RocExs 2017

6th Interndisciplinary Workshop on Rockfall Protection

22 – 24 May 2017, Barcelona, Spain

Jordi Corominas, Jose Moya and Marc Janeras (Eds.)

6th Interdisciplinary Workshop on Rockfall Protection

RocExs 2017

Barcelona, Spain
22-24 May, 2017

A publication of:

International Center for Numerical Methods in Engineering (CIMNE)
Barcelona, Spain

Printed by: Artes Gráficas Torres S.L., Huelva 9, 08940 Cornellà de Llobregat, Spain

ISBN: 978-84-946909-4-5

SUMMARY

CONTENTS

Rockfall hazard characterization, monitoring and modelling

Invited lecture

Rockfall inventory and mapping

Rockfall modelling

Rockfall modelling: fragmentation

Rockfall modelling: parameters’ characterization and tests

Monitoring and alert systems

Hazard analysis

Rockfall mitigation and protective measures

Invited lectures

Evaluation and innovative designs

Parameters' characterization and tests

Modelling of protective measures

Maintenance of protective measures, regulations and case histories

ADVANCES IN ROCK SLOPE CHARACTERIZATION AND MONITORING USING 3D/4D DATASETS (Lidar, Drones and Structure-from-Motion Photogrammetry)

Antonio Abellán[1], Michel Jaboyedoff [2]

This invited talk will summarize the current challenges and future trends on the different techniques and methods dealing with 3D rock slope characterization and monitoring. An overview to the different sensors and systems (Lidar, Drones, *Structure-from-Motion* Photogrammetry) able to acquire a continuum 4D information (3D space + time) will be presented. Then, most of the talk will turn around showing recent applications and modern workflows on the use of point clouds for the investigation of the rockfall phenomena, with emphasis on feature extraction (e.g. characterization of rock slope features such as discontinuities, lithology, etc.) and change detection (pre-failure deformation, rockfall extraction, volume computation, etc.).

Keywords: Rock slope, monitoring, characterization, rockfall, deformation, 3D sensors, close-range photogrammetry, UAV systems.

INTRODUCTION

One of the most significant advances in rock mechanics during the last decades is the use of remote sensors that are able to quickly collect information from the terrain surface in areas that are either inaccessible or too dangerous for direct investigation. Among the different active and passive methods such as Radar, LiDAR, optical, thermal, hyperspectral, etc., there are two systems that are particularly effective for the 3D characterization and monitoring of rock masses: laser scanner and photogrammetry. Both optical and laser sensors can be mounted over terrestrial, aerial (e.g. airborne, helicopter, Unmanned Aerial Vehicles or UAV), satellites, vessel and others ways of transportation. The acquisition of dense terrain information using well-established 3D techniques is entirely varying the way we see, model and eventually interpret the surrounding environment [1], [2], including the investigation of rock slopes and landslides [3], [4]. Examples of applications at different scales ranging from a simple generation of high resolution Digital Terrain Models, to the monitoring of small changes at unprecedented level of detail (e.g. sub millimeter-scale deformation), the detection of changes on real-time, the development of semi-automatic methodologies for the extraction of rock-slope characteristic features including slope discontinuities and lithological units, etc. The interest on the characterization and monitoring of rock slopes using high resolution 3D point clouds created both LiDAR and photogrammetric techniques is continuously growing [5]; Nevertheless, we have been observing during the last few years that both Terrestrial LiDAR

[1] Scott Polar Research Institute, University of Cambridge, Cambridge, CB21ER, UK, aa962@cam.ac.uk
[2] Institute of Earth Sciences, Risk Group, University of Lausanne, Lausanne, 1015, Switzerland

and "classical" photogrammetric techniques are being gradually surpassed by a more flexible and low-cost modern photogrammetric systems, that are combined with efficient post-processing workflows for image treatment (Structure-From-Motion photogrammetry or SfM, [6], [7], [8]). The core of this invited talk is dealing with the main applications that our group have been developing in collaboration with several project partners during the last years. We have classified them into two main avenues of research: feature extraction and change detection, as it will discussed as follows.

ROCK SLOPE CHARACTERIZATION AND FEATURE EXTRACTION

Using 3D point clouds obtained by terrestrial LiDAR or terrestrial photogrammetry is progressively being incorporated into the protocols for rock mass characterization in real practice [9], [10]. Some examples on the use of automatic or semi-automatic techniques for acquiring fundamental rock mass properties include the automatic or semi-automatic extraction of the number and orientation of discontinuity sets [11], [12], [13], spacing [14], persistence [15] as well as the roughness [16], lithology [17], [18], [19], weathering degree, Slope Mass Rating [20], etc. Using semi-automatic techniques is specially indicated in those cases where either a physical accessibility or health and safety cannot be guaranteed. Commercial software includes *Split FX* [21], *Coltop* [11], and *DiAna* [12], while open-source software include *DSE extractor* [13].

ROCK SLOPE MONITORING AND CHANGE DETECTION

Applications on the use of multi-temporal 3D point clouds for the investigation of rock slope processes include: (a) the extraction of rockfall locations, volumes and rates of occurrence [22], [23] for the investigation of either fragmental rockfalls on mountainous areas [24], [25], coastal cliffs [26], [27], [28] and hazardous transportation corridors [29], [30]. In addition, (b) the possibility to detect both precursory deformation and minor scale rockfalls with sufficient time was shown in the past [31], [32], [33]. More recently, (c) other studies are showing the possibility to unlock the photographic archives and to quantify rockfall events along several decades by extracting 3D point clouds from pictures contained in old databases or open repositories, such as Google Street Drive, Flickr, etc. [34], [35], [36]. Finally, (d) recent studies show how to investigate rock slopes in a 4D continuum using both terrestrial LiDAR and time-lapse photogrammetry, which are shedding light on the dynamic of rapidly evolving processes at multiple spatial and temporal scales [37], [38].

FUTURE TRENDS

Apart from the important advances mentioned above, a series of stimulating research outcomes are anticipated for the upcoming decade in the following areas: sensor fusion, development of new algorithms for the acquisition and treatment of massive flows of information in a four dimensional continuum, development of new algorithms with applications in computer vision (process automatization, direct georeferencing, improvements in bundle adjustment and 4D processing chains) and rock mechanics (e.g. feature extraction and real-time monitoring). In addition, it is anticipated that SfM photogrammetry will turn into a standard procedure during the coming two or three years. In addition, the adaptation of techniques from computer vision and the use of Graphic Processing Units (GPU) originally designed for

gamming applications will turn into a higher point cloud processing capabilities. One of the most challenging topics is to adapt the numerical models to take fully advantage of high resolution data, as for instance rockfall trajectories [39] and block stability. Finally, a fast proliferation of open knowledge, including open-access publications, open-data and open methods in public repositories is also highly expected (and desired) during the forthcoming years [40], [41].

ACKNOWLEDGEMENTS

We acknowledge the organizers of the *6th Interdisciplinary Workshop on Rockfall Protection* for their invitation. The financial support from the Spanish Economy and Competitiveness Ministry to the Rockrisk research project [BIA2013-42582-P] and the H2020 Program of the European Commission under the Marie Skłodowska-Curie Individual Fellowships [MSCA-IF-2015-705215] are also acknowledged. This research has been possible thanks to the close collaborations of researchers from the University of Lausanne, Queen's University, Technical University of Catalonia, University of Barcelona, University of Alicante and University of Cambridge.

REFERENCES

[1] TELLING J, LYDA A, HARTZELL P, GLENNIE C (2017) Review of Earth science research using terrestrial laser scanning. Earth-Science Reviews 169, 35-68.

[2] BUCKLEY SJ, HOWELL JA, ENGE HD, KURZ TH (2008) Terrestrial laser scanning in geology: data acquisition, processing and accuracy considerations. Journal of the Geological Society, 165(3), 625-638.

[3] Abellán A, Oppikofer T, Jaboyedoff M, Rosser N J, Lim M, Lato M J (2014) State of science: terrestrial laser scanning on rock slope instabilities. Earth Surface Processes and Landforms 39 (1), 80-97

[4] Jaboyedoff M, Oppikofer T, Abellán A, Derron MH, Loye A, Metzger R, Pedrazzini A, (2012) Use of Lidar in landslide investigations: a review. Natural Hazards 61, 5–28.

[5] ABELLAN A, DERRON M-H, JABOYEDOFF M (2016) "Use of 3D Point Clouds in Geohazards" Special Issue: Current Challenges and Future Trends Remote Sensing 8, 130.

[6] WESTOBY MJ, BRASINGTON J, GLASSER NF, HAMBREY MJ, REYNOLDS JM (2012) Structure-from-Motion" photogrammetry: A low-cost effective tool for geoscience applications. Geomorphology 179, 300–314

[7] SMITH MW, CARRIVICK JL, QUINCEY DJ (2016) Structure from motion photogrammetry in physical geography Progress in Physical Geography 40(2), 247-275.

[8] Eltner A, Kaiser A, Castillo C, Rock G, Neugirg F, Abellán A (2016) image-based surface reconstruction in geomorphometry – merits limits and developments. Earth Surface Dynamics 4 359-389.

[9] OLSEN MJ, RAUGUST JD, ROE GV (2013) Use of Advanced Geospatial Data, Tools, Technologies, and Information in Department of Transportation Projects (Vol. 446). Transportation Research Board.

[10] LATO MJ, GAUTHIER D, HUTCHINSON DJ (2015) Rock Slopes Asset Management: Selecting the Optimal Three-Dimensional Remote Sensing Technology. Transportation Research 2510, 7–14

[11] JABOYEDOFF M, METZGER R, OPPIKOFER T, COUTURE R, DERRON MH, LOCAT J, TURMEL D (2007) New insight techniques to analyze rock-slope relief using DEM and 3D-imaging cloud points: COLTOP-3D software. Rock Mechanics: Meeting Society's Challenges and Demands 2, 61-68.

[12] GIGLI G, CASAGLI N (2011) Semi-automatic extraction of rock mass structural data from high resolution LiDAR point clouds. Int. Journal of Rock Mechanics and Mining Sciences 48 (2), 187-198.

[13] RIQUELME A, ABELLÁN A TOMÁS R JABOYEDOFF M (2014) A new approach for semi-automatic rock mass joints recognition from 3D point clouds Computers and Geosciences 68, 38–52.

[14] RIQUELME A, ABELLÁN A TOMÁS R (2015) Discontinuity spacing analysis in rock masses using 3D point clouds Engineering Geology 195, 185-195.

[15] STURZENEGGER M, STEAD D (2009) Quantifying discontinuity orientation and persistence on high mountain rock slopes and large landslides using terrestrial remote sensing techniques. NHESS 9 (2), 267-287.

[16] BISTACCHI A, GRIFFITH WA, SMITH SA, DI TORO G, JONES R, NIELSEN S (2011) Fault roughness at seismogenic depths from LIDAR and photogrammetric analysis. Pure and Applied Geophysics, 168, 2345-2363.
[17] CARREA D, ABELLÁN A, HUMAIR F, MATTASCI F, DERRON M-H, JABOYEDOFF M (2016) Correction of terrestrial LiDAR intensity channel using Oren–Nayar reflectance model: An application to lithological differentiation ISPRS Journal of Photogrammetry and Remote Sensing 113, 17-29.
[18] HUMAIR F, ABELLÁN A CARREA D MATASCI B JABOYEDOFF M EPARD JL (2015) Stratigraphic layers detection and characterization using Terrestrial Laser Scanning point clouds: example of a box-fold European Journal of Remote Sensing 48, 541-568.
[19] BUCKLEY SJ, KURZ TH, HOWELL JA, SCHNEIDER D (2013) Terrestrial lidar and hyperspectral data fusion products for geological outcrop analysis. Computers & Geosciences 54, 249-258.
[20] RIQUELME A, TOMÁS R, ABELLÁN A (2016) Characterization of Rock Slopes through Slope Mass Rating using 3D point clouds International Journal of Rock Mechanics and Mining Sciences 84, 165-176.
[21] SLOB S, VAN KNAPEN B, HACK R, TURNER K, KEMENY J (2005) Method for automated discontinuity analysis of rock slopes with three-dimensional laser scanning. Transportation Research Board 1913, 187-194.
[22] TONINI M, ABELLÁN A (2014) Rockfall detection from LiDAR point clouds: a clustering approach using R. Journal of Spatial Information Science 8, 95-110.
[23] CARREA D, ABELLAN A, DERRON MH, JABOYEDOFF M, LOYE A, MICHOUD C (2015) Automatic rockfalls volume estimation based on terrestrial laser scanning data. Eng. Geol. for Soc. & Territory, 2, 425–428.
[24] STOCK GM, MARTEL SJ, COLLINS BD, HARP EL (2012) Progressive failure of sheeted rock slopes: The 2009–2010 Rhombus Wall rock falls in Yosemite Valley California USA. ESPL 37, 546–561.
[25] SANTANA D, COROMINAS J ,MAVROULI O, GARCIA-SELLÉS D (2012) Magnitude-frequency relation for rockfall scars using a Terrestrial Laser Scanner. Engineering Geology 145, 50–64.
[26] LIM M, PETLEY DN, ROSSER NJ, ALLISON RJ, LONG AJ, PYBUS D (2005) Combined digital photogrammetry and time-of-flight laser scanning for monitoring cliff evolution. Photog. Record 20, 109–129.
[27] ROSSER NJ, PETLEY DN, LIM M, DUNNING SA, ALLISON RJ (2005) Terrestrial laser scanning for monitoring the process of hard rock coastal cliff erosion Q J Eng Geol Hydrogeol 38, 363–375.
[28] DEWEZ TJ, ROHMER J, REGARD V, CNUDDE C (2013) Probabilistic coastal cliff collapse hazard from repeated terrestrial laser surveys: Case study from Mesnil Val. Journal Coastal Research 65, 702–707.
[29] KEMENY J, HENWOOD J, TURNER K (2006) The use of ground-based LiDAR for geotechnical aspects of highway projects. In Proceedings of the 57th Annual Highway Geological Symposium CO USA, 27–29.
[30] KROMER R, HUTCHINSON DJ, LATO MJ, GAUTHIER D, EDWARDS T (2015) Identifying rock slope failure precursors using LiDAR for transportation corridor hazard management. Eng. Geology 195 93-103.
[31] ROSSER N, LIM M, PETLEY D, DUNNING S, AND ALLISON R (2007) Patterns of precursory rockfall prior to slope failure. Journal Of Geophysical Research: Earth Surface 112(F4).
[32] ABELLÁN A, VILAPLANA JM, CALVET J, BLANCHARD J (2010) Detection and spatial prediction of rockfalls by means of terrestrial laser scanning modelling. Geomorphology 119: 162-171.
[33] ROYÁN MJ, ABELLÁN A, JABOYEDOFF M, VILAPLANA JM, CALVET J (2014) Spatio-temporal analysis of rockfall pre-failure deformation using Terrestrial LiDAR. Landslides, 11 697–709.
[34] ALBER S (2016) Change detection combining SfM and LiDAR techniques: application to the study of rockfalls using archival photographs Katholische Universitat Eichstatt-Ingolstadt MsC thesis num. 653105, 98 pp.
[35] GUERIN A, ABELLÁN A, MATASCI B, JABOYEDOFF, M DERRON, MH RAVANEL L. (under review) 3D reconstruction of a collapsed rock pillar from web-retrieved images and terrestrial LiDAR data – The 2005 event of the West face of the Drus (Mont-Blanc massif) Natural Hazards and Earth System Science.
[36] VOUMARD J, ABELLAN A, NICOLET P, CHANUT MA, DERRON MH, JABOYEDOFF M (under review) Using street view imagery for 3D survey of rock slope failures. Natural Hazards & Earth System Sciences.
[37] ROSSER N, WILLIAMS J, HARDY R, BRAIN M, HUNTER G, DAVIS J (2017) Insights from constant near-realtime laser scanning of actively failing rockslopes. Virtual Geoscience Conference, Norway Sept 2016.
[38] KROMER R, ABELLÁN A, HUTCHINSON J, LATO M, EDWARDS T, JABOYEDOFF M (2015) A 4D Filtering and Calibration Technique for Small-Scale Point Cloud Change Detection with a Terrestrial Laser Scanner. Remote Sensing 7, 13029-13052.

[39] NOËL F., CLOUTIER C., TURMEL D., LOCAT J, (2016) Using point clouds as topography input for 3D rockfall modeling. In Landslides and Engineered Slopes. Experience, Theory and Practice. Napoli, Italy: CRC Press, pp. 1531–1535.
[40] OPENTOPOGRAPY: High-Resolution Topography Data and Tools Available online: http://www.opentopography.org/ (accessed on 25 April 2017).
[41] POINT CLOUD LIBRARY DATA REPOSITORY Available online: http://www.pointclouds.org/news/2013/01/07/point-cloud-data-sets/ (accessed on 25 April 2017).

11 YEARS OF GROUND-BASED LIDAR MONITORING IN THE WEST FACE OF THE DRUS (MONT-BLANC MASSIF, FRANCE)

Antoine Guerin[1], Ludovic Ravanel[2], Battista Matasci[1], Michel Jaboyedoff[1], Marc-Henri Derron[1] and Philip Deline[2]

The Petit Dru West face (Mont-Blanc massif, France) has been scanned every year by terrestrial LiDAR since the collapse of the Bonatti Pillar in June 2005. During the last 11 years, 307 rockfall events were detected with volumes ranging from 0.002 m^3 to 54'731.2 m^3. The average activity is of 0.34 event per year and per hm^2. The distribution of rockfall volumes follows a power-law with an exponent value of 0.37. Since the major event of October 2011, the annual rockfall volume is steadily decreasing.

Keywords: rockfall, rock avalanche, terrestrial laser scanner, power-law distribution, Mont-Blanc massif.

INTRODUCTION

Large rockfall events have been quite well described in the Alps for the last 15 years [1], [2], [3], [4]. On contrary, the countless smaller rockfalls that occurred in high Alpine rock faces are poorly documented. Then the rockfall volume-frequency relationship for high-mountain area is still poorly constrained [5]. To fill this gap, we have monitored the Petit Dru West face (3'730 m a.s.l.; Mont-Blanc massif, France) by terrestrial laser scanners for 11 years (2005-2016). This emblematic peak of the Chamonix valley is made of Hercynian granitic rocks. It has been affected by large rockfall events in 1950, 1997 and 2003 (Fig. 1), and by a little rock avalanche (volume between 265'000 m^3 and 292'680 m^3) in June 2005 [1], [6], [7]. This rock avalanche completely wiped out the Bonatti Pillar and significantly modified the morphology of the face. This present work analyses the rockfall activity in the Petit Dru West face after this major event.

MATERIAL AND METHODS

Terrestrial Laser Scanning (TLS) measurements have been acquired every year in autumn from October 2005 to September 2016. From 2005 to September 2011, only the upper part of the West face was acquired from the Flammes de Pierre ridge (Fig. 1; mean distance: 400 m). Since November 2011, the whole face was scanned from the right lateral moraine of the Drus glacier (Fig. 1; mean distance: 1'000 m). Only the October 2009 dataset could not be used for the monitoring because of a defective LiDAR.

[1] Risk Analysis Group, Institute of Earth Sciences, University of Lausanne, Switzerland, antoine.guerin@unil.ch
[2] EDYTEM, University Savoie Mont-Blanc – CNRS, Le Bourget du Lac, France

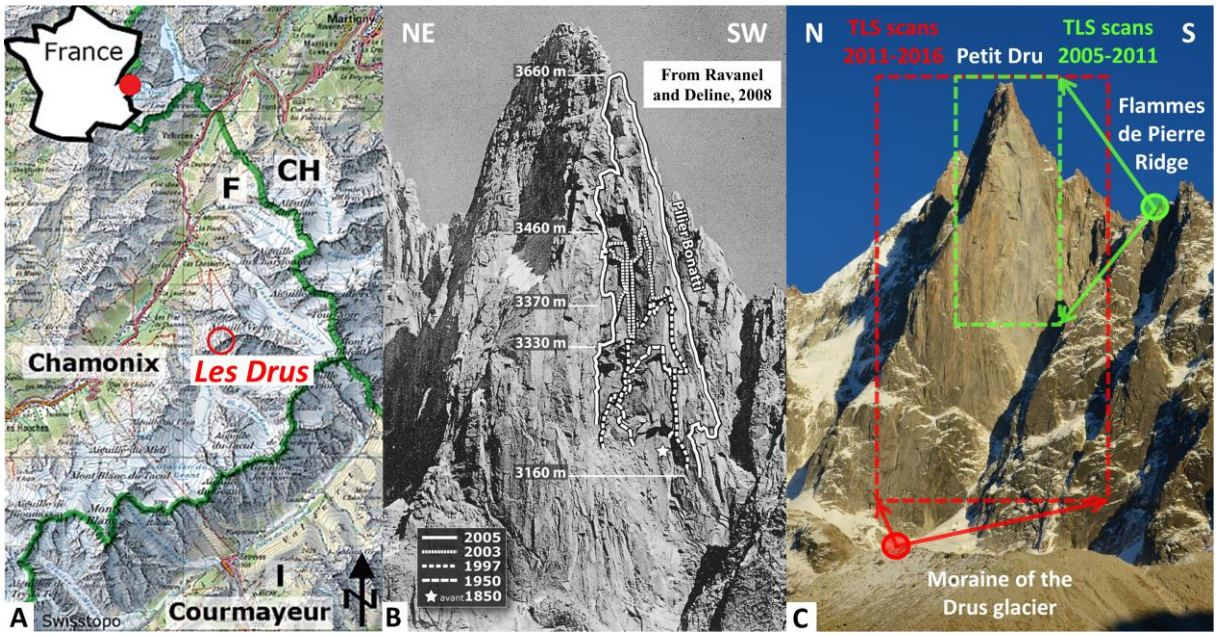

Fig. 1 A: Location of the Petit Dru within the Chamonix Valley (Mont-Blanc massif; map Swisstopo). B: Main rockfall events in the Petit Dru West face since the end of the Little Ice Age (figure modified after [1]). C: West face of the Petit Dru in November 2015 with the scanner locations (circles) and the corresponding scanned surfaces (dashed line) for 2005-2011 (green) and 2011-2016 (red).

All point clouds were then aligned by Iterative Closest Point algorithm. Eleven pairs of point clouds with about 1 year in between two acquisitions (Tab. 1) were compared with a level of detection of 3 cm at an average distance of 1'000 m. Rockfall extraction and volume calculation have been achieved as proposed in [8] and [7].

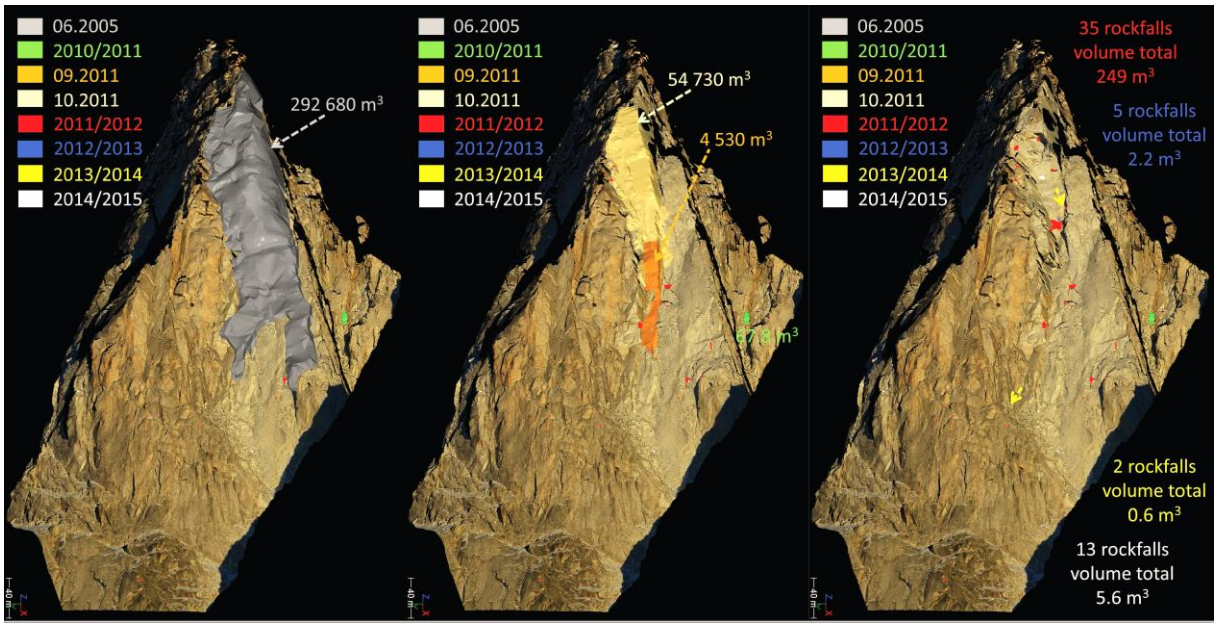

Fig. 2 Photo-realistic model of the Petit Dru West face (high-resolution TLS mesh textured with a picture of November 2015) and front view of the rockfall events detected between October 2010 and November 2015. The gray compartment on the left picture corresponds to the volume of the June 2005 rock avalanche determined by [7].

RESULTS AND DISCUSSION

From October 2005 to September 2016, 307 rockfall events (Tab. 1) were detected in the Petit Dru West face, with volumes ranging from 0.002 m^3 to 54'731.2 m^3. Three major events occurred during this period: a 2'228.2 m^3 event between March and the end of August 2010, and two successive collapses in September and October 2011 (4'532.3 m^3 and 54'731.2 m^3 respectively) in the area of the June 2005 event scar (Fig. 2). The other rockfalls range between 0.002 m^3 and 475.9 m^3 with a median value of 0.2 m^3.

Tab. 1 Inventory of rockfall events detected for each comparison.

TLS comparison	Viewpoint	Number of rockfalls	Eroded volume (m^3)
2005/2006	Flammes de Pierre Ridge	73	556.6
2006/2007	Flammes de Pierre Ridge	46	63.5
2007/2008	Flammes de Pierre Ridge	18	41.4
2008/2010	Flammes de Pierre Ridge	37	2'657.7
2010/2011	Both viewpoints	75	59'750.6
2011/2012	Moraine of the Drus glacier	35	249.4
2012/2013	Moraine of the Drus glacier	5	2.3
2013/2014	Moraine of the Drus glacier	2	0.6
2014/2015	Moraine of the Drus glacier	13	5.6
2015/2016	Moraine of the Drus glacier	3	0.5

Tab. 1 shows that the number of "small-size" rockfalls per year is not constant over the period of survey. This number is higher right after a major event (2005 and 2011) and decreases rapidly afterwards. This trend is also valid for the annual eroded volume (Tab. 1 and Fig. 3). In this inventory, only the periods 2008/2010 and 2014/2015 stand out with an increasing number of rockfalls and/or an eroded volume after three consecutive years of decrease.

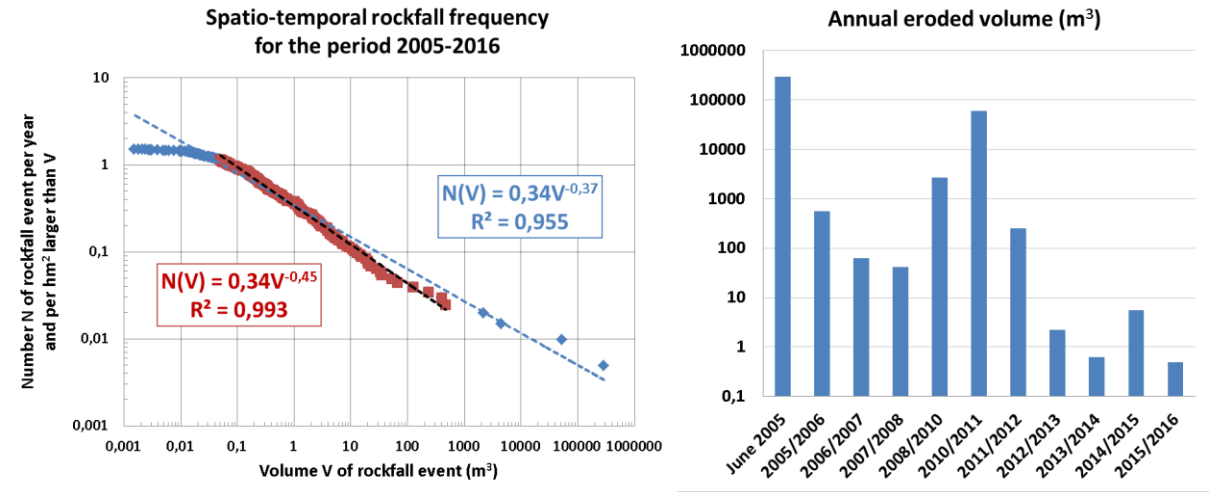

Fig. 3 Left: Cumulative volume-frequency relationships with the power-laws fitting all the volumes (blue) and for 0.05 m^3 < V < 500 m^3 (red). Right: Annual eroded volume during the 11 years of TLS monitoring.

Fig. 3 shows that the resulting spatio-temporal rockfall frequency of the inventory (307 events) is well fitted (R^2=0.955) by a power-law distribution. This magnitude-frequency rela-

tionship includes the June 2005 rock avalanche volume and is characterized by an exponent value of 0.37 and a rockfall activity of 0.34 event per year and per hm^2. Within this distribution, the best-fit (R^2=0.993) was obtained for the volumes of 0.05 m^3 to 500 m^3 (231 events) and this second magnitude-frequency relationship is characterized by an exponent of 0.45 and by the same spatio-temporal rockfall activity. These two exponent values are quite close to the one (0.40) determined by [9] in the Yosemite Valley for Cretaceous granitic rocks. It confirms previous works ([10], [11]) showing that the exponent value depends on the rock type and the erosion processes (glacial) that shape the landscape.

CONCLUSION

The 11 years of ground-based LiDAR monitoring conducted in the Petit Dru West face allowed to determine a rockfall frequency for this high Alpine granitic face between October 2005 and September 2016. Over this period, three major rockfalls (61'491.7 m^3 in total) occurred in 2010 and 2011 in the 2005 rock avalanche scar area, thus continuing the series of large-scale events begun before 1850. Since November 2011, we observe an annual decrease in the number of rockfalls and eroded volume, which we interpret as a gradual stabilization of the West face of the Petit Dru.

REFERENCES

[1] Ravanel, L., & Deline, P. (2008). La face ouest des Drus (massif du Mont-Blanc): évolution de l'instabilité d'une paroi rocheuse dans la haute montagne alpine depuis la fin du petit âge glaciaire. Géomorphologie: relief, processus, environnement, 14(4), 261-272.
[2] Sosio, R., Crosta, G. B., & Hungr, O. (2008). Complete dynamic modeling calibration for the Thurwieser rock avalanche (Italian Central Alps). Engineering Geology, 100(1), 11-26.
[3] Oppikofer, T., Jaboyedoff, M., & Keusen, H. R. (2008). Collapse at the eastern Eiger flank in the Swiss Alps. Nature Geoscience, 1(8), 531-535.
[4] Deline, P., Broccolato, M., Noetzli, J., Ravanel, L., & Tamburini, A. (2013). The December 2008 Crammont rock avalanche, Mont Blanc massif area, Italy. In Landslide Science and Practice (pp. 403-408). Springer Berlin Heidelberg.
[5] Deline, P., Jaillet, S., Rabatel, A., & Ravanel, L. (2008, June). Ground-Based LiDAR data on permafrost-related rock fall activity in the Mont-Blanc massif. In Proceedings of the 9th International Conference on Permafrost (pp. 349-354).
[6] Fort, M., Cossart, E., Deline, P., Dzikowski, M., Nicoud, G., Ravanel, L., ... & Wassmer, P. (2009). Geomorphic impacts of large and rapid mass movements: a review (Vol. 15, No. 1, pp. 47-64). Groupe français de géomorphologie.
[7] Guerin, A., Abellán, A., Matasci, B., Jaboyedoff, M., Derron, M.-H., and Ravanel, L. (in review, 2016). Brief communication: 3D reconstruction of a collapsed rock pillar from web-retrieved images and terrestrial LiDAR data – The 2005 event of the West face of the Drus (Mont-Blanc massif), Nat. Hazards Earth Syst. Sci. Discuss., doi:10.5194/nhess-2016-316.
[8] Tonini, M., & Abellan, A. (2014). Rockfall detection from terrestrial LiDAR point clouds: A clustering approach using R. Journal of Spatial Information Science, 2014(8), 95-110.
[9] Guzzetti, F., Reichenbach, P., & Wieczorek, G. F. (2003). Rockfall hazard and risk assessment in the Yosemite Valley, California, USA. Natural Hazards and Earth System Science, 3(6), 491-503.
[10] Moore, J. R., Sanders, J. W., Dietrich, W. E., & Glaser, S. D. (2009). Influence of rock mass strength on the erosion rate of alpine cliffs. Earth Surface Processes and Landforms, 34(10), 1339-1352.
[11] Barlow, J., Lim, M., Rosser, N., Petley, D., Brain, M., Norman, E., & Geer, M. (2012). Modeling cliff erosion using negative power law scaling of rockfalls. Geomorphology, 139, 416-424.

ESTIMATION OF FALLEN BLOCK VOLUME-FREQUENCY LAW FOR RISK ANALYSIS: AN EXAMPLE

Valerio De Biagi[1], Monica Barbero[1], Maria Lia Napoli[1], Daniele Peila[1]

Quantitative rockfall risk assessment is a powerful tool for land planning and the structural design of rockfall protection systems. In this sense, one of the most critical and discussed aspects is the definition of a design block. In the present paper, a method for formulating a block volume frequency relationship is proposed. Two inputs are necessary: a list of observed falling block events and the results of a detailed survey at the foot of the cliff. An example illustrating the calculations is proposed.

Keywords: rock block size, frequency law, statistics

INTRODUCTION

Modern design Codes aim at guaranteeing the structural safety during buildings' expected life [1]. The expected life of a building depends on the class of consequence of the activities performed in it. Thus, for many natural hazards, say earthquake or strong winds, Building Codes establish a link between the magnitude of the forces exerted by the natural phenomenon and the corresponding return period. The present paper summarizes the methods and findings recently published in NHESS [2], consisting in a novel approach for building a block volume-frequency law for rockfall risk analysis. Such input is required for a probabilistic risk assessment [3]. The approach is in some points similar to the solution found by [4] for hydrological problems with reduced data sets.

BUILDING THE FREQUENCY LAW CURVE

The steps required for the derivation of a block volume-frequency relationship with a reduced number of available data are proposed in the following. The methodology is based on the following hypothesis: temporal occurrences of the falling block events are considered separately from the deposit volumes distribution in a representative area where the rockfall phenomenon occurs. Although a detailed explanation and discussion of the methodology is proposed in [2],[5], the procedure can be summarized in the following steps.

(1) Surveying: the required data for deriving the frequency law are the catalogue of the events, $\mathcal{C}$, i.e., a catalogue containing the size of the falling block and the corresponding temporal information (date), and a list of measured volumes, $\mathcal{F}$, that may have fallen down at any time. Both $\mathcal{C}$ and $\mathcal{F}$ must relate to the same representative area. The representative area is defined as the portion of deposit beyond a defined line, in which the hazard is computed. We consider the foot of the slope as a representative area;

[1] Politecnico di Torino, C.so Duca degli Abruzzi 24, Torino 10129, Italy, +390110904842, valerio.debiagi@polito.it (Corresponding author: V. De Biagi)

(2) Definition of the threshold volume: the catalogue of the events $\mathcal{C}$ contains all the recorded events gathered in a time window of temporal length, t. Since the recording of the events is related to *in-situ* observations after the occurrence, events involving small rock blocks are not always recorded. Therefore, there is the possibility that the catalogue $\mathcal{C}$ contains only a part of these small events. This fact was considered in the proposed analysis with the introduction of a threshold volume, V_t, defined as the minimum size of a fallen block that has always been observed and recorded (after its occurrence).

(3) Creation of the reduced data sets: once the threshold volume V_t is determined, the catalogue of the events and the list of measured blocks are split in two parts. In both data sets, the volumes smaller than V_t are not considered. The remaining constitute the so-called reduced catalogue, $\mathcal{C}^\star$, and the reduced list, $\mathcal{F}^\star$. The temporal length t is increased to $t^\star$ accounting for the fact that the decision of monitoring a rockfall prone slope usually begins after the occurrence of an event larger than the threshold volume;

(4) Choice of the probabilistic models: two probabilistic models (p.m.) are chosen. One should be able to describe the temporal occurrences of the events of the reduced catalogue; the other the distribution of the surveyed volumes. The hypothesis of Poisson point process is adopted for the former p.m., thus a Poisson distribution is considered for the occurrence of the falling blocks. The probability of occurrence of n events during the observation period $t^\star$ is

$$p(n) = \frac{e^{-\lambda t^\star}(\lambda t^\star)^n}{n!} \ , \tag{1}$$

where λ is the occurrence parameter to be determined. A Generalized Pareto Distribution (GPD) is adopted for the latter. Evidences of power laws (GPD is a power-like probability distribution) are present in literature for fragmentation processes [6]. The cumulative distribution function of volume v is

$$F_V(V) = 1 - \left(1 + \xi \frac{v-\mu}{\sigma}\right)^{-\frac{1}{\xi}} \ , \tag{2}$$

where σ, ξ and μ are the scale, shape and location parameters, respectively.

(5) Evaluation of the parameters of the distribution: the estimate of the four parameters can be obtained through maximum likelihood method from the reduced data sets. Poisson distribution parameter is equal to the ratio between the number of observed events larger than the threshold volume and $t^\star$.

Following that, the volume $v(T)$ of a block corresponding to a return period T is

$$v(T) = \mu + \left[(\lambda T)^\xi - 1\right]\frac{\sigma}{\xi} \ . \tag{3}$$

and the return period, $T(v)$, corresponding to a volume v is

$$T(v) = \frac{1}{\lambda}\left(1 + \xi \frac{v-\mu}{\sigma}\right)^{1/\xi} \ . \tag{4}$$

A CASE STUDY

The test is located in Aosta Valley (Northwestern Italian Alps) at an altitude ranging from 1630 m to 1800 m a.s.l. The study area is composed of greenschist facies deposits (metabasites and metamorphosed gabbro) with the foliation plane N 160/80. Large rock blocks are present at the base of the cliff, proving an intense rockfall activity in the past. Recent events have been recorded since 2010. Since this year, risk analyses have been performed and three falling blocks were observed in three different events. The observed size was larger than 0.5 m^3. An onsite survey was performed in order to define the distribution of the fallen blocks in a representative area at the foot of the cliff following the procedure reported in [7]. Block sizes are grouped into size classes in a geometric progression following $\sqrt{2}$ with volume, as reported in the plot of Fig. 2(a). The volume of the measured blocks ranges from 0.008 m^3 to 60 m^3.

Because of the particular attention paid on rockfall events reaching the foot of the cliff where a residential area is located, all the events occurred after 2010 were considered in the catalogue $\mathcal{C}$ and the reduced catalogue $\mathcal{C}^\star$, which are coincident. The threshold volume V_t was set equal to 0.5 m^3, i.e., the minimum size of the observed events in $\mathcal{C}$. The number of events considered in the analysis is equal to $n = 3$. The corrected temporal length of the observation period, $t^\star$ (computed through Eqn. (7) of ref. [2]) is equal to 7.0 years. Thus, the estimate of Poisson parameter modelling the distribution of the occurrences is equal to

$$\lambda = \frac{3}{7} = 0.4285\ yr^{-1}\,. \tag{5}$$

The reduced list $\mathcal{F}^\star$ was created after the survey at the foot of the cliff. The volumes smaller than 0.512 m^2 were not considered in the calculations. Referring to the plot of Fig. 2(a), the excluded block sizes are marked in red, while those that served for getting the volume-frequency law are in black. A maximum likelihood procedure has provided the following estimates of the Generalized Pareto Distribution parameters. The location parameter is equal to the threshold volume, i.e., 0.512 m^3. The scale and the shape parameter are equal to 2.2963 and 0.1955, respectively. Using the equations found at point (5) of the numbered list in the previous section, the volume corresponding to a given return period can be found. The block-volume frequency law is plot in Fig. 2(b).

CONCLUSIONS

Differently from other results found in the literature observed rockfall events [8],[9], where volume-frequency laws were from a database of observed and measured events, exclusively, the procedure herein summarized permits to build a volume-frequency law from a reduced set of observations. The computed frequency law can be used in engineering calculations (risk and design). The independency between the events described by Poisson's probabilistic models in rockfall was discussed in [10], who affirmed that the interaction between a natural hazard and anthropic elements (say, vehicles, buildings) is a rare event that can be ascribed to a Poisson process, i.e., it is random. Despite the fact that precursors of large rockfall events were observed [11],[12], the assumption of random process can be considered true for volumes larger than the threshold volume. In order to have a good estimate of the return period of the events of the reduced catalogue, it is necessary to have a consistent number of observa-

tions. The present case study considers three events in six years with $\lambda = 0.4286\ yr^{-1}$. An additional (missed) event would set $\lambda = 0.5925\ yr^{-1}$, implying that the volumes with 100 and 500 years return period are 12% and 9.8%, respectively, greater than the ones currently expected. Since the bounds are acceptable, the temporal sample can be considered representative. In case of a single observed event in a short observation period, the return period would be strongly underestimated [2].

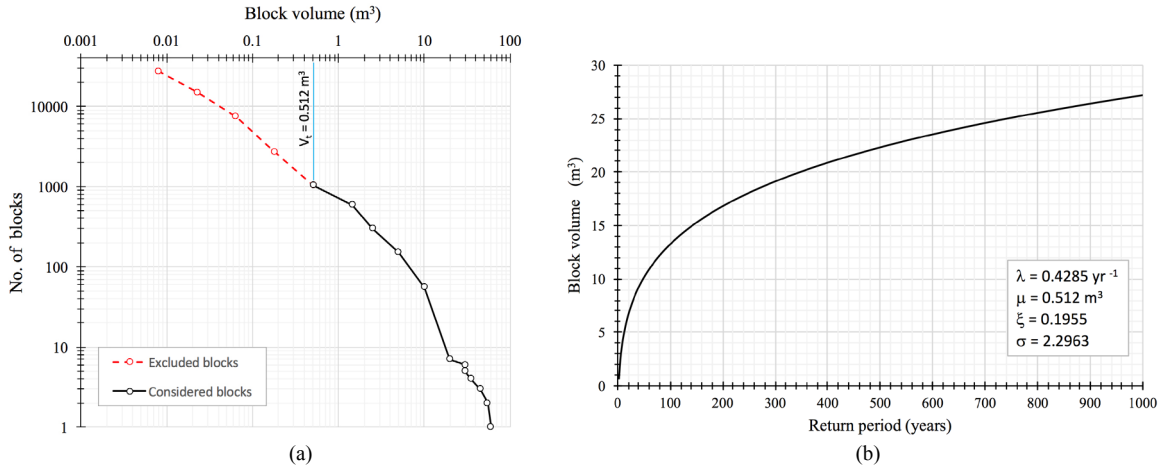

Fig. 2 In (a) the cumulative number of measured blocks versus block volume is plot. In (b) the block volume frequency law is reported

This research was supported supported by Regione Autonoma Valle d'Aosta under the framework of the project "Realizzazione di scenari di rischio per crolli di roccia".

REFERENCES

[1] CEN (2000) EN 1990: Basis of Structural Design (Eurocode 0). European Committee for Normalization.
[2] DE BIAGI V, NAPOLI M L, BARBERO M, PEILA D (2017) Estimation of the return period of rockfall blocks according to their size. Nat. Hazards Earth Syst. Sci., 17, 103-113.
[3] STRAUB D, SCHUBERT M (2008) Modeling and managing uncertainties in rock-fall hazards. Georisk 2, 1-15.
[4] CLAPS P, LAIO F (2003) Can continuous streamflow data support flood frequency analysis? An alternative to the partial duration series approach. Water Resources Research 39, SWC 6-1-11.
[5] DE BIAGI V, BOTTO A, NAPOLI M L, DIMASI C, LAIO F, PEILA D, BARBERO M (2016) Calcolo del tempo di ritorno dei crolli in roccia in funzione della volumetria. GEAM 53(1), 39-48.
[6] CROSTA G, FRATTINI P, FUSI N (2007) Fragmentation in the Val Pola rock avalanche, Italian Alps, Journal of Geophysical Research: Earth Surface 112, F01 006.
[7] RUIZ-CARULLA R, COROMINAS J, MAVROULI O (2015) A methodology to obtain the block size distribution of fragmental rockfall deposits. Landslides 12, 815-825.
[8] DUSSAUGE C, GRASSO J-R, HELMSTETTER A (2003) Statistical analysis of rockfall volume distributions: Implications for rockfall dynamics. J. Geophys. Res.-Sol. Ea.,108, 2286.
[9] HUNGR O, EVANS S, HAZZARD J (1999) Magnitude and frequency of rock falls and rock slides along the main transportation corridors of southwestern British Columbia. Canadian Geotechnical Journal 36, 224-238.
[10] MCCLUNG D (1999) The encounter probability for mountain slope hazards. Canadian Geotechnical Journal 36, 1195-1196.
[11] ROSSER N, LIM M, PETLEY D, DUNNING S, ALLISON R (2007) Patterns of precursory rockfall prior to slope failure. J. of Geophysical Research 112, F04014.
[12] JESÚS ROYÁN M, ABELLÁN A, JABOYEDOFF M, VILAPLANA J M, CALVET J (2014) Spatio-temporal analysis of rockfall pre-failure deformation using Terrestrial LiDAR. Landslides 11, 697-709.

ENHANCING THE INTEGRATION OF THE PROTECTIVE ROLE OF FOREST IN ROCKFALL SIMULATIONS

David Toe[1], Franck Bourrier[2], Luuk Dorren[3], Marco Conedera[4], Frédéric Berger[5]

This study presents an innovative method to enhance the integration of the protective role of forest in rockfall trajectory analysis models. First, a deterministic model which can simulate block-tree impacts was developed and calibrated using field and laboratory experiments for different tree species. Second, the calibrated deterministic model is used to build meta-models which can be easily integrated into classical rockfall trajectory analysis models.

Keywords: Forest, Impact, Rockfall simulations, Meta-model, Discrete Element Method

INTODUCTION

In the field of rockfall hazard assessment, the integration of the protective effect of forest is increasingly being studied. Research studies were mainly dedicated to integrate forest effects into empirical or lumped-mass rockfall models which present efficient computational times and global accounting of forest effects [1]. However, these models do not integrate all the physical processes occurring during block/tree impact. In particular, they do not account for the respective contributions of the tree components - stem, root system and crown - on the impacting block velocity changes and energy reduction.
To integrate these contributions, simulation tools based on mechanical approaches have been developed [2], [3]. However the main difficulties related to these approaches remain the in-situ characterization of the numerous input parameters of the models and the important computational effort needed for the simulations.
In this research work we propose to develop two meta-models that can predict the block energy reduction after an impact on two different tree species. These meta-models models are developed to be easily coupled with probabilistic rockfall models. They are built using a Discrete Element Method (DEM) model that was calibrated using laboratory and field impact tests for the two different tree species: *Fagus sylvatica* (beech) and *Ailanthus altissima* (ailanthus).

[1] Irstea, 2 rue de la papeterie, St Martin d'hères 38400, France, david.toe@irstea.fr
[2] Irstea, 2 rue de la papeterie, St Martin d'hères 38400, France, franck.bourrier@irstea.fr
[3] Bern University of Applied Sciences, Länggasse 85, CH-3052 Zollikofen Switzerland luuk.dorren@bfh.ch
[4] Swiss Federal Research Institute WSL, a Ramèl 18, 6593 Cadenazzo marco.conedera@wsl.ch
[5] Irstea, 2 rue de la papeterie, St Martin d'hères 38400, France, frederic.berger@irstea.fr

DEM MODEL

Modeling the impact of a block on a tree using the DEM (open-source code Yade-Dem [4]) allows taking into account large displacements, material non-linearities and contacts between the block and the tree. Tree stems are represented by flexible cylinders modelled as elasto-plastic beams sustaining normal, shearing, bending, and twisting loading [5]. The root system is modeled using a non-linear rotational spring acting on the bending moment at the bottom of the stem. The crown is taken into account using an additional mass distributed uniformly on the upper part of the tree. The block is represented by a sphere. The contact between the block and the stem is explicitly modeled (see Fig. 1).

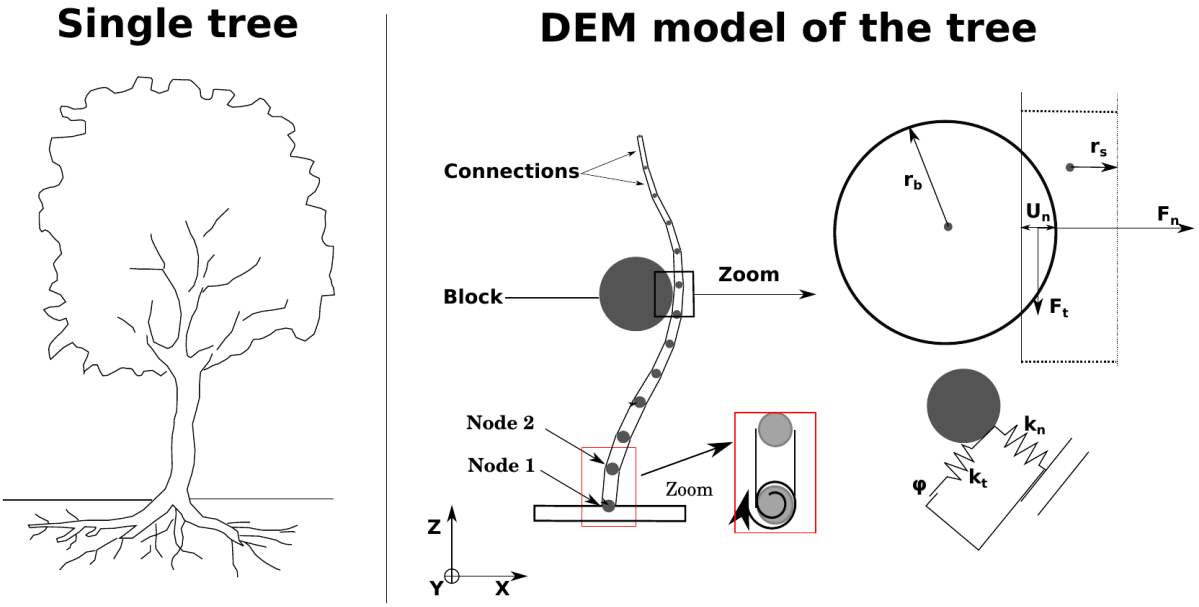

Fig. 1 Sketch of the tree model. DEM model of the tree impacted by a block. U_n is the block overlap with the tree, r_b and r_s are the block radius and tree radius at the contact surface. F_n and F_t are the normal and the tangential forces at the contact surface between the block and the tree. K_n and K_t are the normal and the tangential stiffness at the contact and φ is the local friction angle at the contact. The root system is modeled by a rotational spring depending on the orientation of local coordinate systems associated with node 1 and node 2

LABORATORY AND FIELD EXPERIMENTS

A first calibration of the DEM model was done on beech species which is highly present in the alpine protection forest [6]. The DEM model was calibrated using laboratory impact tests carried out on 41 fresh beech stems. Each stem was 1.3 m long with a diameter ranging from 3 to 7 cm. The wood stems were clamped on a rigid structure and impacted by a 149 kg charpy pendulum.

Over the last 50 years many forests with a protection function against rockfall hazard have been colonized by ailanthus [7]. This invasive species has the ability to grow rapidly, suppressing competition with allelopathic compounds and to re-sprouts vigorously when trees are cut. The development of ailanthus in forests could affect their protective capacity against

rockfall hazard. The mechanical parameters controlling the stem and the root contribution of ailanthus during an impact were calibrated using three types of experiments. 20 winching tests were done on ailanthus with diameter ranging from 6 to 21 cm to analyze the response of the root system when the tree is subjected to a bending effort. 30 three points bending tests were done on freshly cut ailanthus stems with diameters ranging from 8 to 16 cm. Finally, 30 dynamic impact tests were conducted in an ailanthus forest located in Bellinzona (Switzerland). The trees, with diameters ranging from 10 to 20 cm, were impacted by a spherical granite ball (mass: 57 Kg; diameter: 0.35 m) with a mean velocity of 14 m/s. The impacts were recorded using a high speed (250 frames per second).

THE META-MODELS

19 input parameters are required to perform DEM simulations of a block impacting a tree: 11 parameters were related to the tree and 8 parameters to the block. Thus, a sensitivity analysis on the DEM model was done to identify a reduced number of input parameters controlling the block energy reduction after impact. A quantitative sensitivity analysis was conducted calculating the Sobol indices that correspond to the ratio between the partial variance associated with each input parameter and the total variance of the output parameters [8]. The results highlight that the impact velocity, the stem diameter, and the impact point horizontal location are the three input parameters that mainly control the block energy reduction after impact [3]. These parameters correspond to those classically used in the model of rock impacts on trees of classical trajectory analysis tools.

According to those results, we have built two meta-models using two set of 4200 DEM simulations for the two different tree species. In these simulations only four input parameters vary (chosen as input parameters in the meta-model), the other are set to mean values. The ranges of values chosen for the four input parameters are the same as those used in the sensitivity analysis which corresponds to classical values in the field of rockfall assessment. Three of the input parameters are directly calculated in rockfall simulations (velocity [5 – 40 m/s], block volume [0.1 – 1 m^3], and impact location [0 – 100 %]) and the last one is the tree diameter ([0 – 0.6 m]).

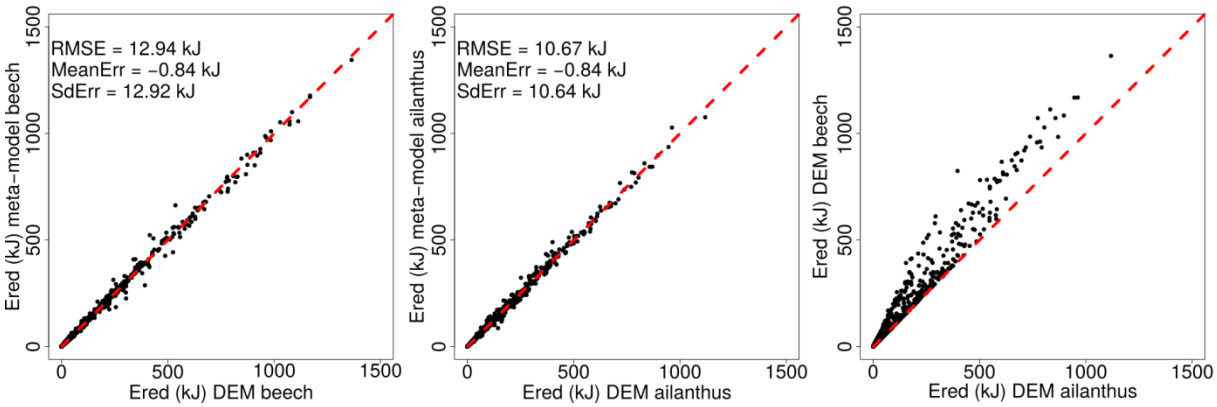

Fig. 2 Comparison between the energy reductions of blocks after an impact on a tree (Ered) predicted by a DEM model and a meta-model for two different tree species. RMSE is the Root Mean Square Error, MeanErr and SdErr are the mean and the standard deviation of the difference between the values predicted by the DEM and the meta-model

The meta-models are then build using multi-linear interpolations for the two set of 4200 DEM results. The robustness of the meta-models to predict the energy lost by the block during the impact was evaluated using a comparison between DEM simulations and meta-model predictions for 1000 new impact configurations randomly defined in the range of the four input parameters. The results show a good agreement between the block energy reduction (Ered) predicted by the meta-models and the DEM model (see Fig. 2). In addition, the results highlight that beech is slightly more efficient to reduce block energy after an impact compared to ailanthus.

CONCLUSION

A DEM model of block impacts on trees was developed and calibrated using laboratory and field experiments for two different tree species. First, a sensitivity analysis allowed identifying the parameters that control the block energy reduction after impact on a tree **(**impact velocity, stem diameter, and horizontal impact point location). Based on these results, two meta-models of the DEM model were developed to tackle the limitations of the DEM approach (important computational effort, huge set of input parameters).

The meta-model developed in this study are limited to be used for beech and ailanthus that have grown in the same condition and have the same sanitary state as the one used for the DEM model calibration. Differences in growth conditions and sanitary state can induce an important variability of the mechanical parameters and modify the capacity of a tree to reduce the block energy. This limitation can induce an over or under estimation of the residual hazard downslope a forest depending more on the wood quality than on the tree species. One perspective would be to study the influence of that variability using rockfall simulations at the slope scale. Another would be to set up a fast and a cost effective technique to estimate the wood quality in the field (multispectral information, vibrational analyses).

REFERENCES

[1] VOLKWEIN, A., SCHELLENBERG, K., LABIOUSE, V., AGLIARDI, F., BERGER, F., BOURRIER, F., DORREN, L., GERBER, W., and JABOYEDOF, M. (2011). Rockfall characterization and structural protection - a review. Natural Hazard and Earth System Sciences 11, pp. 2617-2651.

[2] JONSSON, M. J., VOLKWEIN, A., and AMMANN, W. J. (2007). Quantification of energy absorption capacity of trees against rockfall using finite element analysis. Taylor & Francis Ltd, London. WOS:000252215300044.

[3] TOE, D., BOURRIER, F., OLMEDO, I., MONNET, J.M., and BERGER, F. (2017), Analysis of the effect of trees on block propagation using a DEM model: implications for rockfall modelling, *(Accepted in Landslide*).

[4] SMILAUER, V., CATALANO, E., CHAREYRE, B., DOROFEENKO, S., DURIEZ, J., GLADKY, A., KOZICKI, J., MODENESE, C., SCHOLTES, L., SIBILLE, L., STRANSKY, J., and THOENI, K. (2014). The Yade project.

[5] OLMEDO, I., BOURRIER, F., BERTRAND, D., BERGER, F., and LIMAM, A. (2016). Discrete element model of the dynamic response of fresh wood stems to impact 120, pp.13-22.

[6] JANCKE, O. (2012). Quantifying the mechanical resistance of coppice trees against rockfall. PhD thesis, Hamburg.

[7] KNUSEL, S., MARCO C, ANDREAS R, PATRICK F, JAN W (2015) A tree-ring perspective on the invasion of Ailanthus altissima in protection forests. Forest Ecol. Manage.

[8] SOBOL, I. M. (1993). Sensitivity estimates for nonlinear mathematical models. Math. Model. Comput. Exp. 1, pp. 407-414.

STUDY OF ROCKFALLS IN A QUARRY ENVIRONMENT PHYSICAL AND NUMERICAL EXPERIMENTS

Manolis Fleris[1], Alexander Preh[1] & Bernd Kolenprat[2]

The study of rockfalls in quarries aims at a better understanding of the phenomenon and the improvement of safety conditions for employees. The later can be achieved through a correct identification and dimensioning of hazard zones related to rockfall activity. It is suggested that two different zones can be defined at the toe of a quarry slope and that these zones can be dimensioned according to rockfall associated values, concerning expected distances for runout and first impacts. These *characteristic* distances are influenced by several parameters such as size and form of falling rocks, surface roughness and geometry of the slope, rebound behaviour during impacts, all adding up to a relationship with a strongly random character. After observing and analyzing drop tests conducted on a granite quarry slope, we present results from efforts to calibrate and use an experimental stochastic *3D* code for rockfall numerical simulations.

Keywords: Rockfall, drop tests, numerical simulations in *3D*, hazard zoning

INTRODUCTION

Rockfalls are a common source of danger to employees at quarry sites. It has been suggested from previous research [1], that this kind of hazard could be managed in a preventive logic, by defining danger zones away from the toe of the slope. A first zone of highly destructive impact energy, can be derived from the *95* percentile of expected distance for first impacts (ID_{95}), signifying an area where danger exists even to operators of cabin featured-machinery, and no hauling activity should take place. A second zone of less destructive kinetic energy, can be defined from the *95* percentile of expected runout distance (RD_{95}), signifying an area where danger exists to employees protected through ordinary protective equipment. The dimensions of these zones can significantly vary from site to site and even at different locations of the same slope. This is a case where numerical simulations could be valuable, if only the aforementioned distances could be predicted within some reliability levels.

RESEARCH OBJECTIVES AND METHODS

Our main research objective is to test the performance and applicability of Wurf3D, an experimental rockfall code based on stochastic roughness and hyperbolic restitution factors. The code is scripted in PYTHON programming language and its theoretical framework is based upon the approach reported in [2].

[1] Institute of Geotechnics, Research Center of Engineering Geology, Vienna University of Technology, Vienna, Austria, emmanouil.fleris@tuwien.ac.at, alexander.preh@tuwien.ac.at
[2] Central Labour Inspectorate, Federal Ministry of Labour, Social Affairs and Consumer Protection, Vienna, Austria, bernd.kolenprat@sozialministerium.at

In addition, a developed technique for the post-processing of rockfall simulation data, has enabled the accurate and fast calculation of intersection between- rockfall trajectories and any given surface in *3D*. A *Ray - tracing* algorithm operating through tree - like hierarchical structures of spatial data, consists the core of the technique [3].

Furthermore, a precise visualization of the terrain and of the rockfall trajectories, along with the possibility for an *on the model* measurement of distance, configure a virtual *3D* computational environment for the study of rockfalls (*Fig.1*). By performing drop tests in an active quarry, we have generated data for the calibration of the code. Through a combined study of physical experiments and numerical simulations, we assess rockfall behaviour and calculate characteristic distances which could assist in a correct selection and the optimal design of protective measures. It should also be possible to discuss on the limitations of the numerical approach, and how a careful consideration could improve the interpretation of the results.

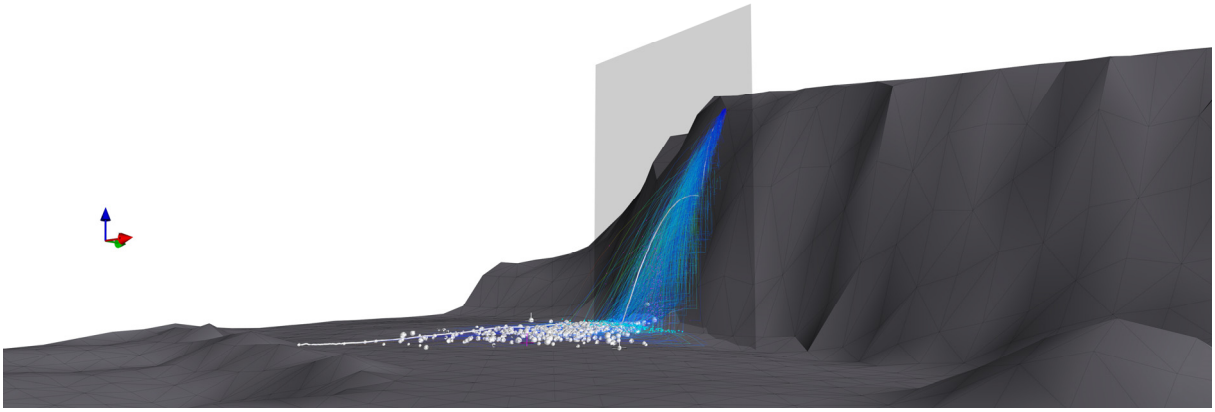

Fig. 1 Visualization of rockfall simulations and the creation of an interactive vitrual environment using Wurf3D.

PHYSICAL EXPERIMENTS

A series of drop tests have been conducted on a granite slope in an active quarry located at Limberg, Maissau, in Austria. In total *64* boulders ranging from *4* to *4720* kg were tested in an experimental procedure similar to the one reported in [4], with two significant enhancements: the use of a digital crane-scale which has enabled direct measurements of boulder mass, and the capturing of rockfall motion through a camera equipped drone, recording in a 'birds-view' mode *(Fig.2)*. From drone photography it has also been possible to create a unified Digital Elevation Model of the quarry slope and its bench, through photogrammetric techniques. Gathered data has initially been explored with the aid of video analysis software, for a precise measurement of impact and runout distances as well as the lateral spreading of rockfall trajectories. The purpose of these tests was to assess and improve rockfall observation techniques and consequently produce a set of quality data, which could facilitate the calibration of a rockfall code. From the analysis of drop tests video data and the manual tracking of rockfall trajectories, it has been possible to measure impact and runout distances in a consistent way, with excellent agreement to on-site registered measurements.

Fig. 2 Drop tests in a granite quarry at Limberg, Lower Austria. Geological unit of the Bohemian Massif. Monitoring with the aid of a video recording drone.

SIMULATION PARAMETERS

The principle of the numerical approach is to simplify the mathematical description of rockfall, following a 'hybrid' lumped mass scheme, and to account for naturally observed random behaviour, through a limited number of stochastic parameters that could be possibly calibrated against actual drop tests. Goldsmith's impact model is being used for the mathematical treatment of impacts and the calculation of translational and rotational rebound velocities [2]. Two input parameters, termed as roughness coefficients C_θ , C_φ are the solely stochastic elements of the simulation. They are controlling the extent of a random change in the inclination of the impact surface in longitudinal and transverse direction respectively, for each impact configuration. A further two parameters, representing energy levels, are marking a 'reference deformation energy' in normal and tangential direction (E_n, E_t) which is used to control the hyperbolic functions [5] relating normal and tangential restitutions factors (K_n, K_t) to the normal component of translation incident velocity and the boulder equivalent radius. Obtaining correct values for the aforementioned parameters is the purpose of the calibration procedure.

CALIBRATION APPROACH AND ITS RESULTS

In terms of programming, it has been possible to automate the calibration process. The numerical code through its calibration module, can be executed several times, being initialized for each run, with its key parameters randomly varied within a user specified range of values. In such a way, model behaviour could be explored in a broad range, by creating a large number of random combinations for model initialization. The accuracy of each simulation can be assessed by computing the root mean square (*RMS*) error between simulated and observed values, for selected parameters. Results from a Kolmogorov – Smirnov test, which is a statistical method to compare two different Cumulative Distribution Functions (*CDFs*), have proved to be useful for the calibration and in agreement with the *RMS* method (*Fig.3*). The calibration process has indicated that model response is very sensitive to the roughness coefficients C_θ, C_φ. In general, it has been possible to arrive at a set of parameters that could produce simulations with higher

than *1m* of accuracy when the *50* and *95* percentiles for both runout and impact simulated distances were to be compared against observations. At the same time, other rockfall characteristics, measured in drop tests, such as the maximum lateral spreading of the first impact points as well as the average lateral spreading of end boulder positions, could also be simulated with fine accuracy.

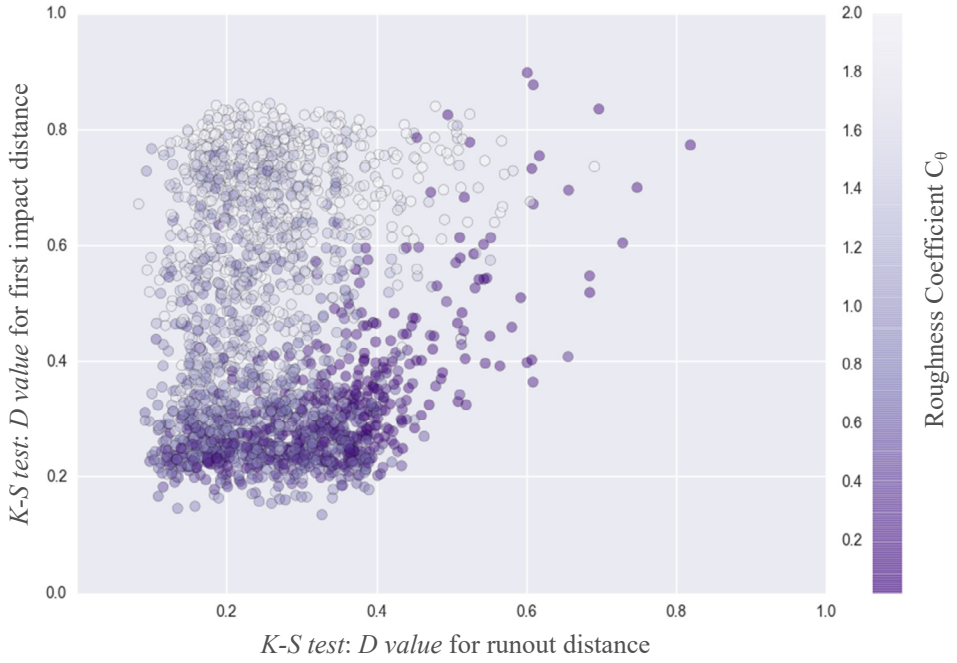

Fig. 3 Typical results from a Kolmogorov - Smirnov statistical test. Comparison of observed against simulated distributions, after a broad calibration procedure through 2000 random realizations.

CONCLUSIONS

Numerical simulations can assist in a better understanding of rockfall behaviour at quarries. Results, generated and interpreted by experts, can be used as to improve safety conditions and to bring site operation in conformity with relevant safety regulations. Data from advanced drop tests has been utilized for the calibration of a stochastic rockfall code in *3D*. Precise visualization and new methods for the post processing of numerical simulations, provide with the possibility for a robust evaluation of *characteristic* rockfall-related distances, within an interactive virtual environment.

REFERENCES

[1] KOLENPRAT B (2012) Tagbauarbeitenverordnung. Berg und Hüttenmännische Monatshefte, Vol. 157(4), S, pp 160-164.
[2] GISCHIG V, HUNGR O, MITCHELL A, BOURRIER F (2015) Pierre3D: a 3D stochastic rockfall simulator based on random ground roughness and hyperbolic restitution factors. Canadian Geotechnical Journal 52, 1360-1373.
[3] KYRIAKOU A (2015) Ray-Casting and Ray-Tracing with VTK. The Source Issue 32, VTK https://blog.kitware.com/the-source-newsletter/
[4] PREH A., MITCHELL A., HUNGR O, KOLENPRAT B (2015) Stochastic analysis of rock fall dynamics on quarry slopes. International Journal of Rock Mechanics & Mining Sciences 80, 57-66.
[5] BOURRIER F, HUNGR O (2011) Rockfall dynamics: a critical review of collision and rebound models. *In* Rockfall engineering. *Edited by* LAMBERT S and NICOT F, ISTE Ltd and John Wiley & Sons Inc., pp 175-203.

THE EFFECT OF SLOPE ROUGHNESS ON 3D ROCKFALL SIMULATION RESULTS

François Noël[1], Michel Jaboyedoff[1], Catherine Cloutier[2], Mélanie Mayers[2], Jacques Locat[2]

The development of a new rockfall simulation program, Trajecto3D, has been initiated. It should better consider the effect of small topographical features, like ditch or natural depression. Several authors using different simulation programs noticed that the terrain's roughness affects the dispersion and runout distances of the simulated rock falls. Simulations were carried on to find if results obtained with Trajecto3D follow the same trends. First, simulations on a fictitious terrain with variable roughness values were done to evaluate the runout variations. Then, simulations with elevation data from a natural terrain were realised to analyse the dispersion effect. By gridding these elevation data and down sampling the resolution, the roughness was gradually smoothed. Preliminary results show a clear trend with the runout distances that increase when roughness decrease for the fictitious terrain. Another clear trend is observed with the increasing dispersion that goes with increasing roughness for the natural terrain. However, the runout trend was not observed with the natural terrain, maybe because its acquire elevation data's roughness is not sufficient.

Keywords: rockfall, simulation, modeling, roughness, dispersion, variability, point cloud, ALS, TLS, photogrammetry

INTRODUCTION

Numerous factors could be considered when modelling rock fall, but compromises often has to be done to keep decent computational time. For now, few available 3D simulation programs allow the consideration of the particle size with a good terrain representation. However, those factors are needed when the effect of present mitigating measures, like a ditch, or small topographical depressions has to be considered [1]. So the development of a new rockfall simulation program, Trajecto3D, has been initiated. Being able to detect impact against point cloud topography, it can use high precision elevation data and consider the size of the particle [2].

Several authors using different simulation programs noted that the terrain representation's accuracy strongly affect the results [1], [3], [4]. Some noted that smoothed terrain's roughness due to low quality elevation data tend to lower the dispersion of the simulated trajectories and sometime accentuate the runout distances [3]. To see if similar observations could be made, Trajecto3D was used to simulate rock falls on fictitious terrain represented by point clouds with different roughness and with the elevation data of a natural terrain. Preliminary results are here presented.

[1] Risk Group, ISTE, Université de Lausanne, Switzerland, francois.noel@unil.ch
[2] Laboratoire d'étude sur les risques naturels, Université Laval, Québec, Canada

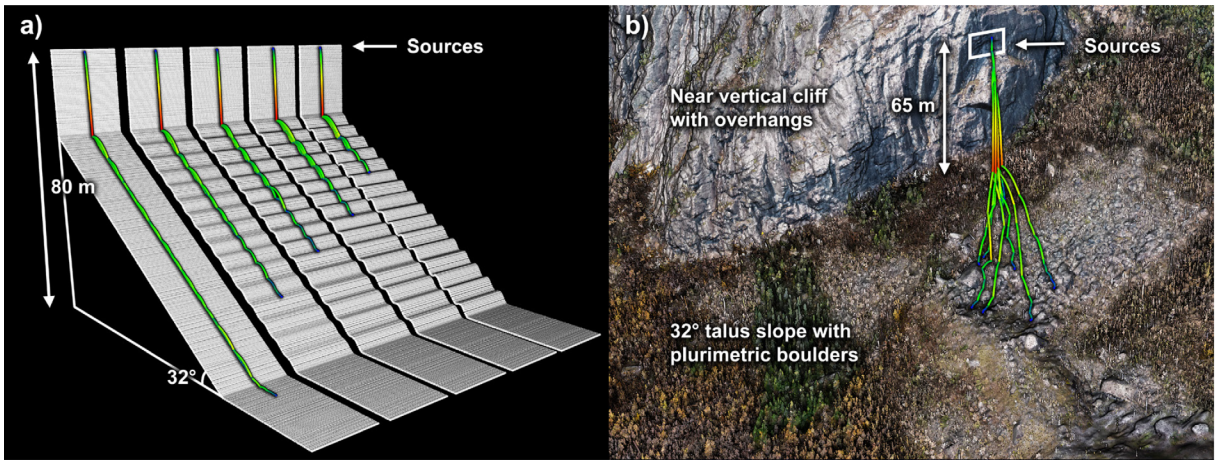

Fig. 1 Terrains used to test the influence of different roughness on the rock fall simulations carried out with Trajecto3D. In a), five fictitious slopes, one without roughness, one with strong roughness and those in-between. In b), Natural terrain with similar geometric features than the fictitious slopes.

METHODOLOGY

The impact model of Trajecto3D is based on the equations proposed by Wyllie [5] and on the empirical measures made by Wyllie [5] and Asteriou et al. [6]. It does not consider for now the sliding mode of motion, the particle's shape or impacts against trees. Particle's size is simplified to a sphere. Its 3D rotation inertia and the air resistance are however considered.

To evaluate the roughness effect on the runout distances, a simple fictitious terrain composed of a 25 m vertical slope followed with a 32° slope was created. The inclined portion was then modified with a sinusoidal function after the point where the first impact occurs in order to introduce some roughness. The resulting slopes are shown at Fig. 1 a) with some simulated trajectories of 1 m particles. Over 32 000 separate rockfalls were simulated per fictitious terrain to get good trends. Simulations were then carried out on a natural terrain to see the effect of roughness over dispersions (Fig. 1 b)). Elevation data were obtained by combining these different acquisition methods: airborne and terrestrial laser scans and structure from motion photogrammetry. They were then smoothed by gridding the elevation point data and then by lowering the grid resolution in order to get different roughness values. Again, between 300 000 and 1 600 000 separate rockfalls were simulated per terrain to get good trends.

RESULTS

Results of the simulations with the fictitious terrain are summarised in Tab. 1. A clear correlation is observed between the roughness of the terrain and the energy lines obtained. However, there is no clear trend for the runout dispersion.

Results of the simulations with the natural terrain are shown in Tab. 2.

Tab. 1 Energy lines on the fictitious slopes.

Ficticious terrain's roughness	Energy lines			
	Mean (°)	Std. (°)	95th pct. runout (°)	Max runout (°)
Smooth	49.6	6.9	40.8	30.1
Very light roughness	51.8	7.9	40.3	33.1
Light roughness	57.8	7.1	45.3	34.9
Moderate roughness	61.4	6.1	50.0	35.2
Rough	66.6	5.0	57.0	43.2

Tab. 2 Characteristics of the simulated rockfall trajectories on the natural terrain.

Elevation data's type	Spacing / cellsize (m)	Surface orientation method	Simulated trajectories	Energy lines				Directions	
				Mean (°)	Std. (°)	95th pct. runout (°)	Max runout (°)	Mean (°)	Std (°)
Points	0.2	3D Triangulation	1 588 399	46.4	4.1	40.2	29.3	58.8	11.8
Grid / raster	1	2.5D Triangulation	344 064	46.5	4.0	40.5	30.6	56.0	11.0
Grid / raster	2	2.5D Triangulation	319 488	46.3	3.8	40.3	30.5	54.0	10.1
Grid / raster	5	2.5D Triangulation	401 408	46.1	3.6	40.5	30.1	50.2	3.6
Grid / raster	10	2.5D Triangulation	434 176	45.0	3.6	39.6	28.8	48.5	4.1
Grid / raster	1	GIS slope & aspect	1 376 256	59.6	15.3	42.0	29.4	42.6	27.7
Grid / raster	2	GIS slope & aspect	1 277 952	52.6	10.8	40.9	30.2	45.1	14.4
Grid / raster	5	GIS slope & aspect	1 601 837	59.9	12.4	43.0	29.3	44.8	7.0

In contrast with the first results, there is no evidence of a correlation between the roughness of the natural terrain and the energy lines obtained. Indeed, the five simulations with elevation data that had theirs surface orientations calculated by triangulation almost have the same mean energy lines around 46° and standard deviation around 4°. All simulations on the natural terrain have max runout close to a 30° corresponding energy line, which is close to the values given in [7]. Simulations with elevation data surface's orientations calculated with GIS method [8] have different mean energy lines and standard deviation compared to the ones with triangulated orientations.

Concerning the rockfall path's directions, there is a slight shift toward the north in the mean directions as the roughness decrease for the simulations with the triangulated orientations. Dispersion clearly decreases for the simulations with gridded data from 2 m to 10 m cellsize. This change, still present, is subtler from points to 1 m raster and 2 m raster. This trend of dispersion decreasing with smoother roughness is also clearly visible on Fig. 2.

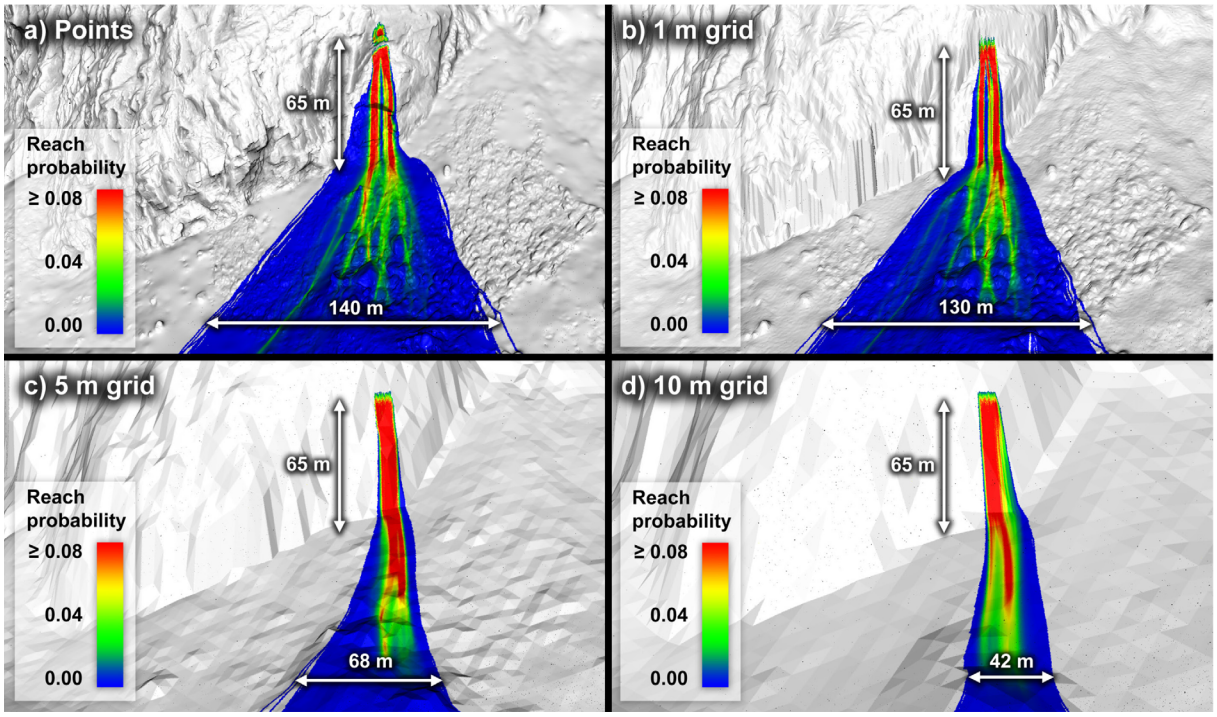

Fig. 2 Some of the results obtained for the natural terrain with different roughness values.

DISCUSSION AND CONCLUSION

The lateral dispersion of the simulated trajectories seems clearly correlated with the terrain's roughness, as seen with the results on the natural terrain. However, these results do not show the same trend of the ones with the fictitious terrain concerning the runout distances. This may be explained by the fact that the natural terrain elevation data, even if it seems detailed, does not have a lot more roughness compared to its smoothed copies (Fig. 3).

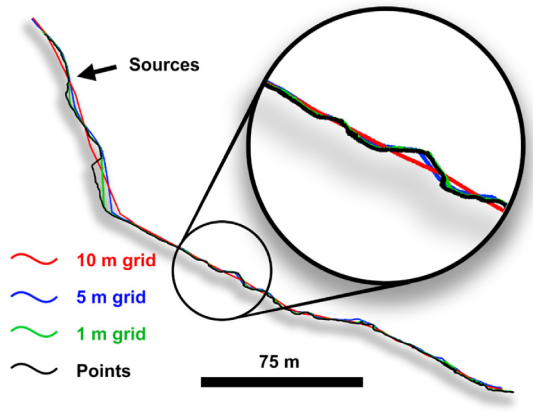

Fig. 3 Four slope profiles of the natural terrain.

The differences between the simulations with triangulated and GIS surface's orientations are probably caused by errors induced by the later ones. In fact, GIS surface's orientations method does not work properly with 3D rockfall simulation programs because obtained orientations are smoothed compared to the real elevation data's orientations. This can lead to erroneous simulated particles passing through or getting stuck in the surface. Therefore, such method for determining the surface orientations should be avoided with 3D rockfall simulations.

It's been shown that Trajecto3D can simulate numerous rockfalls with different kind of elevation data and that the results follow the trends that have been previously observed with other simulation programs. As Trajecto3D can take into account very detailed terrain representations, further work will extend those preliminary results to terrains with protective measures and with more prominent metric surface roughness.

REFERENCES

[1] LAMBERT, S., BOURRIER, F. & TOE, D., (2013). Improving three-dimensional rockfall trajectory simulation codes for assessing the efficiency of protective embankments. International Journal of Rock Mechanics and Mining Sciences, 60, pp.26–36.
[2] NOËL, F., CLOUTIER, C., TURMEL, D., LOCAT, J., (2016). Using point clouds as topography input for 3D rockfall modeling. In Landslides and Engineered Slopes. Experience, Theory and Practice. Napoli, Italy: CRC Press, pp. 1531–1535.
[3] CROSTA, G.B., AGLIARDI, F., FRATTINI, P., LARI, S., (2015). Key Issues in Rock Fall Modeling, Hazard and Risk Assessment for Rockfall Protection G. Lollino et al., eds., Springer International Publishing.
[4] BÜHLER, Y., CHRISTEN, M., GLOVER, J., CHRISTEN, M., BARTELT, P., (2016). Significance of digital elevation model resolution for numerical rockfall simulation. In 3rd International Symposium Rock Slope Stability. Lyon, France, pp. 101–102.
[5] WYLLIE, D.C., (2014). Rock fall engineering: development and calibration of an improved model for analysis of rock fall hazards on highways and railways. The University of British Columbia.
[6] ASTERIOU, P., SAROGLOU, H. & TSIAMBAOS, G., (2012). Geotechnical and kinematic parameters affecting the coefficients of restitution for rock fall analysis. International Journal of Rock Mechanics and Mining Sciences, 54, pp.103–113.
[7] JABOYEDOFF, M. & LABIOUSE, V., (2011). Technical Note: Preliminary estimation of rockfall runout zones. Natural Hazards and Earth System Science, 11(3), pp.819–828.
[8] BURROUGH, P.A., MCDONNELL, R.A. & LLOYD, C.D., (2015). Principles of geographical information systems Third Edit., Oxford University Press.

SIMULATION OF ROCKFALL TRAJECTORY ON MOUNTAIN SLOPE CONSIDERING ROUGHNESS OF SLOPE SURFACE

Yukinari Nishikawa[1], Hiroshi Masuya[2], Yuko Moriguchi[3]

The estimation of risk due to rockfall is mostly achieved empirically. Simulation of rockfall trajectory helps to describe the motion of rockfall on a slope. Fundamental idea is shown to consider the roughness of the slope surface to reproduce the state that is close to the real slope. A treatment method of the roughness at that moment of the collision between a rock fall and a slope was developed. The method expressed the roughness of the slope by adding an angle in the normal vector of the triangular plane. The validity of proposed simulation method becomes clear by the application to rock falls on a simple slope.

Keywords: rockfall, simulation, roughness, slope surface

INTRODUCTION

Performance based design is required to rationally evaluate the safety against dynamic natural actions such as rock fall, debris flow, avalanche, tsunami, and design the structure according to the required performance[1]. It is naturally considered that extremely high risk should be avoided in the structures that undergoes such natural action. However, it is possible to consider designs that allow a certain risk. The acceptable risk is generally less but not zero.
The actual phenomenon of rock fall is complicated by the influence of the shape of the ground surface and geological conditions, the shape of falling rocks and the presence of vegetation. In practice, predictions of the occurrence of rock falls, design conditions such as kinetic energy are often set empirically[2][3][4]. In this study, the analysis method was developed taking into account a three-dimensional irregularities of the slope surface in order to reproduce the further state close to the actual slope. We describe the details including formulation, and show the validity and usefulness of this method from numerical analysis results applied to analysis of falling rock behavior on a simple slope.

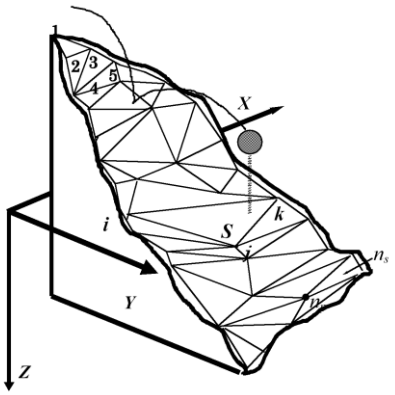

Fig.1 Model of the slope by triangle planes

[1]Kokudo Kaihatsu Center Co., Ltd, Design Division, Yatsukaho 3-7, Hakusan 924-0838, Japan,+81 76 274 8800, nishikawa_yukinari@kokudonet.co.jp
[2]Kanazawa University, Institute of Science and Engineering, Faculty of Environmental Design, Kakuma-machi, Kanazawa 920-1192, Japan, +81 76 234 4603, masuya@se.kanazawa-u.ac.jp
[3] Mie Prefecture, Ise Construction office, Seitatyou 628-2, Ise 516-8566, Japan, +81 596 27 5197, m-guppy3@ch-i.jp

THREE-DIMENSIONAL SIMULATION METHOD CONSIDERING UNEVENNESS OF SLOPE

The slope is divided and modeled by triangular planes as shown in Fig. 1. If it is assumed that the slope is expressed with n_s triangle planes and n_p nodal points, the arbitrary triangle plane of a slope is expressed by

$$aX + bY + Z = d \qquad (1)$$

Where, a, b, d are constant.

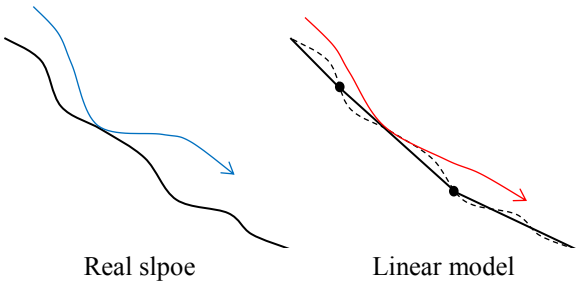

Fig.2 Modeling of slope roughness

The falling rock movements are influenced in many ways, such as shape of rocks and its characteristics, slope shape and geologic rock quality, the influence of vegetation. In this study, the slope is divided into triangular planes and modeled, but there are large and small irregularities on the actual slope, which influences exercise including the rock shape. Although it is possible to model the falling rock form to some extent in detail, it is thought that it is not easy to reproduce it by modeling the roughness of the slope in detail. Even if modeling the surface roughness of the slope surface, as shown in Fig. 2, depending on the modeling of the slope, the simulation result greatly differs.

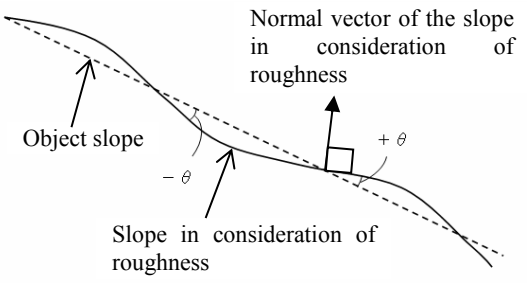

Fig.3 Concept of the roughness

In this research, a method considering the influence of randomness at the time of falling rock collision by the unevenness of the slope was studied. Specifically, as shown in Fig.3, only at the moment the falling rock collides with the slope, add an angle to the normal vector of the triangular plane and then return to the original normal vector to maintain continuity of the slope to express irregularities on the slope. Here, is the angle (roughness angle) representing the degree of roughness of the slope (roughness).

Fig.4 shows the unit normal vector n_1 of the plane considered and the vector n_2 of the plane considering the roughness angle θ. Here, components of vector n_1 and n_2 are respectively $n_1 = (l_1, m_1, n_1)$ and $n_2 = (l_2, m_2, n_2)$. And the roughness angle θ is randomly changes between zero to an arbitrary determined angle. A vector n_1 is rotated vector n_2 by arbitrary angle ϕ around a unit vector n_1. Point P is the end

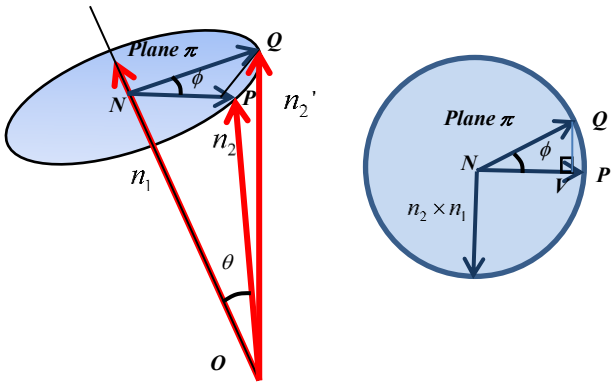

Fig.4 Relations with a normal vector n_1 an angle of roughness θ and the vector n_2' having angle of rotation

point of one normal vector OP of a certain plane in consideration of roughness and Q indicated by $n_2' = (l_2', m_2', n_2')$ is a point rotated by random angle ϕ around vector ON in consideration of roughness $(0 < \phi < 2\pi)$.

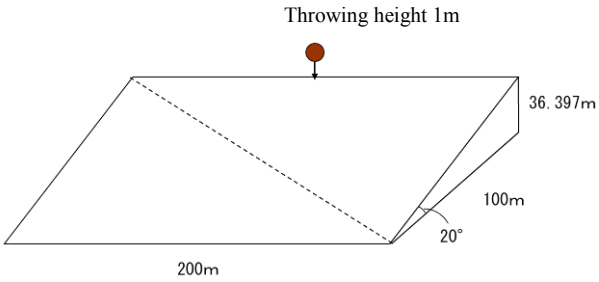

Fig.5 The slope used for simulation

RESULTS OF SIMULATION

As shown in Fig. 5, the slope used for the analysis was a uniform two-dimensional simple slope with a width of 200 m, a depth of 100 m, and a slope of 20 degrees. The initial condition of rock falls in the analysis is shown in Tab. 1 and the characteristic values of falling rocks in Tab. 2. In addition, it was assumed that there were no vegetation such as trees on the slope.

Analysis was carried out by changing the roughness angle representing the unevenness of the slope using the above conditions. Changes in the trajectory of the falling rock movement, the number of collisions and the final speed were compared. The number of trials of analysis was set to 300 times, respectively.

Tab. 1 Initial condition of rockfall

Item	x(m)	y(m)	z(m)
Throwing down position (m)	0	90	-37.397
Initial velocity (m/s)	0	0	0
Initial angular velocity (rad/s)	0	0	0

Tab. 2 Characteristics of rock

Rock mass (t)	0.17
Rock diameter(m)	0.50
Coefficient of restitution of the slope	1.00
Coefficient of friction of the slope	0.10

Fig. 6 shows the trajectory diagram on the X-Y plane and the trajectory diagram on the Y-Z plane when the roughness angles are 5 degrees and 20 degrees. The average value and the standard deviation of the number of collisions with the slope and the final velocity are shown in Tab.3.

When the roughness angle is 20 degree, the spread of the trajectory in the XY plane becomes larger than the roughness angle 5 degree. It has become clear that the change in the jumping height of rock falls increases as the roughness angle increases from the trajectory of the Y-Z cross section. This can clearly be confirmed at the bottom of the slope. Concerning the velocity of rock falls f, as shown in Table 3, the final velocity of rock falls is 24.1 m/s for the roughness angle is 5 degree. On the

Tab. 3 Effect of roughness

θ (degree)	Final velocity (m/s)		Frequency of collision	
	Average	Standard deviation (Variation index)	Average	Standard deviation (Variation index)
5	24.1	0.90 (0.037)	5.1	2.6 (0.51)
20	22.4	1.9 (0.085)	7.6	4.2 (0.55)

other hand, when the roughness angle increases to 20 degree, the final velocity becomes as small as 22.4 m / s. It was confirmed that the result of considering the unevenness of the slope affects the fluctuation of the final velocity and spreads the spatial distribution of the rock fall trajectories including the jumping height.

CONCLUSIONS

In this study, we developed and investigated the falling rock motion simulation method, which can consider the ruggedness of the three dimensional slope.
As a result, we showed how to represent the irregularities of the slope with random inclination in the normal vector of the triangle plane modeled at that moment when the falling rock collides with the slope.
Using this method, we developed a method to reproduce the collision behavior of complicated rock falls by three-dimensional simulation and showed the effectiveness of the method by examples using a simple slope.

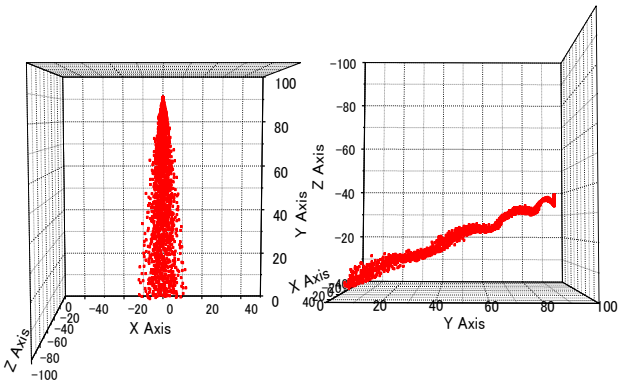

Plane of X-Y Plane of Y-Z

(a) θ =5 degree

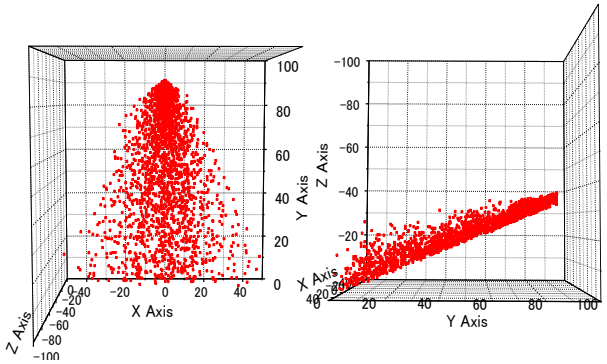

Plane of X-Y Plane of Y-Z

(b) θ =20 degree

Fig.6 Trajectories of rockfall in planes

REFERENCES

[1] MASUYA H, ENO S, NAKAMURA S, SATOH A (2014) Study on the characteristic of dynamic response of the frame structure under impact for performance based design of rockfall protection, Interdisciplinary Rockfall Workshop 2014 ROCEXS.
[2] JAPAN ROAD ASSOCIATION (2000) Handbook of preventatives against rock-falls, Japan road association, Japan Road Association (in Japanese).
[3] HUNGR, O (2011) Characterization of rockfall and rockslide hazards for the design of protective measures, Interdisciplinary Rockfall Workshop 2011 ROCEXS, Keynote lecture.
[4] MASUYA, H, AMANUMA, K, NISHIKAWA, Y, TSUJI, T (2009): Basic rockfall simulation with consideration of vegetation and application to protection measure, Natural Hazards and Earth System Sciences 9, 1835-1843.

THE ROCKRISK PROJECT: ROCKFALL RISK QUANTIFICATION AND PREVENTION

Jordi Corominas[1], Nieves Lantada[1], Josep A.Gili[1], Roger Ruiz-Carulla[1], Gerard Matas[1], Olga Mavrouli[2], M. Amparo Núñez-Andrés[1], Jose Moya[1], Felipe Buill[1], Antonio Abellán[3], Càrol Puig[1], Albert Prades[1], Joan Martínez-Bofill[1], Lluís Saló[1]

Rockfalls are frequent instability processes in road cuts, open pit mines and quarries, steep slopes and cliffs. The orientation and persistence of joints within the rock mass define the size of the kinematically unstable rock volumes and determine the way how the detached mass becomes fragmented upon the impact on the ground surface. Knowledge of the size and trajectory of the blocks resulting from fragmentation is critical for calculating the impact probability and intensity, the vulnerability the exposed elements and the performance of protection structures. In this contribution we summarise the main goals and achievements of the RockRisk project. We focused on the characterization of the rockfall fragmentation by means of the analysis of the fracture pattern of intact rock masses, the development of a fragmentation model and its integration into rockfall propagation analysis. The ultimate goal of the project is to quantify risk due to rockfalls and develop tools for the improvement of prevention and for protection from its occurrence.

Keywords: Rock falls, fragmentation, vulnerability, quantitative risk assessment, digital photogrammetry, LiDAR

1. INTRODUCTION

The RockRisk project aims at quantifying the risk induced by rockfalls and to provide tools to improve its prevention and mitigation. The project has three work packages: (a) the spatially explicit determination of rock volumes kinematically unstable and characterization of the rock mass fracture pattern using high resolution remote techniques such as: Terrestrial Laser Scanner (TLS) and terrestrial or aerial digital photogrammetry; (b) definition of fragmentation laws using data collected from recent rockfall events and real-scale tests. Incorporation of the fragmentation mechanism in rockfall propagation models and in the calculation of impact energies; (c) Quantitative risk assessment, by developing of methods for quantifying the vulnerability of different types of masonry structures and buildings against rockfalls and the preparation of fragility curves.

[1] Department of Civil and Environmental Engineering, Universitat Politècnica de Catalunya, C. Jordi Girona 1-3, Barcelona 08034, Spain, +34 93 401 68 61, jordi.corominas@upc.edu
[2] ITC (ESA) University of Twente (Nederland)
[3] Scott Polar Research Institute (University of Cambridge).

2. CHARACTERIZING DETACHABLE ROCK MASSES AND FRAGMENTATION

The initial rockfall volume is a required input parameter of the trajectographic analysis. The detached mass may be either a single block or a rock mass containing discontinuities. The impact on the ground may cause the disaggregation of the rock mass and breakage of the blocks, thus producing new rock fragments. Although, fragmentation has been frequently observed in rockfalls this phenomenon is rarely considered in the rockfall analysis.

Fragmentation of a rock mass may result from the division of detached volume by either the breakage of the rock pieces, the disaggregation of joint-determined blocks, or both. The analysis of fragmentation requires considering the In-Situ Block Size Distribution (IBSD) of the detached mass at the cliff face. Due to the frequent lack of accessibility of the rockfall sources that difficult the direct measurement of joints, a 3D Digital Surface Model (DSM) of the rock wall is generated with digital photogrammetry and then the fracture pattern is extracted using the software Rhinoceros [1].

The volume distributions of the fragments of several rockfall events and from real scale tests can be fitted to power laws [2 & 3]. However, the scaling factors or exponents of the tails range between 0.5 and 1.3 and that the scaling factors are an expression of the intensity of the fragmentation process. The highest exponents are found in the rockfalls showing high height of fall and mobilised volume. Large exponents mean a substantial reduction of the particle size and implicitly the breakage of large blocks.

We have developed a rockfall fractal fragmentation model (RFFM) that generates rockfall block size distribution (RBSD) from the volume of the initial detached mass and its fracture pattern (IBSD) [1]. This model is based on a generic fractal fragmentation model of Perfect that considers a cubic block of unit length which is broken into small pieces according to a power law. The size distribution of the elements in a fractal system is given by:

$$(1/b^i) = k[1/b^i]^{-Df} \; ; \; i=0,1,2,\ldots\infty$$

Where N $(1 / b^i)$ is the number of elements at the level "i" of the hierarchy; "k" is the number of initiators of unit length; "b" is a scaling factor > 1; and D_f is the fractal dimension of fragmentation, which can be defined as:

defined as:

$$D_f = 3 + \frac{log[P(1/b^i)]}{log[b]}$$

Where P $(1 / b^i)$ or P_f is the probability of fracture that determines the proportion of the original block that breaks and generates new fragments. The fractal fragmentation model has been adapted for the case of the rockfall. First, instead of k initial volumes of unit length, the IBSD is used as input, classifying it in bins. Second, not all the blocks of the IBSD break upon impact

on the ground. To consider this, a survival rate, Sr, representing the proportion of blocks that do not break is defined.

The RFFM has been implemented in an Excel worksheet, allowing the adjustment of the model parameters and generating a range of rock fragments distribution. The model input is the IBSD. The model parameters "Sr", "P_f" and "b", control the intensity of fragmentation and the resultant RBSD. The model generates the RBSD through the iterative adjustment of the model parameters. Real-case inventories are used to calibrate the model for different scenarios. The Excel file is freely available in the tool tab at https://rockrisk.upc.edu/en

Finally, a method simulating the volume and number of fragments of rockfall events, based on the size distribution of blocks deposited at the talus slope, has also been developed [4]

3. ADDING FRAGMENTATION TO THE ROCKFALL SIMULATION

In the project we have developed RockGIS, a GIS-Based tool that simulates stochastically the fragmentation of the rockfall, based on a lumped mass approach [5]

The model requires as input data a digital surface model with the release points of the rockfall, the volume of the detached mass and its IBSD, the land use coverage map and the model parameters. In RockGIS, the fragmentation initiates with the disaggregation of the detached rock mass through the pre-existing discontinuities just before the impact with the ground. An energy threshold is defined in order to determine whether the impacting blocks break or not. The conservation of energy during the impact is written as follows:

$$E_k^{bi} = E_k^{ai} + E_d + E_b$$

Where E_k^{bi} is the kinetic energy before impact, E_d is the energy dissipated in the impact with the ground, E_b is the energy dissipated due to the breakage process and E_k^{ai} is the sum of the kinetic energy of the fragments. The main hypothesis of the model is that the energy loss from the impact of the block with the ground and the energy released by the breakage of the block are considered uncoupled processes. Thus the breakage of the block will take place after the computation of the rebound velocity, independently of the rebound model used. The distribution of the initial mass between a set of newly generated rock fragments is carried out stochastically following a power law. This criterion has been support by the results of the rockfall inventories and real scale tests. The trajectories of the new rock fragments are distributed within a cone while the remaining energy after breakage is distributed proportionally to the mass of each fragment. Finally, all fragments generated are simulated as new rockfalls and the process continues iteratively until all fragments stop their propagation. The fragmentation model has been calibrated and tested with real cases.

4. VULNERABILITY OF BUILDINGS DUE TO ROCK BLOCK IMPACTS

Vulnerability has been often analysed using empirical and/or judgmental approaches that do not provide objective and quantitative information on the expected damage and do not take into consideration the kinematical characteristics of the rock block impact. Moreover, differentiation between different structural typologies is seldom made. These are limiting the application of these approaches for damage prediction.

Our research group has developed analytical methodologies for evaluating the vulnerability of reinforced concrete buildings impacted by rockfalls. These approaches incorporate the kinematic properties of the block, their size and the probability of impact on key structural elements for the stability of a building. The obtained vulnerability is expressed in quantitative terms and can be directly integrated into the QRA using fragility curves. In Rockrisk an analytical procedure to evaluate the damage caused by blocks impacting on different masonry typologies, which are typical structures of buildings in rural and mountainous areas [6]. This methodology takes into consideration the characteristics of the exterior walls of a building (e.g. natural stone or brick walls) for the assessment of the damage due to a rock block impact.

The procedure comprises three stages: (i) Determination of the rockfall impact actions which are applied to a masonry structure, in terms of external forces, using the Particle Finite Element method; (ii) Evaluation of the mechanical properties, modelling of the masonry structure, and calculation of the internal stresses, using the finite element method; (iii) Assessment of the damage due to the rockfall actions, applying a failure criterion adapted to masonries, and calculation of the damage in terms of the percentage of the damaged wall surface. An Excel tool, called RockDamage, has been developed for the automatic calculation of fragility curves for masonry walls and is freely available in the tool tab at https://rockrisk.upc.edu/en

ACKNOWLEDGEMENT

The Rockrisk research project is funded by the Spanish Ministry of Economy and Competitiveness on the framework of the State Plan of Scientific-Technical Research and Innovation with reference code BIA2013-42582-P.

REFERENCES

[1] RUIZ-CARULLA, R., COROMINAS, J. & MAVROULI, O. (2016). A fractal fragmentation model for rockfalls. Landslides doi:10.1007/s10346-016-0773-8. Editorial version http://rdcu.be/mncX
[2] RUIZ-CARULLA, R., COROMINAS, J. & MAVROULI, O (2016). Comparison of block size distribution in rockfalls. In: Aversa S, Cascini L, Picarelli L, Scavia C (eds) Landslides and engineered slopes, 3: 1767-1774
[3] GILI JA, RUIZ R, MATAS G, COROMINAS J, LANTADA N, NÚÑEZ MA, MAVROULI O, BUILL F, MOYA J, PRADES A, MORENO S (2016) Experimental study on rockfall fragmentation: in situ test design and firsts results. In: Aversa S, Cascini L, Picarelli L, Scavia C (eds) Landslides and engineered slopes, 2: 983-990.
[4] MOYA J, COPONS R (2017) Monte Carlo simulation of the volume and number of rockfall fragments using talus deposits. 6th RocExs workshop, May 22 – 24, 2017, Barcelona (this volume).
[5] MATAS G, LANTADA N, COROMINAS J, GILI JA, RUIZ-CARULLA R, PRADES A (2017). RockGIS: A GIS-based model for the analysis of fragmentation in rockfalls. Landslides. doi: 10.1007/s10346-017-0818-7
[6] MAVROULI, O., GIANNOPOULOS, P.G., CARBONELL, J.M.& SYRMAKEZIS, C. (2016). Damage analysis of masonry structures subjected to rockfalls. Landslides. doi: 10.1007/s10346-016-0765-8 (in press)

MONTE CARLO SIMULATION OF THE VOLUME AND NUMBER OF ROCKFALL FRAGMENTS USING TALUS DEPOSITS

José Moya[1], Ramon Copons[2]

Volume of blocks produced by rockfall fragmentation can be regarded as a random variable having a site-dependent probability distribution. Once the probability model is identified, both the volume and the number of block can be simulated for a given rockfall volume using the inversion technique. Model identification requires a large number of blocks, which is not readily available in rockfall inventories. We used blocks of the talus slope, deposited by rockfalls along centuries, to overcome this shortcoming. The method was applied to a test site in the Andorra Principality. Volume of blocks of rockfall events was also available in the site and used to test the method. Block volume in the site follows a truncated power law which depends on the rockfall volume. 20000 distribution curves were simulated for several rockfall volumes. Both the inventoried and the simulated block volumes show a large variability even for a given rockfall volume. The inventoried volumes are scattered within the 90% band of the simulated ones. This finding shows that the simulation results are realistic.

Keywords: rockfalls, fragmentation, block volume, random simulation, validation.

INTRODUCTION

Fragmentation reduces the size of the falling rock pieces and increases the number of blocks of a propagating rockfall. As a consequence, rockfall volume-frequency curves are not directly applicable to the hazard assessment of fragmental rockfalls [1, 2]. The average hazard can be obtained by means of the estimation of the mean number of blocks of a given volume [1-4]. However, for an event based hazard analysis, the size and number of the blocks produced in events must be determined, as it was carried out in [5] using a fractal model. The random nature of the process of rockfall fragmentation has been clearly shown by in-situ tests [6, 7]. This latter suggests that Monte Carlo methods are useful for simulating blocks volumes and emulating fragmentation. This is the approach we used. The basis of the method and its application to a site in the Andorra Principality are described. The simulated block volume distributions are compared with those of events inventoried in the site.

GENERAL METHOD

The method assumes that the volume of blocks (V_f) resulting from rockfall events follow a given distribution, which depends on the site and on the rockfall volume. The first step is to infer this distribution. Using data from inventoried events would be the best way to do this. However, inventories usually contain only just the larger blocks. In sites where repeated rock-

[1] Universitat Politècnica de Catalunya BarcelonaTech, Division of Geotechnical Engineering and Geosciences, C. Jordi Girona 1-3, Building D2, Barcelona 08034, Spain, + 34 934 010 736, jose.moya@upc.edu
[2] Institut d'Estudis Andorrans, Centre d'Estudis de la Neu i la Muntanya d'Andorra, Av. Rocafort 21-23, Edifici El Moli 3er pis, Sant Julià de Lòria AD600, Andorra, +376 742630, rcopons.cenma@iea.ad

falls accumulate at the cliff bottom V_f can be measured at talus deposits. Talus blocks should have a distribution similar to that of the rockfall events. The latter is true provided the conditions in the source and propagation areas did not change significantly in time. It is worth noting that V_f has an upper limit, V_{sup}, which depends on the rockfall volume, V_r.

The next steps in the method are: a) fitting a probability model to the empirical distribution of the block volume, b) inferring the V_{sup} value conditioned on V_r, and c) simulating block volumes, using the inverse equation of the fitted model, until V_r is reached. Further details of the method are described below by means of their application to a talus of the Solà d'Andorra.

SIMULATING BLOCK VOLUMES FOR THE SOLÀ D'ANDORRA

Distribution of volume of block fragments of inventoried rockfall events

The Solà d'Andorra is a granodioritic cliff where rockfalls occur frequently menacing the Andorra la Vella city, the capital of the Principality. Thirteen rockfalls with a volume from 4 to 150 m^3 have been inventoried there since 1999 [2, 8]. All of them fragmented. On the other hand, the volume of 2041 blocks measured at the Borrasica – Forat Negre talus of the Solà d'Andorra was also available [8]. The minimum V_f measured at the talus was 0.001 m^3.

Fig. 1 shows the empirical exceeding cumulative probability ($S = P(V_f \geq v)$) of V_f for block-sized fragments of inventoried events and for talus blocks. Data corresponding to $V_f \geq 0.9$ m^3 for the event data set (48 blocks) and to $V_f \geq 0.2$ m^3 for the talus set (539 blocks) are plotted in Fig. 1. A clear rollover effect was found in below these values, which is regarded as due to undersampling of the smaller blocks. The empirical distribution s of V_f for talus blocks and for event blocks are quite similar. They can be well fitted by power laws that have exponents statistically identical. This is even clearer if the distribution of the talus blocks is calculated using only blocks larger than 0.9 m^3 (Fig. 1). Standard power laws can be fitted to these data (e.g. thin green line in Fig. 1); however it is worth noting that such a distribution has no upper limit ($V_{sup} = \infty$), which is not realistic and would lead to nonsense results in the simulation.

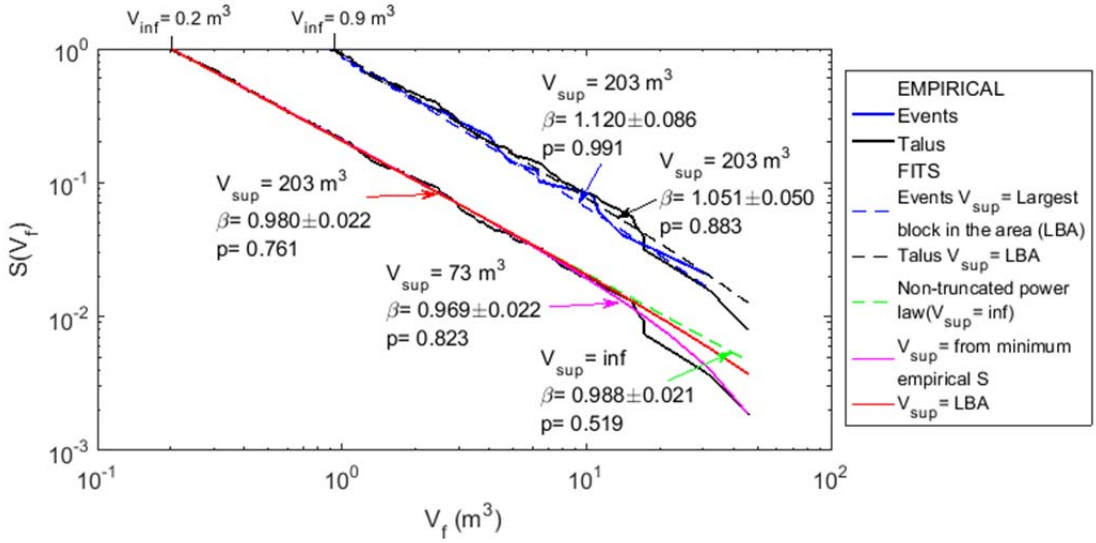

Fig. 1 Empirical and fitted distributions of the volume of blocks measured for rockfall events and on the Borrasica – Forat Negre talus slope (Solà d'Andorra, Andorra Principality).

The models fitted to the empirical data are truncated power laws, which general expression is:

$$S(V_f) = \frac{(V_{inf}/V_f)^{\beta} - (V_{inf}/V_{sup})^{\beta}}{1 - (V_{inf}/V_{sup})^{\beta}} \quad \text{(Eq. 1)}$$

Where V_{inf} and V_{sup} are the minimum and maximum limit values for V_f, respectively, and the exponent β is a shape parameter. S probability is null for V_{sup}; i.e. no blocks may be equal or larger than it. It must be highlighted that the estimate for β exponent depends on V_{sup}. A volume greater than the largest block observed in the lower part of the talus, or even below in the fluvial plain, should be used for V_{sup}. The largest block found in the talus (46 m^3) is located in their middle part; however, it could be not representative of V_{sup} because the lower part of the talus, where usually the largest blocks are located, is urbanised. The volume of the largest block identified in the cliff face (203 m^3) [8] was instead considered for V_{sup}. Using this latter bound, a value of 0.969 ± 0.022 was estimated for β, using the maximum likelihood method.

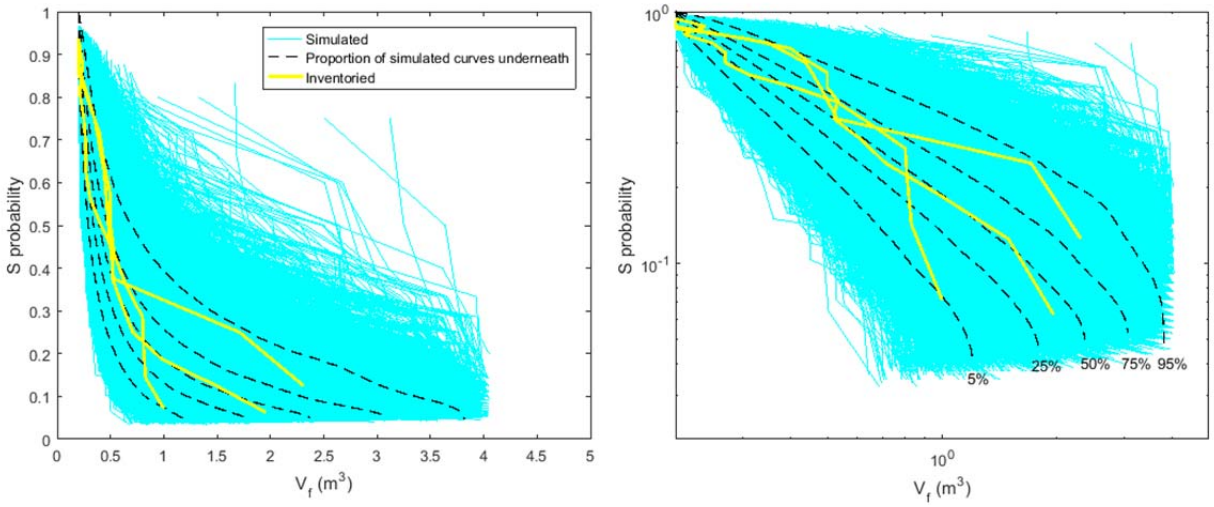

Fig. 2. Simulated V_f distributions (20000) and empirical distributions of three recent events in the Solà d'Andorra for 10 m^3 rockfalls. Data are plot using linear scales (left) and log scales (right).

Simulating the volume and number of fragments and comparison with events observed

Block volumes were simulated using the inverse of Eq. 1, to show the block volume as depending on S, and giving random values to S generated from the uniform distribution. To emulate fragments of a rockfall of a given volume V_r, random V_f values were generated until their sum reached V_r, within an 1% tolerance margin. Sets of simulated V_f within this margin were retained (otherwise were rejected). The number of simulated V_f in a set is taken as corresponding to the number of blocks resulting from fragmentation of the rockfall.

Simulations for the test site were carried out setting β to 0.980 and V_{inf} to 0.2 m^3. It should be noted that V_{sup} depends on V_r in this case (i.e. it will be different than the used for the overall distribution of the talus blocks). V_{sup} was determined, first, using the regression between the largest block ($V_{f,\,max}$) and V_r in the inventoried rockfalls, and, second, carrying out several simulation trials for determining the equation relating the maximum $V_{f,\,max}$ ($\cong V_{sup}$) and mean $V_{f,\,max}$ and then trying to fit the mean $V_{f,\,max}$ - V_r relationship shown by the inventoried events.

Once V_{sup} was calibrated, 20000 rockfall events were simulated for several V_r. Fig. 2 shows the results obtained for 10 m^3 rockfalls (cyan lines). The V_f distributions for the events inventoried having this V_r are also shown in the plots. To make easier the comparison between the simulated and the inventoried distributions, several lines showing the proportion of the simulated curves for each V_f were also drawn (e.g., 95% of the simulated curves are located below the 95% line) . The variability in the simulated cases is noticeable, as it can be expected for power law behaviour and for a very large number of runs, though it is also very large for the inventoried events. V_f data from 11 rockfalls occurred in the Solà d'Andorra were used to check the method. They scattered between the 5 and 95% of the simulated cases and around the line corresponding to 50% of the simulations. This suggests that most of the curves simulated are realistic. Such results are encouraging though data from additional rockfall events are required in order to test the goodness of the method accurately.

CONCLUSIONS

The volume of blocks both in the Borrasica-Forat Negre talus site and in the inventoried rockfalls follows a truncated power law, which depends on the rockfall volume. Exponent β ranges from 0.969 to 0.980 in the site depending on the value used for the upper limit of the distribution model. The volume of blocks in the inventoried events shows a large variability even for the same rockfall volume. The comparison of the simulated distributions and those of the events occurred in the site shows that the method provides realistic results. Major advantages of the method are its ability to reproduce the variability of the fragmentation process and to provide the distributions of the random variables related (e.g. the volume of the largest block for a given rockfall volume).

ACKNOWLEDGEMENTS

The authors acknowledge the support of the Spanish Economy and Competitiveness Ministry to the RockRisk research project (BIA2013-42582-P), in which this research was done.

REFERENCES

[1] JABOYEDOFF M, DUDT JP, LABIOUSE V (2005) An attempt to refine rockfall hazard zoning based on the kinetic energy, frequency and fragmentation degree. Nat. Hazards Earth Syst. Sci. 5: 621–632.
[2] COROMINAS J, MAVROULI O, SANTANA D, MOYA J (2012) Simplified approach for obtaining the block volume distribution of fragmental rockfalls. In: Eberhardt E, Froese C, Turner AK, Leroueil S (eds) Landslides and engineered slopes. Taylor and Francis. V2:1159–1164.
[3] HANTZ D, VENTROUX Q, ROSSETTI JP, BERGER F (2016) A new approach of diffuse rockfall hazard. In: Aversa et al. (eds) Landslides and Engineered Slopes. Experience, Theory and Practice, pp 1063-1067.
[4] DE BIAGI V, NAPOLI ML, BARBERO M, PEILA D (2017) Estimation of the return period of rockfall blocks according to their size. Nat. Hazards Earth Syst. Sci. 17, 103-11.
[5] RUIZ-CARULLA R, COROMINAS J, MAVROULI O (2016) A fractal fragmentation model for rockfalls. Landslides doi:10.1007/s10346-016-0773-8.
[6] GIACOMINI A, BUZZI O, RENARD B, GIANI GP (2009) Experimental studies on fragmentation of rockfalls on impact with rock surfaces. International Journal of Rock Mechanics & Mining Sciences 46, 708-715.
[7] GILI JA, RUIZ-CARULLA R, MATAS G, COROMINAS J, LANTADA N, NÚÑEZ MA, MAVROULI O, BUILL F, MOYA J, PRADES A, MORENO S (2016) Experimental study on rockfall fragmentation: in situ test design and firsts results. International Symposium Landslides 2016, Napoli. Balkema, 7 pp.
[8] COPONS R (2004) Avaluació de la perillositat de caigudes de blocs rocosos al Solà d'Andorra la Vella. PhD Thesis, Universitat de Barcelona. Published in Monografías del CENMA, 2007. 235 pp.

APPLICATION OF A ROCKFALL FRACTAL FRAGMENTATION MODEL TO THREE CASE STUDIES

Roger Ruiz-Carulla[1], Jordi Corominas[1]

A simple rockfall fractal fragmentation model (RFFM) is used to simulate rockfall fragmentation in three inventoried events. The inputs to the model are the detached rock mass volume and the In situ Block Size Distribution (IBSD). The latter is generated applying a Discrete Fracture Network to the rock mass volume. In this communication we discuss the influence of the model parameters that control the average size reduction, the shape of the final volume distribution, and the degree of fragmentation. The model is calibrated with the observed Rockfall Block Size Distribution (RBSD) of the deposits of the inventoried rockfalls.

Keywords: rockfall, fragmentation, fractal fragmentation model, real cases

INTRODUCTION: FRAGMENTAL ROCKFALLS

Rockfall fragmentation involves the separation of a rock mass into several smaller pieces upon the first impact(s) on the ground surface, leading to independent trajectories of the resultant blocks. The fragmentation causes the redistribution of the initial rock mass into smaller blocks; it affects the runout distance, the impact energy and consequently, the rockfall hazard.

A rock mass detached from the slope face is composed of intact rock blocks bounded by discontinuities. The range of sizes of the blocks within the rock mass may be characterized by the In Situ Block Size Distribution (IBSD). After the first impact(s), disaggregation of the rock mass and breakage of intact blocks modify the initial volume distribution, generating a new one, the Rockfall Block Size Distribution (RBSD).

FRACTAL MODEL

We have proposed a Rockfall Fractal Fragmentation Model (RFFM), based on the models proposed by [1] and [2], which have been adapted to the case of rockfalls [3]. The model considers a cubic block of unit length that breaks into small pieces according to a power law. The size distribution of the elements in a fractal system is given by:

$$N(1/b^i) = k\left[1/b^i\right]^{-D_f} \quad ; i = 0,1,2,\ldots\infty \quad [Eq.\,1]$$

Where $N\,(1/b^i)$ is the number of elements at the level i of the hierarchy; k is the number of initiators of unit length; b is a scaling factor greater than 1, that defines the geometric relation

[1] Technical University of Catalonia, C/ Jordi Girona 31, Barcelona, 08034, Spain, roger.ruiz@upc.edu, jordi.corominas@upc.edu

between the original block and the new generated blocks; and D_f is the fractal dimension of fragmentation, which is defined as:

$$D_f = 3 + \frac{log\left[P\left(1/b^i\right)\right]}{log[b]} \quad [Eq.2]$$

Where $P(1/b^i)$ or P_f : It is the probability of fracture that determines the proportion of the original block that breaks and generates new fragments. P_f is physically related to the interfaces of the fragments and maximum strength.

The first stage of the fragmentation is the disaggregation of the intact blocks present within the rock mass. The degree of disaggregation is controlled by the Survival rate, S_r. If the terrain is soft and/or the impact energies are low, the blocks may remain unbroken. In this case, a S_r equal to 1 is assigned to the model (Case study 1). If the impact energy is high enough to break a number of blocks, then, a fractal distribution law is applied to generate the volume distribution of the resultant fragments. The sum of all the new fragments generated and the surviving disaggregated blocks, define the calculated RBSD. The geometric factor b controls the reduction of the average size of blocks that takes place between the IBSD and the RBSD. P_f, controls the mass conservation in the blocks that break and the fractal shape of the final block size distribution (Case study 2 and 3).

MODEL CALIBRATION IN THE INVENTORIED ROCKFALL EVENTS

All the details on the 3 cases used in this work, can be found in the website https://rockrisk.upc.edu/en/field-work/inventories and in the publication [4].

Case 1 is the **Pont de Gullerí rockfall**. The volume of the detached rock mass is 2.6 m^3 and the height of fall, 12 meters. The failure mechanism is identified as wedge sliding. The rock mass is composed of schists affected by highly persistent joint pattern. As most of the fallen blocks were fully bounded by preexisting joints, it is assumed that the rock mass was simply disaggregated. Only one block showed fresh fracture. The RBSD was obtained by measuring 116 blocks of the deposit, and it is the same as the IBSD. The minimum block volume measured is $1.2*10^{-4}$ m^3, and the maximum is 0.28 m^3. In this case the S_r was made equal to 1 (Fig. 1-a). The parameters b and P_f are not used due to the lack of breakage. Therefore, S_r is the parameter that characterizes the disaggregation process. The high strength of the rock and the low energy scenario produce a rockfall event without new breakage, even the energy was enough to completely disaggregate the rock mass by the preexisting joint pattern.

Case 2 is the **Omells de na Gaia rockfall.** It is a small-size rockfall that propagated on a stepped soft ground. It initiated with a free fall of 0.8 m, and the farthest block stopped after impacting a building wall located at 22 m from the source. The blocks trajectories crossed a paved road and damaged a barrier. The detached rock mass is a weak sandstone of Oligocene age with a total volume of 4.2 m^3. We measured 48 blocks, with a minimum and maximum volume of $7*10^{-4}$ and 1.1 m^3, respectively. Rockfall blocks showed fresh faces formed by breakage as well as preexisting discontinuities, mostly bedding planes. This rockfall event is considered a low energy event due to the low free fall height. Anyhow, the weakness of the rock allowed the breakage of the blocks generating new fragments, developing a completely redistribution of the mass, modifying the trajectories of the blocks and the impact energies. The

RBSD measured can be fitted by a power law with a negative exponent of 0.53. The IBSD is generated applying a Discrete Fracture Network to the detached rock mass volume. The shape of the latter has been reconstructed using a 3D photogrammetric model of the cliff. We used a reduced Xi^2 criterion to reduce the difference between the RBSD measured in the deposit and the one generated with the RFFM, combining the parameters *b*, P_f, and *Sr*.

In the Omells rockfall, all blocks show new broken faces. In this case we made S_r=0. The scaling factor was set to *b*=1.8, which reduces the average size of the blocks almost two orders of magnitude. The Xi^2 value is optimized for a probability of failure of P_f=0.4, which determines that the 40% of the volume of the blocks breaks generating new fragments. Model fit and the measured RBSD are shown in Fig. 1-b). The total number of blocks increases by a factor of 10, from 5 blocks in the IBSD to 48 in the deposit. The block size distributions are represented in terms of percentage of volume passing certain block volume in cubic meters, showing the two orders of magnitude translation of the d50. The combination of *b*=1.8 and P_f =0.4 defines a fractal fragmentation dimension of 1.44. In this case, where all blocks show new fresh faces, the model parameters *b* and P_f allow generating a RBSD that fits reasonably well to the measured RBSD.

Case 3, **the Malanyeu rockfall.** Is a large rockfall, with a total volume detached close to 5000 m^3. The failure mechanism is unconfined toppling, that introduces rotational energy to the first impact. The rock is a high-strength Cretaceous limestone. The free fall height is less than 10 meters while the detached mass had a height of 60 m. The maximum run-out distance is 100 meters, reaching the valley bottom. We measured 2721 blocks, with a minimum volume of $4.2*10^{-5}$ m^3 and a maximum of 445 m^3. The deposit includes 7 blocks greater than 100 m^3, and more than 60 blocks greater than 10 m^3. A Young Debris Cover (YDC) was formed in the upper part of the deposit with a high concentration of small-size blocks, as consequence of the height of fall and probably crushing due to the large mass involved. The RBSD was obtained by extrapolation of the block sizes measured in sampling plots using the methodology detailed in [5]. The obtained RBSD estimates 25000 blocks in the deposit bigger than 0.001 m^3, and may be well fitted to a power law with a negative exponent of 0.72. The IBSD includes 235 blocks bigger than 0.01 m^3. This event is considered as a high energy rockfall due to the total volume detached and the free fall height.

Most of the blocks in the deposit show several faces that are preexisting discontinuities (joints and bedding surfaces). Suggesting than only a small proportion of the block have been broken. In this case, fragmentation is related to both the disaggregation and breakage. Fragmentation decreases the average size of the blocks up to four orders of magnitude. The best fit is obtained by assigning *b*=4.2 and P_f=0.2. These parameters indicate that breakage affects 20% of the initial block volume. S_r=0.2 allows the 20% of the original blocks propagate downhill unbroken, thus preserving their large volumes. A proof of this is the presence of huge blocks, bounded by preexisting discontinuities in the lower part of the deposit and, on the other side, the blocks of the YDC, showing multiple new faces and a highly decreased volume (in part due to crushing effect). The combination of the parameters *b*=4.2 and P_f =0.2 defines a fractal fragmentation dimension equal to 1.87. The bigger total volume, and then the bigger impact energies, in this third case, may justify a bigger fractal fragmentation dimension. Fig. 1-c) shows the estimated IBSD, the measured RBSD in the deposit, and the modelled RBSD. Again, the reduced Xi^2 is

used in order to minimize the difference between both the measured and modelled RBSD, combining the parameters S_r, b and P_f.

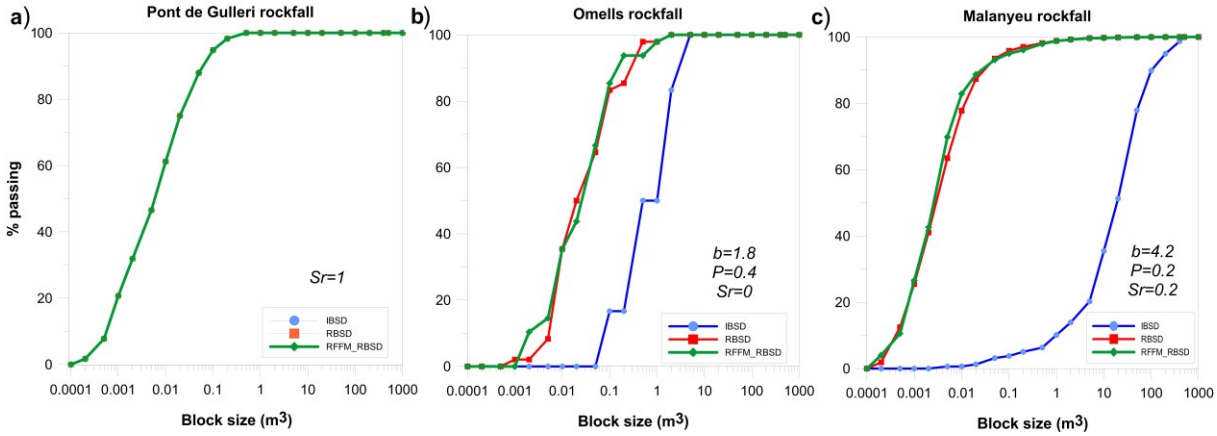

Fig. 1 Plots of the IBSD estimated from the cliff, RBSD measured on the deposit, and RBSD generated using the RFFM, in terms of % of volume passing versus block size, for 3 different cases: 1) Pont de Gulleri , 2) Omells de na Gaia, and 3) Malanyeu.

CONCLUSIONS

The three rockfall events analyzed in this study represent different fragmentation scenarios and how the fragmentation model parameters can be adjusted to each case. Pont de Gulleri rockfall is a case of pure disaggregation, where the RBSD and the IBSD are the same. S_r =1 allows reproducing this behavior. The cases 2 and 3 show different degree of block breakage. In the case 2, Omells de na Gaia, all the measured blocks show new fresh faces, and therefore S_r =0. This low energy scenario implies a low proportion of volume reduction, given by the value of b=1.8. However, the low rock strength allowed that almost all blocks were broken, typically splitting in two big parts and few small fragments. In this case, 40% of the blocks broke generating new fragments (P_f =0.4). Finally, the third case, Malanyeu rockfall, is the highest energy scenario analyzed, resulting in a significant reduction of the average block size, with a reduction of up to four orders of magnitude with a geometric factor b=4.2. Despite of this, some blocks remained unbroken (S_r =0.2). Due to the high rock strength, P_f =0.2. Only 20% of the mass of the block broke into new fragments. More calibration analysis should be carried out in order to define a range of values to be used for the prediction of the behavior of fragmental rockfalls and for the definition of hazard scenarios.

REFERENCES

[1] PERFECT E (1997) Fractal models for the fragmentation of rocks and soils: a review. Engineering Geology 48:185-198
[2] TURCOTTE D (1986) Fractals and Fragmentation. Journal of Geophysical Research 91. NO B2: Pages 1921-1926
[3] RUIZ-CARULLA R, COROMINAS J AND MAVROULI O (2016) A fractal fragmentation model for rockfalls. Landslides doi: 10.1007/s10346-016-0773-8
[4] RUIZ-CARULLA R, COROMINAS J AND MAVROULI O (2016) Comparison of block size distribution in rockfalls. International Symposium on Landslides 2016 (ISL2016), pp: 1767-1774, Napoli (Italia).
[5] RUIZ-CARULLA R, COROMINAS J AND MAVROULI O (2015) A methodology to obtain the block size distribution of fragmental rockfall deposit. Landslides. Vol. 12, Issue 4, pp 815-825 doi: 10.1007/s10346-015-0600-7

ROCKFALL FRAGMENTATION ANALYSIS: VILANOVA DE BANAT CASE STUDY

Gerard Matas[1], Nieves Lantada[1], Jordi Corominas[1], Josep A. Gili[1], Roger Ruiz-Carulla[1], Albert Prades[1]

Fragmentation is a critical mechanism for the calculation of the trajectories of the blocks and the impact energies, for the assessment of the potential damage and for the design of protective structures, although few rockfall models account for it. In this contribution we present an application of the trajectory simulation tool RockGIS, which explicitly accounts for fragmentation, to a recent rockfall event occurred near Vilanova de Banat (Spain). All parameters of the model controlling the kinematics of the propagation and fragmentation have been calibrated in order to reproduce the number of fragments generated and trajectories followed by the blocks. Several performance criteria have been considered and simulations with and without accounting for fragmentation have been performed to assess their influence. The results considering fragmentation show a reasonable matching with the observations in the field.

Keywords: rockfall, fragmentation, GIS, rockfall simulation

INTRODUCTION

A rockfall is a mass instability process frequently observed in road cuts, open pit mines and quarries, steep slopes and cliffs. It is frequently observed that the detached rock mass becomes fragmented due to the impacts upon the slope surface. However, accounting for this phenomenon in rockfall models is not trivial. In this work we have modelled the fragmentary rockfall of Vilanova de Banat using RockGIS tool, which incorporates the fragmentation. First, an overview of the model is presented. Then, we describe all data available from different previous studies of Vilanova de Banat site and the calibration process. Finally, the results of some simulations considering or not fragmentation are shown and discussed.

ROCKGIS MODEL

RockGIS is a GIS-Based model that simulates stochastically the fragmentation of rockfalls, based on a lumped mass approach [1]. The model requires as main input data a digital surface model, the soil type coverage map and the release coordinates for triggering the movement of the blocks. In RockGIS, the fragmentation initiates by the disaggregation of the detached rock mass through the pre-existing discontinuities. An energy threshold is defined in order to determine whether a block break or not at each impact upon the ground surface. The distribution of the initial mass between the set of newly generated broken rock fragments is carried out stochastically following a power law since it has been proved to represent reasonably the phenomena in several real scale tests [2]. The output velocities of the new rock fragments are

[1] Department of Civil and Environmental Engineering, Universitat Politècnica de Catalunya, C. Jordi Girona 1-3, Barcelona 08034, Spain, +34 93 401 69 25, gerard.matas@upc.edu

distributed within a cone and the remaining energy after breakage is distributed proportionally to the mass of each fragment. Finally, all fragments generated propagate downslope and the process continues iteratively until all fragments stop.

VILANOVA DE BANAT ROCKFALL

In November 2011 a fragmental rockfall event occurred on a limestone cliff in the Cadí Sierra, Eastern Pyrenees near the village Vilanova de Banat. A field inventory carried out by [3] estimated the initial detached mass to be 10,000 m³. This mass became substantially fragmented, generating a Young Debris Cover (YDC) extending over an area of approximately 30,000m². Many Large Scattered Blocks (LSB) propagated far beyond the YDC. In [3] the Rockfall Block Size Distribution (RBSD) was extrapolated from the measurements in representative sampling plots within the YDC. All the LSB were measured one by one. The input to our models is the In Situ Block Size Distribution (IBSD) of the detached rock mass, which was obtained in [3] by applying a Discrete Fracture Network to the missing volume of the rockfall source. The rockfall deposit is shown in Fig. 1c while the measured ISBD and RBSD are shown in Fig. 2.

CALIBRATION AND VALIDATION

The model requires the calibration of both the runout of the resultant blocks and the spatial distribution of the volumes of fragments generated by both disaggregation and breakage during their propagation. As this is a coupled process which is controlled by several parameters, a set of performance criteria to be met by the simulation have been defined. The criteria include: position of the centre of gravity of the whole block distribution, histogram of the runout of the blocks, extent and boundaries of the young debris cover over the slope surface, lateral dispersion of trajectories, total number of blocks generated after fragmentation, volume distribution of the generated fragments, the number of blocks and volume passages past a reference line and the maximum runout distance. We tested several sets of parameters varying each parameter using fixed intervals. Finally, the set of parameters fitting better the field data according the mentioned performance criteria was selected.

RESULTS

In this contribution we used all data collected in [3,4] to perform trajectory simulations considering and without considering fragmentation in RockGIS. Each block of the ISBD is released in a randomly chosen point inside the estimated detachment area. As all the propagation process is stochastic, 5 simulations in each case where performed to check the variability of the results.

Fig. 1 shows the locations stopped blocks in two of the simulations runs: not considering (Fig. 1a) and considering block breakage (Fig. 1b). The size of the circles is proportional to the volume of the blocks. The distances between the observed and simulated centre of gravity of the fragments (c.o.g) are 1.57, 1.18, 2.82, 2.36 and 5.67 meters for simulations 1 to 5, respectively. The simulations without fragmentation show an average excessive distance of 79m for the modelled c.o.g.

For the proper visualization of the spatial distribution of the simulated blocks, a set of polygons defining specific percentages of the total number of simulated blocks has been plotted. Fig. 1c shows the results of this procedure in the fragmentation case overlaid with the field data. It is observed that the YDC boundary is quite similar to the contour of the polygon containing 80% of the simulated blocks.

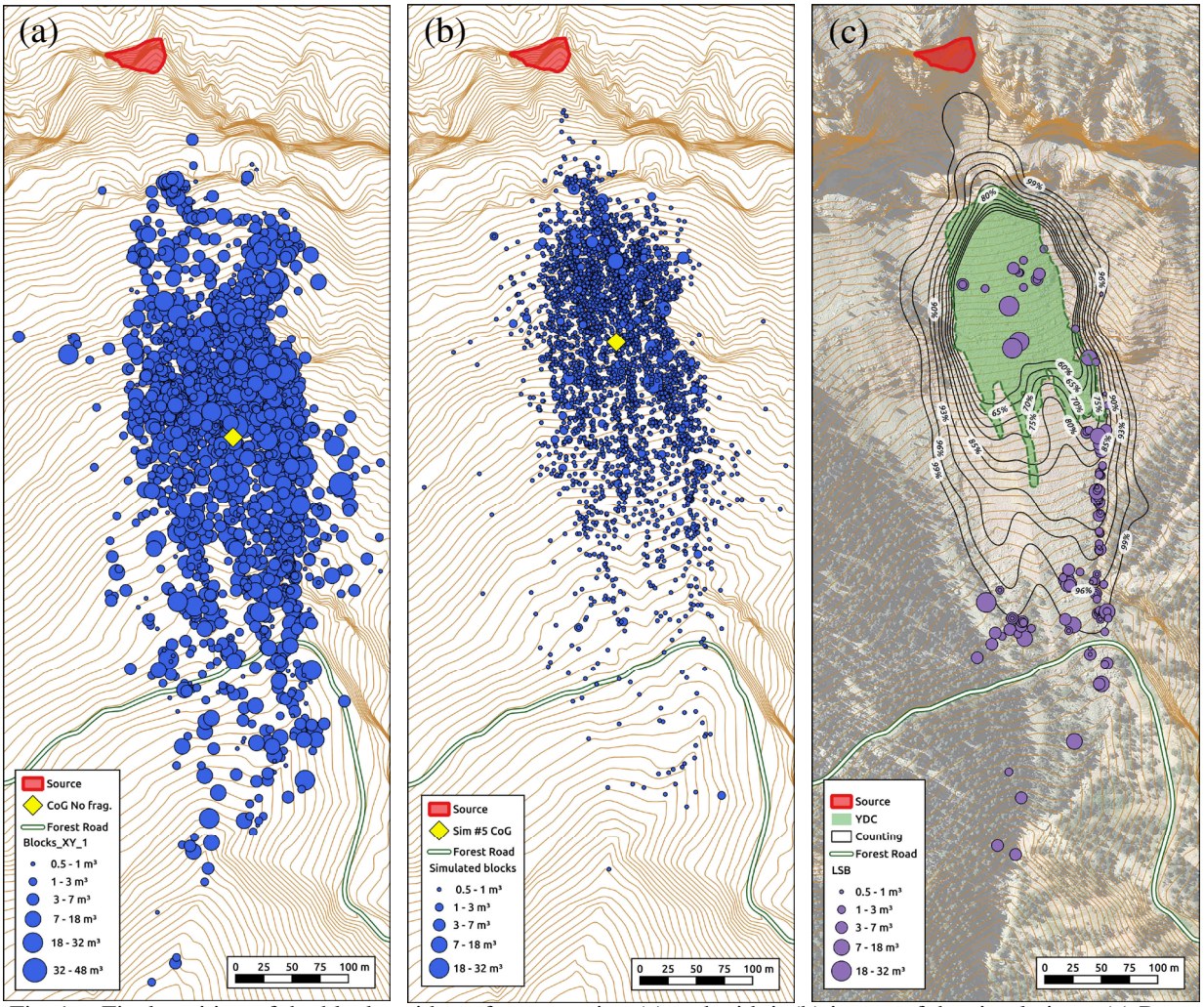

Fig. 1 Final position of the blocks without fragmentation (a) and with it (b) in one of the simulations. (c) Density map of the accumulated blocks of the simulation with fragmentation superposed with the field YDC and LSB measured in the field, [modified from 1].

Fig. 2 shows the five RBSD obtained by the RockGIS simulations considering fragmentation against the field RBSD and IBSD. The five simulation runs yield similar RBSD, which may be well fitted to the observed in the field. They nearly coincide in the domain corresponding to the power law used for distributing the mass of the fragments during breakage but differ slightly in the part of the curve representing the largest volumes. This can be explained by the stochasticity of both the process for generating the fragments and the energy threshold for triggering breakage. In a simulation, a block may break into smaller fragments than the same block in same impact conditions in other simulations. Moreover, not all blocks break and then the RBSD obtained strongly depend on the IBSD used.

DISCUSSION

The model has shown a high sensitivity of the rockfalls to the fragmentation process. The number of large blocks reaching the lowest parts of the slope is reduced significantly with the fragmentation and the whole debris mass remains close to the rock wall as shown by the locations of the centres of gravity.

Several factors affect the breakage of a block during an impact and some tests [2] have shown it cannot be characterized by a single parameter. However, the simple assumption of an energy threshold that triggers breakage has shown to be useful for modelling purposes when considering fragmentation. Moreover, using power laws to distribute the mass has proven to be a simple way of representing the breakage process.

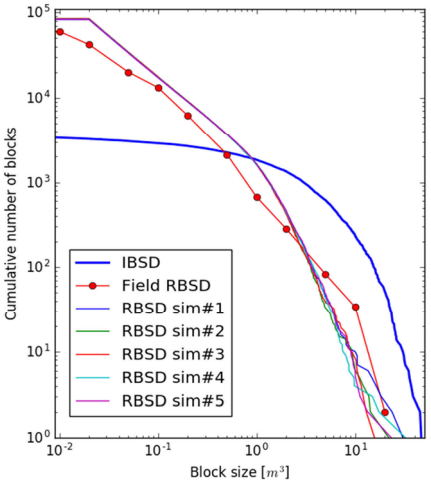

Fig. 2 RBSD obtained from five simulations in RockGIS considering fragmentation against field data RBSD.

The model uses the lumped mass approach whose restrictions are already known: it does not explicitly take into account the shape of the blocks, their rotational movement nor the relative position of the internal fractures of a block with respect to the impacting angle. Despite these limitations, the RockGIS model has been able to reproduce the study case.

The model approached the position of the centre of gravity of the field distribution with an average error of 2.72m considering fragmentation. The extend boundaries of the YDC matched the polygon containing 80% of the blocks in the performed simulations, whilst the polygon containing 96% of the blocks had an average lateral divergence of 23m.

CONCLUSION

RockGIS functions successfully and accomplishes the goal of representing the fragmentation process during a rockfall as we were able to reproduce the runout of the blocks and the RBSD measured in the Vilanova de Banat case farely well. The fulfilment of the performance criteria when adding the fragmentation parameters to the simulation makes the calibration process a delicate exercise that ends with a compromise between all the criteria.

REFERENCES

[1] MATAS G, LANTADA N, COROMINAS J, GILI JA, RUIZ-CARULLA R, PRADES A (2017). RockGIS: A GIS-based model for the analysis of fragmentation in rockfalls. Landslides. doi:10.1007/s10346-017-0818-7
[2] GILI JA, RUIZ R, MATAS G, COROMINAS J, LANTADA N, NÚÑEZ MA, MAVROULI O, BUILL F, MOYA J, PRADES A, MORENO S (2016) Experimental study on rockfall fragmentation: in situ test design and firsts results. In: Aversa S, Cascini L, Picarelli L, Scavia C (eds) Landslides and engineered slopes, 2: 983-990.
[3] RUIZ-CARULLA R, COROMINAS J, MAVROULI O (2015) A methodology to obtain the block size distribution of fragmental rockfall deposits, Landslides, 12 (4): 815-825.
[4] RUIZ-CARULLA R, COROMINAS J, MAVROULI O (2015) An empirical approach to rockfall fragmentation. EUROCK 2015 & 64th Geomechanics Colloquium, Schubert (ed): 151-156.

COMPARISON OF MONTE-CARLO MODEL SIMULATIONS AND RECENT DEPOSITED BLOCKS TO DETERMINE REALISTIC ROCKFALL RUNOUT ZONES

Luuk Dorren[1], Frédéric Berger[2], Franck Bourrier[3], Christine Moos[4], Thomas Planzer[5], David Toe[6]

Rockfall trajectory modelling is one of the methods that provide an important basis for predicting realistic rockfall propagation or runout zones. To account for the many unknowns in the rockfall process, models generally use stochastic variables in their algorithms. When interpreting rockfall simulation results, extreme long, low probability trajectories, need to be separated from all other trajectories in the modelled rockfall runout distribution. This preliminary study evaluates simulated propagation probability values on the basis comparisons with deposited blocks of recent rockfall events.

Keywords: rockfall trajectory modelling, simulation, probability, silent witnesses, validation

INTRODUCTION

The yearly damage due to rockfall on Swiss national roads is, based on a recent risk evaluation, expected to be at least 12 million Swiss francs [1]. Although rockfall hazard analyses have been improving considerably over the last decades, it remains a challenge to fully grasp the stochastic behaviour of this natural hazard process both with respect to time and space.

To come up with a realistic hazard prediction, rockfall modelling is one of the methods that provide an important basis. Rockfall models generally use stochastic variables in their algorithms to account for the many unknowns in the rockfall process. These are, for example, the precise location of the release area, the release volume, the fragmentation of the initial volume during impacts on the slope surface (especially during the first one after descending a cliff), the size and shape of the individual blocks, the transformation and dissipation of energy during rebounds on the slope surface,

Since such algorithms, also called Monte Carlo methods, rely on repeated random sampling, the numerical results represent probability distributions, which in the case of rockfall generally include runout zones, kinetic energies and passing heights. Usually, the first step in the interpretation of rockfall simulation results is the definition of the realistic runout zone for the modelled scenario, by separating extreme long, low probability trajectories, or outliers, from all other trajectories in the modelled rockfall runout distribution.

[1] Bern Univ. of Applied Sciences - HAFL, Länggasse 85, CH-8052 Zollikofen, Switzerland (CH), luuk.dorren@bfh.ch
[2] IRSTEA Centre de Grenoble, 2 rue de la papeterie, F-38402 St. Martin d'Hères cedex, frederic.berger@irstea.fr
[3] IRSTEA Centre de Grenoble, 2 rue de la papeterie, F-38402 St. Martin d'Hères cedex, franck.bourrier@irstea.fr
[4] Bern Univ. of Applied Sciences - HAFL, Länggasse 85, CH-8052 Zollikofen, Switzerland (CH), christine.moos@bfh.ch
[5] Bern Univ. of Applied Sciences - HAFL, Länggasse 85, CH-8052 Zollikofen, Switzerland (CH), thomas.planzer@bfh.ch
[6] IRSTEA Centre de Grenoble, 2 rue de la papeterie, F-38402 St. Martin d'Hères cedex, david.toe@irstea.fr

At present, clearly defined propagation probability threshold values based on sound statistical comparisons with silent witnesses (deposited blocks) of recent rockfall events are missing. These threshold values would allow an objective definition of the realistic runout zone.

The objective of this study is to analyse probability values by comparing results generated by a Monte-Carlo based rockfall simulation model on 4 different sites in the French and Swiss Alps, where rockfall events occurred during the last decade, with individual blocks ranging from 0.4 – 33 m^3.

METHODS

The Monte-Carlo based rockfall simulation model used in this study is Rockyfor3D (RF3D, cf. [2]), which is a probabilistic process-based rockfall trajectory model simulating falling of individual blocks in three dimensions. RF3D was developed on the basis of real-size, field-based rockfall experiments and uses raster maps describing topography (Digital Elevation Model, DEM), rockfall source cells, the elasticity of the surface material, slope surface roughness, the number of trees per cell, DBH of trees in each cell and tree species per cell as input data. For each rockfall source cell, the trajectories of a given number of rocks are simulated by sequences of flying and bouncing phases. Rolling is considered as multiple rebounds on the slope surface with very short flying phases in between.

The density of the impacted material is calculated based on the normal coefficient of restitution (Rn) which is determined using seven different categories of soil types. Surface roughness is represented by a mean obstacle height (MOH) representative for 70, 20 and 10%, respectively, of each cell. RF3D explicitly calculates the deviation and energy loss after impacts with trees dependent on tree diameter, impact position, and the kinetic energy of the rock before the impact. The main output of RF3D used for this study consists of a raster map containing information on the reach probability, as defined by [2] in a version published in 2011 and the propagation probability. Additional outputs generated by RF3D are, amongst others, raster maps with information on the kinetic energies, the passing heights, the number of deposited rocks and the number of tree impacts per cell.

The reach probability (P_reach) is calculated by:

(*Nr_passages* * 100) / (*Nr_simulations_per_source_cell* * *Nr_sourcecells*) [in %]

Where *Nr_passages* is the number of blocks passed through each cell; *Nr_simulations_per_source_cell* is the number of individual blocks simulated from each source cell; *Nr_sourcecells* is the number of source cells "feeding" a given cell [-]. In other words, the raster *Nr_sourcecells* shows for each cell, from how many different source cells the blocks arrived in that given cell.

The propagation probability (P_prop) is calculated by:

(*Nr_passages* * 100) / (*Total_Nr_simulations*) [in %]

Where *Total_Nr_simulations* is the total number of executed simulations (= *Nr_simulations_per_source_cell* * the total number of source cells).

At each of the 4 study sites, we carried out 1000 trajectory simulations per start cell. Here, the start cells corresponded to the mapped release areas of the real events. All input rasters (elevation model, surface properties, start areas, etc.) had a resolution of 2 × 2m. We simulated the exact volume of the extreme runout blocks, mapped at the four sites. For the block form we chose one of the four standard options available in RF3D (rectangular, ellipsoid, sphere and disc), that represented best the mapped block in the field. In a following step, we defined the simulated P_reach and P_prop value at the location of the mapped block. For this study, we assessed firstly whether a distinct probability value range exist for the blocks deposited in the extreme runout zone. Secondly, we analyze if this value range is dependent on block volume. Since we are just beginning with this study, the results presented here are only based on 29 mapped blocks. Half of these blocks were individual rockfalls with block volumes between 0.4 and 1 m^3), the other half were individual blocks that ran out of a rock mass falls with block volumes between 4 and 33 m^3).

RESULTS

The results at the 4 sites show that both the reach and propagation probability (P_reach resp. P_prop) give good indications of the locations of the extreme propagation distance or runout zone of rockfall events, both for individual rockfall, as well as for individual fragments originating from rock mass falls (cf. Fig. 1).

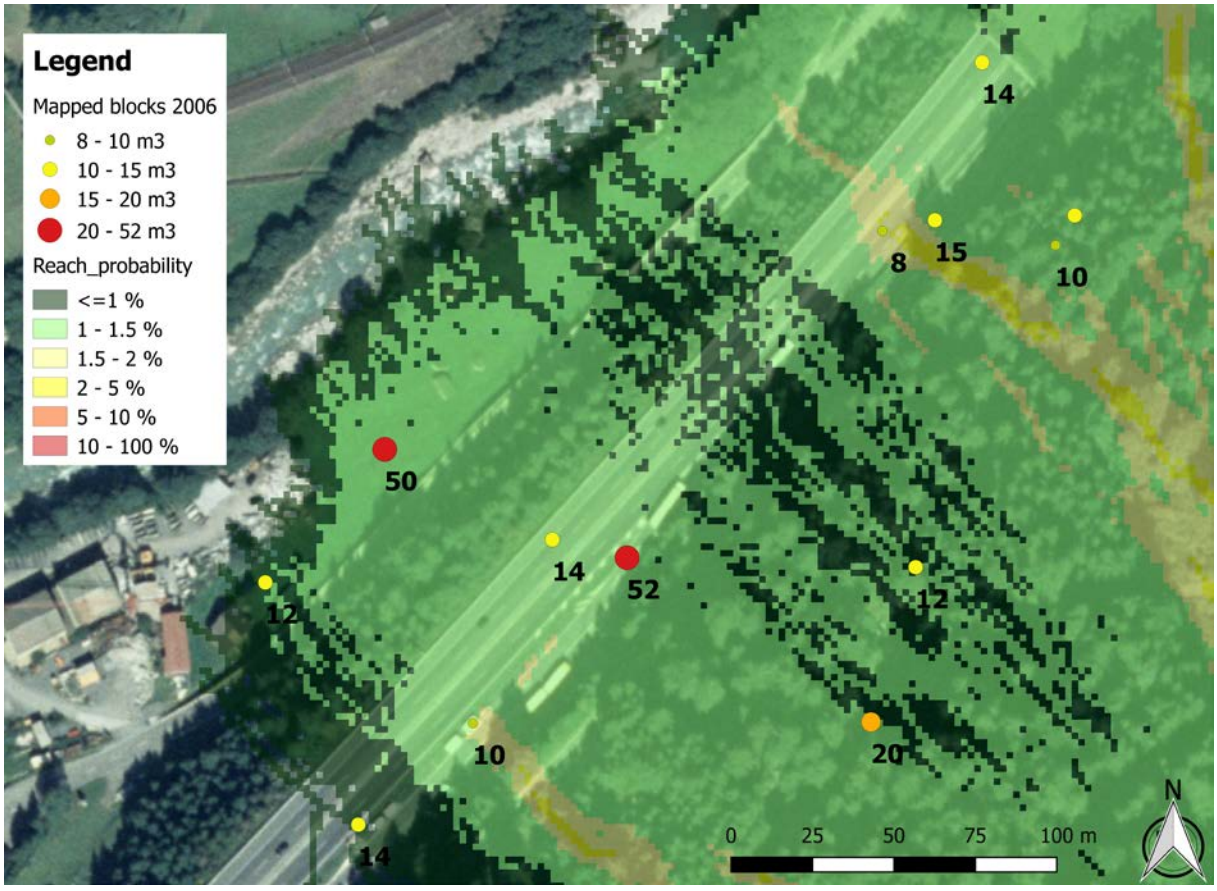

Fig. 1: Stopping positions of the largest individual blocks in the extreme runout zone of the rock mass fall of 2006 in Gurtnellen, Switzerland. The reach probability map in the background is the result of 1000 simulations with blocks of 14 m3.

When comparing P_reach with P_prop, the results indicate that the values of P_reach allow for a more distinct definition of the realistic runout zone within the large range of simulated probabilities. Especially for block volumes > 4 m^3, P_reach values are confined between 1 and 2%, whereas corresponding P_prop values are more scattered. Both P_reach and P_prop values are scattered for block volumes < 1 m^3 (Fig. 2).

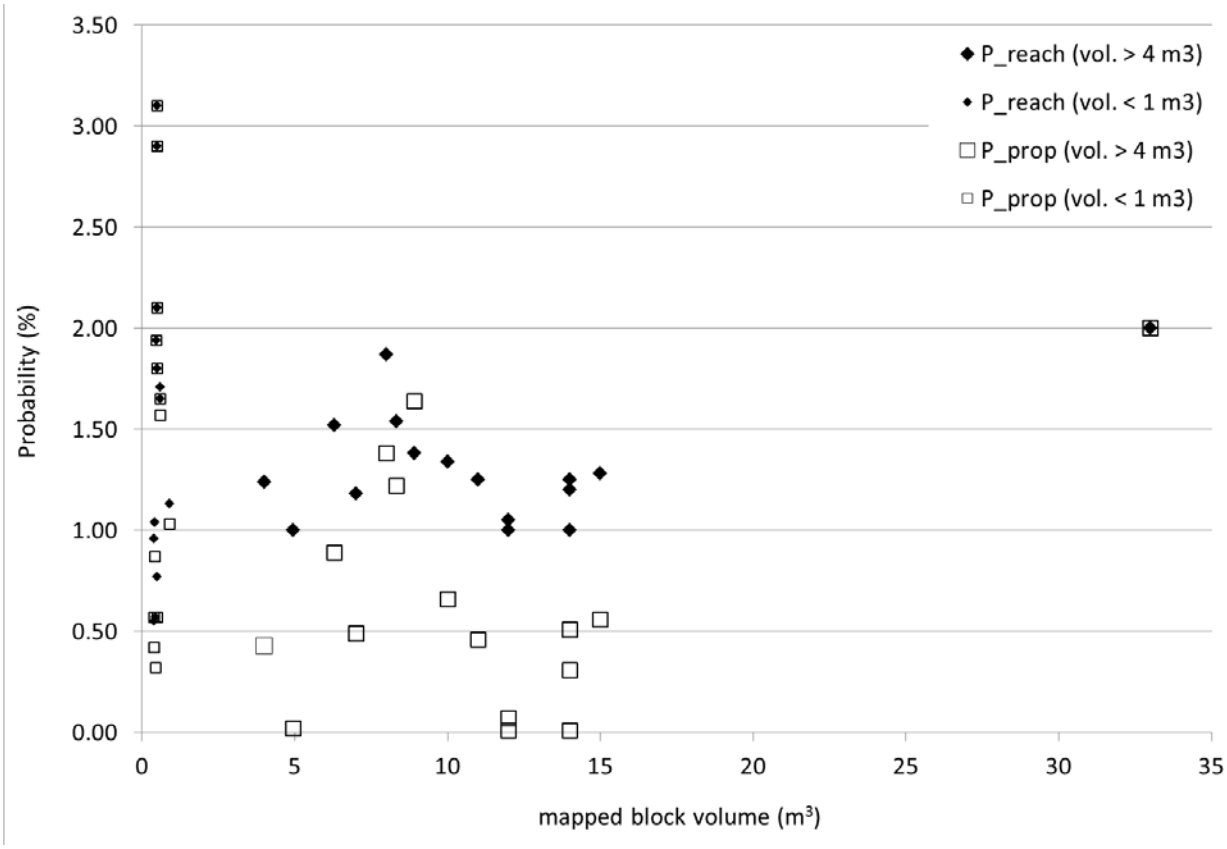

Fig. 2: Volume of the blocks mapped in the extreme runout zones versus the simulated reach and propagation probabilities (P_reach and P_prop).

CONCLUSION

Based on the results of this study, we conclude that the reach probability gives the most distinct indication of the realistic runout zone of rockfall events, especially for individual fragments originating from rock mass falls with volumes larger than 4 m^3. The block volume range from 1 - 4 m^3 needs to be covered in a more extensive follow-up study.

REFERENCES

[1] DORREN, L. ARNOLD, PH. (2016) Key results of the Swiss wide natural hazard risk assessment on national roads. Interpraevent 2016 – Conf. Proceedings: 479 – 485.
[2] DORREN L. (2015) Rockyfor3D (v5.2) revealed – Transparent description of the complete 3D rockfall model. ecorisQ paper: 32 p.

CALIBRATION METHODS FOR NUMERICAL ROCKFALL MODELS BASED ON EXPERIMENTAL DATA

Andrin Caviezel[1], Marc Christen[1], Yves Bühler[1], Perry Bartelt[1]

Experimental data sets of induced rockfalls are used to enhance calibration methods for the existing RAMMS::ROCKFALL software package. Repeated release of the same rocks instrumented with acceleration and gyroscopic sensors yields statistical information of their deposition points and provides direct measurements of the rotational speeds and acting impact forces. The presented data and the subsequent calibration of the software code via real experimental data outlines an objective path for selection of terrain parameters.

Keywords: rockfall, experimental data, simulation, RAMMS calibration

INTRODUCTION

Residents in mountainous areas are well aware of the necessity of mitigation of rock fall hazards in order to prevent damage of infrastructure such as roads, railway lines, or houses. Mitigation of this hazard relies on the combined use of the different data sources such as observations, measurements and information gathered through numerical simulations. It is key that all available information is as objective as possible, without interpretation bias and that a quantitative measure of the information is provided

Amongst many other methods such as topographical analysis, consulting natural hazard registers, event maps, etc., information gathered via numerical modelling has become of growing importance over the past years. Several different mechanical models and thus simulation software tools have been developed ([1-6] and references therein) and are available for risk assessments. These 3D approaches bear the strong advantage that they include detailed terrain information and improve the estimation accuracy for outliers. Whereas its output is basically free of interpretation, the reliability and user friendliness relies on well calibrated input parameters for any given conditions. Due to the scarcity of real-world data most often a numerical model is calibrated via case studies. This approach already yields good results, however, the direct comparison with experimental data is preferred. Here, we present data gathered with an in-situ sensor node [7] and a similar in-

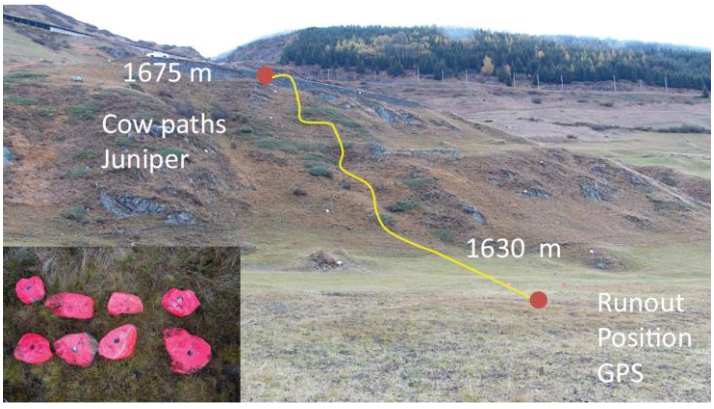

Fig. 1: Experimental site with indicated trajectory paths located close to Tschamut (Grisons, Switerland)

[1] WSL Institute for Snow and Avalanche Research SLF, Flüelastr. 11, 7260 Davos Dorf, Switzerland, +4181 417 03 61,surname@slf.ch

house development. While only a few of such sensors have been developed so far [8,9] with either dated components or not sufficient sensor ranges the used sensors focus on improved ruggedness, form factor, update rates and convenient data retrieval. Details of the design and components can be found in Ref. [7]. We present typical data sets and provide a preliminary comparison to simulated data which drafts the up-coming calibration work.

EXPERIMENTAL SETUP

The experimental site in Tschamut is located at 696607/167726 (CH1903 LV03) near the small settlement Tschamut on the road to Oberalppass. The start position on the road is situated at roughly 1675 m.a.s.l, the runout situated at ca. 1630 m.a.s.l. with a rather uniformly alpine meadow. The slope consists of a inclined area of 40 degree, offering typical coexistence of alpine meadow, rocky sections, juniper vegetation and is shown in Figure 1. The Tschamut site offers good accessibility of the release and runout zones due to road access. The inset in Fig. 1 shows eight rocks collected in the Bondasca valley in Bergell. These granite rocks have been collected with the goal to overcome the frequent problem of fragmentation observed in previous experiments. Additionally to the eight Bergell rocks, the heaviest rock from a previous experiment and a normed shape EOTA rock are added to a second experimental campaign. A drilled hole of 68 mm diameter allowed to fix the used sensors closely to the center of mass. Figure 2 shows, that according to the Sneed and Folk classification (1958) the used rocks belong to the equant, compact bladed and elongated categories. Table 1 summarizes the specifications of the rocks taken from the digitized point cloud later used for RAMMS::ROCKFALL simulations.

RESULTS AND DISCUSSION

The first experimental campaign (*RF04*) has been conducted after heavy rain falls on rather soft terrain. It consisted of six releases of Rock 1-8, yielding 48 deposition points of which 25 trajectories have been successfully recorded with in-situ intruments. Figure 3a shows the overview of the experimental site with all of the deposition points as well as the release point. The second experimental campaign (*RF05*) depicted in Fig. 3b has been conducted on frozen ground with six releases of Rock 1-8 and TS2 and seven releases of the EOTA block totalling to 57 deposition points due to the destruction of Rock 7 in the third release. In-situ data are available for 26 trajectories. The larger runout distances for frozen ground are evident.

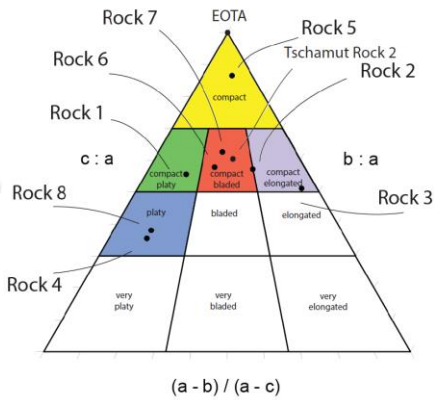

Fig. 2: Sneed and Folk classification (1958)

Rock	Dimensions (m)	Weight (kg)	Volume (m^3)
1	0.36/0.32/0.20	30.5	0.011
2	0.41/0.30/0.24	34.8	0.013
3	0.49/0.25/0.27	42.4	0.016
4	0.43/0.48/0.18	34.8	0.012
5	0.37/0.34/0.32	42.6	0.016
6	0.45/0.37/0.26	41.1	0.016
7	0.33/0.40/0.25	29.9	0.011
8	0.52/0.58/0.22	52.2	0.019
TS2	0.50/0.39/0.30	78.4	0.030
EOTA	0.3/0.30/0.30	44.0	0.016

Tab. 1: Dimensions, weights and volumes of the used rocks

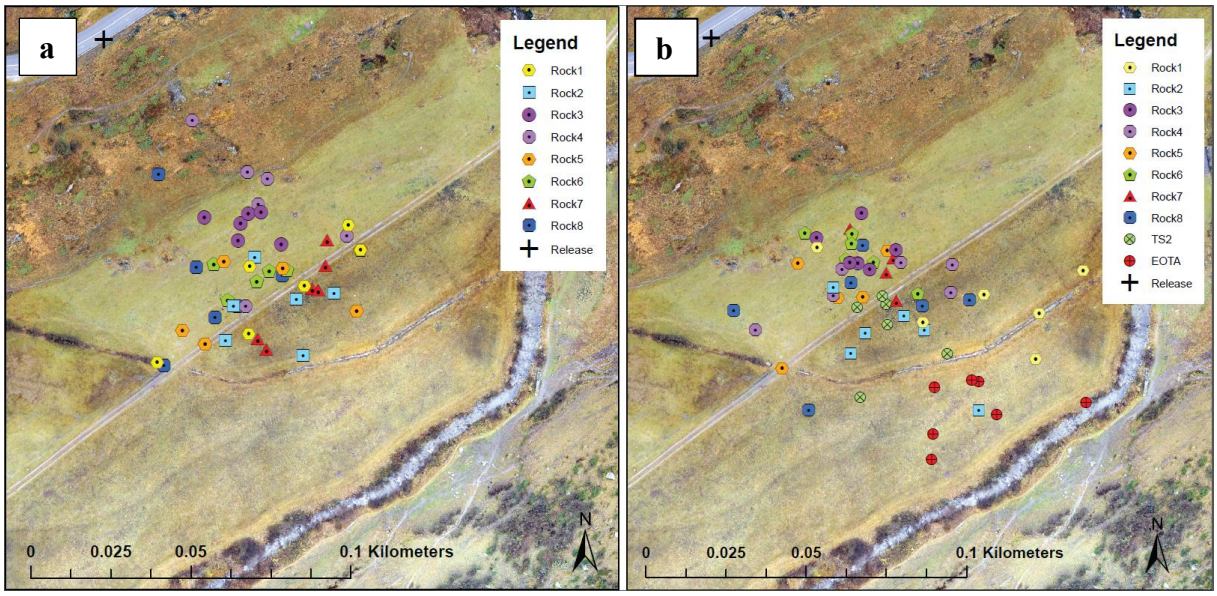

Fig 3: Release point and deposition points for two different experimental campaigns *RF04* and *RF05*: the left panel was conducted at rather soft soil conditions, the right panel at frozen ground.

A parameter sweep for RAMMS::ROCKFALL simulations is conducted. Due to the close to ideal runout area, the center of mass and the principal axis orientations of the two dimensional Gaussian ellipsoids are chosen to be the parameters of interest. Figure 4a shows the best fit for Rock 1, while Fig. 4b depicts the simulation result with these parameters for the entire rock ensemble Rock 1-8 and is in good agreement with the experimental result. The limitations of the principal axis criterion for circular distributions becomes obvious. Additionally, Fig. 5 shows the comparison of experimental sensor data of Rock 1 during the *RF04* campaign with simulation output using the best parameter fit of the previously conducted parameter search. The qualitative and quantitative agreement is striking.

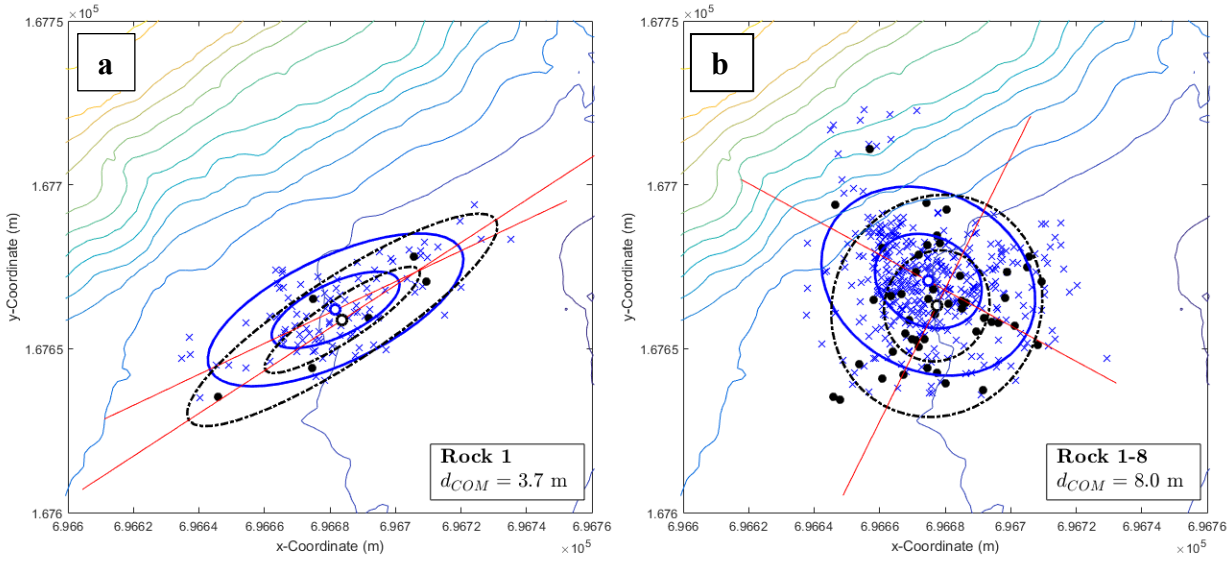

Fig. 4: Parameter evaluation for Rock 1 (a), and Rock 1-8 (b) for the deposition points conducted on soft ground. Accuracy of the evaluated parameters is judged via the offset in the center of mass of the deposited rocks as well as the deposition angle of the distribution.

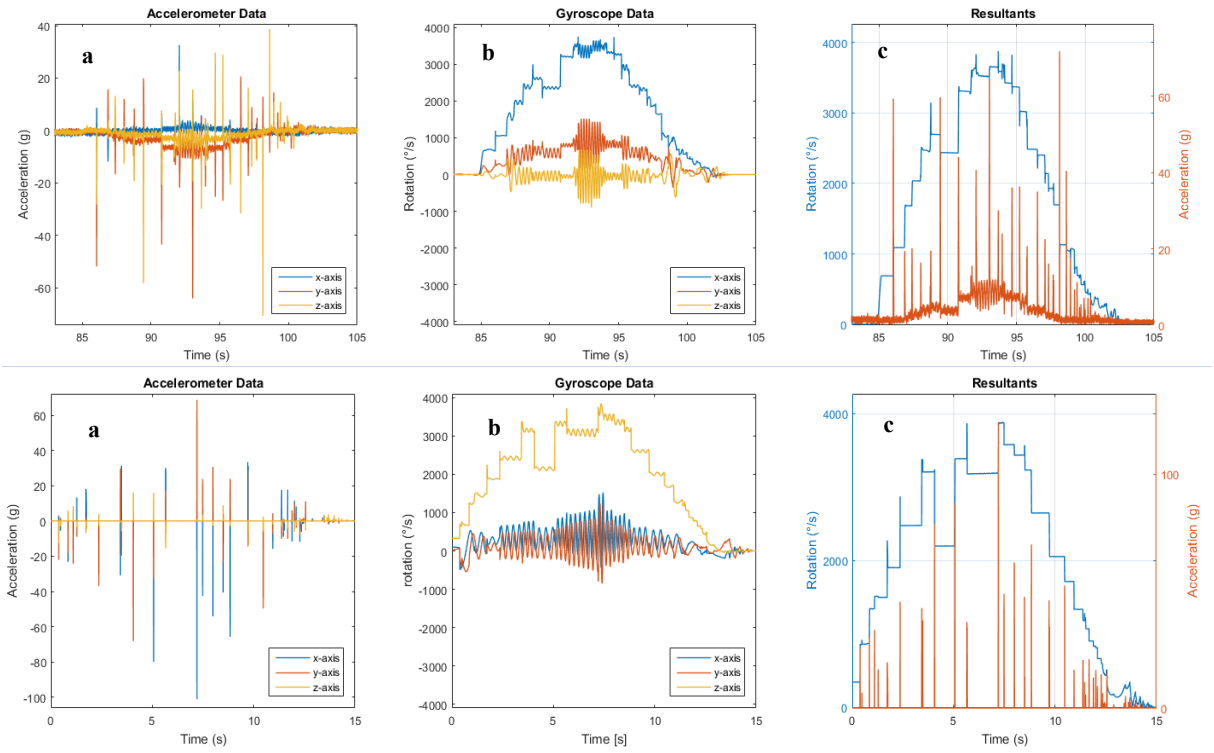

Fig. 5: Typical measurement traces (upper panel): (a) tri-axial accelerations, angular velocities (b), and (c) absolute magnitudes representing the third run of the compact bladed *Rock 1* in RF04. The lower panel shows a single simulated trajectory of Rock 1.

CONCLUSION AND OUTLOOK

Experimental data of induced rockfall experiments are used as calibration input for the simulation module RAMMS::ROCKFALL. Terrain parameters are chosen corresponding to the best congruence of the respective Gaussian ellipsoids. Strong qualitative and quantitative agreement of acting accelerations and rotations between simulation outputs and experimental data are found. Extended analysis routines will involve congruence fitting of all used rocks and comprehensive cross-checking for best fits. Therefore, a stringent routine has to be determined to tackle this multidimensional problem.

REFERENCES

[1] CHRISTEN M, BÜHLER Y (2012) Integral Hazard Management Using a Unified Software Environment Numerical Simulation Tool RAMMS, Proc. Congress Interpraevent, pp. 77–86
[2] LAN H, MARTIN D, and LIM C (2007) RockFall analyst: A GIS extension for three-dimensional and spatially distributed rockfall hazard modeling, Comput. Geosci., 33, 262–279
[3] DORREN LKA Rockyfor3D revealed – description of the complete 3D rockfall model, Tech. rep., EcorisQ, http://www.ecorisq.org, 2010.
[4] H. MASUYA H, AMANUMA K, NISHIKAWA Y. and TSUJI T (2009) Basic rockfall simulation with consideration of vegetation and application to protection measure, NHESS, vol. 9, no. 6
[5] JONES CL, Higgins JD, and Andrew RD (2000) Colorado Rockfall Simulation Program: Version 4.0
[6] AGLIARDI F, CROSTA GB (2003) High resolution three-dimensional numerical modelling of rockfalls. International Journal of Rock Mechanics and Mining Sciences 40, 455-471
[7] NIKLAUS P, BIRCHLER T, AEBI T, SCHAFFNER M, CAVIGELLI L, CAVIEZEL A, MAGNO M, and BENINI L (2017) StoneNode: A Low-Power Sensor Device for Induced Rockfall Experiments. Proc. 2017 IEEE Sensors Application Symposium, (accepted)
[8] GRONZ O, HILLER PH., WIRTZ S, BECKER K, ISERLOH T, SEEGER M,BRINGS C. ABERLE J, CASPER MC, RIES JB (2016) Smartstones: A small 9-axis sensor implanted in stones to track their movements, CATENA,142, 245 - 251
[9] A. VOLKWEIN A, KLETTE A (2014) Semi-automatic determination of rockfall trajectories, Sensors, vol. 14, no. 10

DIVERSITY OF THE RESULTS FROM DROP WEIGHT TESTS

Werner Gerber[1], Andrin Caviezel[2]

Here we show results of deceleration measurements from drop weight tests with cubic concrete bodies on soil layers with different compaction. In each experiment, the maximum deceleration was compared with an average deceleration resulting from the impact speed and the deceleration time. These *deceleration factors* show values in the range of 1.3-2.4. Also a *penetration factor* is determined for each test, which compares the penetration depth with a theoretical distance during the brake time. The combination of the two values reveal a large diversity of impact behavior.

Keywords: impact forces, drop weight test, deceleration, rockfall, penetration depth

INTRODUCTION

The dimensioning of protective dams against rockfalls depends on forces acting upon impacts. The calculation of such forces achieved by different methods [1]. However, the results are partly contradictory and show corresponding differences. Many models use parameters of the ground material as well as parameters of the stone itself, while other use only the energy to determine the impact force. In order to investigate these contradictions, more than 250 drop weight tests with cubic concrete blocks have been carried out at the WSL test side over the past years.

METHODS

Various soil strengths were used to stop the falling masses, but also combinations of concrete slabs and different layers were tested [2]. In this paper, we focus mainly on soil layer tests where different masses of 800 kg, 4000 kg and 8000 kg were dropped from different heights (2.5 m, 5 m, 10 m and 15 m), resulting in impact energies of 20-1200 kJ. Each impact process is filmed with high speed cameras and the deceleration has been measured with different sensors [3, 4]. Measured values like maximum deceleration values a_{max} and penetration depths p are shown in Figure 1.

Figure 1 depicts not only results of 186 experiments, but also lines representing the relationship between the maximum deceleration and the penetration depth given by the simple relation

$$a_{max} = \frac{v^2}{p} \qquad (1)$$

With a_{max} the maximum deceleration, v the velocity, and p the penetration depth [5].

[1] Swiss Federal Institute for Forest, Snow and Landscape Research WSL, Zuercherstrasse 111, 8903 Birmensdorf, Switzerland, +4144 7392111, werner.gerber@wsl.ch
[2] WSL Institute for Snow and Avalanche Research SLF, Fluelastrasse 11, 7260 Davos, Switzerland, +4181 4170111, andrin.caviezel@slf.ch

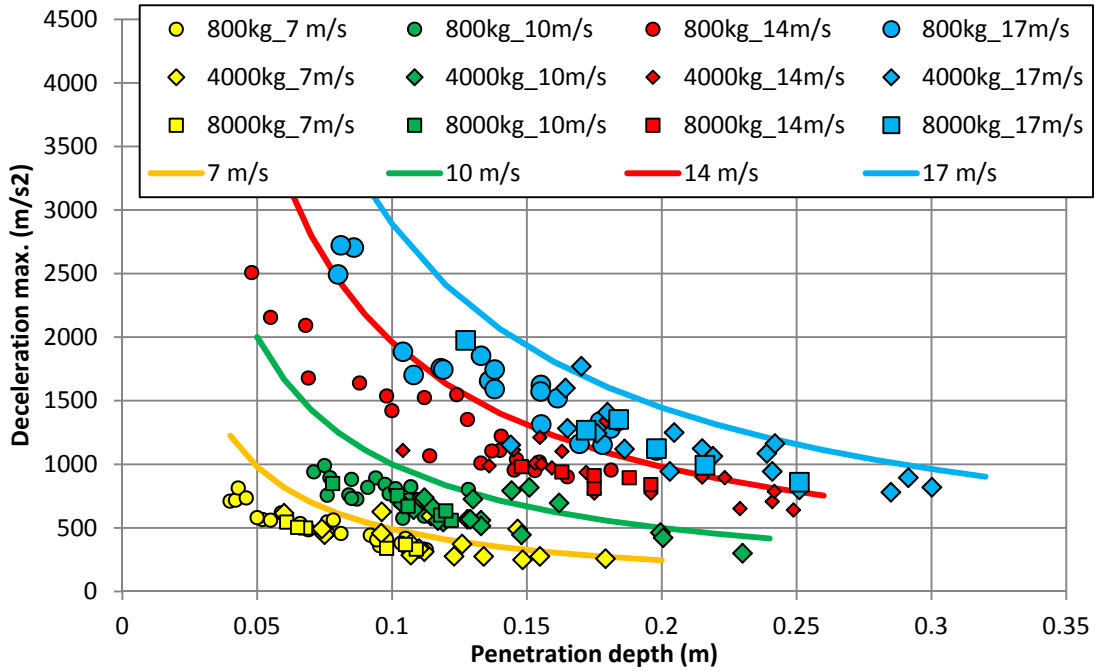

Fig. 1 Results of deceleration and penetration depth from 186 Impact tests.

The results show that almost all values are below the corresponding line with a few isolated values above the corresponding lines. In this article, we will clarify these diversities and calculate a deceleration factor f_d and a penetration factor f_p

$$f_d = a_{max} \frac{t}{v} \tag{2}$$

$$f_p = \frac{d}{v \cdot t} \tag{3}$$

Where t is the deceleration time during which the velocity v is reduced to zero and the penetration depth d is reached. The deceleration factor f_d compares the maximum deceleration a_{max} with an average deceleration calculated from the velocity v and the braking time t. The penetration factor compares the penetration depth with a distance theoretically traveled over braking time. In both of these factors, the acceleration due to gravity has been omitted since its influence is relatively small during the observed deceleration times of 10-50 milliseconds.

RESULTS

The results of the whole experimental ensemble bear no uniform distribution. There exist two areas, where the deceleration factors reach higher values than 2. This is, on the one hand, a penetration factor less than 0.44 and, on the other hand, a value of more than 0.58 (Figure 2).

Detailed analysis of the data set reveal, that for those two areas special experimental conditions have prevailed, which significantly differ from "normal" conditions, i.e. an uncompacted, thick enough deposition layer. In the area of small penetration factors, the results of tests with 800 kg mass are mainly based on compacted soil, as they were dropped into existing footprints of a larger block. These have relatively high deceleration factors of 1.8-2.4 and small penetration factors of 0.34-0.46. The other results with high penetration factors are tests

with a thin soil layer an relatively large mass. The masses of 4000 kg have been dropped on a layer of only 0.5 m in these 12 tests. They also show high decelerations factors of 1.5-2.1, but relatively high penetration factors of 0.57-0.64 (Figure 3). Due these differing experimental condition, those values - 15 data pairs (800 kg) on compacted soils, 12 data pairs (4000 kg) with the thin soil layer – have been discarded from further treatment. In addition, eleven data points from the other series offered similar experimental deficiencies an have been consequently omitted as well. Thus, 148 experiments yield the basis for the performed statistical analysis.

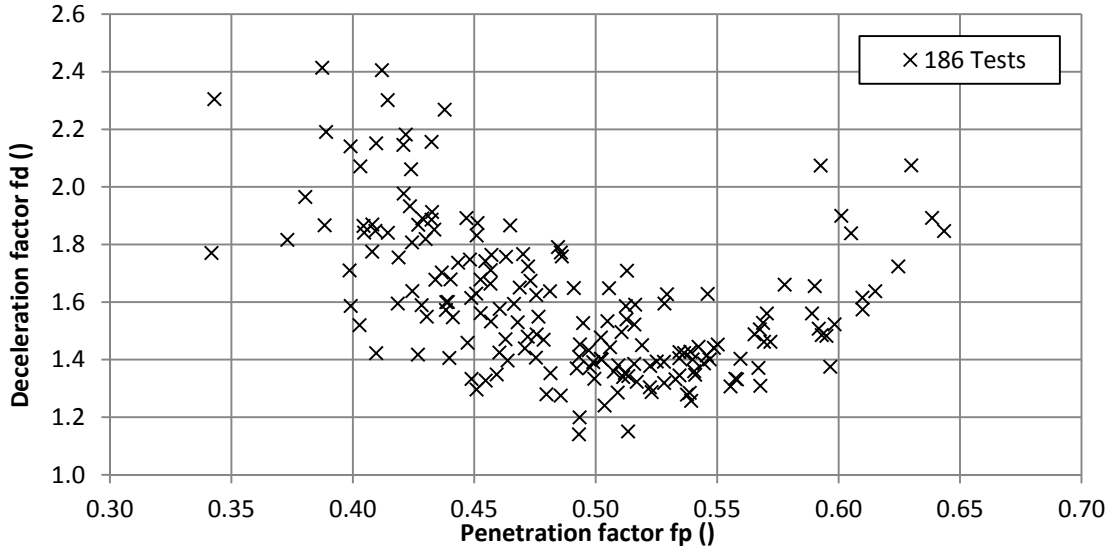

Fig. 2 Results of deceleration factors and penetration factors.

In the case of the deceleration factors, a mean value of f_d = 1.52±0.18. The penetration factors shows an average value of f_p = 0.49±0.05 (Figure 4).

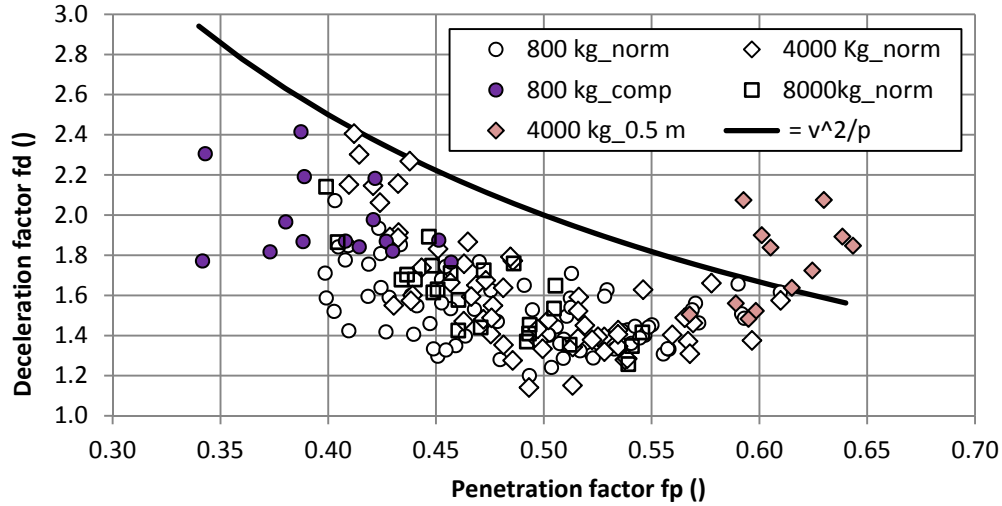

Fig. 3 Results of the different test series “compacted”, “normal” and “thin layer”.

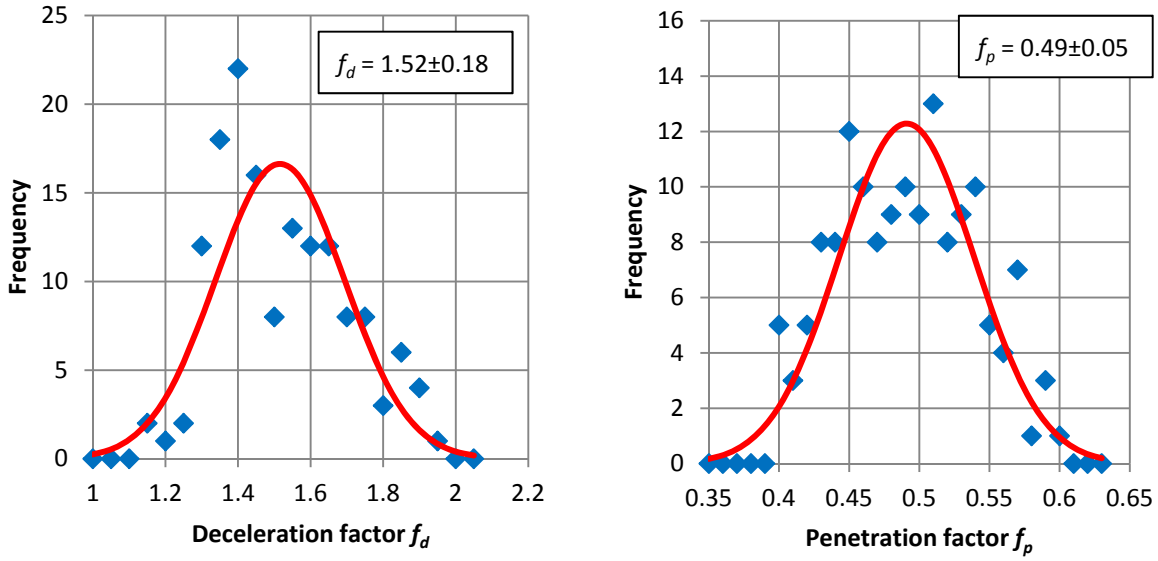

Fig. 4 Results of a 0.05 interval binning for the deceleration factor and a 0.01 interval binning for penetration factor.

CONCLUSIONS

The forces when impacting rocks depend not only on the properties of the soil, but also on the shape of the stone. In the presented data, standardized concrete bodies with flat ground surfaces have been used and therefore the decelerations are rather large and the penetration depths have been relatively small. On average, deceleration factors of 1.5 have been measured. Higher values occur with rather hard impacts. The harder the impact, the greater the deceleration factor. A deceleration factor of 1 means that an almost constant deceleration acts and the velocity decreases almost linearly. The penetration factor indicates the temporal occurrence of the maximum deceleration. For small values ($fp < 0.5$), the maximum lies in the first half of the braking time. At very high values ($fp > 0.6$), the maximum deceleration does not occur until nearly the end of the braking time. Whereas the penetrations factors have a relatively small standard deviation, the spread in the deceleration factors shows the diversity of impact behaviors even under standardized conditions as presented above.

REFERENCES

[1] ASTRA (2015) Erarbeitung von Grundlagen zur Bemessung von Steinschlagschutzdämmen. Eidgenössisches Departement für Umwelt, Verkehr, Energie und Kommunikation UVEK, Bundesamt für Strassen ASTRA, Bern. 295 S.

[2] SCHELLENBERG, K. (2008) On the design of rockfall protection galleries. Dissertation Nr. 17924, ETH Zürich.

[3] GERBER W, VOLKWEIN A (2010) Impact loads of falling rocks on granular material. In: Darve, F.; Doghri, I.; El Fatmi, R.; Hassis, H.; Zenzri, H. (eds) Euromediterranean Symposium on Advances in Geomaterials and Structures. Third Edition, Djerba, 337-342.

[4] GERBER W, VOLKWEIN A (2012) Fallversuche auf Bodenmaterial, Messung der Verzögerung. In: Koboltschnig, G.; Hübl, J.; Braun, J. (eds), 12th Congress INTERPRAEVENT Proceedings, International Research Society Klagenfurt, Vol 1, 143-149.

[5] ASTRA (2008) Einwirkungen infolge Steinschlags auf Schutzgalerien. Eidgenössisches Departement für Umwelt, Verkehr, Energie und Kommunikation UVEK, Bundesamt für Strassen ASTRA, Bern. 21 S.

CONDITION MONITORING SYSTEM FOR ROCKFALL CATCH FENCES

Hassan Al-Budairi[1]*, Zhiwei Gao[1], Andrew Steel[2], Trevor Davies[1], Simon Wheeler[1]

Rockfall incidents on catch fences along railways are generally monitored by regular site inspections. This inefficient and laborious process cannot ensure a high level of safety because incidents can happen between inspections. An alarm system is needed to signal these events in real-time to prevent accidents. A real-time condition monitoring system (CMS) for rockfall catch fences is currently under development. The proposed CMS is a compact device which is attached to the posts of catch fences: the device is activated by a built-in shock sensor. Proper selection of sensor characteristics is needed in order to provide reliable monitoring; to prevent the sensor from damage due to overloading and to prevent false alarms. In this study, a finite element model analysis of rockfall catch fences is used to predict CMS sensor requirements by simulating various impact scenarios.

Keywords: Rockfall monitoring, explicit finite element modelling, shock sensor

INTRODUCTION

The records of the British Geological Survey (BGS) show that there has been a significant increase in the number of rockfall accidents in the UK in recent years (Fig.1.) Rockfall accidents present a significant threat to transportation routes such as railways. Figure 2 shows a derailed train after collision with a fallen rock on a train line in Scotland, UK [2].

Low-energy rockfall catch fences are frequently used to protect railway infrastructure but these fences need to be monitored to ensure that they provide reliable protection. Currently, regular site inspections are conducted for catch fence maintenance but these are inefficient, time-consuming and expensive, as most catch fences are built in remote areas. Crucially, they cannot ensure a high level of safety because rockfall accidents can happen between inspections. In addition, when a rockfall event occurs, a rapid response is needed to avert accidents and to minimize disruption. Thus, a monitoring system with real-time notification capability can provide significant benefits.

[1] University of Glasgow, School of Engineering, Glasgow G12 8LT, UK, +44-141-330 5348,
*Corresponding author. Hassan.Al-Budairi@glasgow.ac.uk
[2] QTS Group, Strathaven, Scotland ML10 6QJ, UK, +44-1357 440 222, AndrewSteel@qtsgroup.com

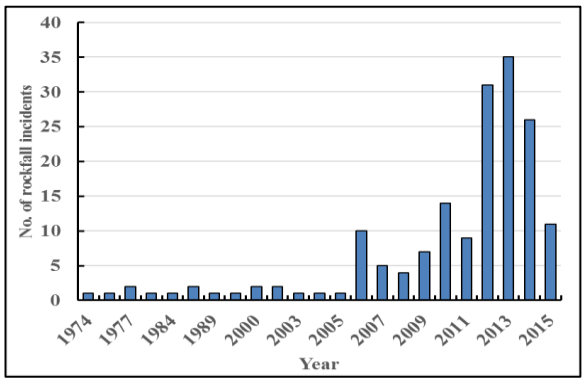

Fig. 1 Major rockfalls in the UK [1].

Fig. 2 Derailed train after collision with a fallen rock. [2]

A condition monitoring system (CMS) to remotely monitor rockfall catch fences is currently under development. The device has an integral shock sensor to monitor vibrations. When a rock impacts the catch fence, the sensor activates the CMS which transmits a signal through the mobile telephone network to pre-defined users. CMS has the ability to:

- send real-time warnings of rockfall incidents;
- provide detailed information of incident via photos/videos;
- work as an autonomous unit, thus increasing its reliability;
- run as a self-powered device, re-charged by solar cells;
- provide regular check data on the serviceability of the catch fence;
- perform health checks on itself.

The communication system between the CMS device and the control centre is illustrated schematically in Fig. 3.

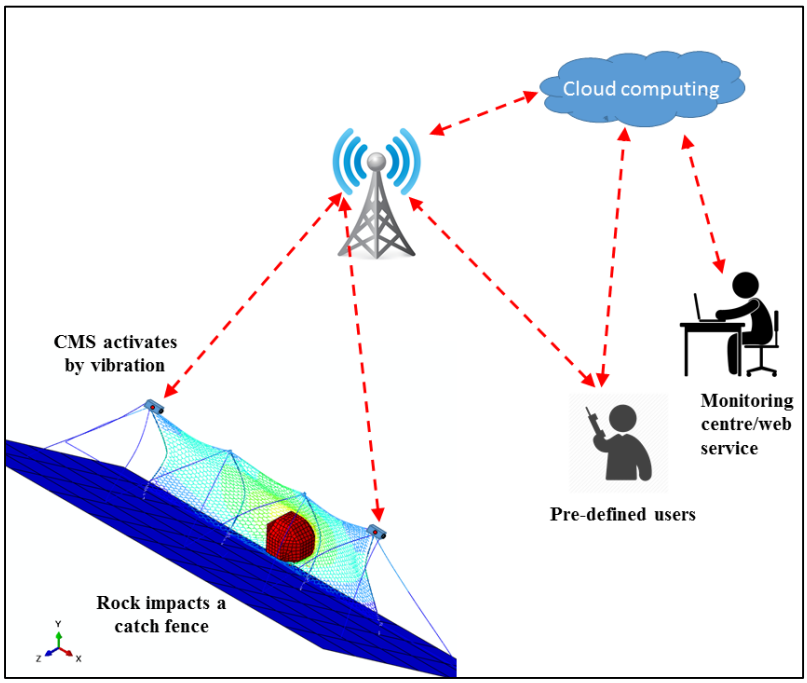

Fig. 3 CMS communication diagram.

MODELLING OF ROCKFALLS ON CATCH FENCES

To ensure that the monitoring device is only activated by serious rockfall incidents, the shock sensor should only trigger the CMS when predefined threshold vibrations are exceeded. To predict the required dynamic characteristics of the sensor (such as sensitivity, dynamic range and frequency response), a numerical model to simulate impacts on catch fences was created in Abaqus/Explicit [3]. A number of impact loading scenarios, involving a range of masses with various impact velocities, were simulated. The acceleration responses at the top of the posts, where the CMS devices would be located, were extracted.

The model can simulate a very wide range of catch fence designs, including arbitrary separation between the posts. For illustrative purposes, Fig. 4 shows a model of 12 m section of a low-energy catch fence with seven posts; the simulated acceleration responses on Post 5 due to the impact of a 1 tonne polyhedral boulder travelling at a speed of 10 m/s is presented in Fig. 5. Acceleration responses (raw) data are recorded for every time increment of the explicit solver in order to include the highest possible frequency response. The figure shows that the highest accelerations (which exceed 10E3 g) can be observed between 0.02 s and 0.06 s after impact.

However, explicit dynamic analysis of elastic-plastic impact behaviour using the finite element method can be corrupted by noise at high frequencies [4]. This particularly affects the calculation of accelerations. In order to remove this effect, data filtering using digital signal processing (DSP) was conducted by using a low-pass filter to delete the responses obtained at frequencies higher than a prescribed frequency threshold (cutoff frequency). The filtered acceleration data are presented in Fig. 5 which reveals in this case a peak vertical acceleration of c580 g and a peak lateral acceleration of c550 g.

To demonstrate that the filtered data are valid, and to avoid corrupted results by aliasing, these data were integrated to calculate velocity and displacement components. For illustrative purposes, the integrated results for displacements are compared in Fig. 6, with the data obtained directly from the Abaqus/Explicit analysis for Post 5 (P5). The agreement in the y and z directions is excellent and the difference in the x-direction is not significant. These differences might be reduced by further signal processing.

These data can be used to optimise the separation between CMS devices on the catch fence, by examining the attenuation of accelerations at neighbouring posts. Evidently, the interplay between sensor sensitivity, magnitude of the impact event and its remoteness from the sensor requires careful consideration in order to avoid false alarms on the one hand and the risk of failing to detect significant incidents on the other.

CONCLUSIONS

A condition monitoring system (CMS) which provides real-time notification of rock fall incidents enhances the capacity of rockfall catch fences to provide reliable protection for railways. A numerical approach has been developed to simulate rockfall impact on catch fences which shows promise as an aid to designing an optimum system.

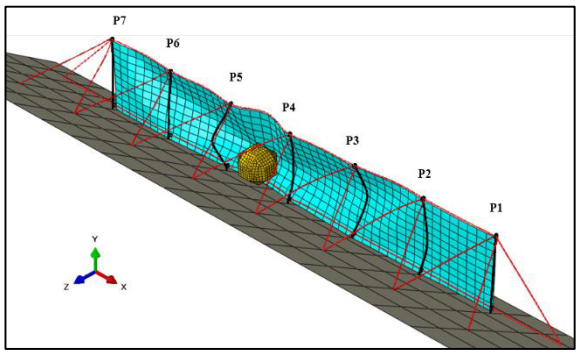

Fig. 4 Modelling of a rock impact on a low-energy catch fence.

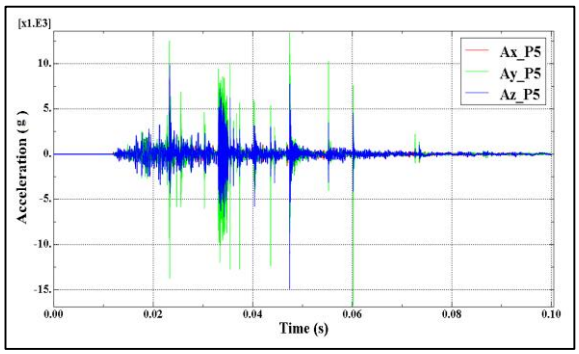

Fig. 5 Acceleration response components (raw data) of P5.

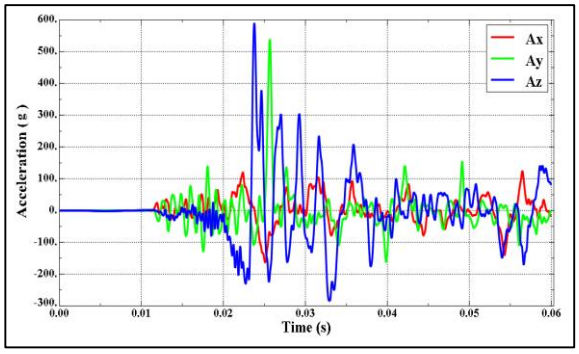

Fig. 6 Acceleration response components (filtered data) of Post 5.

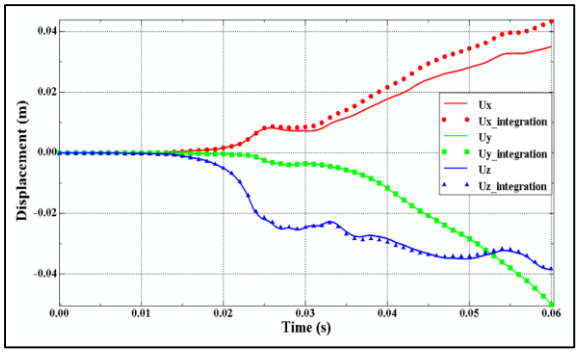

Fig. 7 Comparison between filtered and unfiltered displacement components of Post 5.

AKNOWLEDGEMENT

This research is funded by the Knowledge Transfer partnerships (KTP) programme (Project no. 9980) and QTS Group Ltd., a leading railway infrastructure services company in the UK (http://www.qtsgroup.com/). We acknowledge the contribution of **Mr Mark Craig** of QTS and the use of the High Performance Computing facilities provided by the School of Engineering, University of Glasgow.

REFERENCES

[1] DEPARTMENT OF TRANSPORT (2011) Rail Accident Investigation Branch (RAIB): Rail Accident Report.
[2] ABAQUS ANALYSIS USER'S MANUAL (2014) Dassault Systems Simulia Corp, Providence, RI.
[3] AL-BUDAIRI H, GAO Z, STEEL A, WHEELER S, DAVIES T (2016) Modelling and optimising of a light-weight rockfall catch fence system. NAFEMS UK Conference, pp 129-132.
[4] DIEHL T, CARROLL D, NAGARAJ B (2000) Applications of DSP to explicit dynamic FEA simulations of elastically-dominated impact problems. Shock and Vibration 7, pp 167-177.

WIRELESS MONITORING FOR CLIFF STABILIZATION AT LA CLUA (PRE-PYRENEES, SPAIN)

Clàudia Abancó[1], Carles Raïmat[2], Juan Pérez[1]

SUMMARY

La Clua is a village at the foot of a conglomerate cliff (Pre-Pyrenees, Spain), eventually affected by rockfalls. After last big event, in 2009, that affected a house of the village, a rope net was installed to protect the village. In order to obtain information about the performance of the protecting net, but also to gain knowledge on the triggering mechanism a wireless monitoring system was installed. The system is equipped with sensors (4 crackmeters, 2 biaxial tiltmeters, 2 rope tension load cells and 2 thermistors) that are measuring the changes on two unstable boulders (one protected with the net, the other not). Sensors are connected to wireless dataloggers, installed next to the sensors and send data to the gateway. In this site, gateway is located 250 m far from the furthest logger, but thanks to the long range technology of the system, loggers can be up to several km far from the gateway and the data which is pushed to an internet server every 15 minutes. Preliminary results show that no relevant movements have been observed in the boulders, since February 2016. Only some slight changes of around 0.15º have been observed after heavy rainfall events in spring.

Keywords: wireless, sensors, Pyrenees, rockfall, stabilization

INTRODUCTION

The conglomerate's cliff at La Clua village is located at the Southern part of the Pre-Pyrenees, near the village of Artesa de Segre (Lleida). The cliff, that has more than 300 m of longitude, where three families of discontinuities are present. The two vertical ones are almost orthogonal, which provide the cliff of a columnar aspect. The stratification is subhorizontal with clay levels, that invidualize the columns in the vertical. The combination of the three discontinuities, helped by the effects of weathering, makes big boulders susceptible of being unstable.
In 2009 a large rockfall event occurred, during a heavy rainfall episode. The event affected a house of the village, which was partially destroyed [1]. According to the amount of boulders cumulated at the foot of the cliff, the open joints, clearly visible, and the evidences of recent instabilities, the rockfall risk at the village appears to be high.
After several studies at the site to evaluate the instabilities, several potentially unstable blocs were identified, representing a total volume of 1700 m3. The main unstable areas were selected and, considering the elevated risk they were producing over the houses and people in the village, some actions were taken to stabilize them.

[1] Worldsensing, C/ Aragó 383, 4th , Barcelona 08013, Spain, 934180585, cabanco@worldsensing.com
2 Geobrugg Ibérica, C/ Gomera, 8, 1st B, Madrid 28703, Spain, carles.raimat@geobrugg.com

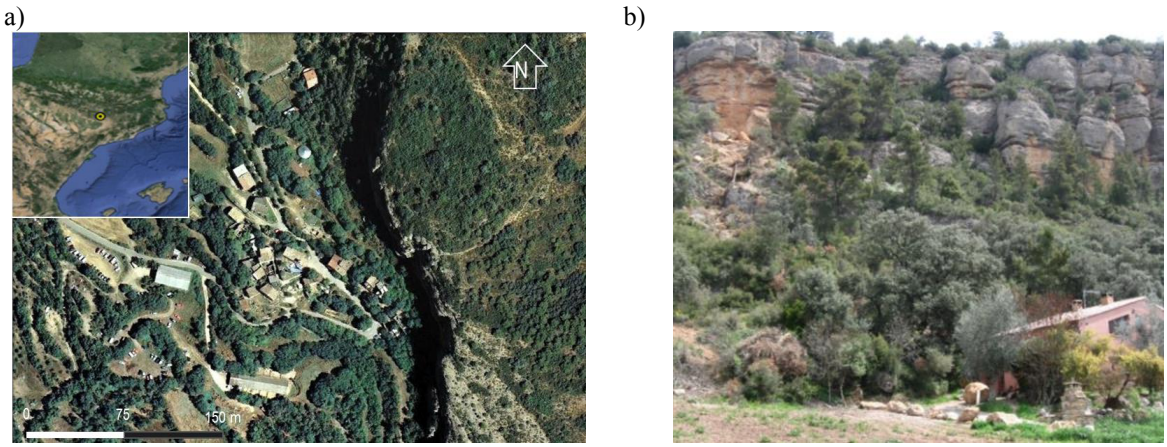

Figure 1: a) Aerial view of La Clua, and location of La Clua in Catalonia's map; b) Event occurred in 2009, it can be observed both the source area at the cliff and the affected house.

Punctual actions were carried out in three main unstable areas: a flexible stabilization system (SPIDER®, [2]) consisting in a spiral rope net made from high-tensile wire was installed covering the selected unstable area. Large flexible anchorages are fixing the net. The mission of the whole system is to increase the safety factor of the potential unstable boulders, which was close to 1. Additionally to the net installation, a wireless monitoring system was installed.

LONG RANGE WIRELESS MONITORING SYSTEM

The long range wireless monitoring system has a threefold purpose: a) to identify the triggering factors and the mechanism of instability, b) to study the behavior of the protecting elements and c) to get preliminary data for the design of an Early Warning System based on the monitoring of the triggering factors and protecting elements. The system consists of 4 analog dataloggers, reading data from a variety of sensors, and 1 gateway, equipped with wireless communications of very long range. In order to perform the purpose b), some part of the sensors were installed in the protected area, while others were installed in boulders where no protecting action was taken, so that the effect of the protecctng elements can be analyzed.
In Boulder 1 (no protecting net installed), 2 crackmeters, 1 biaxial tiltmeter and 2 thermistors, were installed. In Boulder 2 (protected), 2 other crackmeters, 1 biaxial tiltmeter and 2 rope tension load cells (installed in the horizontal wires that are reinforcing the protecting system) were installed. Sensors in Boulder 1 are located in two different locations, connected to two analog wireless dataloggers. All the loggers read and store data from sensors and send it to the gateway [3].
The long range radio technology that this system uses is based on a frequency band of 868 MHz. Thanks to this technology, the gateway can be installed up to 15 km far of the loggers (in best situation). In this specific project, gateway was placed in the front wall of one of the houses of the village, 250 m far from the loggers in Boulder 1 and Boulder 2. The gateway is powered by the standard electrical power, and it is connected to the internet using a GSM SIM card. The gateway has an embedded software, available for the user through a tunnel in a server. The software permits to visualize the data, download it, see the performance of the radio communications, but also permits to change the sampling rate of the sensors remotely. Thanks to this software, data can be automatically pushed to a FTP server, every 15 minutes.

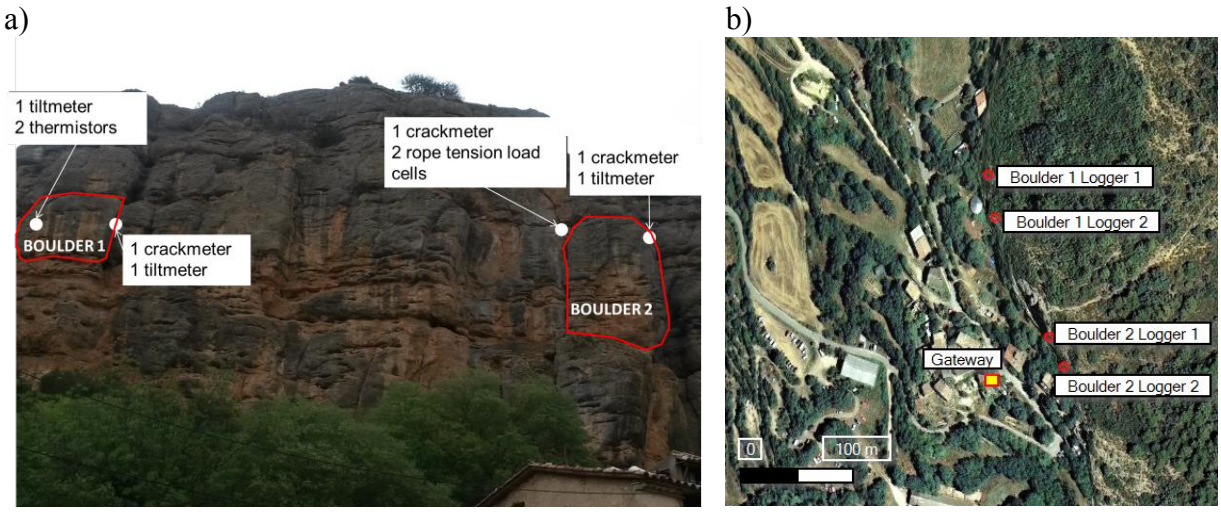

Figure 2: a) Location of the sensors at the cliff. Boulders 1 and 2 are identified; b) aerial view of the site. Gateway and loggers are located.

FIRST PRELIMINARY RESULTS

Installation of the monitoring system finished on February 2016. Since then, data sampling has been done with a hourly frequency for all the sensors. No rockfall event has occurred since then, neither in the protected nor the unprotected parts. Analysis of data series has been performed and some preliminary results can be highlighted.

On one side, no movement in the cracks other than the daily oscillation due to temperature has been observed. Also the rope tension load cells are showing daily oscillations due to contraction-retraction of the steel (Figure 3).

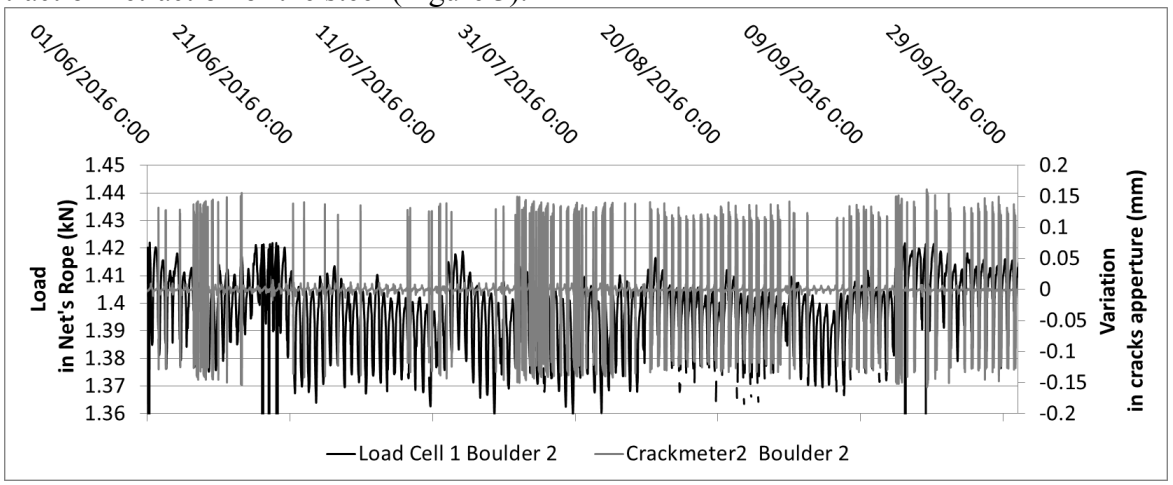

Figure 3: Data from Load Cell 1 in Boulder 2 and Crackmeter 2 in Boulder 2 from June to October 2016.

The tiltmeters did not show relevant movements along time, only some specific events when the tilt increased. Some of these events were correlated with rainfall data from a nearby meteorological station (Baldomar, from the public network, Figure 4). Between 9th and 13th of May, a special event was detected. A daily cummulated rainfall of 38,4 mm was detected. This rainfall episode had a maximum hourly precipitation of 12,3 mm. The correlation between the rainfall and the delayed movement of the boulder has been observed.

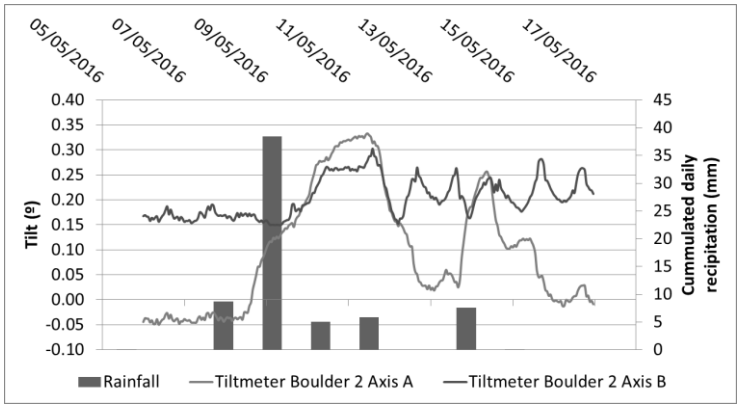

Figure 4: Correlation between daily cumulated rainfall in Baldomar (nearby station) and tilt in Boulder 2.

CONCLUSIONS

Wireless monitoring systems are a suitable system for remote monitoring in situations where wired systems are difficult to install, such as rockfall prone sites. The wireless long range radio communications make possible to have data from sensors spread in a extense area remotely available. Data collected in La Clua since February 2016 is the beginning of a dataseries that will be completed after a period of time and that will permit to develop an early warning and alarm system for the rockfall prone cliff.

Triggering mechanisms of the instability have still not been clearly identified, but the correlation between the rainfall and some small episodes of movement in the tiltmeters has been detected.

ACKNOWLEDGEMENTS

The authors of this work want to acknowledge collaboration from: Ajuntament Artesa de Segre, Institut Cartogràfic i Geològic de Catalunya, and the company Eurogeotècnica.

REFERENCES

[1] Geobrugg, Spider Technical datasheet
[2] WORLDSENSING S.L., Loadsensing user guide v1.7.

REAL-TIME ROCKFALL DETECTION WITH DOPPLER RADARS

Lorenz Meier[1], Mylène Jacquemart[1], Susanne Wahlen[1], Bernhard Blattmann[1]

Rockfall presents a threat to roads, railways and building infrastructure as well as livelihoods in mountainous areas around the world. Traditional protection measures, such as tunnels and protection netting, are often expensive to build, impractical to install and maintain. We have successfully applied Doppler radar systems for automatic rockfall detection and mapping in real time and we propose they be integrated into rapid response alarm systems. This type of radar system allows the control of transportation corridors at risk of rockfall by reacting with automatic closure of roads or other infrastructure only seconds after an event was indicated.

Keywords: rockfall, detection, radar, warning system, alarm system

INTRODUCTION

Rockfall mitigation is traditionally addressed with massive constructive structures, such as nets or dams, and galleries or tunnels. In an alternative approach, it is accepted that rockfalls occur, however, safety is guaranteed by continuously monitoring and detecting rockfall to provide an alarm signal which closes the hazardous zone. Two different types of early warning systems exist; Warning and alarm systems [1]. *Warning systems* measure slow deformations, such as rock instabilities or glaciers, and detect accelerating areas as precursors of an event, e.g. rock or ice failures. In this case, an interferometric radar is used to monitor these changes [2]. Lead times for warning systems range from several hours to months. Mitigation measures are then organized by experts and include road closures, evacuation or the installation of additional equipment. In contrast, *alarm systems* measure an event in real-time permitting automatic and immediate action that are already in place. Lead times for alarm systems are between seconds and minutes. For this purpose, Doppler radar systems are applied due to their ability for instantaneous measurement of various types of movements in the target area.

We report on a site where we installed a Doppler radar system that permanently monitors about 0.5 km^2 of terrain and automatically sends an alarm message if rockfall activity is detected. For events with sufficient warning time, the signal can be used to temporarily close a road or a railway within seconds, preventing cars or trains from running into a hazardous zone. To date, we have installed and successfully operated ten similar systems worldwide to detect snow avalanches, for example in Zermatt/Switzerland. The village of Zermatt has single access road which is prone to avalanches. Two radars scan the avalanche slope and automatically control four traffic lights covering the according road sections at risk. [3].

[1] GEOPRAEVENT AG, Technoparkstrasse 1, 8005 Zürich, Switzerland

METHODS

Radar technology has become increasingly popular in the field of natural hazards. The main advantages of radar are:

- Radar works independently of weather conditions and visibility, i.e. at night, during fog, rain or snow fall;
- One radar system can cover an area up to several km^2;
- No instrumentation is required inside the target area.

For this application, Doppler radar systems are used over interferometric radars [4] as Doppler radars detect movements of velocities above a few meters per second, whereas interferometric radars measure small scale deformations (e.g. submillimeter) between two acquisitions.

The rockfall detection radar system was installed during the summers of 2015 and 2016 in the village of Brinzauls in Switzerland at 1144 m a.s.l. The *Igl Slide* is a well-known active landslide, with a relief of 1 km wide and 400 m high, situated close to the village (Fig. 1). The road to the village crosses below the slide. Rockfall events happen on a regular basis, especially during days with heavy precipitation. Rocks are released in the upper scarp of the slide and quickly disintegrate to form 'rock avalanches' with thousands of particles involved. Larger rocks on the order of a few cubic meters have almost come as far as the road (Fig. 2).

The radar system installed in the village of Brinzauls 'sees' all movements in the slide area within the antenna field of view (FOV) if the target cross section is large enough to exceed the detection threshold within a certain distance from the radar. For example, the system can detect a person walking at a distance of up to 1'300 m from the radar. This roughly corresponds to a rock with a volume of 0.5 m^3. The FOV measures 90° horizontally by 10° vertically. Fig. 3 shows the simulated coverage obtained with a digital terrain model. All movements in this area with a sufficient cross section are registered by the radar. Proprietary algorithms analyze the data in real-time and decide whether the movement is a relevant mass movement (e.g. rockfall or snow avalanche) or something else (e.g. birds or a helicopter). If an event is detected, immediate action can be taken. The event is localized and displayed on an online map within minutes (Fig. 4). In the case of the snow avalanche system in Zermatt, immediate measures involve automatic road closures and informing the authorities via text messages.

To date, the ten real-time radar systems of this kind have detected more than 1'600 snow avalanches with very high probability of detection (no missed events known up to now) in addition to keeping a very low false alarm rate (less than 10 false alarms up to now). The Brinzauls system applied the same algorithms with parameters adapted to rockfall.

RESULTS

In summer 2015, the system was working in 'passive mode', i.e. data was acquired but not analyzed in real-time. We used this data to optimize the detection algorithms for rockfall. From June 14, 2016, to December 6, 2016, the system was operational in 'real-time mode' and detected 50 rockfall events during this period. All events were automatically mapped online and camera images were taken. Events were verified manually using these camera images. When

visibility was bad, we used the audio signal of the video camera for verification of events. Additionally, raw radar data was manually inspected after each event to confirm the rockfalls. Lastly, we compared camera images taken before and after an event and searched for impact craters in the terrain caused by the falling rocks. We are convinced the 50 detected events all were actual rockfalls and the system did not miss any significant event. It is important to note that there is no 'reference data set' containing a perfect list of events. Nonetheless, we strongly believe that radar is the most reliable tool to detect mass movements, such as rockfall or snow avalanches, and that currently there is no superior technology with the ability to generate a reference data set to use as a benchmark.

During the measurement period in 2016, a total of three false alarms were registered by the radar, all related to heavy thunderstorms and high speed rain fronts moving towards the radar. The false alarm rate was considerably higher than for avalanches in winter due to strong signals from heavy rain. This issue has been addressed in a revised software version.

CONCLUSIONS

We have successfully operated a radar system for real-time detection and mapping of rockfall events in Brinzauls. An area of approx. 0.5 km^2 was monitored from June to December 2016 and 50 rockfall events were identified. The system did not miss any relevant events. We currently plan to add traffic lights for summer 2017 and include automatic road closure.

Given that in most cases rockfall does not reach the road, the system is designed to function as follows:

- The road is closed immediately as soon as rockfall activity is detected.
- The falling rocks are tracked by the radar: If they do not exceed a predefined boundary towards the lower portion of the slide, the event is considered 'small' and the road is reopened automatically.
- If the rocks pass beyond the boundary, the road remains closed and the authorities are informed. They can then inspect the road remotely using a pan-tilt-zoom camera. If debris is not visible on the road, it can be reopened remotely.

Fig. 1 The landslide area behind the village of Brinzauls with a typical event captured in the area left of the slide.

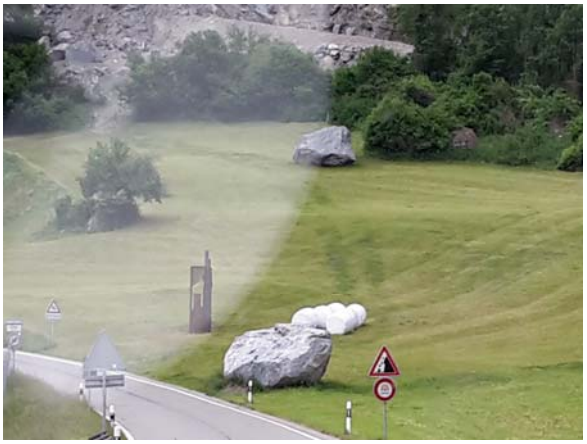

Fig. 2 Most – but not all – rocks come to a stop on the debris cone or are retained in the protection dam.

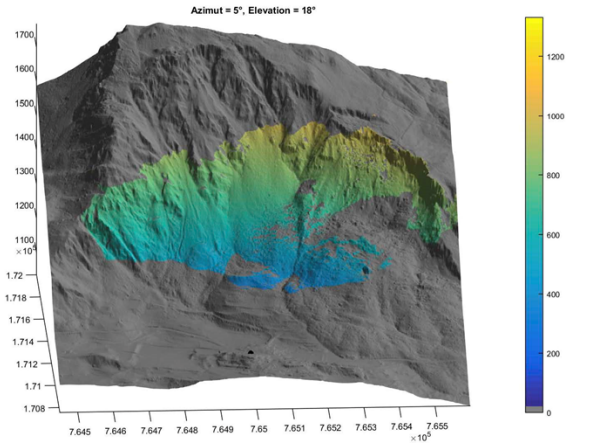

Fig. 3 Simulated radar coverage area. Colors indicate distance from the radar in meters.

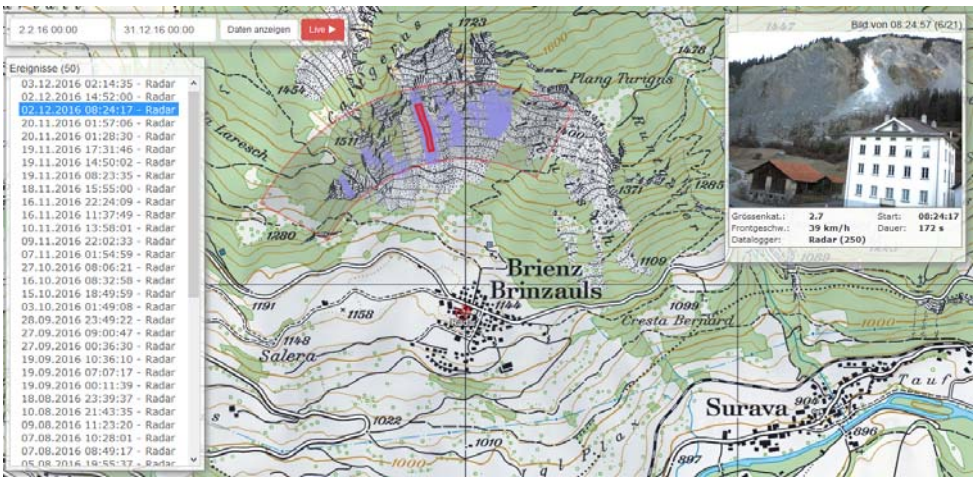

Fig. 4 All events are mapped immediately after detection on an online web portal. In addition, camera images are taken and uploaded automatically.

REFERENCES

[1] Martina Sättele, Michael Bründl, Daniel Straub, Classification of warning systems for natural Hazards, Proceedings of the 10th International Probabilistic Workshop, Stuttgart 2012

[2] Monserrat O., Corsetto M., Luzzi G. (2014). A review of ground-based SAR interferometry for deformation measurement. ISPRS Journal of Photogrammetry and Remote Sensing, Vol. 93, pp. 40-48.

[3] Lorenz Meier, Mylène Jacquemart, Bernhard Blattmann, Bernhard Arnold: Real-Time Avalanche Detection with Long-Range, Wide-Angle Radars for Road Safety in Zermatt, Switzerland. Proceedings, International Snow Science Workshop, Breckenridge, Colorado, 2016, p. 304 ff.

[4] Lorenz Meier, Mylène Jacquemart, Bernhard Blattmann, Sam Wyssen, Bernhard Arnold, Martin Funk, Radar-based Warning and Alarm Systems for Alpine Mass Movements, INTERPRAEVENT 2016 Conference Proceedings.

ACKNOWLEDGEMENTS

The authors would like to thank the authorities of Brinzauls and the Canton of Grisons.

A PROBABILISTIC APPROACH TO INTEGRATE THE EFFECT OF PROTECTION SYSTEMS INTO ROCKFALL HAZARD ASSESSMENT

David Toe[1], Alessio Mentani[2], Franck Bourrier[1], Laura Govoni[2], Guido Gottardi[2], Stéphane Lambert[3]

The paper introduces the essential features of a new strategy to develop reliable and computationally cost-effective models of the mechanical response of a rockfall barrier subjected to realistic impact conditions. The approach combines the use of three-dimensional, non-linear and dynamic finite element models of a rockfall barrier with a reliability-based probabilistic approach. The strategy may apply to any type of rockfall barrier in presence of any condition of impact and it is devised so it can be implemented in rockfall propagation simulation tools. Applications of the approach are wide and includes the evaluation of the residual hazard down existing protection works and the reliable planning of new interventions.

Keywords: rockfall hazard, FEM, non-linear dynamic analysis, probabilistic approach, protection structures

INTRODUCTION

Rockfall propagation simulation tools generally use a process-based probabilistic approach to predict the energy and the trajectories of blocks falling along potentially unstable slopes. These tools play a crucial role in rockfall hazard assessment and design of mitigation interventions. The effect of the protection structures is described within these tools by a location, a height and a capacity [1, 2]. The value of capacity, which might not be available, is given as a result of full-scale tests on prototypes carried out in standardised conditions, assuming that impact parameters other than the kinetic energy have no influence on the barrier ultimate response. Suitably calibrated and developed numerical models of these structures [4, 5] could certainly allow a more comprehensive description of the rockfall barrier within these tools through a simulation of the likely response of the barrier during each rockfall propagation. However, the high computational cost associated to a procedure as such would make the approach unpractical. On the other hand, in order to have a reliable prediction of the residual hazard down the structure, the effect of impact conditions on the structure response should be accounted for. This is especially crucial for semi-rigid, low to medium energy barriers (less than 250 kJ), whose capacity have been shown to be very much dependent on the impact conditions [6, 7, 8]. In this context, a strategy to develop reliable and computationally cost-effective models of the mechanical response of a rockfall barrier subjected to realistic impact conditions is presented with reference to a semi-rigid barrier currently installed within the Alpine arc. Numerical analyses carried out in ETAG-like conditions, which involved the cen-

[1] Irstea, 2 rue de la papeterie, 38402 Saint Martin d'hères, France, franck.bourrier@irstea.fr
[2] University of Bologna, Department of Civil, Chemical, Environmental and Materials Engineering, Vial Risorgimento 2, Bologna 40136, Italy, 051 2093521, l.govoni@unibo.it
[3] Irstea, 2 rue de la papeterie, 38402 Saint Martin d'hères, France, stephane.lambert@irstea.fr

tral impact of a prismatic block of length equal to one third of the barrier height, showed that the barrier capacity was about 200 kJ. The FE model was then subjected to further 600 simulations in which the impact related parameters were varied within a range typical of rockfall trajectory analyses. Results were used to build a meta-model of the barrier response. The scope of the meta-model is to reproduce the barrier effect for any impact event into a common rockfall simulation model. The meta-model uses a reliability-based approach and provides, for a low cost-efficiency ratio, the response of the structure in terms of its ability in stopping the block and residual block kinetic energy in case of structure failure.

FE INVESTIGATION OF THE PERFORMANCE OF A SEMI-RIGID BARRIER

Rockfall protection barriers are structures composed by a certain number of single functional modules. Each module is made of an interception structure, a supporting structure and connecting components. In the following, a semi-rigid barrier is analysed with the aim of predicting its response to impact events. The studied barrier is 3.2 m high with three modules of 5 m width each [10]. The principal interception structure, composed by 15 longitudinal cables of 12 mm diameter, is connected to the posts, which constitute the supporting structure. Internal and lateral posts are IPE 200 and IPE 300, respectively. As secondary interception structure, a double-twisted hexagonal meshwork is installed. Whereas its presence is not of interest when modelling flexible barrier with high energy absorption capacity, it can considerably affect the performance of semi-rigid systems [10]. Finally, side cables of 18 mm diameter connect the head of the lateral posts to the ground (Fig. 1).
The numerical model is built using one-dimensional elements with elasto-plastic constitutive laws assigned to each element. Details of the mechanical properties are provided in [10], while the behaviour of the double-twisted mesh refers to [7]. The barrier is considered installed vertically to the ground. 600 non-linear explicit dynamic simulations, with different loading conditions, are carried out to investigate its response to polyhedral shaped impacting bodies. Analyses were run by varying five parameters of the event conditions: the block volume, translational and rotational velocities, impact point position and inclination of the incident trajectory. The system is considered failed when the block is not arrested and goes beyond the structure. Figure 2 illustrates the results of the simulations in terms of block volume and horizontal velocity at impact. Green symbols represent cases where the block was arrested, while the other colours indicate the failure mechanisms associated to each simulation.

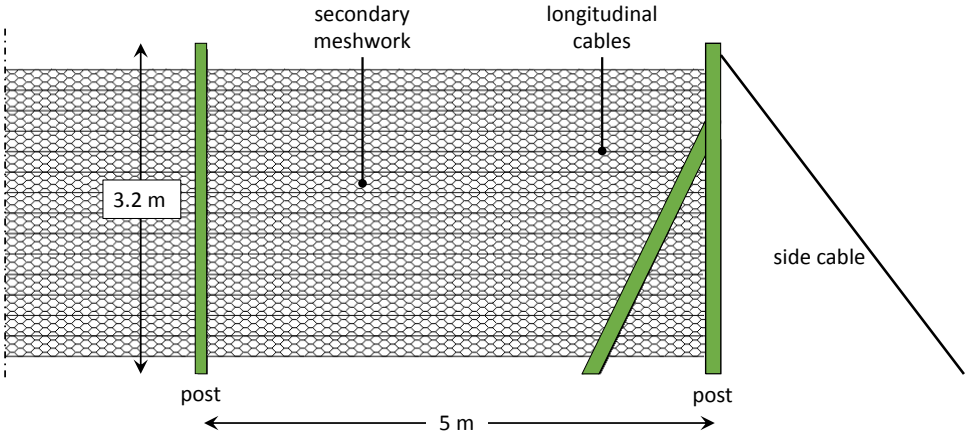

Fig. 1 The semi-rigid barrier studied (half model)

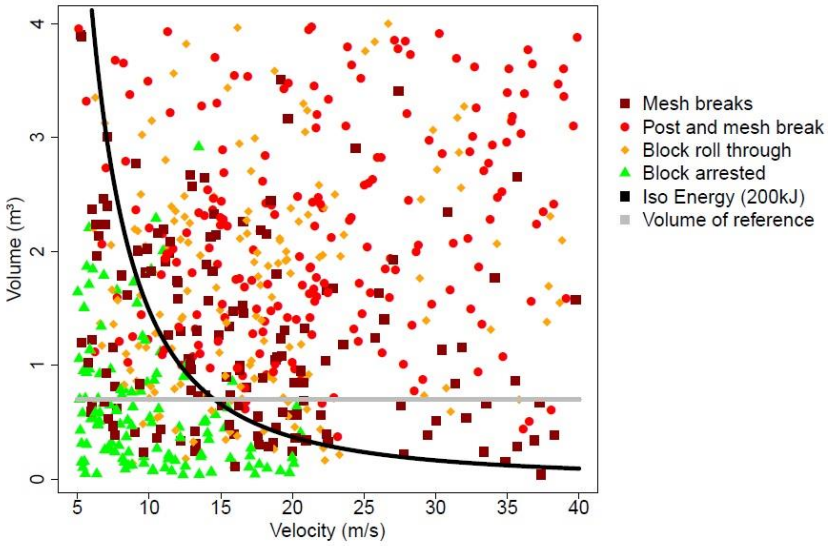

Fig. 2 FEM results of simulations to different impact events

When rupture of the system is reached, red dots stand for failure of the posts, while brown nodes are cases for which the mesh failed after the block passed through the longitudinal cables and orange symbols represent for the cases where the block rolls over the structure i.e. block impacting the mesh at the top). The black curve represents the limit energy level identified in [10]. Similarly, the grey line is the maximum volume to be considered following [9] (i.e. 1/3 of barrier nominal height).
It can be seen that none of this two lines allow differentiating failure and non failure cases. In particular, a significant number of mesh ruptures are observed below these limits. This demonstrates that, due to the high dependence of the structure performance on the impact conditions, currently used design methods based on deterministic approaches fail in addressing the performance of a semi-rigid barrier. The FE model helps to identify the barrier behavior, both in case of failure or not. On the other hand, it also provides several data for each simulation about the post-impact trajectory of the block. These data can be implemented in a probabilistic approach to create a meta-model of the barrier, able to predict its response for every impact event, as illustrated in the next section.

PROBABILISTIC MODEL OF THE BARRIER RESPONSE

The probabilistic approach allows developing a meta-model of the response of the structure. It basically corresponds to the response envelop of output parameters depending on the 6 parameters defining the impact conditions. The response is addressed in terms of structure capacity in arresting the block, via the performance function G proposed in [11], and residual energy of the block if not stopped by the barrier. For example, Fig. 3 (a) gives the cumulative probability of these two variables in the case of the structure presented previously and considering the widest possible ranges for the 6 input parameters.
The meta-model of the response of the structure may be implemented into block propagation models to integrate the effect of the protection structure. Such improved propagation model can be used to quantify the efficiency of protection structures on endangered sites. This quantitative assessment of structure efficiency is of major interest for the optimal design and location of protection structures.

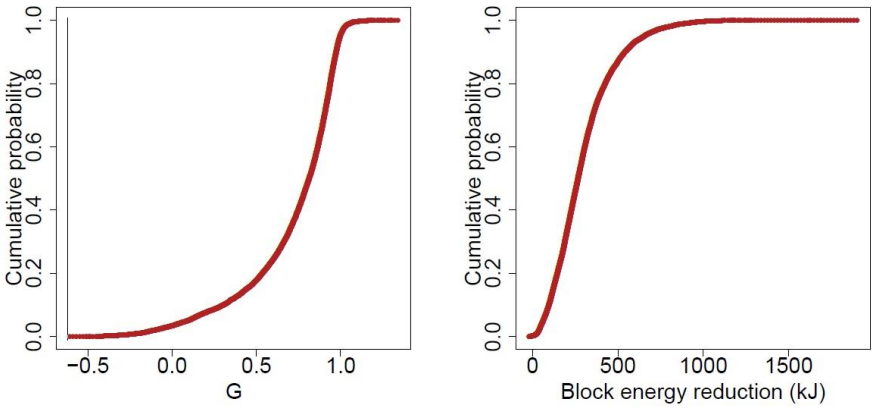

Fig. 3 Meta-modeling results in terms of (a) perfomance function G and (b) and block kinetic energy reduction.

CONCLUSION

The combination of three-dimensional, non-linear and dynamic finite element models of a rockfall barrier with a reliability-based probabilistic approach presented allowed developing computationally efficient meta-model of the response of the structure. This meta-model allows assessing the structure capacity in arresting the block and the residual energy of the block if not stopped by the barrier.
It can easily be implemented into block propagation models to integrate the effect of the protection structure. Such an improved propagation model can be used to quantify the efficiency of protection structures on endangered sites. This quantitative assessment of structure efficiency is of major interest for the optimal design and location of protection structures.

REFERENCES

[1] AGLIARDI F, CROSTA GB, FRATTINI P (2009) Integrating rockfall risk assessment and countermeasure design by 3D modelling techniques. Natural Hazards and Earth System Sciences 9, 1059-1073
[2] BOURRIER F, DORREN L, NICOT F, BERGER F, DARVE F (2009) Toward objective rockfall trajectory simulation using a stochastic impact model. Geomorphology 110, 68-79
[4] VOLKWEIN A, VOGLE A, GERBER W, ROTH A (2009) Flexible rockfall barriers subjected to extreme loads. Struct. Eng. Int. 19, 327-332
[5] GENTILINI C, GOTTARDI G, GOVONI L, MENTANI A, UBERTINI F (2013) Design of falling rock protection barriers using numerical models. Engineering Structures 50, 96-106
[6] SPADARI M, GIACOMINI A, BUZZI O, HAMBLETON JP (2012) Prediction of the bullet effect for rockfall barriers: a scaling approach. Rock Mechanics and Rock Engineering 45, 131-144
[7] MENTANI A, GIACOMINI A, BUZZI O, GOVONI L, GOTTARDI G, FITYUS S (2016) Numerical modelling of a low-energy rockfall barrier: new insight into the bullet effect. Rock Mechanics and Rock Engineering 49, 1247-1262
[8] MENTANI A, GOVONI L, GOTTARDI G, LAMBERT S, BOURRIER F, TOED D (2016) A new approach to evaluate the effectiveness of rockfall barriers. Proc. 6th Italian Conference of Researchers in Geotechnical Engineering, CNRIG 2016, Bologna, Italy pp 398-403.
[9] EOTA (2013) Guideline for European technical approval of falling rock protection kits (ETAG 027), Brussels, 59p
[10] DE MIRANDA S, GENTILINI C, GOTTARDI G, GOVONI L, MENTANI A, UBERTINI F (2015) Virtual testing of existing semi-rigid rockfall protection barriers. Engineering Structures 85, 83-94
[11] BOURRIER F, LAMBERT S, BAROTH J (2014) A reliability-based approach for the design of rockfall protection fences. Rock Mechanics and Rock Engineering 48 (1), 247-259

A METHOD FOR INTEGRATING THE EFFECTS OF FORESTS ON ROCKFALLS INTO QUANTITATIVE RISK ANALYSIS – A CASE STUDY IN SWITZERLAND

Christine Moos[1], Michael Fehlmann[2], Daniel Trappmann[3], Markus Stoffel[4], Luuk Dorren[5]

Although the protective effect of forests against rockfall is widely recognised, a holistic approach to include forests in quantitative risk analyses is missing. In this study, we present a general framework to integrate forests into quantitative rockfall risk analysis and apply it in a case study. The results demonstrate that risk is critically reduced on the forested compared to the non-forested situation. The presented methodology allows for quantification of the forest effects in monetary terms.

Keywords: rockfall, protection forest, quantitative risk analysis, rockfall simulation model

INTRODUCTION

Quantitative risk analyses have successfully been applied for designing and assessing structural measures that protect from natural hazards such as rockfalls [1]. They allow quantification of the positive effects of the protective structure and the associated uncertainties in monetary terms and evaluation of its efficiency in a cost-benefit analysis [2]. Although quantitative risk analyses have been well established for structural protection measures [3, 4], they have hardly been applied to forests that serve as natural protection from rockfalls [5]. This, however, would be necessary in order to compare them to structural measures and make their benefits quantifiable. Several studies showed that trees can stop falling rocks or reduce their energy after collisions [e.g. 6, 7]. Hence, many forests serve as effective barriers and reduce the intensity and propagation probability of rockfall at a given element at risk [8]. In this study, we firstly present a general framework for integrating protection forests into quantitative rockfall risk analysis. Secondly, we apply the proposed methodology in a case study in Switzerland and quantify the risk reduction due to forest effects by comparing rockfall risk for forested and non-forested conditions.

GENERAL FRAMEWORK

The methodological framework presented here is based on the effects of forests in the transit and deposit zone. Forests do hardly influence the release of rocks and have therefore no effect on the onset probability. In contrast, they do influence the propagation of rocks and their kinetic energy. Therefore, it can be expected that the propagation probability and thus the occurrence probability, as well as the intensity, at a given element at risk differ between forested and non-forested conditions. The onset frequency of rockfalls depends on its magnitude M and can be described with a magnitude-frequency relationship. Power law distributions have proved to fit the release volume distribution of rockfalls [9]. In case the power law is fitted based on a catalogue of block volumes with a minimum volume V_0, the annual exceedance frequency can be written as:

[1] Bern Univ. of Applied Sciences - HAFL, Länggasse 85, CH-8052 Zollikofen, Switzerland (CH), christine.moos@bfh.ch
[2] Institute for Environmental Science, University of Geneva, 66 Bvd Carl Vogt, CH-1205 Geneva, CH, michael.fehlmann@unige.ch
[3] Institute for Environmental Science, University of Geneva, 66 Bvd Carl Vogt, CH-1205 Geneva, CH, daniel.trappmann@dendrolab.ch
[4] Institute for Environmental Science, University of Geneva, 66 Bvd Carl Vogt, CH-1205 Geneva, markus.stoffel@unige.ch
[5] Bern Univ. of Applied Sciences - HAFL, Länggasse 85, CH-8052 Zollikofen, Switzerland (CH), luuk.dorren@bfh.ch

$$F(V \geq V_j) = A \times (V_j/V_0)^{-\beta} \quad (1)$$

Where $F(V \geq V_j)$ is the exceedance frequency of volume V_j. A is the anuall onset frequency of blocks with $V \geq V_0$ [10]. For a specific scenario j of a volume range from V_j to Vj_{+1}, the onset frequency is calculated as:

$$F_{onset,j} = F(V_j \leq V < V_{j+1}) = F(V \geq V_j) - F(V \geq V_{j+1}) \quad (2)$$

The propagation of the falling blocks depends on their size and shape and the slope conditions, such as the damping capacity of the soil, the surface roughness or standing or lying trees [11, 12].There is a wide range of empirical or physical models in 2 or 3D for analyzing rockfall trajectories of which only a few integrate the effect of trees [e.g. 13, 7]. The propagation probability $P_{prop,j,i}$ at a certain element at risk i for a certain volume scenario j can be determined as the ratio of the potential rockfall paths of volume j passing through position i (number of passages $Nrp_{i,j}$), and the total number of simulated blocks from the rockfall source, Nrp_{tot}. The occurrence frequency $F_{occ,i,j}$ of a specific volume scenario j at the element at risk i is consequently:

$$F_{occ,i,j} = F_{onset,j} \times P_{prop,i,j} \quad (3)$$

The kinetic energy of blocks at position i is usually used as measure for their intensity I. Since rocks from different sources can reach the location i, their energy distribution has to be considered [2]. Based on the simulation results, the relevant components of the forest effect can be quantified in terms of risk. For a specific element at risk i, the risk $R_{i,j}$ of volume scenario j is defined as:

$$R_{i,j} = F_{onset,j} \times P_{prop,i,j} \times E_i \times P_{presence,i} \times \frac{1}{Nrp_{i,j}} \sum_{Nrp} V(I)_{i,j} \quad (4)$$

With E_i the total value of the objects and persons of element at risk i considering their presence probability $P_{presence}$, and $V(I)_{i,j}$ their vulnerability to possible impacts $Nrp_{i,j}$ of volume scenario j depending on the intensity I.

CASE STUDY

We applied this framework to a forested rockfall slope in Täsch, in the southern part of Switzerland. We derived the onset frequency based on a magnitude-frequency relationship of block deposits behind a dam. Additionally, dendrochronological data was used to estimate the annual onset frequency of past rockfall events [14]. For determination of the propagation probability $P_{prop,i,j}$ and the intensity I, block trajectories were simulated with the rockfall module Rockyfor3D for forested and non-forested situations for 23 volume classes between 0.05 and 20 m^3 derived from the magnitude-frequency relationship. Terrain roughness and soil types were assessed in the field and mapped in homogenous polygons according to the parametrization in RockyFor3D [15; Fig.1]. They were used for simulations with and without trees. The forest was represented based on the mean number of trees per ha and mean and standard deviation of their diameters at breast height (DBH). We estimated these parameters based on measurements of 10 representative plots (20 x 20 m). The monetary value E_i of an element at risk i is the sum of object values and the monetized values of persons present. The parameters required for the calculation were estimated based on geodata, data from municipal and cantonal authorities and field surveys and mapped in a GIS.

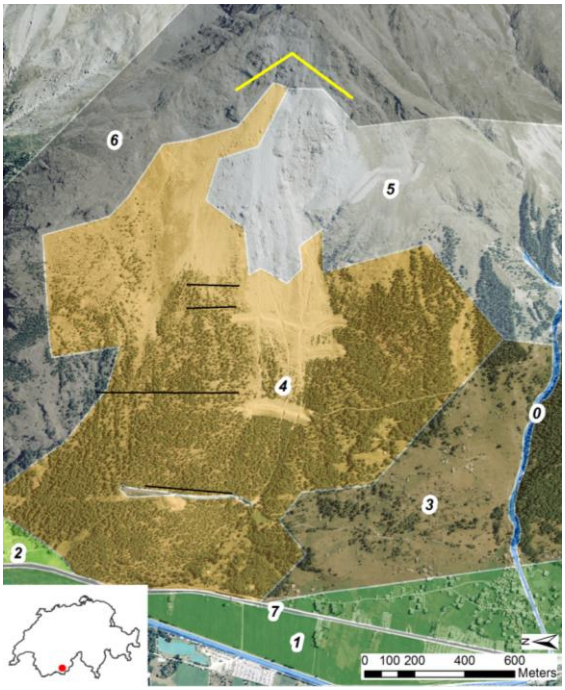

Fig. 1: Study site in Täsch with release line (yellow) and slope type parameterization for rockfall simulations. Slope types in Rockyfor3D: 0 = River, 1= Fine soil material (> 100 cm), 2 = Fine soil material (< 100 cm), 3 = Scree or medium compact soil with small rock fragments, 4 = Talus slope or compact soil with large rock fragements, 5 = Bedrock with thin weathered material or soil cover, 6 = Bedrock, 7 = Asphalt road [19]

RESULTS

Under current forest conditions, the total risk in Täsch, expressed as the sum over all scenarios, amounts to 135'360 CHF*yr^{-1}. It critically increases under the non-forested scenario (1'485'000 CHF*yr^{-1}). The risk reduction due to the forest effects is therefore 1'349'640 CHF*yr^{-1} or ~9'000 CHF*yr^{-1}/ha. Smaller rockfall volumes (~ < 3 m^3) occur most frequent and, consequently, the forest effect on the risk reduction is most significant for such events. Furthermore, for volumes ≥ 3 m^3, the risk reduction is considerably reduced, but not negligible, as it still reaches values between 20 and 70 % (Fig. 2).

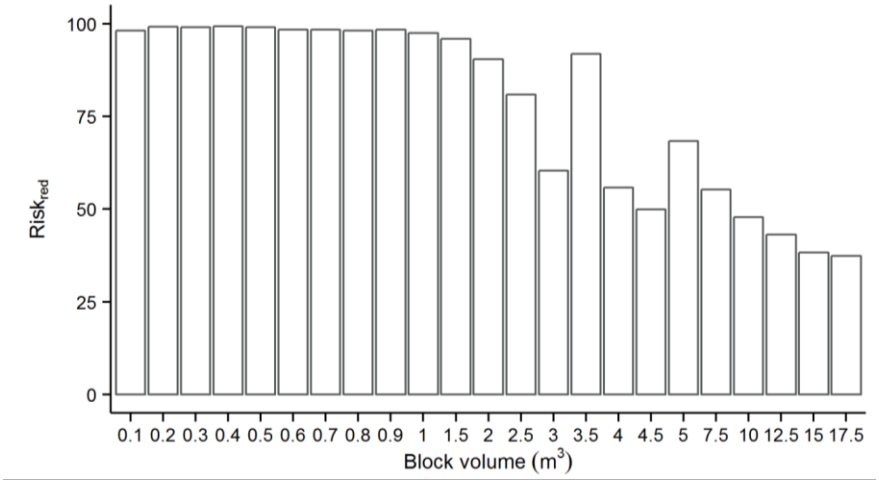

Fig. 2: Risk reduction by forest (in %) per block volume.

Isolating individual forest effects on rockfall risks reveals their contribution to the total risk reduction. If only the effect of forests on the intensity is considered, we observe a marginal risk reduction only (Fig. 3), although the intensity is distinctly reduced by forests. The risk

reduction effect of forest must, in this case study, mainly be attributed to the reduction of rockfall occurrence frequency.

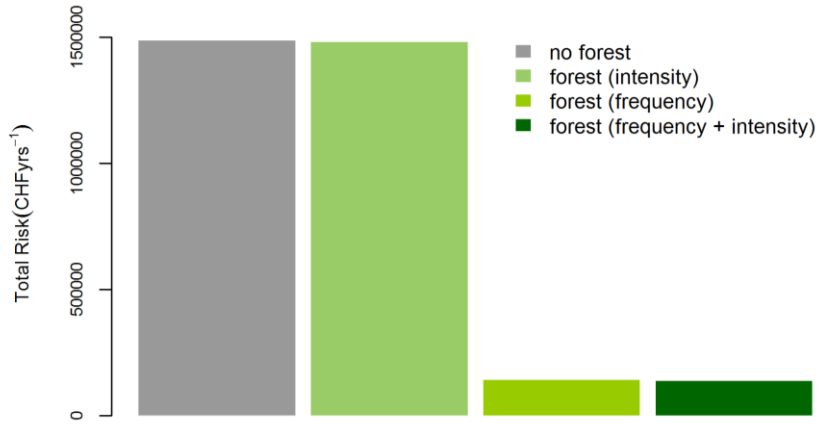

Fig. 3: Total risk for the considered elements at risk in Täsch without forest and for different forest effects (solely reduction of intensity by forests, solely reduction of frequency by forests, combined reduction of frequency and intensity by forests).

CONCLUSIONS

The results of this case study in Täsch demonstrate that the current forest reduces total risk of rock volumes between 0.05 and 20 m^3 by about 90 % compared to a hypothetical non-forested situation. The analysis is based on a general methodological framework which can be applied at other sites and may also be transferred to other hazard processes. In doing so, forests can be compared to other protection measures and evaluated in cost-benefit analyses allowing a standardized and objective assessment of the forest effect.

REFERENCES

[1] STRAUB D, SCHUBERT M. (2008) Modeling and managing uncertainties in rock-fall hazards. Georisk: Assessment and Management of Risk for Engineered Systems and Geohazards 2(1): 1–15.
[2] AGLIARDI F, CROSTA GB FRATTINI P. (2009) Integrating rockfall risk assessment and countermeasure design by 3D modelling techniques. Natural Hazards and Earth System Science **9**: 1059–1073.
[3] BRÜNDL M, ROMANG HE, BISCHOF N, RHEINBERGER CM. (2009) The risk concept and its application in natural hazard risk management in Switzerland. Natural Hazards and Earth System Science 9: 801–813.
[4] MIGNELLI C, PEILA D, LO RUSSO S, RATTO SM, BROCCOLATO M. (2014) Analysis of rockfall risk on mountainside roads: evaluation of the effect of protection devices. Natural Hazards 73(1): 23–35.
[5] RENAUD FG, SUDMEIER-RIEUX K, ESTRELLA M (eds). (2013) The role of ecosystems in disaster risk reduction. United Nations University.
[6] PERRET S, DOLF F, KIENHOLZ H. (2004) Rockfalls into forests: Analysis and simulation of rockfall trajectories ? considerations with respect to mountainous forests in Switzerland. Landslides 1(2).
[7] DORREN L, BERGER F, PUTTERS US. (2006) Real-size experiments and 3-D simulation of rockfall on forested an non-forested slopes. Natural Hazards and Earth System Sciences 6: 145–153.
[8] DUPIRE S, BOURRIER F, MONNET J-M, BIGOT S, BORGNIET L, BERGER F, CURT T. (2016) Novel quantitative indicators to characterize the protective effect of mountain forests against rockfall. Ecological Indicators 67: 98–107.
[9] HANTZ D, VENTROUX Q, ROSSETTI J, BERGER F. (2016) A new approach of diffuse rockfall hazard. In Landslides and Engineered Slopes. Experience, Theory and Practice, Aversa S, Cascini L, Picarelli L, Scavia C (eds). CRC Press; 1063–1067.
[10] LARI S, FRATTINI P, CROSTA GB (2014) A probabilistic approach for landslide hazard analysis. Engineering Geology 182: 3–14.

[11] DORREN L. (2003) A review of rockfall mechanics and modelling approaches. Progress in Physical Geography 27(1): 69–87.
[12] BARTELT P, BIELER C, BÜHLER Y, CHRISTEN M, CHRISTEN M, DREIER L, GERBER W, GLOVER J, SCHNEIDER M, GLOCKER C, LEINE R, SCHWEIZER A. (2013) RAMMS rapid mass movements system - User manual v1.6 rockfall: A numerical model for rockfall in researc hand practice. WSL Institute for Snow and Avalanche Research SLF: Davos.
[13] WOLTJER M, RAMMER W, BRAUNER M, SEIDL R, MOHREN, G M J, LEXER MJ (2008) Coupling a 3D patch model and a rockfall module to assess rockfall protection in mountain forests. Journal of environmental management 87(3): 373–388
[14] MOYA J, COROMINAS J, PÉREZ ARCAS J, BAEZA C. (2010) Tree-ring based assessment of rockfall frequency on talus slopes at Solà d'Andorra, Eastern Pyrenees. Geomorphology 118(3-4): 393–408.
[15] DORREN L. (2015) Rockyfor3D (v5.2) revealed – Transparent description of the complete 3D rockfall model. ecorisQ paper: 32.

MULTI-TECHNIQUE APPROACH TO ASSESS ROCKFALL PROPAGATION : A CASE STUDY FROM LES FORGES, JURA, SWITZERLAND

Caroline Lefeuvre[1], François Noël[1], Marc-Henri Derron[1], Michel Jaboyedoff[1], Andrea Pedrazzini[2]

For the purpose of a case study, the propagation of a potentially instable column has been simulated with several techniques. First, we used a model based on the shadow angle in order to get a quick and simple result of the possible run-out. We also computed, with RocFall software, the propagation of the boulder on several profiles. Finally we used 3D data (GIS and points cloud data) to model rockfalls. The results comparison regarding the energy lines reveals that, in this study case, the falls modelled with Rocfall are similar to a propagation within a 27° shadow angle and that falls modelled with 3D GIS data are approximatively located within a 30° energy line. Points cloud data give results positioned within a shorter distance with an energy line about 67°.

Keywords: rockfall, propagation, numerical modelling

INTRODUCTION

Rockfalls propagation is an important issue in hazard and risk assessment. In this study we used several methods to estimate run-out and compared the results as well as the advantages and disadvantages of each method.

STUDY SITE

The study site is located near Undervelier, Jura, Switzerland (see Fig. 1). The suspected rock instability is a column located on the west edge of a Jurassic limestone cliff of approximately 60 m high. There is a crack between the column and the cliff that can reach 1.7 m and the column is threatening a dam and a road below. Indicators of existing rockfall activity are observed with small boulders located in the forest at the bottom of the cliff.

Fig. 1 Location and profile view of the cliff and the instable column, Les Forges, Jura, Switzerland

[1] University of Lausanne, FGSE, ISTE, Géopolis, Quartier Mouline, CH-1015 Lausanne, Switzerland, +41 21 692 43 45, caroline.lefeuvre@unil.ch
[2] Environment Office, Republic and county of Jura, CH-2882 St-Ursanne, Switzerland

METHODS

We scanned the study area with the terrestrial laser scanner (TLS) Ilris3D from OPTECH. We acquired three scans around the cliff in order to cover the entire surface. We processed the data with Canupo tool [1] from CloudCompare v.2.7 and geo-referenced these acquisitions with aerial laser scanning data, cleaned from the vegetation and interpolated in no data areas with Poisson surface reconstruction. These data were then used to model rockfall propagation.
Four methods of modelling have been used in this study. First the propagation has been estimated with the shadow angle and energy lines method [2], [3]. The models were performed with CONEFALL software. We selected a 35° energy line to model falls from the top of the cliff [2] and a 27° shadow angle from the top of the talus slope at the bottom of the cliff [3].
The RocFall software (RocScience©) was then used to model 2D propagation along several profiles. Eleven profiles were selected every 20° from orientations from 130° to 330°. Points cloud data acquired by TLS were used to reproduce elevation. We performed models with the rigid body approach in order to take into account the size and shape of the block and its interaction with the slope [4]. We estimated the column dimensions using the α-shapes method for concave volumes [5] and took a block with a diameter of 3 m. We chose several boulder shapes according to these proportions. Falls were then modelled on each profile and these linear data were transformed into surface data using a natural neighbor interpolation and a Gaussian to take into account preferential propagation directions.
Finally we used 3D data to model propagation. We firstly simulated rockfalls with GIS data using the software Rockyfor3D. For this purpose the points cloud data were rasterized. In a second part, we modelled rockfall propagation with Trajecto3D using data from points cloud to simulate the topography [6]. The size of the block modelled for these two methods was the same as in the 2D method.

RESULTS

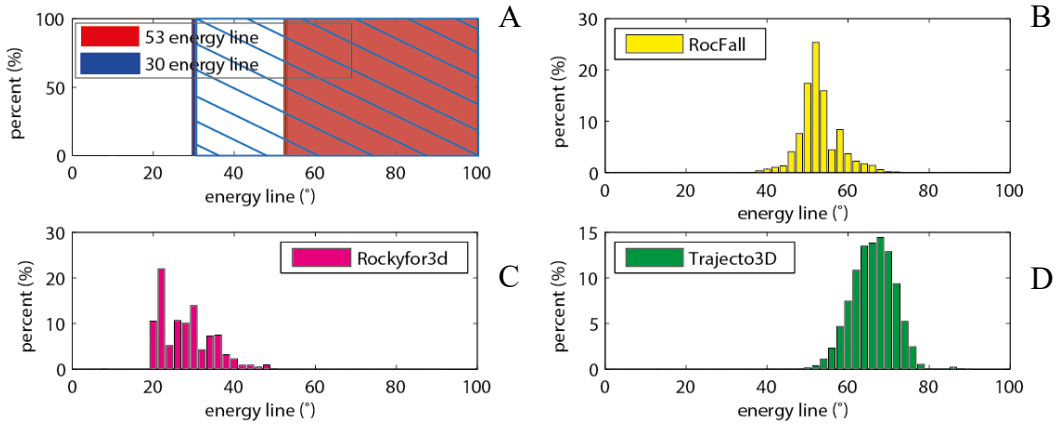

Fig. 2 Comparison of histograms of energy lines between the methods : A. shadow angle method with CONEFALL with a shadow angle of 27° approximately equivalent to a 53° energy line and 30° energy line; B. 2D modelling on profiles with RocFall 5.0 from RocScience©; C. 3D modelling on raster data with Rockyfor3D v5.2 (ecorisQ); D. 3D modelling on points clouds data with Trajecto3D.

We chose to use the energy line to compare the results from the four methods (see Fig. 2). We used a shadow angle of 27° with CONEFALL to estimate the maximal propagation distance from the top of the talus (see Fig. 2.A). This gives a 53° equivalent energy line for this site. The

results from RocFall and Rockyfor3D simulations show approximate normal distributions around respectively 50° and 30° comparable to the results from CONEFALL. However the results from Rockyfor3D are more scattered. This can also be seen on figure 3. C: the rocks spread more in the propagation area with this model. The restitutions coefficients used in RocFall were chosen according to [7] and [8] and those for Rockyfor3D according to [9]. The last are higher for areas defined as rock and forest (Rockyfor3D : 0. 43 and 0.38 / RocFall : 0.35 and 0.3) and thus contribute to the further propagation. In this study, the least conservative results are obtained with Trajecto3D. This method used normal restitution coefficients based on the impact angle [10]. For an impact angle higher than 30° they are mainly smaller than 0.4. Besides, the energy line is a minimal value equivalent to a maximal run-out distance. Rockyfor3D minimal value is 19°, RocFall's is 35° and 95% of falls simulated with Trajecto3D stopped at 57° and more. So these last results are still conservative compared to a 53° energy line.
The propagations computed are shown on figure 3. With the first estimation we can only access the likely maximal area of propagation. The three others simulation give the reach probability of fallen rocks within this area. The location of high reach probability is quite comparable for each method (see Fig. 3). The higher value of probability is about 0.4 for the three simulations.

DISCUSSION AND CONCLUSION

The advantage of using the shadow angle or energy line to estimate the propagation area is that it is quick and simple: it does not require a lot of data. Moreover, in comparison with the other methods, the results are quite comparable. However a low quality of the input data can distort the results particularly if the heights are inaccurate.
Simulations with Rocfall are quick to model but it requires some time to interpolate the 2D results to 3D. Furthermore unlike the two following methods, RocFall does not give preferential propagation directions, but only the possible run-out for a given direction. However the results enable the isolation of each trajectory and the identification of those that reach an infrastructure.
Another advantage of these simulations is that they take the shape of blocks into account and thus interaction with the slope closer to the reality [4].
The results from Rockyfor3D provide a lot of data about the propagation such as blocks energies, passage heights, the number of passage in each cell, velocity, … This method is time efficient and the output can easily be pictured on a map.
Trajecto3D gives the position of deposited boulders, trajectories with their velocities and height at any point and their first impacts against infrastructures when there are. The results also highlight cliff's portions which had sources that produced trajectories of boulder impacting infrastructures as well as their velocity at impact which is interesting to establish the areas that must be monitored in priority and to take protective measures.
For now, we cannot establish which model is the closest to the real propagation the studied boulder could have. However, the fallen blocks observed on the field, in the forest at the bottom of the cliff, suggest that the simulation obtained with Trajecto3D would be the closest to the reality.

ACKNOLEDGMEMENT

The authors thank the Office of environment and Andrea Pedrazzini who provided funding and data for this project.

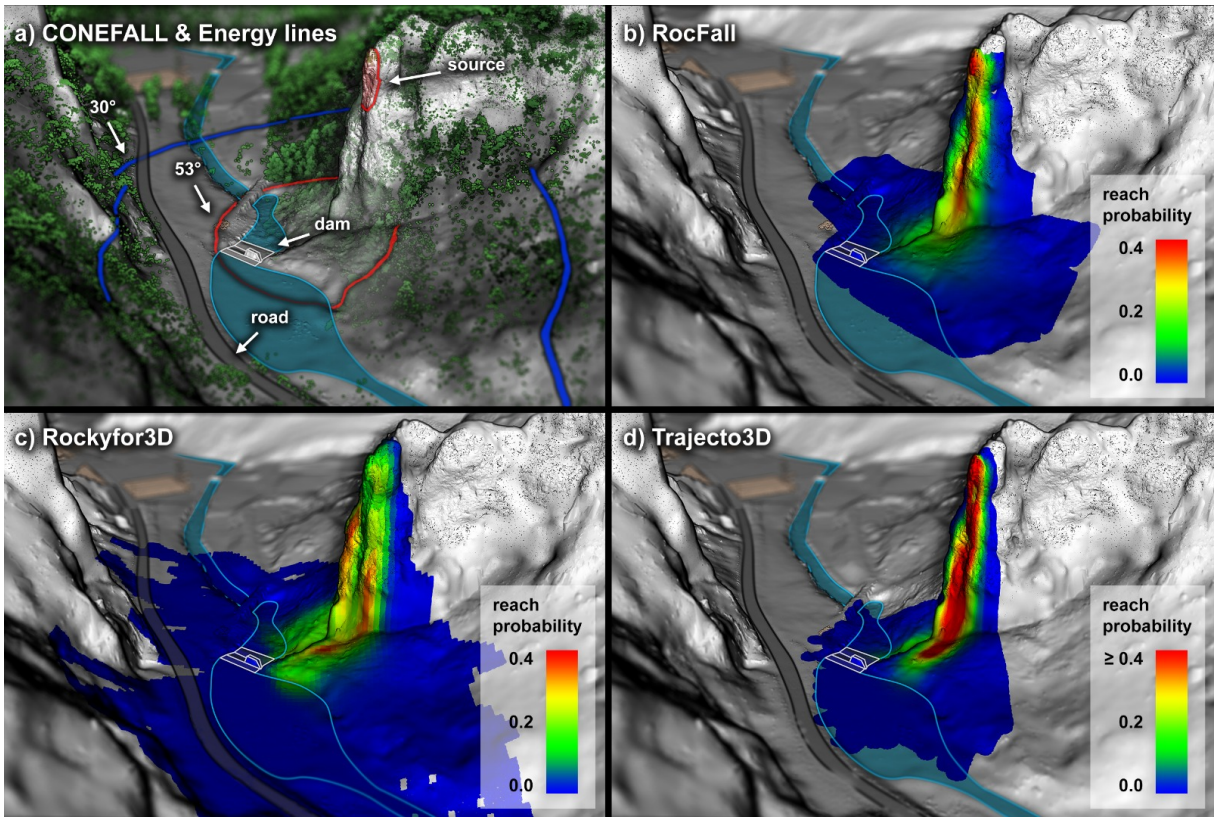

Fig. 3 Results from modelling: a) results from CONEFALL with a shadow angle of 27° approximately equivalent to a 53° energy line, and a 30° energy line; b) 2D modelling on profiles with RocFall 5.0 from RocScience©; c) 3D modelling on raster data with Rockyfor3D v5.2 (ecorisQ); d) 3D modelling on points clouds data with Trajecto3D.

REFERENCES

[1] BRODU N, LAGUE D (2011) 3D Terrestrial lidar data classification of complex natural scenes using a multi-scale dimensionality criterion: applications in geomorphology

[2] JABOYEDOFF M, LABIOUSE V (2011) Technical Note: Preliminary estimation of rockfall runout zones. Natural Hazards and Earth System Sciences 11, 819-828

[3] EVANS S.G, HUNGR O (1993) The assessment of rockfall hazard at the base of talus slopes. Can. Geotech. 30, 620-636

[4] CHAI S, YACOUB T, CHARBONNEAU K, CURRAN J. H (2013) The effect of rigid body impact mechanics on tangential coefficient of restitution, Geo-Montréal 2013 Conference, 09/29- 10/03/2013, Montréal, Canada

[5] CARREA D, ABELLAN A, DERRON M.-H, JABOYEDOFF M (2014) Automatic rockfalls volume estimation based on terrestrial laser scanning data. Engineering Geology for Society and Territory - Volume 2. Published on line 01/29/2015. DOI: 10.1007/978-3-319-09057-3_68

[6] NOEL F, CLOUTIER C, TURMEL D, LOCAT J (2016) Using point clouds as topography input for 3D rockfall modeling. Landslides and Engineered Slopes. Experience, Theory and Practice, Napoli, Italy: CRC Press, 1531-1535

[7] HOEK E (1987) Rockfall – a program in Basic for the analysis of rockfall from slopes. Unpubl. Notes, University of Toronto/Golder Associates

[8] PITEAU D, CLAYTON R (1977) Discussion of paper Computerized design of rock slopes using interactive graphics for the input and output of geometrical data by Cundall P, in: Proceedings of the 16th Symposium on Rock Mechanics, Minneapolis, USA, 62-63

[9] DORREN L (2015) Rockyfor3D (v5.2) revealed – Transparent description of the complete 3D rockfall model. EcorisQ paper, 31p

[10] WYLLIE D. C. (2014) Calibration of rock fall modeling parameters. International Journal of Rock Mechanics and Mining Sciences, vol. 67, p. 170-180

THE AUSTRIAN APPROACH FOR ROCK-FALL HAZARD ZONING: EXPERIENCES, PROBLEMS AND POSSIBLE SOLUTIONS FOR THE DEVELOPMENT OF A STANDARDIZED PROCEDURE

Michael Moelk[1] & Benedikt Rieder[1]

The Austrian Torrent and Avalanche Control produces maps depicting natural hazards such as avalanches and torrential processes to enable the relevant authorities to avoid those dangers when designating new land for the development of new settlements. Until recently, the processes rock-fall and landslide were referred to "hazard indication zones" which were incomplete and used empirical information such as chronicles and reports of the local population. Due to the frequently increasing investments for protection measures against those natural hazards, a more sustainable approach to avoid such hazardous areas in spatial planning had to be developed. To provide a reproducible and state of the art approach, a working party was installed in 2011. As a result, a standard procedure was drafted and published in a compendium by the Austrian conference on spatial planning (ÖROK). To integrate this procedure in the standards applied by the Austrian Torrent and Avalanche Control, several test communities were selected where the hazard mapping for rock-fall processes was executed by using 3D computer models. The experiences from these pilot-projects were summarized and analyzed thus leading to a new approach for the hazard zoning of rock-fall prone areas.

Keywords: hazard zoning, rock-fall hazard, standard procedure

INTRODUCTION

To provide a reproducible and state of the art approach for the assessment and delineation of rock-fall prone areas in alpine communities, a top-down approach is described starting with an empirical method such as the geometrical angle and zooming in to a detailed 3D modelling of rock-fall processes which requires extensive field work and thorough investigation on site, including cronicles, mapping of blocks and rock outcrops in the field. The described procedure forms the basis for new technical guidelines which are to be applied by the Austrian Torrent and Avalanche Control itself as well as by private engineering geologists executing the hazard zoning in the framework of a tender. The description of the tasks to be performed is also part of the results of the development of the standard procedure.

LEGAL FRAMEWORK FOR THE HAZARD ZONING IN AUSTRIA

[1] Austrian Torrent and Avalanche Control, Wilhelm Greil Str. 9, A-6020 Innsbruck, Austria. Phone: +43512584200, Email: michael.moelk@die-wildbach.at & benedikt.rieder@die-wildbach.at

The Österreichische Raumordnungskonferenz (ÖROK) installed a partnership in 2011 dealing with ”Risk management for gravitational natural hazards in spatial planning“. As gravitational natural hazards have a decisive influence on spatial development in the Alpine Region, standard procedures for the assessment of the relevance of these processes for spatial planning was developed ([1] Bäk et al 2015). This contribution describes the recommended procedure to assess the hazards imposed to permanent settlements by rock-fall in a top-down approach.

The §11 Forstgesetz 1975 (Gefahrenzonenplanung der WLV, see [2]) does not foresee hazard zones caused by rock-fall processes but asks for an optional delineation of rock-fall indication areas (brown rock-fall and/or landslide indication areas). These areas show regions, which are possibly, exposed to rock-fall without any further assessment of the rock-fall processes itself. The same applies for the Gefahrenzonenplanverordnung BGBL 436/1976 (Gegenstand der Gefahrenzonenplanung, see [3]). Continuous requests from federal land use planning authorities for a more detailed evaluation of those natural hazards led to the necessity to develop a standard procedure to assess the dynamics and reach of rock-fall processes in a way that is reproducible and reflects the state of the art. The “Strategie 2020” defined by the Austrian Torrent- and Avalanche Control concluded to develop this procedure in one community for each federal state.

STANDARD PROCEDURE FOR DELINEATION OF ROCK-FALL HAZARD ZONES IN A TOP DOWN APPROACH

A first step to define potential conflicts between the maximum run-out of rock-fall processes and the presence of settlements is a conservative empirical assessment based on rock outcrops potentially serving as detachment zones and a maximum reach of such rock-falls leading to a hazard indication map. This approach is based on existing cartographic information only, field investigations are not necessarily involved at this stage. To ensure a conservative result, the use of a high-resolution 1 m terrain model to identify rock outcrops is recommended. Every pixel of the terrain model showing a slope inclination of $\geq 45°$ is treated as a potential detachment source for rock-fall. The maximum reach (run-out) is delineated by a geometric angle of 30° starting from the detachment points, both in drop line and with a lateral deviation of 45°. A polyline depicting the worst-case run-out of rock-falls summarizes all such maximum reaches (see figure 1).

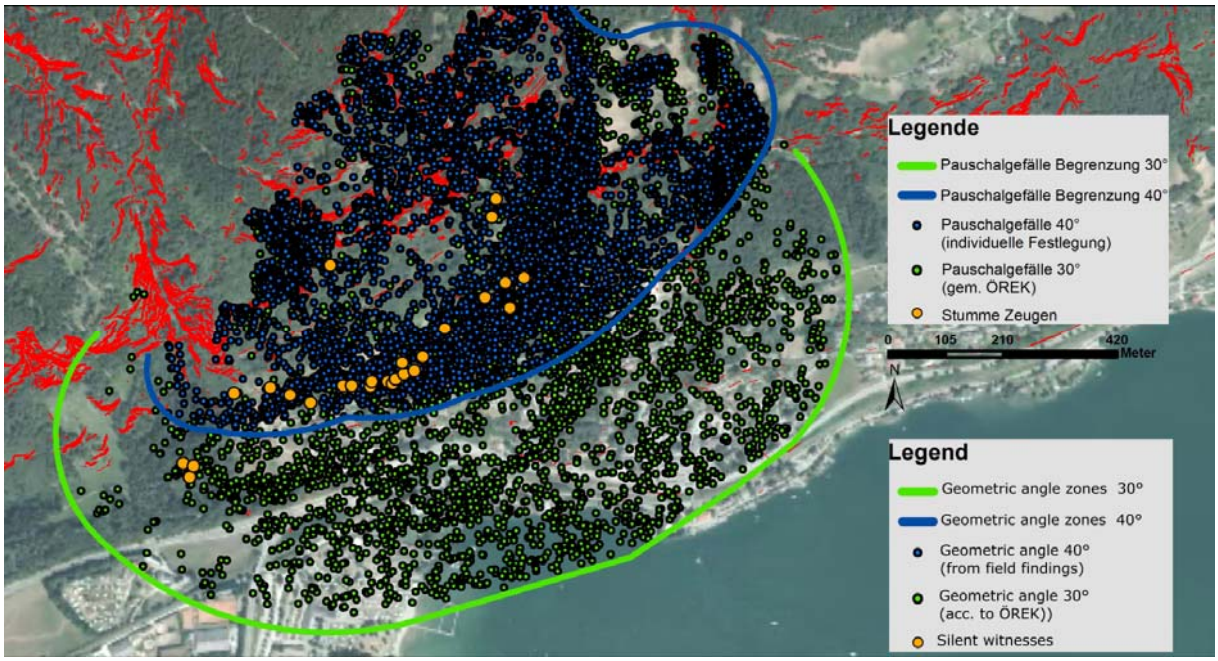

Fig. 1 First and rough estimation of maximum reach by geometric angle approach (green line/dots: no field data included, geometric angle 30° blue line/dots: with evaluation by field findings, geometric angle 40°, orange dots: endpoints of historic rockfall events)

With this information, areas with potential conflicts between existing settlements and buildings with rock-fall processes are identified. In these areas a thorough field work has to be executed in order to map the maximum reach of historic events, to identify potential detachment zones and their respective failure mechanisms and to get a good knowledge of the block-sizes involved in the rockfall processes. A relevant design block for the modelling of the rockfall processes is defined by ÖREK which is consequently implemented in a physical 3D rockfall model (e. g. *RAMMS::Rockfall* or *Rockyfor3D*). The trajectories derived by the model are color coded and according to the "ÖREK recommendation" (see [1] Bäk et al) show red colors for energies > 100 kJ and yellow colors for energies ≤ 100 kJ (see figure 2).
New developments in areas showing red zones are not recommended, while buildings in yellow rockfall zones can be erected under certain precautions.

CONCLUSIONS

First experiences with a standardized procedure to show rockfall hazard zones derived from 3D rockfall modelling are generally positive. Some fields of potential problems could be identified for example

- selection of design-block-size,
- handling of outliers,
- definition of number of simulations and
- evaluation of the effect of existing buildings on runout.

A procedure to tackle these and other critical topics will be included in the best practice description which is foreseen as a final document of the trial-stage.

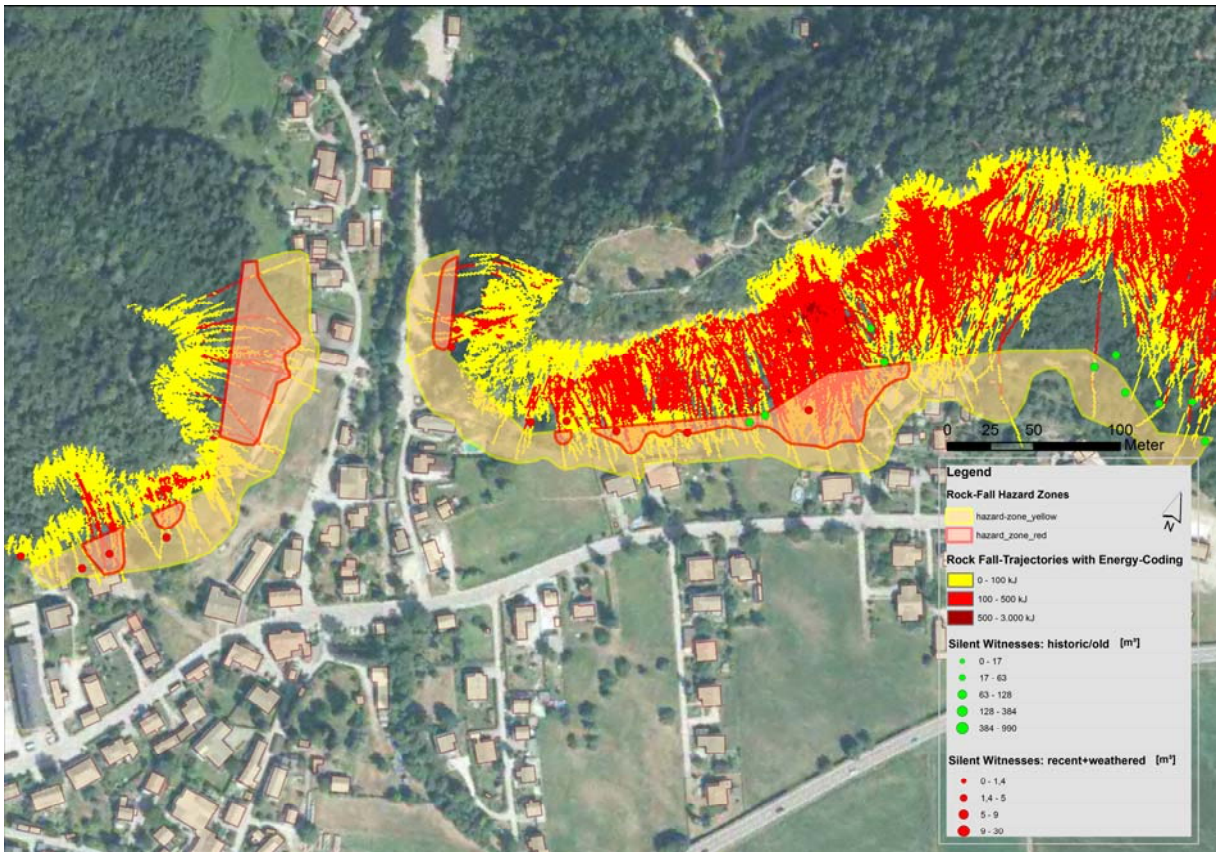

Fig. 2 Example of a rock-fall hazard zone map. Red zones: new developments are not recommended, yellow rockfall zones: new buildings can be erected under certain precautions.

REFERENCES

[1] Bäk R., Braunstingl R., Hagen, K., Kociu A., Kolmer C., Melzner S., Mölk M., Preh A. & Schwarz L.: Materialien und Arbeitspapiere – Arbeitsgruppe Geologie, S. 155-195. In: ÖROK (Hrsg.) (2015): Risikomanagement für gravitative Naturgefahren in der Raumplanung. – Wien (=ÖROK-Schriftenreihe 193)

[2] Bundesgesetzblatt 440/1975: Bundesgesetz vom 3. Juli 1975 mit dem das Forstwesen geregelt wird (Forstgesetz) II. Abschnitt, § 11: Gefahrenzonenpläne

[3] Bundesgesetzblatt 436/1976 Gefahrenzonenplanverordnung

CHALLENGES IN ROCK FALL HAZARD ZONING IN AUSTRIA

Sandra Melzner[1]

This contribution summarizes challenges in the implementation of a standardised procedure for rock fall hazard zoning in Austria. The discussion focuses on the impact of mapping strategy applied to rock size distributions and the frequency of rock fall, the applicability of different 3D rock fall simulation models for hazard zoning in different topographic and geologic environments, and the cartographic presentation of results.

Keywords: Rock fall, standard, rock size distributions, event frequency, 3D rockfall trajectory modelling, hazard zoning.

INTRODUCTION

Many areas in the Eastern Alps are recurrently affected by rock fall processes which pose a significant hazard to settlements and infrastructures (Fig. 1). In Austria, a ÖNORM rules dealing with technical rock fall protection-constructions (ONR 24810) was published in 2013[1], [2]. In 2012, the Austrian Conference on Spatial Planning (ÖROK) installed a ÖREK partnership dealing with "Risk management for gravitative natural hazards in spatial planning", lead partners of this cooperation being the Federal Ministry for Agriculture, Forestry, Environment and Water Management and the Geological Survey of Austria. The results of the ÖREK partnership provide recommendations for a standard procedure to assess landslide and rock fall hazards in residual areas [3].
The present work focuses on the challenges in the implementation of these standards/recommendations into the praxis. Emphasise is put on the determination of block size distributions, rock fall event frequencies and the application of 3D rock fall simulation models, forming a major part in this standard hazard procedure.

DEFINITION OF A BOULDER SCENARIO

The volume of detachable blocks or rock masses are determined by structural geological factors such as joint spacing, persistence and orientation towards to the slope. The frequency of rock fall events is generally assessed separately for all rock size classes.
According to ONR 24810, boulder scenarios are defined based on the event frequency class (EF) and according to percentile class ($V_{98\text{-}95}$) within the block size distribution (table 1). To define boulder scenarios, rock fall release areas defined as frequently affected (> 10 events/year), the 98th percentile of block size distribution is considered. Whereas release areas of low frequency rock fall events (1 event/30 years), the 95th percentile of the block size distribution is considered in the boulder scenario.

[1] Geological Survey of Austria, Department of Engineering Geology, Neulinggasse 38, 1030 Vienna, Austria, 0043 1 7125674 393, sandra.melzner@geologie.ac.at

Tab. 1 Definition of boulder scenario for the dimensioning of preventive measures based on the event frequency and percentile of frequency size distributions (Source: ONR 24810, p. 31).

Classes of event frequency	Rock fall frequency n (1/a)	Percentile of block size distribution
EF 4 (frequent)	n≥ 10 (> 10 events/year)	V_{98}
EF 3 (often)	1≤n< 10 (1-10 events/year)	V_{97}
EF 2 (not often)	0.03≤n< 1 (1 event/1 to 30 years)	V_{96}
EF1 (seldom)	n< 0.03 (1 event/ 30 years)	V_{95}

Depending on the source of rock fall information and the method/technique used to collect the data, the content and detail of an inventory can vary significantly. Standards and guidelines for the preparation of rock fall inventories and for their quality evaluation are lacking [4], [5]. Several rock fall inventories of rock size and rock fall time series in Austria, Italy and USA in different geological settings were analysed according the mapping method/strategy and/or source of information. The objective of this comparison may form the basis for the definition of a concept for the definition of boulder scenarios for hazard zoning.

3D ROCKFALL TRAJECTORY MODELLING

Various approaches exist to simulate rock fall runout distances and/or rock fall dynamics, ranging from simple empirical models to complex process-based models (Dorren 2003, Melzner & Preh 2012, Melzner 2015). According to the ÖREK partnership, rock fall hazard classes are defined accordingly: areas out of reach (no rock fall hazard), areas with potential impact energies ≤ 100 KJ (low intensity) and areas with potential impact energies > 100KJ (high intensity) [3].

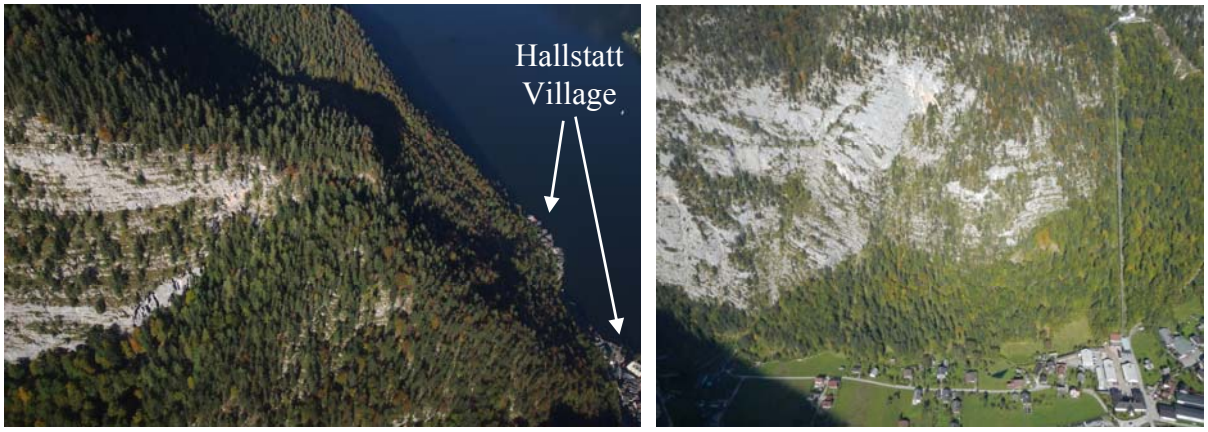

Fig. 1 Carbonate rock faces above the World heritage site "Hallstatt Village" (left) and "Echern Valley" (right), Upper Austria, Austria (photos taken in 2015).

The present study compares the capacity of two 3D process-based models (Rockyfor3D, RAMMS) to predict rock fall trajectories in different topographic and geological settings, with and without considering the protection function of forest.

The objective of the model comparison is to provide decision makers with a transparent overview of the limitations and advantages of the tested 3D models. The discussion about the model application includes required model input parameters, as well as required time and costs for model set-up, model calibration and data collection in the field. The evaluation of the applicability of model results is focused on the model sensitivity to the scale-dependent accuracy of input data and on the quality of the simulated travel distances and dynamics (energies, passing heights, velocities). A very important fact is the cartographic presentation of the simulation results with the field mapping results. The combination of the results of the different methods forms the basis for the final hazard zoning.

CONCLUSIONS

Assessment/mapping strategy has a great influence on the representativeness of frequency size distributions and rock fall time series. Detailed field knowledge and experience with different rock fall simulation models but as well experience in various landscapes are essential, when it comes to the implementation of 3D modelling results into spatial planning decision making issues.
ONR 24810 accounts for the planning and maintenance of rock fall protection-constructions at slope scale. The concept for the definition of boulder scenario according ONR 24810 may be adjusted to a less- conservative attempt (lower percentile) to be used for hazard zoning at local scale. ÖNORM rules should be supplemented with guidelines explaining in more detail different mapping strategies/techniques and model decisions to end users.

REFERENCES

[1] ONR 24810 (2013): Technischer Steinschlagschutz- Begriffe, Einwirkungen, Bemessung und konstruktive Durchbildung, Überwachung und Instandhaltung, Austrian Standards, 15.1.2013.
[2] MOELK M, HOFMANN R (2013) Design of rock-fall embankments according to the Austrian ÖNORM Rule ONR 24810:2013, Mitteilungen für Ingenieurgeologie und Geomechanik Band 10, 6th Colloquium "Rock Mechanics- Theory and Practice", Vienna, pp 33- 50.
[3] ÖROK (Österr. Raumordnungskonferenz) (Eds) (2015): Risikomanagement für gravitative Naturgefahren in der Raumplanung. Fachliche Empfehlungen und Materialienband, Schriftenreihe Nr. 193, 288 pp.
[4] MELZNER S, GUZZETTI F (2014) A comparison of rock fall inventories in Austria and Italy. Geophysical Research Abstracts, Vol. 16, EGU2014-5072-1, Vienna.
[5] MELZNER S (2015) Analyse des Gefahrenpotentials durch primäre Sturzprozesse (Steinschlag/ Felssturz)- Gemeindegebiet Hallstatt. Unpublished GBA report, 185 pp.
[6] DORREN L (2003) A review of rockfall mechanics and modelling approaches, Progress in Physical Geography 27,1, 69-87.
[7] MELZNER S, MOELK M, DORREN L, REICHENBACH P., GUZZETTI F (2011) Rock fall runout modelling for susceptibility evaluation: a multi-scale comparison at different sites, extended abstract 4th International Workshop on Rock fall Protection, Austria.
[8] MELZNER S, PREH A (2012) Sturzmodelle und ihre Anwendbarkeit in der Praxis. Zeitschrift für Wildbach-, Lawinen-, Erosions-und Steinschlagschutz, Heft Nr. 169, 78-101.

ROCKFALL TRAJECTORY ANALYSIS FOR QUARRY PLANNING AND OPERATION

Cesare Castiglia[1], Thomas Frenez[2]

The Authors were retained to provide civil and geomechanics consultancy services to support mining operation and planning at a marble quarry located north of Jeddah city, on the west part of Saudi Arabia Kingdom.
Request was received to provide a study of rock fall trajectories generated by chuting of blasted material from the top of the quarry to the mucking level, located approximately 150m below: the scope of the study was to evaluate rock fall risk for the quarry activities and to support alignment choice for the design of a new quarry road.
The paper presents the approach adopted for field data collection and for trajectory simulation, as well as the findings of the study.

Keywords: trajectory analysis, chuting, mine planning, mine operation

INTRODUCTION

The study site is located north to Jeddah city in Kingdom of Saudi Arabia, where marble is extracted to be used as main part of raw cement mix (beside Schist rock, Iron and Bauxite).
The marble rock forms the top of a mountain in a region with complex thrust faulting and over-thrust features of regional extent. The mountain shows rough topography, with maximum elevation about +700 m above sea level in a relatively small surface area, which reflects in very steep slopes.
Quarry operations are concentrated in the top of the quarry mountain: because the haul road to the top of the quarry is still under development, blasted material is dropped along existing morphologic depressions (called “chutes”) and then mucked from lower levels located approximately 150m below and then transferred to the nearby cement plant through a conveyor belt.
Golder Associates was contracted to provide a study of rock fall trajectories generated by chuting of blasted material from the top of the quarry to the mucking level: the scope of the study was to assess interference between falling rocks and quarry activities, to highlight most viable mucking areas and to support alignment choice for the design of a new haul road to the top.

[1]Golder Associates S.r.l., Via Antonio Banfo 43, Torino 10155, Italy, +39 011 2344211, ccastiglia@golder.it
[2]Incline S.r.l., p.zza San Giovanni 2, Mezzolombardo (TN)38017, +39 0461 600131, mail@theincline.it

Fig. 1 View of the south side of the quarry mountain, with rock chute and accumulation areas.

SIMULATION STRATEGY

The Rockyfor3D – V 5.2 software was used for the simulation (Dorren L.K.A – Ecorisq consortium). The input data of Rockyfor3D consist of a set of ASCII raster maps which define the topography and the slope surface characteristics, as well as a set of parameters, which define the release conditions. These parameters are loaded in the software together with a digital elevation model (DEM) of the slope surface.

The following input data were used as boundary conditions for all the simulations:

- DEM with ground resolution 5m x 5m provided by quarry owner, built from satellite remote sensing data integrated by conventional total station surveys.
- Block Shape: a rectangular block shape was selected based on statistical analysis of blocks observed on site;
- Block Size: based on the average and median block size measured in the field, 2m x 1m x 0.8m dimensions were used. Also, 4m long blocks were used to capture the high energy events generated by falls of the larger potentially unstable volumes that could be mapped on existing outcrops.
- Surface parameters: the quarry area was surveyed and mapped to assign vertical rebound values within typical variation ranges. Values were then calibrated to match actual observed arrest areas and trajectories.

In order to collect the information needed for the simulation, extensive field surveying and mapping was conducted at the site. Data collected were processed and interpreted in order to produce a general engineering geology model of the study area. The following activities were performed:

- preparation of an interpretive geomorphological and geological map of the study area;
- execution of extensive site surveys, including collection of joint set data through geostructural surveys of accessible outcrops and statistical size and shape analysis of rock blocks comprising surface scree deposits;

- processing and interpretation of structural and geomechanical data;
- rock mass classification using Slope Mass Rating index (SMR, Romana, 1985-2015) and Geological Strength Index (GSI, Hoek, 2005);
- preliminary slope stability assessment of the study area using Markland's kinematic approach to determine natural rock release areas and mode of failure (Hoek&Bray, 1981).

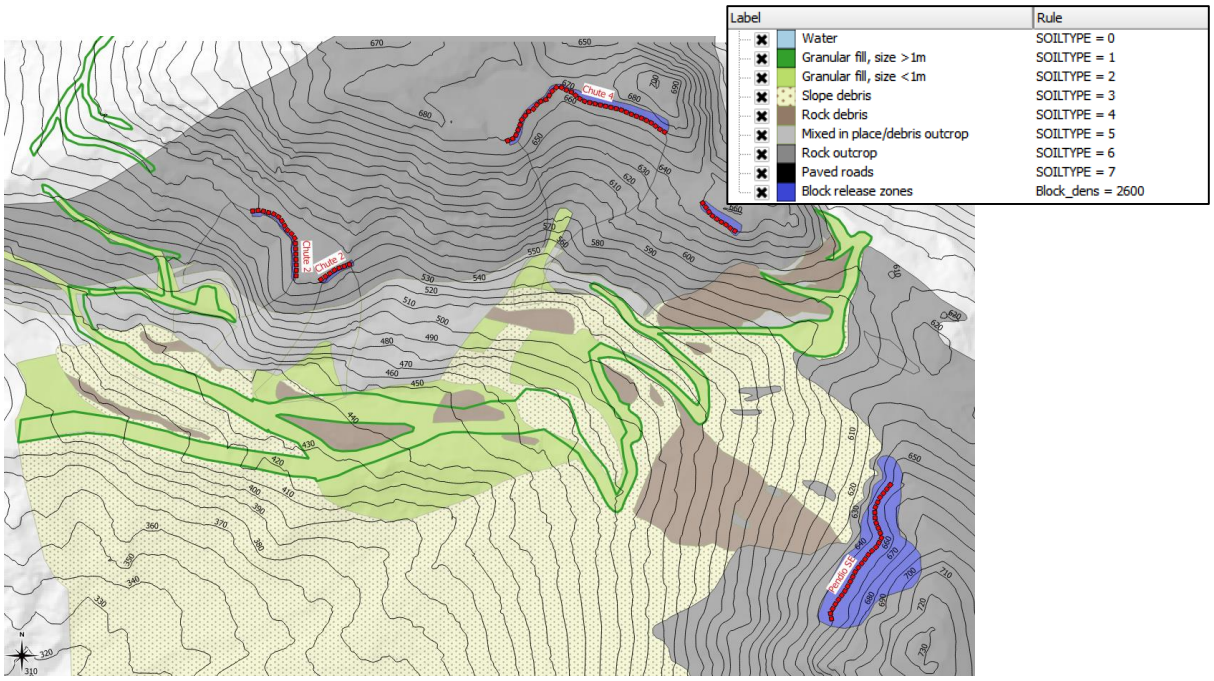

Fig. 2 GIS map of surface characteristics and soil types

SIMULATION FINDINGS AND CONCLUSIONS

The simulation was calibrated to match main accumulation areas and rockfall path as seen on site. Maps such as those in Figure 3 were prepared for the mine manager to improve muck planning, quarry road protection works as well as to support alignment definition of the new haul road:

- maps of most probable landing areas (left), where it is suggested to avoid presence of manned equipment in those areas, as well as to avoid temporary parking of equipment even when chutes are not being operated. Areas should be also be signalled as potentially dangerous;
- maps of most probable passage areas (right), which together with energy and height plots can be used to identify the optimal rock fall protection works in order to improve transit safety on quarry roads or to pick the best alignment for future quarry roads.

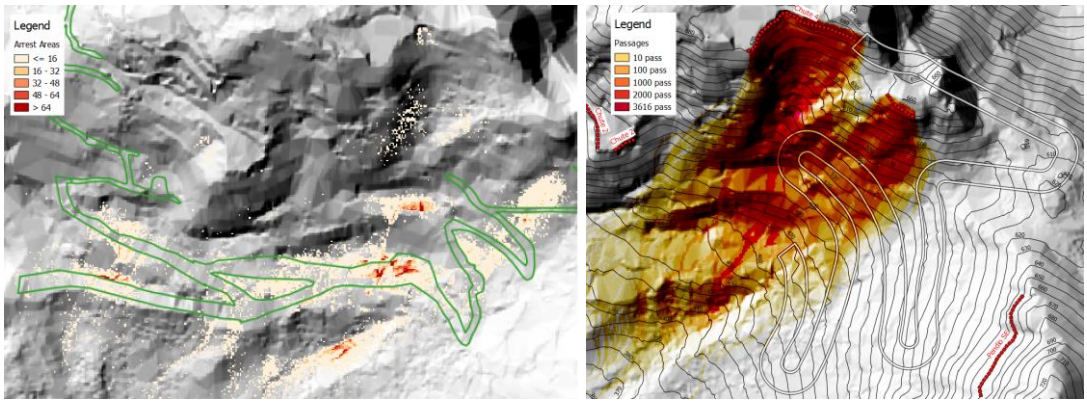

Fig. 3 Graphical output of rockfall simulation from the quarry chutes: accumulation areas (colors indicate number of stops in each cell) and trajectories

The following conclusions could be drawn:

- rock fall trajectory analysis can be an effective engineering tool for quarry planning and safety management, both to control natural rockfall hazard as well as hazard induced by blasting and chuting operations. Rockfall risk can also be assessed by combining hazard with exposure (number of passages of vehicles, time spent in exposed areas for material loading) and consequences.
- collection of input data can be efficiently collected even in remote and wild areas by using remote sensing combined with traditional field mapping;
- Rockyfor 3D demonstrated to be an efficient simulation tool, able to match field evidences and to provide reliable predictions of rockfall trajectories even in complex ground conditions;
- due to the continuous evolution of the release zones and of the chutes surface, that are continuously eroded by collisions with falling material, predictions should be routinely updated as part of the mining control process.

REFERENCES

[1] Hoek E., Bray J.D., (1981). Rock Slope Engineering. CRC Press.
[2] Guzzetti, F., Crosta, G., Detti, R. and Agliardi, F., 2002. STONE: a computer program for the three-dimensional simulation of rock-falls, Comp. & Geosc. 28: 1079–1093.
[3] Jaboyedoff, M. and Labiouse, V., 2003. Preliminary assessment of rockfall hazard based on GIS data. ISRM 2003 – Technology roadmap for rock mechanics. South African Inst. of Mining and Metallurgy: 575-578.
[4] Marinos V., Marinos P., Hoek E. (2005). The geological strength index: applications and limitations. Bull EngGeol Environ (2005) 64: 55–65.
[5] Bourrier, F., Dorren, L.K.A., Nicot, F., Berger and F., Darve, 2009. Toward objective rockfall trajectory modelling using a stochastic rebound algorithm. Geomorphology 110: 68-79.
[6] Lundström, T., Jonsson, M.J., Volkwein, A. and Stoffel, M., 2009. Reactions and energy absorption of trees subject to rockfall: a detailed assessment using a new experimental method. Tree Phys. 29: 345-359.
[7] Dorren L.K.A. (2015). Rockyfor3D (v5.2) revealed – Transparent description of the complete 3D rockfall model. EcorisQ paper
[8] Romana, M., Serón, J.B., Montalar, E. (2003). SMR Geomechanics classification: Application, experience and validation ISRM 2003–Technology roadmap for rock mechanics, South African Institute of Mining and Metallurgy, 2003.
[9] Romana, M., Tomás, R., Serón, J.B. (2015). Slope Mass Rating (SMR) geomechanics classification: thirty years review. ISRM Congress 2015 Proceedings - International Symposium on Rock Mechanics, Quebec, Canada, May 10 to 13 2015. ISBN 978-1-926872-25-4.

QUANTITATIVE ROCKFALL HAZARD ASSESSMENT AT THE MONT SAINT-EYNARD (FRENCH ALPS)

Didier Hantz[1], Jean-Pierre Rossetti[2], Damien Valette[1], Frank Bourrier[3]

A methodology is proposed for quantitative assessment of impact frequency on an element at risk located on a slope under a rock cliff, from the volumetric retreat rate of the cliff, the distribution of the block volumes and the simulation of the block trajectories. The volumetric retreat rate is derived from diachronic terrestrial laser scanning and integration of a power law distribution of the rockfall volume. The frequency and the size of the falling blocks are determined from the power law distribution of the block volume, which is derived from a survey of the blocks fallen on the slope. Finally, the impact frequency is obtained from the simulation of block falls occurring during a given period, using the computer program Rockyfor3D. The method is applied to the Mont Saint-Eynard cliff, which overhangs the Grenoble urban area.

Keywords: rockfall, hazard, cliff, retreat rate, block size distribution, impact frequency

INTRODUCTION

A methodology for impact frequency assessment is applied to the Mont Saint-Eynard cliffs, which overhang the Grenoble urban area (Fig. 1). The lower cliff is 240m high, separated from the 120 m high upper cliff by a ledge covered with forest. The upper cliff consists of massive limestone (bed thickness >1 m) while the lower cliff consists of fractured thin bedded (10–50 cm) limestone. The bedding planes dip inside the cliff. This anaclinal configuration, completed by subvertical fractures, produces overhanging compartments falling mainly by toppling.

Fig. 1 The Mont Saint-Eynard limestone cliff (left); the 1500 m^3 rockfall (middle); orthophoto of some blocks of the 1500 m3 rockfall.(right).

[1] Univ. Grenoble Alpes, ISTerre, Grenoble, France, +33 476 63 51 68, didier.hantz@univ-grenoble-alpes.fr
[2] Alp'géorisques, Domène, France, jeanpierre.rossetti@alpgeorisques.com
[3] IRSTEA, Grenoble, France, franck.bourrier@irstea.fr

VOLUMETRIC RETREAT RATE OF THE CLIFF

The volumetric retreat rate of the cliff has been estimated by integrating the volume-frequency relation for the rockfalls occurring yearly in the cliff [1]. The volume-frequency relation has been obtained from a TLS (Terrestrial Laser Scanner) survey of the cliff during 3 years, which allowed to detect 344 rockfalls bigger than 0.05 m^3 [2]. It is described by a power law:

$$F = A\ V^{-B} \quad (1)$$

Where F is the frequency of rockfalls bigger than V and A the frequency of rockfalls bigger than 1 m^3. For the integration, a maximal possible rockfall volume V_{max} must be fixed, which can be much bigger than the maximal observed volume. The volumetric retreat rate is [1]:

$$W = V_{max}^{(1-B)}\ A/(1-B) \quad (2)$$

Methods for the determination of the maximum credible rockfall volume in a cliff have been presented in [3]. If one assumes that the power law is valid for the whole volume range, the smallest volumes (which have not been observed) are also taken into account. For he Mont Saint-Eynard, $A = 10^{-4}.m^{-2}.year^{-1}$, B = 0.75 and a maximal volume of 10^6 m^3 has been considered. The retreat rate obtained is 0.012 $m.year^{-1}$. The rockfall frequency in the upper cliff is much lower than in the lower one [4], so the former has been neglected in this analysis.

DISTRIBUTION OF THE BLOCK VOLUMES

The distribution of the volumes of the blocks released when a rock compartment falls from a rock cliff can be obtained by measuring the volumes of the blocks deposited during a recent rockfall [5-11]. Haas [6], Hantz et al. [7,10] and Ruiz et al. [9,11] have shown that it is well fitted by a power law with a scaling exponent (b) varying from 0.6 to 1.3:

$$n = a\ v^{-b} \quad (3)$$

Where n is the number of blocks with volume higher than v and a is the number of blocks bigger than 1 m^3. Fig. 2 shows the distribution of the block volumes observed on a recent 1500 m^3 rockfall occurred in the Mont Saint-Eynard (Fig. 1). It has been obtained from a drone photographic survey [12] (Fig. 1). Assuming the scaling exponent depends only on the rock mass structure, the value obtained from a single rockfall can be considered representative of the whole homogenous cliff and Equation (3) represents also the volume distribution of all the blocks falling yearly from the cliff. The volumetric retreat rate (W) can then be derived by integrating the volume in Equation (3):

$$W = v_{max}^{(1-b)}\ a_y/(1-b) \quad (4)$$

Where a_y is the number of blocks bigger than 1 m^3 falling yearly from the cliff and v_{max} is the maximal possible volume of a block. It has to be estimated from the observation of the rock cliff. Knowing W, v_{max} and b, a_y can be derived from Equation (4). Hence the distribution of the volumes of the blocks which fall yearly is known and can be used as input data in the

simulation of the trajectories. For the Mont Saint-Eynard, assuming a maximal volume of an individual block (v_{max}) of 63 m^3, a value of 1.1 10^{-3} $year^{-1}.m^{-2}$ has been obtained for a_y.

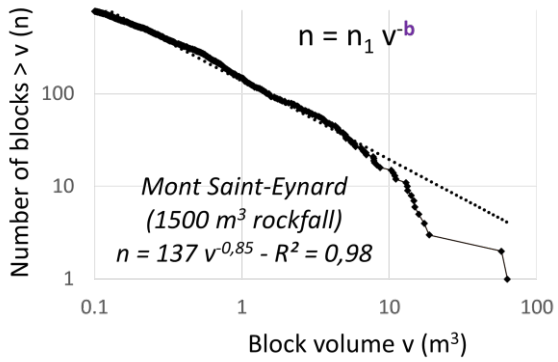

Fig. 2 Distribution of the block volumes observed on a rockfall deposit.

SIMULATION OF THE BLOCK TRAJECTORIES

From the distribution obtained above, the trajectories of all the blocks which fall during a chosen time length can be simulated to determine the impact frequency on each pixel of the slope. A probabilistic modelling has been used with the software Rockyfor3D [13]. The length of the simulated period (1000 years) has been chosen so that a sufficient number of blocks start from each pixel of the DEM (455 blocks > 0.1 m^3 per 5x5m pixel). The contour lines corresponding to different impact frequencies has then been drawn, as shown in Fig. 3. The mean kinetic energy (and different percentiles) can also be given as well as the mean flying height (and different percentiles).

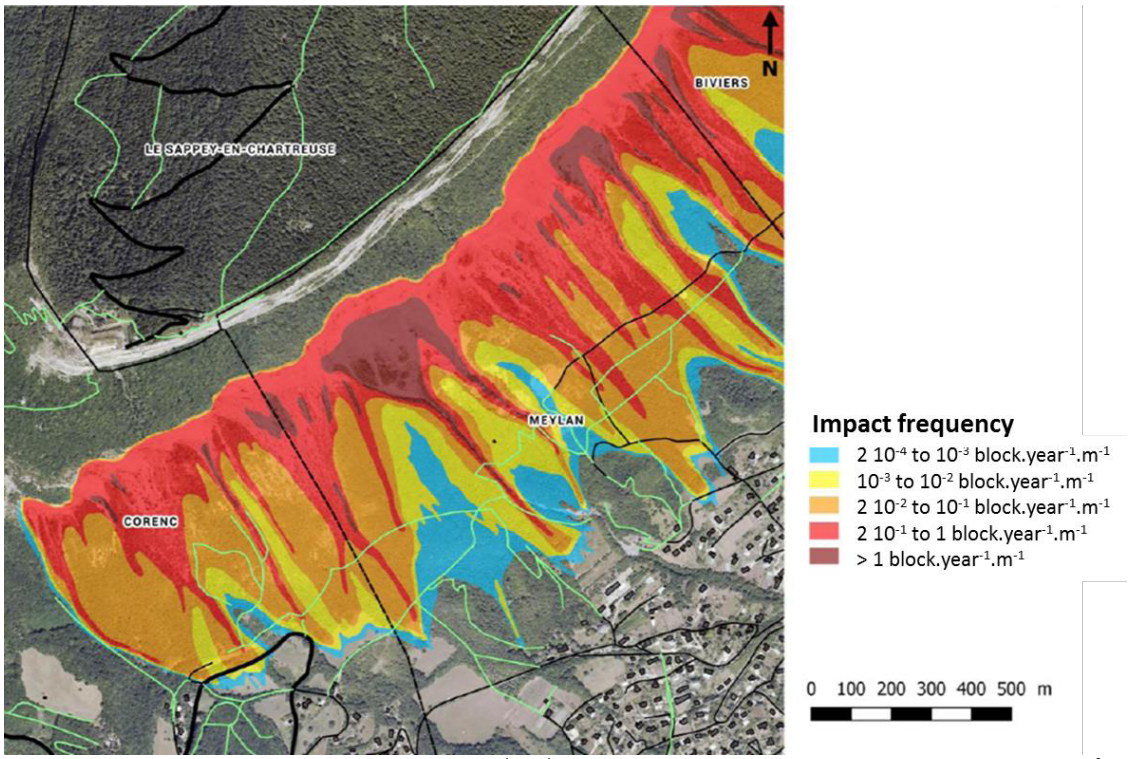

Fig. 3 Annual impact frequency (block.$year^{-1}.m^{-1}$) under the Mont Saint-Eynard for volume > 0.1 m^3.

CONCLUSION

A quantitative approach for rockfall hazard assessment is increasingly used. A methodology is proposed for quantitative assessment of rockfall impact frequency, which consist in: (a) estimating the volumetric retreat rate of the cliff (taking into account the extrem events); (b) dividing this volume into individual blocks (using a power law distribution for the block volumes); (c) simulating the trajectories of the blocks falling during a given period. The application of the method needs the knowledge of the rockfall volume-frequency relation and the distribution of the individual block volumes. It makes it possible to quantify the natural risk, and the residual risk after mitigation measures have been taken.

Acknowledgements. The authors thank the research project C2ROP for funding.

REFERENCES

[1] HANTZ D, DUSSAUGE-PEISSER C, JEANNIN M, VENGEON J-M (2003) Rock fall hazard assessment: from qualitative to quantitative failure probability. Proc. Int. conf. on Fast Slope Movements, Naples, Italy, pp 263-267.
[2] GUERIN A, HANTZ D, ROSSETTI J-P, JABOYEDOFF M (2014) Brief communication "Estimating rockfall frequency in a mountain limestone cliff using terrestrial laser scanner". Nat. Hazards Earth Syst. Sci. Discuss., 2, 123–135.
[3] MAVROULI O, COROMINAS J (2016) Comparing rockfall scar volumes and kinematically detachable rock masses. Engineering Geology, Available online 1 September 2016.
[4] D'AMATO J, GUERIN A, HANTZ D, ROSSETTI J-P, BAILLET L, MARISCAL A, JABOYEDOFF M (2015) Influence of geological and meteorological factors on the frequency of rockfalls. Eurock2015, Salzburg, Austria.
[5] COUTURE R (1998) Contribution aux aspects mécaniques et physiques des écroulements rocheux Université Laval, Québec, Ph. D. Thesis.
[6] HAAS F, HECKMANN T, WICHMANN V, BECHT M (2012) Runout analysis of a large rockfall in the Dolomites/Italian Alps using LIDAR derived particle sizes and shapes. Earth Surf. Process. Landforms 37, 1444–1455.
[7] HANTZ D, ROSSETTI J-P, SERVANT F, D'AMATO J (2014) Etude de la distribution des blocs dans un éboulement pour l'évaluation de l'aléa. Rock Slope Stability 2014, Marrakech, Morocco.
[8] MACCIOTTA R, MARTIN C.D (2015) Remote structural mapping and discrete fracture networks to calculate rockfall volumes at Tornado Mountain, British Columbia. 49th US Rock Mechanics / Geomechanics Symposium, ARMA.
[9] RUIZ-CARULLA R, COROMINAS J, MAVROULI O (2015) A methodology to obtain the block size distribution of fragmental rockfall deposits. Landslides, 12, 815-825.
[10] HANTZ D., VENTROUX Q., ROSSETTI J-P., BERGER F. (2016) A new approach of diffuse rockfall hazard. Proc. 12th Int. Symp. on Landslides, Napoli, Italy, pp 1063-1067.
[11] RUIZ-CARULLA R, COROMINAS J, MAVROULI O (2016) Comparison of block size distribution in rockfalls. Proc. 12th Int. Symp. on Landslides, Napoli, Italy, pp 1767.
[12] VALETTE D (2016) Evaluation quantitative de l'aléa rocheux en termes de fréquence d'impact. Université Grenoble-Alpes, Master Thesis.
[13] DORREN L (2015) Rockyfor3D (5.2) revealed - Transparent description of the complete 3D rockfall model. www.ecorisq.org.

METHODOLOGY FOR ASSESSING ROCKFALL SUSCEPTIBILITY WITHIN THE AMBIT OF CIVIL PROTECTION: THE SAFETY PROJECT.

Roberto Sarro[1], Rosa María Mateos[1], Gerardo Herrera[1], Inmaculada García-Moreno[1], Paola Reichenbach[2], Inocente P. Carralero[3], Jorge Naranjo[3], Marta Béjar-Pizarro[1], Oriol Monserrat[4], Lorenzo Solari[5], Roberta Onori[6], Anna Barra[4], Silvia Bianchini[5], Carmen López[7], Sandro Moretti[5], Elena González-Alonso[7], Sergio Ligüérzana[8], Francesca Ardizzone[2], Michele Crosetto[4], Paola Pagliara[6]

The mission of the SAFETY European project is to provide to Civil Protection Authorities (CPA´s) the capability of periodically evaluating and assessing the potential impact of geohazards on prone sites, and specifically rockfalls. We present the methodology applied in a strategic road (GC-200) located in Gran Canaria (Canary Islands, Spain). We have exploited STONE [1], a GIS based rockfall simulation software which computes 2D and 3D rockfall trajectories starting from the identification of the sources areas and maps of the dynamic rolling friction coefficient and of the normal and tangential energy restitution coefficients. The appropriate identification of these parameters determines the accuracy of the simulation. We have developed a method to calibrate and validate STONE in a volcanic context for the first time, to provide to the Canarian CPA a reliable tool to assess hazard posed by rockfall at regional scale, which could be later applied in any island of the archipelago.

Keywords: Rockfall modelling, Methodology, Civil Protection, Canary Islands

INTRODUCTION

Geohazards are contemplated in the Spanish legislation in the Basic Civil Protection Regulation (1992) which establish the drafting of territorial emergency plans for each Autonomous Community. The Basic Regulations also establish the possibility of producing special plans focusing

[1] Geohazard InSAR Laboratory and Modelling Group. Geological Survey of Spain (IGME), Ríos Rosas, 23, Madrid, 28003, Spain. E-mails: r.sarro@igme.es, rm.mateos@igme.es, g.herrera@igme.es, m.bejar@igme.es, inmaculada.garcia@igme.es
[2] Istituto di Ricerca per la Protezione Idrogeologica (IRPI), National Research Council (CNR), Via Madonna Alta 126, I-06128 Perugia, Italy; E-mails: paola.reichenbach@irpi.cnr.it, francesca.ardizzone@irpi.cnr.it
[3] Dirección General de Seguridad y Emergencias, Consejería de Política Territorial, Seguridad y Sostenibilidad, Gobierno de Canarias, Spain; E-mails: icarjai@gobiernodecanarias.org, jnarbor@gobiernodecanarias.org
[4] Centre Tecnològic de Telecomunicacions de Catalunya (CTTC/CERCA), Avinguda Carl Friedrich Gauss, 7, Castelldefels, 08860, Spain; E-mails: omonserrat@cttc.cat, abarra@cttc.cat, mcrosetto@cttc.cat
[5] Earth Sciences Department, University of Firenze, Via La Pira, 4, I-50121 Firenze, Italy; E-Mails: lorenzo.solari@unifi.it, silvia.bianchini@unifi.it, sandro.moretti@unifi.it.
[6] Italian Civil Protection Department, Rome 00189, Italy; E-mails: roberta.onori@protezionecivile.it, paola.pagliara@protezionecivile.it
[7] Observatorio Geofísico Central, Instituto Geográfico Nacional (IGN), C/ Alfonso XII, 3 Madrid, 28014, Spain. E-mails: clmoreno@fomento.es, egalonso@fomento.es
[8] Centro Nacional de Información Geográfica, Instituto Geográfico Nacional, C/ General Ibáñez de Ibero, 3. Madrid, 28003, España. E-mails: cnig.slr@fomento.es

on particularly significant hazards in each region. These special plans are an important development, since they must necessarily involve in-depth knowledge and characterization of geohazards prior to the operational structure in the emergency state, and have to base on quite thorough scientific research. Due to the volcanic origin of the Canary Islands, the authorities approved in 2010 the Special Emergency Plan for Volcanic Hazards that provides an inventory of means and resources, and lays down action protocols to apply in the case that a volcanic event comes true, including other related geohazards. Rockfalls in the Canary Islands are very common and they represent a major threat to society, costing lives, disrupting infrastructures and destroying livelihoods. During the volcanic crisis in El Hierro (2011) numerous rockfalls were triggered, affecting the road network of the island and causing a great social alarm. The SAFETY European project aims to develop accurate tools to provide to Civil Protection Authorities (CPA´s) the capability of periodically evaluating and assessing the potential impact of rockfalls. In the present work, we show the procedure carried out in a strategic road located in Gran Canaria (GC-200) by applying STONE rockfall modeling.

DESCRIPTION OF THE TEST SITE

The Canary Islands is a populated outermost Spanish region and one of the most popular touristic destinations in Europe. The steep topography and geological complexity of the archipielago, influences the activation of intense slope dynamics and many slope failures occur. Rockfalls are the most frequent and damaging landslide type in the Canary Islands, producing damages on built-up areas and communication networks. Taking into account the priorities indicated by the CPA of Canaries, a pilot area was selected in the western extreme of the island of Gran Canaria. It is the GC-200 road, located between the localities of Agaete and Aldea (Fig. 1). The GC-200 road constitutes the main transportation corridor between both localities. With a length of 34 km, the road path is very tortuous following the contour of the coast, a very step coastline with the highest cliffs in Europe (Risco Faneque, 1027 m a.s.l.). From the point of view of mobility, the GC-200 is a strategic road with a heavy traffic estimated at 1500 vehicles per day. The geology of the test-site area is within the domain of the basaltic shield stage, Middle Miocene in age. Along the road, an alternance of alkaline basaltic deposits and pyroclastic flows can be observed. Both materials can be the rockfall sources. The road is frequently cut off by rockfalls and numerous boulders invade the road every month (Fig.1).

Fig. 1 The GC- 200 road between the localities of Agaete and Aldea. It is considered one of the most hazardous roads in Europe. Numerous rockfalls cut the road off every year.

METHODOLOGY

This work develops a methodology to provide to civil protection authorities the capability of evaluating and assessing rockfall hazard. The methodology is based on rockfall simulations, and involves three main phases: (1) inventory, (2) simulation, and (3) validation.
In the first stage, we have recorded the information and observations carried out by the Canarian CPAs about rockfall events occurred from January 2010 to March 2016, along the first 15 km of the GC-200 road. A total of 7811 rockfall events were reported. Based on this, a rockfall inventory map was developed defining accurately the location of each impact on the road. The information for each event includes wide data, such as kilometer point (PK), number of events, date, boulder size, etc. In parallel, we generated a database including all information available for each rockfall and we have also design and unified tab to be used by CPAs to collect future rockfall events data.
The goal of the simulation stage is the rockfall modeling at regional scale. Rockfalls are difficult to model with accuracy because it is necessary to determine precisely factors such as: the location of the source area, the size and shape of the boulder, the parameters of the bedrock, etc. [3]. To assess rockfall susceptibility in the test site, STONE was applied. It is a physically based software capable of modelling rockfall processes in three dimensions (3D), and of providing the potential rockfall trajectories [1]. The software requires the following input data: the location of the source areas, a digital elevation model (DEM), the starting velocity, and the coefficients of normal and tangential energy restitution and friction to simulate the loss of energy when rolling and at impact points. DEM was generated by the National Geographic Institute at a 5m x 5m resolution (www.ign.es). All the cells with slopes above 40º were considered as the sources areas, and five rocks for each cell were launched. In addition, we have compared some LiDAR point clouds, taken from different time-periods, to identify the areas with material losses to adjust better the source areas. According to the field observations and the geological map available -GEODE from IGME (www.igme.es)- four lithological units were differentiated and their coefficients were firstly obtained from the literature [4] [5] and then, they were calibrated with some well-known rockfall events occurred in the Canary Islands. The starting velocity in the preliminary simulation is null, but we will carry out new simulations considering different starting velocities for potential seismic scenarios. The software computes, for each DEM cell, the cumulative count of rockfall trajectories, the maximum computed velocity, and the largest flying height produced.
The third stage consists on validation, that is, to determine the accuracy of the developed simulations. The validation consists on quantifying the matching/mismatching between the rockfall inventory map and the simulated rockfall map. The analysis was applied considering the 7811 rockfall events documented in the road during the last 6 years, and calculating the percentage of computed rockfall trajectories that cross the rockfall inventory areas, as well as the percentage of the rockfall inventoried areas within the simulated outputs (Fig. 2).

RESULTS AND CONCLUSION

This study presents a methodology to provide to the Civil Protection Authorities of the Canary Islands the capability of evaluating and assessing rockfall susceptibility. The comparison of the map of the potential rockfall trajectories obtained by STONE with the well-known location of the impact points of the historical rockfalls along the road during the last 6 years, confirmed a

preliminary spatial representation for the potential extent of rockfalls along the GC-200 road. This map provides the percentage of trajectories that cross each cell. In the study area the highest density of trajectories is located in between the PKs 7 and 9 km, where high densities of rockfall events were identified (Zone A). Additionally, between the PKs 9 and 11 km high densities were also observed (Zone B). Overall, the numbers of trajectories are in agreement with the information and observations carried out by the Canarian CPAs (Fig. 2).

The validation stage makes evident that the travel paths and the depositional areas are successfully ascertained through numerical modelling. Results show success in 73.33% of the largest rockfalls inventoried (11 events).

We have calibrated and validated the STONE software [1] for the first time in a volcanic context, developing a reliable tool, which can be applied in any rockfall prone area of the archipelago.

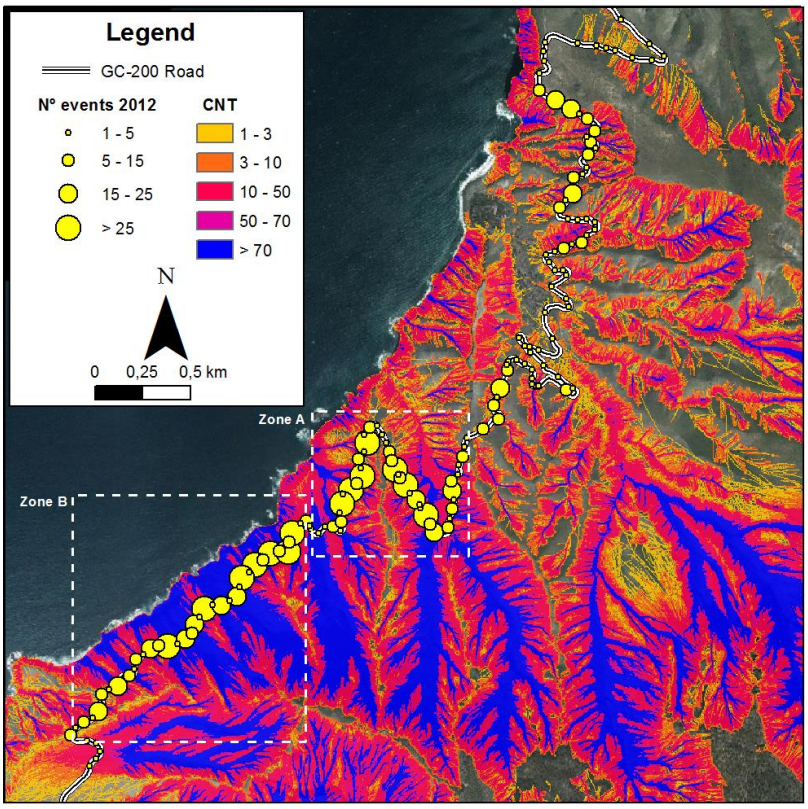

Fig. 2 Comparison between the rockfalls identified in 2012 and the simulated rockfall map

REFERENCES

[1] GUZZETTI F, CROSTA G, DETTI R, AGLIARDI F (2002) STONE: A computer program for the three-dimensional simulation of rock-falls. Computers Geosciences 28 (2002): 1079-1093.

[2] ABBRUZZESE JM, SAUTHIER C, LABIOUSE V (2009) Considerations on Swiss methodologies for rock fall hazard mapping based on trajectory modelling. Natural Hazards and Earth System Sciences, 9(4), 1095.

[3] GUZZETTI F, REICHENBACH P (2010) Rockfalls and their hazard. Tree Rings and Natural Hazards. Springer Netherlands, 2010. 129-137.

[4] MATEOS RM, GARCÍA-MORENO I, REICHENBACH P, HERRERA G, SARRO R, RIUS J, FIORUCCI F (2015) Calibration and validation of rockfall modelling at regional scale: application along a roadway in Mallorca (Spain) and organization of its management. Landslides, 1-13.

[5] SARRO R, MATEOS RM, GARCÍA-MORENO I, HERRERA G, REICHENBACH P, LAÍN L, PAREDES C (2014) The Son Poc rockfall (Mallorca, Spain) on the 6th of March 2013: 3D simulation. Landslides, 11(3), 493-503.

10 YEARS OF ROCKFALL ANALYSIS IN MONTSERRAT (NE SPAIN)

Xabier Blanch[1], Manuel J. Royán[1], Marta Guinau[1], David García-Sellés[1], Joan M. Vilaplana[1]

After 10 years of monitoring using terrestrial LiDAR data in the Montserrat massif (NE Spain), detailed information about rockfall source zones and pre-failure movements is acquired. The study comprises a detailed joint analysis (revealing the existence of at least 5 joint sets) and an exhaustive rockfall inventory (with volumes greater than 0.0001 m^3). Moreover, pre-failure movements of two unstable blocks were analysed. This results are a great advance forrisk management and were included in the Risk Mitigation Plan leaded by the *Institut Cartogràgfic i Geològic de Catalunya* (ICGC).

Keywords: rockfall monitoring, rockfall detection, joint sets detection, LiDAR data

INTRODUCTION

Montserrat Mountain is one of the most visited touristic places in Catalonia (NE Spain). In this mountain there is a monastery which is visited for more than 2.5 million people every year [1]. Geologically, Montserrat massif is characterized by almost vertical conglomerate slopes affected by frequent rockfalls that reach volumes up to 1000 m^3 [2]. The rockfalls suppose a remarkable risk for visitors and infrastructures. Since 2014 the *Institut Cartogràgfic i Geològic de Catalunya* (ICGC) has been leading the Risk Mitigation Plan in Montserrat [2]. For this purpose, almost 10 years of terrestrial LiDAR (TLS) monitoring of different slopes in Montserrat have been achieved. The main goal of this work is to show a summary of the results obtained with LiDAR data analysis, which could be structured in: a) a detailed structural analysis of the rockfall source zones, which revealed the existence of at least 5 different joint sets [3], that together with the presence of soft layers of siltstone/sandstone interspersed with massive conglomerates play an important role in rockfall occurrence; b) the time-lapse comparison of LiDAR data, obtaining an exhaustive rockfall inventory with an unprecedented level of detail, detecting volumes greater than 0.0001 m^3 and c) the monitoring of pre-failure movement of two unstable blocks, providing data about the failing mechanism and about the movement acceleration.

This work was developed in three slopes located at the East extreme of the massif (Tab. 1): a) The Monestir cliff, located behind the monastery and surrounding buildings (SW-NE orientation, maximum height 150 m, 49000 m^2); b) The Degotalls cliff, where one of the most important rockfalls (1000 m^3) occurred in December 2008, has a dihedral shape with two orthogonal rock faces (rock face N: W-E orientation, and 150 m-wide and rock face E: N-S orientation and 200 m-wide), both cliffs are 170 m-high; and c) The Collbató cliff, that is located next to the B-112 road, at 3.5 Km from Monistrol the Monserrat to Collbató (20000 m^2, 90 m-high).

[1] RISKNAT Res. Grp., GEOMODELS Res. Inst. Dept. of Earth and Ocean Dynamics, Earth Sciences Faculty, Universitat de Barcelona-UB. C/ Martí I Franquès s/n, 08028 Barcelona, Spain. xabierblanch@gmail.com

METHODOLOGY

Data acquisition

Data acquisition was performed using an ILRIS-3D (Optech) TLS, in different field campaigns from different positions to cover the whole area (see Tab. 1). The start of the scans as well as the frequency is variable in each studied sector.

Tab. 1 Field campaigns and scanning period in each slope involved in the study

Location	LiDAR position	Scans	Field campaigns	Scanning period
Monestir Cliff	Fra Garí	3	16	2011.02-2017.01
Degotalls cliff	Rock face N	1	17	2007.05-2017.01
	Rock face E	2	18	2007.05-2016.12
Collbató cliff	Road B-112	4	3	2015.07-2015.12

Data pre-treatment

Pre-treatment of the point clouds acquired consists of; a) alignment based on the assignment of homologous points, b) distance between point clouds reduction by applying the ICP algorithm [4], and c) differences between two point clouds computation using the point-to-surface distance in Polyworks software. The weighted distance in the X, Y and Z axes was calculated. This distance can be negative or positive depending on whether a rockfall (loss of material) or deformation has occurred. In order to improve the methodology, the M3C2 distance algorithm [5] was used in the Collbató cliff. Using this pre-treatment, the minimum distance between scans to detect a rockfall was reduced from 3 cm to 1.5 cm.

Rockfall source identification

In order to detect rockfall sources, all distance values that are lower than the minimum detection value were filtered. The rockfall detection process involves three steps; a) DBSCAN algorithm [6] was applied to group the distance-filtered points that can be a rockfall and to remove noise, b) manual filtering was performed to remove erroneous clusters and DBSCAN was reapplied to individualize each rockfall, and c) triangulation of the points of each individual rockfall to calculate the volume. As a result of applying this methodology the minimum volume detected was 0.001 m^3, except for Collbató cliff, where it was possible to detect values up to 0.0001 m^3 due to the smaller scanning distance.

Deformation detection

The NN-3D technique [7 and 8] was applied in order to detect centimeter-scale displacements between two point clouds. This technique consists of searching the nearest neighbour points around each point of the point clouds in a maximum radius and the median calculation of the differences between point clouds. As a result, detection was reduced from 3 cm to 1 cm.

Joint analysis

After point cloud georreferencing, the joint analysis starts with a planar regression using the SEFL program [9]. The planar regression resides in associating a set of points in a generated plane that contains them. The process calculates the strike and dip of the plane. The coplanarity and collinearity evaluation permits one controlling the planes adjustment, before the construction of planes by clustering points. The planes orientation were analysed to identify the joint sets.

RESULTS

Rockfall source identification

The rockfall source inventories are composed of the exact location of the rockfalls and its volume. The results obtained in this topic are summarized in Tab. 2.

Tab. 2. Number of rockfalls identified in each slope and range of volumes (in m^3)

DEGOTALLS N			DEGOTALLS E			MONESTIR			COLLBATÓ		
Time Lapse	Nº of rock falls	Volume range	Time Lapse	Nº of rock falls	Volume range	Time Lapse	Nº of rock falls	Volume range	Time Lapse	Nº of rock falls	Volume range
2007.05 2017.01	115	min. 0,001 max. 8832 90% <0,1	2007.05 2016.12	126	min. 0,001 max. 0,276 95% <0,1	2011.02 2017.01	142	min. 0,001 max. 0,483 93% <0,1	2015.07 2015.12	29	min. 0,0001 max. 0,014 100% <0,1

Pre-failure deformation

Two unstable blocks were detected in Degotalls N (Fig. 1A). The movement of block A was detected between May 2007 and Dec. 2009. This instability was related to the great event occurred in Dec. 2008 (1000 m^3), since it was characterized by an initial mean movement of 2 cm followed by inactivity periods until Oct. 2016 (Fig. 1A). Stabilizing tasks carried out in this block after the great event could induce this inactivity.

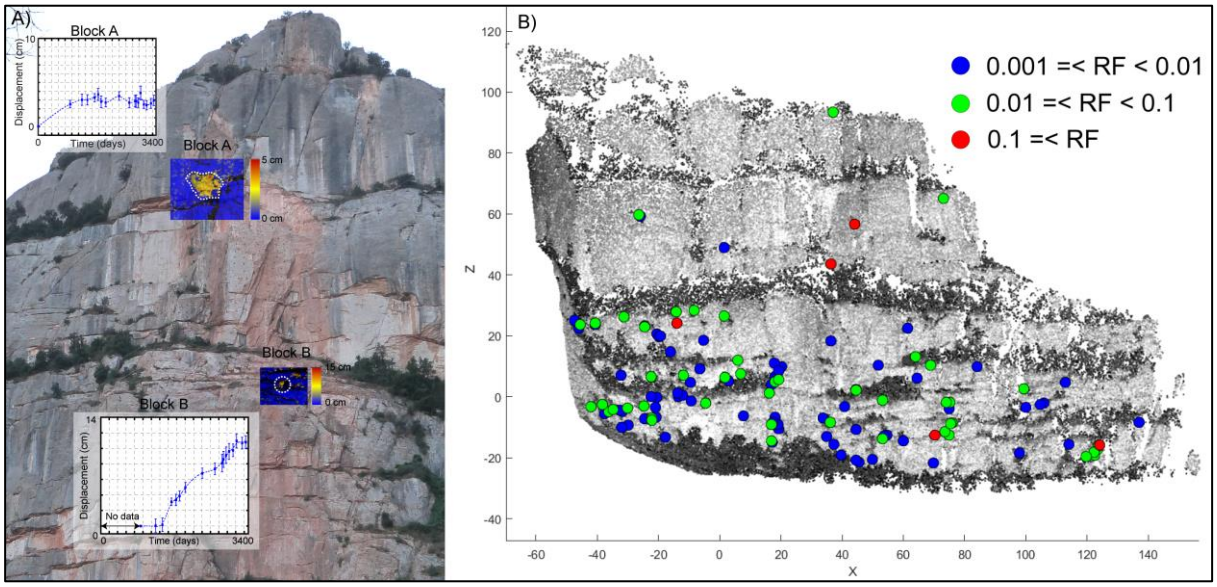

Fig. 1 A) Unstable areas (block A and B) detected in Degotalls N wall. B) Rockfalls detected in Degotalls E wall, with volume ranges indicated in colours (RF: rockfall; volumes in m^3).

Block B, was detected between May 2011 and Dec. 2011. The initial movement was linked with the detachment of a neighbour block occurred in the same period. The dynamic of this instability is fully different compared with block A. In this case, the initial mean displacement was 4 cm followed by an increase that reached 11 cm until October 2016 (Fig. 1A).

Joint Analysis

Table 3 shows the results for the joint analysis and the comparison with the joint sets revealed by [3]. Sets 1, 5 and 6 were found in the three studied cliffs and coincide with the main joint sets defined [3]. Sets 2, 3 and 4 were found in two of the studied cliffs but only Set 2 coincide

with the joint set B_{NW} [3], may be because they are the result of local stress-fluctuations or because they appear in the studied localities as lineaments which cannot be detected by the analysis performed from LiDAR data. In addition, Set 7 has a local significance only as it was found exclusively in the Monestir cliff.

Tab. 3 Structural analysis results and comparison with joint sets defined [3].

Set of joints	Dip/Dip Direction				
	Monestir Cliff	Degotalls Cliff	Collbató Cliff		Alsaker et al. (1996)
Set 1	71/182	86/014*	75/196		Set E (W-E) / Set C (WNW-ESE)
Set 2	81/225		79/230		Set B_{NW} (NW-SE)
Set 3	83/245		81/274		
Set 4		85/065	80/054		
Set 5	72/144	83/141	78/147		Set A (NNE-SSW)
Set 6	70/122*	80/120*	80/335		Set B_{NE} (NE-SW)
Set 7	73/103				

CONCLUSIONS

TLS monitoring allows one detecting rockfall sources otherwise undetectable, obtaining rockfall inventories where the 90-95% of the rockfalls have volumes < 0.1 m^3. The analysis of rockfall source density and volume distribution revealed zones with higher activity where to prioritize surveillance and protective works. In addition, TLS monitoring release the movement of one block destabilized because of a large detachment, which reminded stable after the stabilization works. A second unstable block was detected with an almost lineal displacement evolution over time. Joint analysis concludes that the principal joint sets that contribute to the cliffs instability are joint sets 1, 5 and 6. All this information is crucial for the design and implementation of protective elements and actuations making possible a better risk management in an area with a high level of exposure.

REFERENCES

[1] FONTQUERNI S, VILAPLANA JM, GUINAU M, ROYÁN MJ (2013) El factor exposición en el análisis del riesgo geológico. Aplicación a los desprendimientos de roca en la montaña de Montserrat. Seguridad y Medio Ambiente, 131, 8-25

[2] JANERAS M., JARA JA, ROYÁN MJ, VILAPLANA JM, AGUASCA A, FÀBREGAS X, GILI JA, BUXÓ P (2017): Multi-technique approach to rockfall monitoring in the Montserrat Massif (Catalonia, NE Spain). Engineering Geology, 219 (9), 2 - 20. http://dx.doi.org.sire.ub.edu/10.1016/j.enggeo.2016.12.010

[3] ALSAKER E, GABRIELSEN RH, ROCA E (1996) The significance of the joint patterns of Late-Eocene Montserrat fan-delta, Catalan Coastal Ranges (NE Spain). Tectonophysics 266, 465–91

[4] CHEN Y, MEDIONI G (1992) Object modelling by registration of multiple range images. Image Vis Comput, 10, 145–155

[5] LAGUE D, BRODU N, LEROUX J (2013) Accurate 3D comparison of complex topography with terrestrial laser scanner: Application to the Rangitikei canyon (N-Z). ISPRS journal of Photogram. and Remote Sensing, 82, 10-26 http://doi.org/10.1016/j.isprsjprs.2013.04.009

[6] ESTER M, KRIEGEL H, SANDER J, XIAOWEI XX (1996) A density-based algorithm for discovering clusters in large spatial databases with noise. Proc. 2nd Int. Conf. on Knowledge Discovery and Data Mining

[6] ABELLÁN A, JABOYEDOFF M, OPPIKOFER T, VILAPLANA JM (2009) Detection of millimetric deformation using a terrestrial laser scanner: experiment and application to a rockfall event. Nat Hazards Earth Syst Sci, 9, 365–372

[7] ROYÁN, MJ (2015). Caracterización y predicción de desprendimientos de rocas mediante LiDAR Terrestre. PhD Thesis, Universitat de Barcelona, November 2015

[8] GARCÍA-SELLÉS D, FALIVENE O, ARBUES P, GRATACOS O, TAVANI S, MUNOZ JA (2011) Supervised identification and reconstruction of near-planar geological surfaces from terrestrial laser scanning. Computers & Geosciences, 37 1584-1594

A BRIEF HISTORY OF ROCKFALL BARRIER TESTING

John Duffy[1]
James Glover[2]

Since Arthur M. Ritchie first conducted his rock rolling tests along American state highways in the late 1950s, rockfall design and mitigation has come a long way. To date there have been on the order of 15,500 rocks rolled from various research campaigns. Each campaign has advanced our understanding of rockfall mechanics. Some campaigns to calibrate computer models or to determine the degree of hazard associated with rockfall, and others to test the capacity or utility of specific rockfall protection measures. Building upon Richie's landmark research, rockfall mitigation measures have been under a constant state of development. Immense effort and capital have been expended in the research and design of mitigation measures. Of all four types of mitigation i.e., avoidance, stabilization, protection and management, none have seen more improvements than protection systems. Every aspect of these systems has been and continues to be researched and developed resulting in ever-evolving rockfall mitigation designs. This contribution provides a brief history of rockfall testing where rocks were released into a slope to evaluate rockfall protection methods and in some cases develop numerical rockfall models.

Keywords: Rockfall testing, rockfall protection systems, numerical rockfall models.

ROCK ROLLING EXPERIMENTS THROUGH TIME

In the early 1960s Arthur M. Ritchie of Washington State Department of Transportation performed one of the first comprehensive testing series where rocks were rolled, filmed, and analysed (Ritchie, 1963). The primary goal of these tests was evaluating catchment width criteria, with some rocks rolled into various flexible fence barriers. Following this, in the USA, D'Appolinia Consulting Engineers in 1978, under contract with the North Carolina Department of Transportation, conducted rock rolling tests used to design rockfall mitigation measures and these data were later used to develop a computer model for the Beaucatcher Mountain Highway project (Evans, 1989). In Canada the Ministry of Highways and Public Works conducted rock-rolling tests along the Trans Canada Highway to support a slope stabilization project near the Ferrabee Tunnel (Elstron, et al., 1978) to test the effectiveness of a proposed wall and ditch. Then in North America the Canadian Railways rolled rocks into a cable net attenuator system constructed in Kicking Horse River Canyon near Golden, B.C., Canada (Wyllie, 1991). In California, USA, as part of a rockfall mitigation study, the California Department of Transportation rolled rocks into catchment ditches and catchment fences on numerous road cuts around California (McCauley, et al., 1985). Then in 1987 the California Department of Transportation rolled rocks as part of the Gaviota Pass rockfall project near Santa Barbara, California, USA to design catchment ditches with flexible rockfall fences and

[1]Yeh & Associates, Inc. 2000 Clay St, Denver CO 80211, USA, 303-781-9590, jduffy@yeh-eng.com
[2] Mountain Geohazards, Flüelapassstr. 5 CH-7260 Davos Dorf Switzerland +41 79 350 70 97 jmh.glover@gmail.com

draperies (Duffy, 1989). A few years later the California Department of Transportation began a research project to test and evaluate manufactured flexible rockfall barriers used in Europe (Smith & Duffy, 1989) to construct, test, and evaluate the effectiveness of flexible rockall fences (Fig. 1).

Figure 1: California Department of Transportation Rockfall Barriers Tests (Smith & Duffy, 1989).

Finally, the Colorado Department of Transportation began a series of tests, near Rifle, Colorado, USA, on flexible barriers (constructed of railroad ties and used tires) designed to attenuate the impact energy (Barrett & Pfeiffer, 1989).

In the 90s the testing trend continued with greater enthusiasm and more tests than ever before. In the United States Hearn (1991) was testing the Flex-Post fence at the Rifle, Colorado test site. Colorado DOT (Buroughs, et al., 1992) was testing reinforced earthen berms designed to stop large impact energies. Kane & Duffy (1993) performed a low energy flexible barrier test at the Shale Point test site in California. A comprehensive testing program in Oberbuchsiten, Switzerland (Duffy & Haller, 1993) was completed on steep hard rock slopes. Kurz (1993) with the Railway Department in Stuttgart, Germany tested rail and tie walls at the Oberbuchsiten, Switzerland test site. The Oregon Department of Transportation pioneered a new rockfall runout design criteria for 4:1 (V:H) slopes (Pierson, et al., 1994). Duffy & Hoon (1996) tested flexible rockfall fences with different meshes and infrastructure configurations at the Shale Point test site. In Shayupin, Taiwan flexible fence barriers were studied to evaluate performance and collect data on rockfall trajectories (Bau-Lin & Spang, 1997). In Switzerland testing continued at the Bekenried test site where rocks were rolled into a flexible barriers (Gerber, et al., 1998). In Japan at the Maeda Kosen Quarry, rocks were rolled into a rein-

forced earthen berm (Yoshida & Momura, 1998). Mean while back in the USA, Andrew, et al., (1998) performed tests at the Rifle test site of a recently developed flexible cable net fence. The California Department of Transportation (Duffy & Hoon, 1998) tested flexible rockfall fences with different meshes and infrastructure configurations at the Shale Point test site in California, USA.

Figure 2: Flexible rockfall fence testing with different meshes and infrastructure configurations at the Shale Point test site in California, USA (Duffy & Hoon, 1996).

Figure 2 Rockfall fence Tests in Oberbuchsiten, Switzerland (Duffy & Haller, 1993).

By the 2000's a standard test for testing flexible rockfall fences was developed where rocks be dropped directly into the test fence without ground contact (Gerber, et al., 2001). These new standards decreased the number of rock rolling tests performed. Fortunately rock rolling tests continued largely for the purpose of developing rockfall catchment design guidelines, calibrating computer models and to a lesser extent testing barrier systems. The California Department of Transportation tested a temporary flexible rockfall barrier for use during construction (Duffy & Jones, 2000). In Colorado, USA, between 2004 and 2009 at the Georgetown incline site four test series were performed, to validate the rock rolling models used by CRSP 4.0 and to test a rockfall attenuator system (Arndt, et al., 2009). In Europe two rock rolling tests were performed at the Apennines test site near Parma, Italy and the Leopontine test site in northern Italy (Giani, et al., 2004) to study trajectory analysis, the suitability of existing barriers and the need for new barriers. In France real-size experiments and 3-D simulation of rockfall on forested and non-forested slopes were being performed (Dorren, et al., 2006). At a test facility near Meano, Italy the University Degli Studi Di Trieste tested a hybrid fence commonly referred to as an attenuator (Badger, et al., 2008) to evaluate its performance. In 2012 the California Department of Transportation together with California Polytechnic State University rolled rocks into a flexible fence with an accelerometer inserted into the rocks to measure the roackfall trajectory (Turner, et al., 2012). Testing continued in France to study rockfall rebound and compare detailed field experiments and alternative modelling approaches (Bourrier, et al., 2012). In 2014 repeated controlled rockfall trajectory testing was performed in Switzerland to study the different phases of trajectories (Volkwein, et al., 2015). Most recently in 2015 rock rolling experiments were performed in Hope BC, Canada to test the capabilities of an attenuator system (Glover, et al., 2016).

SUMMARY
The importance of rock rolling studies has been clearly demonstrated and acknowledged world-wide as an important task in rockfall science. For more than 60 years practitioners have been testing barriers, developing numerical models, and creating design guidelines nearly all of which are based on actual rock rolling events. Over 15,500 rocks have been rolled and analysed to various degrees. Of those over 1250 were rolled to evaluate specific rockfall protection measures. Over 670 rocks for flexible rockfall fence systems. Nothing can replace the value of witnessing a rolling rock impact a barrier and observing the impact forces and subsequent response of the barrier. Nor is there any replacement to watching a rock roll and bound down a slope outside of the constraints of a computer model; and as if in protest at our attempts to capture this behaviour in numerical formulations, rebound in spectacular unexpected nature to reveal another feature of the fascinating mechanics of rockfall. Experience has proven that rolling tests have provided otherwise unknown insights into rockfall behaviour and barrier performance.

REFERENCES

ANDREW R D, FRY D A & BOOKWALTER R E (1998) Field Testing and Evaluation of Various Rock Fall Control Systems, prepared for Chama Valley Productions, LLC, Chama Valley, New Mexico, 44 p.

ARNDT B, ORTIZ T, & TURNER A K (2009) Colorado's Full Scale Testing of Rockfall Attenuator Systems, Transportation Research Board, Washington, DC, Circular Number E-C141, 113 p.

BADGER T C, DUFFY J D, SASSUDELLI F, INGRAHAM P C, PERREAULT P, MUHUNTHAN B, RADHAKRISHNAN H, BURSI O S, MOLINARI M E, & CASTELLI E (2008), Hybrid Barrier Systems for Rockfall Protection, In: Proceedings, Interdisciplinary Workshop on Rockfall Protection (A.Volkwein et al., editors), Morschach, Switzerland, pp. 10-12.

BARRETT R K, & PFEIFFER T (1989) Rockfall Modelling and Attenuator Testing, Colorado Department of Transportation Report CDOH-DTD-ED3/CSM-89-2, Denver, Colorado, USA, 44 p.

BAU-LIN H & SPANG R, (1997) Field Tests of a 750 Kilojoule Brugg RockfallBarrier, video recording developed by Chung Cheng Institute of Technology for Geobrugg, Romanshorn, Swit-zerland.

BOURRIER F, BERGER F, TARDIF P, DORREN L, HUNGR O (2012), Rockfall rebound: comparison of detailed field experiments and alternative modelling approaches. Earth Surf. Process. Landforms, 37: 656–665. doi:10.1002/esp.3202

DORREN L K A, BERGER F, PUTTERS U S (2006). Real-size experiments and 3-D simulation of rockfall on forested and non-forested slopes. Natural Hazards and Earth System Sciences 6: 145–153.

DUFFY J D' (1989) Gaviota Rockfall Mitigation Project Memorandum, California Department of Transportation, San Luis Obispo, California, pp. 1-15.

DUFFY J D & HALLER B (1993) Field Tests of Flexible Rockfall Barriers, Proceedings of the Conference on Transportation Facilities Through Difficult Terrain, Aspen Snowmass, Colorado, USA, pp. 465-473.

DUFFY J D, & HOON W (1996a) Field Tests and Evaluation of Hi-Tech Low Energy Chain Link Rockfall Fence, Report No. CA/05-96-01. California Department of Transportation, San Luis Obispo, California, USA, 39 p.

DUFFY J D, & HOON W (1996b) Field Tests and Evaluation of Hi-Tech 50 and 70 foot-ton Rockfall Fence, Report No. CA/05-96-02, California Department of Transportation, San Luis Obispo, California, USA, 42 p.

DUFFY J D, HOON W, & SERAFINI D (1998) Field Tests and Evaluation of Cuesta Grade Chain Link Fence, Gawk Screen, Fence and Jersey barrier, Report No. CA/05-98-01, California Department of Transportation, San Luis Obispo, California, USA, 63 p.

DUFFY J D, & JONES C, (2000) Field Tests and Evaluation of Temporary Construction Chain Link Fence, Report No. CA/05-00-01, California Department of Transportation, San Luis Obispo, California, USA, 4 p.

ELSTON M G, RICHARDS W A, & EASTMAN B W R (1978) Slide 5 Trans-Canada Highway Slope Stabilization, British Columbia Ministry of Highways and Public Works, Highway Engineering Division, Geotechnical and Materials Branch, 45 p.

EVANS C L (1989) The Design of Catch Bench Geometry in Surface Mines to Control Rockfall, Thesis, Department of Mining and Geological Engineering, University of Arizona, 170 p.

GERBER W (1998) Kräfte in Steinschlagverbauungen. In: Steinschlag als Naturgefahr und Prozess. Tagungsband zum Symposium vom 3. und 4. September 1997 in Salzburg. Institut für Wildbach und Lawinenschutz, Universität für Bodenkultur Wien; Institut für Geologie und Paläontologie, Universität Salzburg. 33-41

GERBER W, GRASSL H, BÖLL A, & AMMANN W, (2001) Flexible Rockfall Barriers – Development, Standardisation and Type-Testing in Switzerland. - In: International Conference on Landslides - Causes, Impacts and Countermeasures, 17-21 June 2001, Davos, Switzerland, (Kuehne, M., Einstein, H.H., Krauter, E., Klapperich, H. & R. Poettler, eds.), Verlag Glueckauf Gmbh, Essen, pp. 515-524.

GIANI G P, GIACOMINI A, MIGLIAZZA M, & SEGALINI A (2004) Experimental and Theoretical Studies to Improve Rock Fall Analysis and Protection Work Design, Rock Mechanics and Rock Engineering, Vol. 37, No. 5, pp. 369–389.

GLOVER J, WYLLIE D, BUCHER R, (2016) Attenuator systems — an old method to deviate rocks but a new testing method for developing a design concept, The First Asia Pacific Slope Stability in Mining (APSSIM) Brisbane, Australia.

HEARN G, (1991) CDOT Flex-Post Rockfall Fence, Colorado Department of Transportation, University of Colorado at Boulder, USA, Report CDOH-R-UCB-91-6, 11 p.

KANE W F & DUFFY JD (1993) Brugg Low Energy Wire Rope Rockfall Net Field Tests, Technical Research Report 93-01, The University of the Pacific, Dept. of Civil Engineering, 34 p.

KURZ G, (1993) Rechnerische Untersuchung von Schwellenzaunnen als Schutz gegen Steinschlag und Felssturz, Bundesbahndirektion, Heilbronner Str. 7-9, 70174 Stuttgart.

MCCAULEY M T, WORKS BW, & NARAMORE SA (1985) Rockfall Mitigation, California Department of Transportation, Sacramento, California, USA, 147 p.

BURROUGHS, K., HENSON, H., JIANG, S., 1992. Full Scale Geotextile Rock Barrier Wall Testing, Analysis and Pre-diction, Colorado Department of Transportation, Denver, Colorado, USA, 28 p.

PIERSON L A, DAVIS S A, PFEIFFER T J, (1994), The Nature of Rockfall as the Basis for a New Fallout Area Design Criteria for 0.25:1 Slopes, Engineering Geology Group, Oregon Department of Transportation, Salem, Oregon, USA, 31 p.

RITCHIE A M (1963) Evaluation of Rockfall and Its Control, Highway Research Record 17, Highway Research Board, National Research Council, Washington, DC, pp. 13-28.

SMITH D D & DUFFY J D (1989) Field Tests and Evaluation of Rockfall Restraining Nets, Final Report No. CA/TL-90/05, California Department of Transportation, Sacramento, California, USA, 138 p.

SPANG R M & R BOLLIGER R, (2001) From the Timber Fence to the High Energy Net: Developments in Rockfall Protection from the Origins to the Present, Geobrugg Jubilee Conference, Bad Ragaz, Switzerland, June 2001.

TURNER R T, TURNER J T, DUFFY J D, BALABAN S, 2012, Rock Rolling Experiments to Evaluate Stone Node Accelerometer Data Collection Capabilities and Durability, Internal California Department of Transportation Memorandum, San Luis Obispo, California, 10 pp.

VOLKWEIN A, KRUMMENACHER B, GERBER W, LARDON J, GEES F, BRUGGER L, OTT T (2015) Repeated controlled rockfall trajectory testing. [Abstract] Geophys. Res. Abstr. 17: EGU2015-9779.

WYLLIE D C (1991) Evaluation of Performance of a Rockfall Catch Fence Test Section, British Columbia, Canada, Golder and Associates, 8 p

YOSHIDA Y & NOMURA T, (1998) Latest Experimental Study for Rockfall Mitigation, Protection Engineering, Maedakoson Co. LTD.Japan, 10 p.

FULLY RECORDED ROCKFALL TRAJECTORIES

Axel Volkwein[1], Peter Kummer[1], Tobias Sutter[1]

Rockfall simulation software is increasingly used to predict the energy content and reach of rockfalls as well as existing deterministic or probability based process models. Their validity and calibration usually is based on data originating from natural rockfalls. This contribution presents data from fully recorded rockfall experiments in natural terrain including acting accelerations, rotational speed, position and velocities over time and the runout of the single rock-falls. The total of 111 experiments allow for an statistical analysis regarding single values of interest.

Keywords: rockfall, trajectory, testing, measurements

INTRODUCTION

Both traditional rockfall models and numerical simulation software rely on field data against which they are calibrated and validated. But no simulation or model is able to exactly follow a natural rockfall. There are too many unknown or probabilistic issues affecting the trajectory such as the irregular shape of the falling block, its release mechanism with the resulting starting conditions and the variety of the terrain the block has to cross. The latter can be described in the easiest by the use of different soil types and the general gradient of the topography. In reality, however, the soil types vary constantly regarding their deformation capacities, their surface orientation and their composition. Especially, blocks on the slope have an enormous influence on a single trajectory. Therefore, simulations or models will reflect rather the overall distribution of trajectories in the field resulting in statistical output.
If field data from a natural block is available [1] it has to be checked whether the single event fits into the distributed output. But even then it is not clear whether the single rockfall stands for an average or an extreme event. Therefore, field data ideally are also reflect several events. Such data can be collected in the field from past events [2] or special testing series [3, 4] where blocks artificially are released repeatedly. Both, quality and quantity of data receivable during such experiments increased a lot in the past years due to the advantages of today's technical measurement possibilities [5].
This contribution gives some first results obtained from tests described in [4]. Averaging over all tests allows some first simple statistical analyses. Then, the measurements of a single trajectory are shown. If the single trajectories are analyzed more in detail further results can be presented as exemplified in this contribution for so far ten trajectories.

OVERALL RESULTS

During the testing series first mentioned in [4] six different blocks with masses between 19 and 79 kg and volumes up to 0.031m^3 were released altogether 111 times along a mostly

[1] Swiss Federal Research Institute WSL, Zuercherstr. 111, 8903 Birmensdorf, Switzerland, volkwein@wsl.ch

Fig. 1 Rockfall test slope at Tschamut (CH): (a) starting zone marked in red, (b) runout zone. (c) Start and end positions of single trajectories coloured according to different starting positions.

smooth and grassy slope (Fig. 1a). The testing series concentrated not only on the block dynamics in the so-called transit zone of a rockfall trajectory [6] but also the natural runout on a homogenous slope. The test slope's profile starts with an about 2 m vertical drop followed by terrain with an average inclination of 36°. The runout zone's inclination is almost horizontal (2°). Starting and resting position of each trajectory has been determined using a tachymeter (Fig. 1c). Typical maximum velocities reach 15 m/s.

The average horizontal travel distance of the single trajectories was 92.8 m (standard deviation σ = 20.1 m) with an average height difference of 48.2 m (σ = 4.7 m). This corresponds to an average shadow angle of 28.5° (= 54%). The lateral spread along the starting line was 54.5 m, the maximum horizontal distance between the trajectories end points was 102.4 m. This results in a horizontal lateral spreading of 14°.

Above numbers of course only represent the averages without reflecting the full variability of the single trajectories. Calibration or validation of rockfall simulation codes therefore can be visualized within a GIS environment (e.g. [7]) to better see the influence of local topography.

SINGLE TRAJECTORY MEASUREMENTS

During the tests the total/non-directional accelerations acting on the blocks and their rotational velocities were recorded at about 1 kHz sampling rate (Fig. 2). Based on such data, a trajectory can be analysed over the time. The block has been rolled to the starting position around time t = 6s. The first drop lasted about 0.5s. Acceleration peaks then occur during every impact. At the same times also the rotational speed changes. During the single jumps the rotational speed remains constant. The maximum acceleration during test 109 with a released mass of 79 kg has been detected after the first drop with about 83g (~810m/s^2). The maximum rotational speed during a jump was about 2890°/s which corresponds to eight rounds per second. The block's rotation increases until time about 13 s at the highest terrain inclination of 41° and then slows down

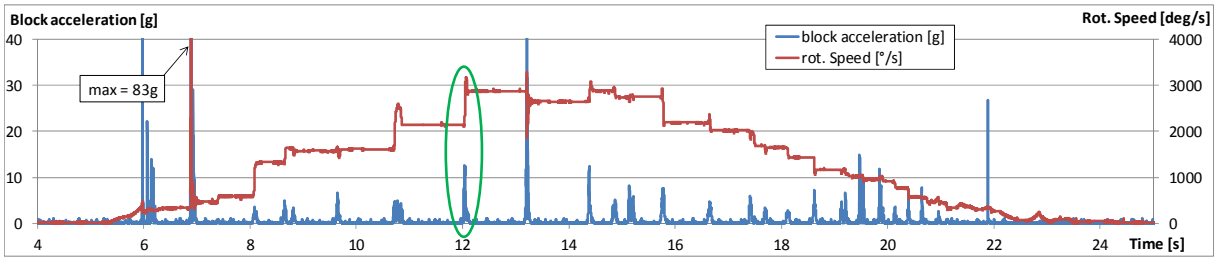

Fig. 2 Block acceleration and rotational speed during trajectory 109 measured over time.

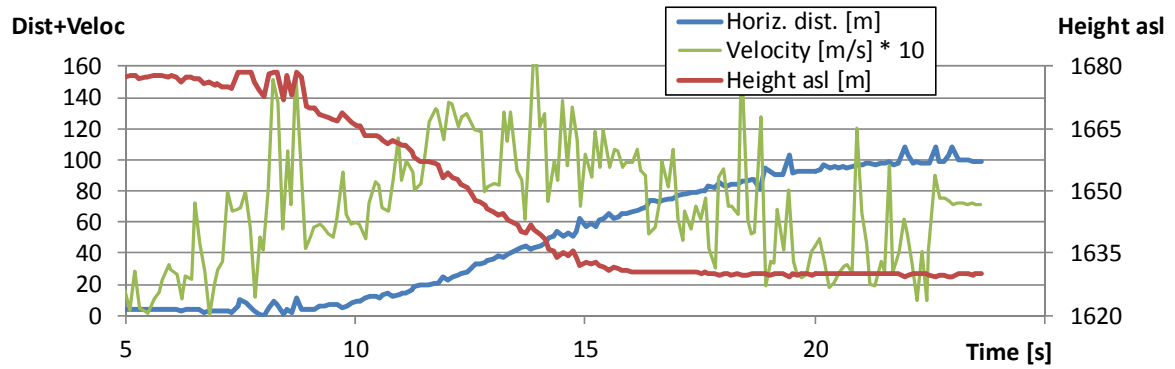

Fig. 3 Block position ground over time during test 109 together with the corresponding ground height a.s.l. and the horizontal block velocity.

again. The 2D position (no jump heights were measured) in the field over the time was recorded at 10Hz using a so-called LPS (local positioning system) [5]. Fig. 3 shows the horizontal distance from start position, the current height of the ground at that position and the horizontal velocity over time. The runout in the horizontal part of the slope is nicely visible because the block still travels about 40 m on the flat ground. We estimate the maximum velocity to ~13 m/s. However, the block's velocity curve over time has high noise.

Video records at 50 frames per second tracked full trajectories but also single jumps of the blocks during in the runout zone of the trajectories (Fig. 4). The vertical movement of the block during a single jump follows gravity and the video scale can be adjusted that a perfect parabola ($s = \frac{1}{2}gt^2$) is obtained.

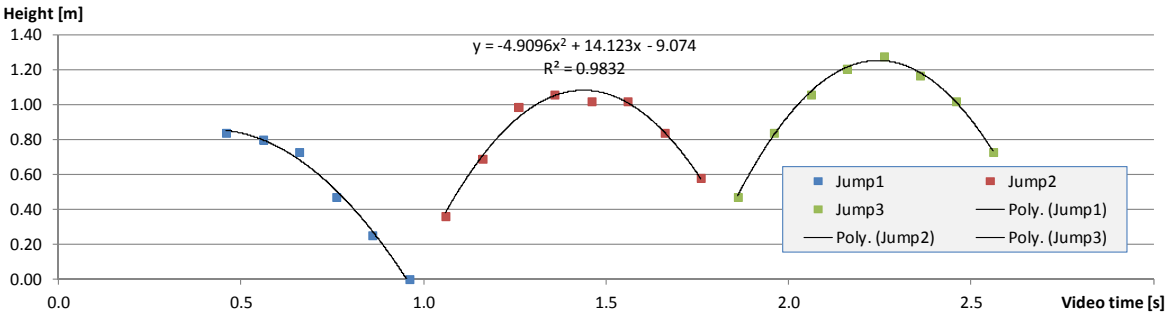

Fig. 4 Block height over time during three jumps in the runout zone. The video scale has been set to obtain a suitable free flight parabola for a single jump.

The combination of the single measurement techniques allows also for an evaluation of their precision. Table 1 shows a comparison of single redundant measurements. The rotational speeds of video analysis and block internal measurement fit very good. The velocity measurements of the LPS vary up to 40% during the runout phase (see explanation above). The accelerations determined from video analysis are usually smaller than measured within the block due to the small picture rate and limited video resolution.

Table 1 Comparison of redundant measurements of trajectory 109 between t = 15s and 17.5s.

	Measurement within block	Video analysis	LPS
Rotational speed [°/s]	2758	2571	
	2192	2250	
	2031	2000	
Velocity [m/s]		10.6	11.9
		8.3	10.7
		7.6	10.7
Acceleration [m/s²]	76	60	
	46	36	

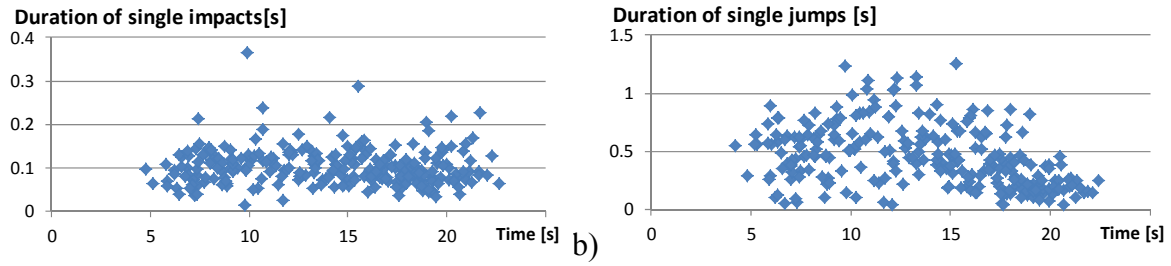

Fig. 5 Duration of (a) single impacts and (b) jumps over the time for 10 different trajectories.

AVERAGE TRAJECTORY ANALYSES

If the single trajectories are separated into single impacts, jumps and runout rolling, their properties deliver additional data for potential comparisons with simulation software. In the following the results of ten selected trajectories are combined. The average duration of these trajectories is about 15.9 s (σ = 2.0 s). Every trajectory has in average 25.9 jumps each lasting in average 0.45 s (σ = 0.26 s) with 1.9 s of final rolling before full stop. The single jumps had an average slope parallel length of 4.5 m (σ = 4.2 m) at an average velocity of 11.5 m/s. The average rotational speed was 4.7 rounds per second (σ = 2.6 rps). The single impacts lasted 0.10 s (σ = 0.04 s) and had an average intensity/acceleration peak of 12 g (σ = 20.6 s).

SUMMARY & CONCLUSIONS

Measurement results of a field test series are presented that cover the full trajectories of the blocks including path, accelerations, rotational velocity and runout. No information are available on the jump heights. Care has to be taken if above data are interpreted as stochastically distributed. For example, Fig. 5 shows the duration of the single impacts and jumps. A Shapiro-Wilk-test on the impact durations reveals that they are not normal distributed. The durations of the single jumps (Fig. 5right), however, seem to be linked to the terrain inclination: in the flat runout zone the jump times decrease.

REFERENCES

[1] GERBER, W. (2015) Geschwindigkeit und Energie aus der Anlayse von Steinschlagspuren - Velocity and kinetic energy from the analysis of rockfall trajectories. Österr. Ing.- Archit.-Z. 160, 1-12: 171-175.
[2] RUIZ-CARULLA, R., COROMINAS, J., MAVROULI, O. (2015) A methodology to obtain the block size distribution of fragmental rockfall deposits. Landslides, 12: 815.
[3] DORREN, L. K. A., BERGER, F., PUTTERS, U. S. (2006) Real-size experiments and 3-D simulation of rockfall on forested and nonforested slopes, Nat. Hazards Earth Syst. Sci., 6, 145–153.
[4] VOLKWEIN, A., KRUMMENACHER, B., GERBER, W., LARDON, J., GEES, F., BRÜGGER, L., OTT, T. (2015) Repeated controlled rockfall trajectory testing. [Abstract] Geophys. Res. Abstr. 17: EGU2015-9779.
[5] VOLKWEIN, A., KLETTE, J. (2014) Semi-Automatic Determination of Rockfall Trajectories. Sensors 14: 18187-18210.
[6] VOLKWEIN, A., SCHELLENBERG, K., LABIOUSE, V., AGLIARDI, F., BERGER, F., BOURRIER, F., DORREN, L.K.A., GERBER, W., JABOYEDOFF, M. (2011) Rockfall characterisation and structural protection - a review. Nat. Hazards Earth Syst. Sci. 11: 2617-2651.
[7] BÜHLER, Y., CHRISTEN, M., GLOVER, J., BARTELT, P. (2016) Significance of digital elevation model resolution for numerical rockfall simulations. [Abstract] In: 3rd International Symposium Rock Slope Stability 2016. Proceedings. 15-17 November, 2016, Lyon (France). Lyon, C2ROP. 101-102.

IMPACT LOADS ON PROTECTION GALLERIES

Axel Volkwein[1], Daniel Fergg[1], Reto Hess[2], Kristian Schellenberg[2]

Full-scale drop tests were performed to evaluate the load bearing capacity of an existing reinforced concrete protection gallery originally constructed in 1940. Blocks with a weight of up to 3.2 tons dropped onto the gallery roof with a falling height of 25 m. The roof was covered by a 40 cm layer of soil. The impact of the block and the reaction of the gallery roof are analyzed in detail and compared with an existing load model. The impact energies were between 80 and 800 kJ.

Keywords: rockfall, protection, gallery, impact, testing

INTRODUCTION

The prediction of the load bearing capacity of a reinforced concrete rockfall protection gallery is complex. This task is on the one hand necessary to design new galleries according to corresponding guidelines [e.g. 1]. On the other hand, the evaluation of existing galleries regarding their remaining capacities considering aging or changing hazard conditions might benefit from different approaches such as improved models [e.g. 2, 3], improving the cushion layer on top [e.g. 4, 5] or numerical simulations [e.g. 6].
Usually, for such models experimental data is essential to allow for calibration and/or validation. An avalanche protection gallery along the Swiss road over the pass "Oberalp" (Fig. 1a) was to be dismantled. Prior to the deconstruction a few tests could be conducted to study the capacity of the gallery regarding rockfall.

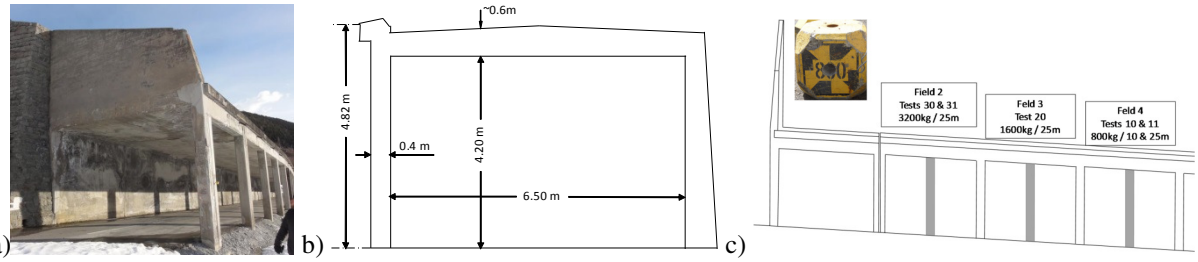

Figure 1 Protection gallery Parde 1: a) upper portal with first gallery fields = sections between valley side columns; b) cross section; c) testing fields & details with position of additional wooden columns and photograph of one test specimen.

TEST SETUP

The gallery has been erected in 1940, some renovation works took place in 1987. The existing drawings described the structural dimensions only. Details on concrete strength and rein-

[1] Swiss Federal Research Institute WSL, Zürcherstr. 111, 8903 Birmensdorf, Switzerland, volkwein@wsl.ch
[2] Canton Grisons, Road Office, Sägenstr. 78, 7001 Chur, Switzerland, kristian.schellenberg@tba.gr.ch

forcement were not available in advance. The about 0.6 m thick gallery roof was line supported by a retaining wall on the mountain side and point supported at the valley side (Fig. 1b,c). A 0.4 m soft soil cushion layer covered the roof before the tests.
In order to setup a suitable testing program the model presented in [2] has been used to predict possible maximum loads to force failure of the roof due to bending of the roof plate. To avoid failure of the valley side support columns additional wooden columns were installed (Fig. 1c). The test specimen with weights of 800kg, 1600kg and 3200kg were shaped according to [7] (see Fig. 1c). They were positioned by a mobile crane above the centers of the gallery fields and lifted into heights of up to 25 m above the roof. After release they free fell onto the cushion layer and the roof.
Figure 1c shows the test details and impact locations. In total, five tests 10, 11, 20, 30 & 31 were performed. The impacts 11 and 31 occurred onto the previously loaded position of tests 10 and 30. During the tests, the vertical accelerations of the test specimen and the bottom side of the gallery roof were measured at 10 kHz. The impact has been recorded by high-speed video camera with a frame rate of 1000 fps. Before and after the tests the elasticity of the soil cushion has been measured using a light drop-weight tester.

TEST RESULTS

The main results of the current testing series are the impact loads F_{max} transferred to the gallery roof. These loads are derived from the maximum block accelerations a_{max} and the block masses m to $F_{max}=a_{max}m$. Hence, it is relevant to obtain the peak values of the accelerations. Figure 2 shows the measurement of the block accelerations of test 20 over time during the impact. The maximum deceleration reaches 2064 m/s^2. The acceleration increases directly after the first contact with the cushion layer and reaches its maximum about 9 ms later. The raw accelerations show strong vibrations, faster ones until time 20 ms, slower ones afterwards. The load impulse is of such a short time that the sensor's limits regarding its own Eigen-frequency might have been reached. So, self-agitation could be possible. The acceleration curve has therefore being smoothed by (i) the use of a running average or (ii) applying a low pass filter (Fig. 2). Both approaches reduce the maximum acceleration significantly down to about 1500 m/s^2 (see Table 1 for all tests).

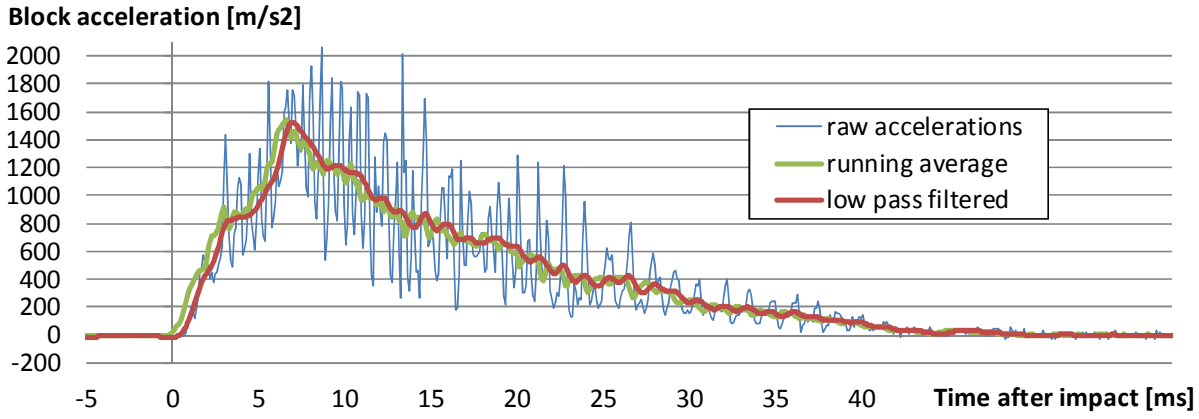

Figure 2 Block acceleration during impact of test 20. Two different approaches (running average/low pass filter) were used to smooth the raw data that are influenced by sensor related vibrations.

Both smoothing approaches have been used to obtain a velocity and a displacement curve through (double) integration of the acceleration data over time (see Figure 3 for method i). In the end we found method (i) to produce a displacement curves that fit better to the video records. The block's velocity has been dissipated after 30 ms. The maximum displacement since first impact was 277 mm.

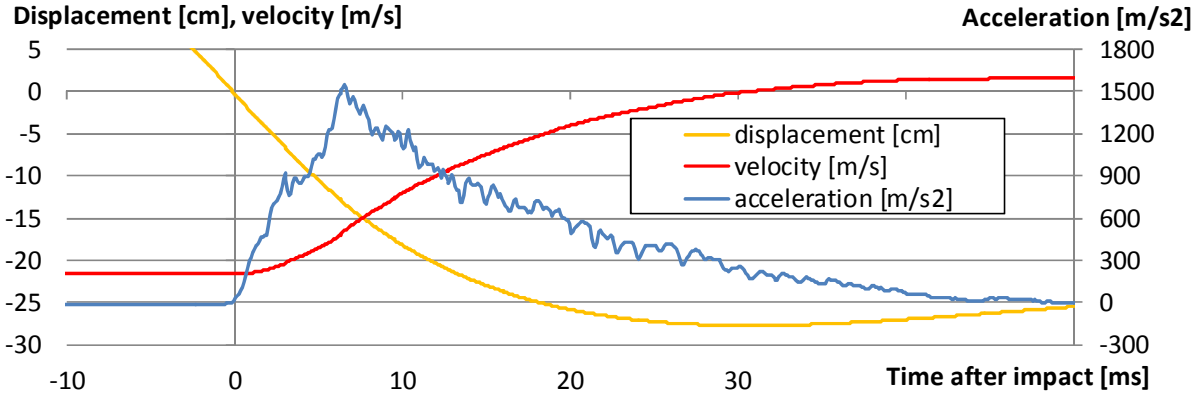

Figure 3 Velocity and displacement of block during impact of test 20 in dependency of the measured accelerations smoothed by a moving average.

The same approaches in recording of accelerations close to the impact location, smoothing and integration over time were also used for the gallery roof. Figure 4 shows its kinetics for test 20. The roof was first accelerated downward during approximately 10 ms and moving up again until time 25 ms. Table 1 shows a summaryof the maximum accelerations.

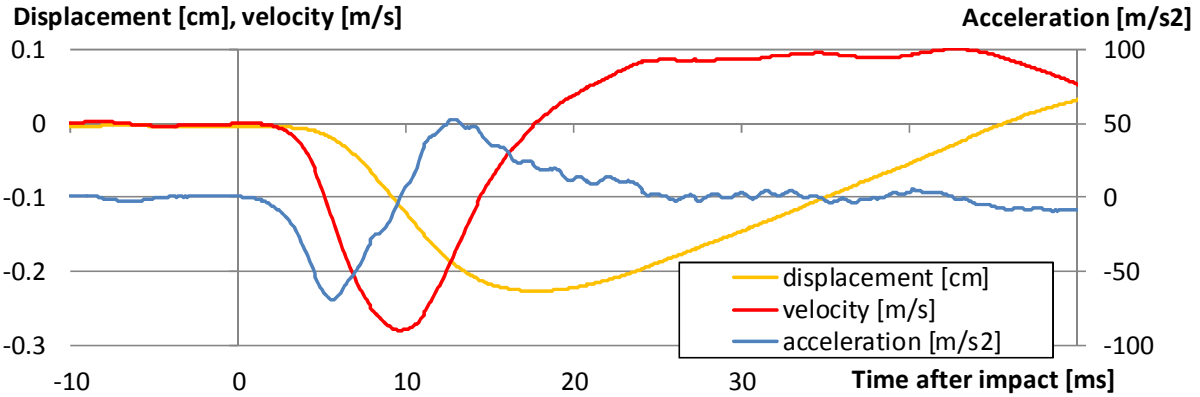

Figure 4 Kinetics of gallery roof during test 20: Velocity and displacement of block in dependency of the measured accelerations smoothed by a moving average.

MODEL RESULTS

The model described in [2] has been setup to match above tests. Table 1 shows a comparison between the model and the test results without additional fine tuning of the model. This allows to compare e.g. impact durations or maximum block accelerations. The test results now allow to further calibrate the model to perfectly match the tests [9]. Based on this calibration a similar structure is assessable resulting in significantly reduced design loads compared to a standard quasi-static approach.

Table 1 Measured and filtered acceleration maxima with comparison between model according to [2] and experimental results. The model has not been specially calibrated for the tested gallery.

Test no.			*P10*	*P11*	*P20*	*P30*	*P31*
Impact duration	*Model*	*ms*	*22*	*12*	*25*	*31*	*12*
	Test	*ms*	*56*	*27*	*43*	*47*	*16*
Time to max. block acceleration	*Model*		*55 %*	*58 %*	*60 %*	*65%*	*67%*
	Test		*27 %*	*19 %*	*21 %*	*15 %*	*31 %*
Maximum block acceleration	*Model*	*g*	*195*	*578*	*258*	*213*	*731*
	measured	*g*	*207*	*608*	*210*	*295*	*536*
	averaged	*g*	*83*	*201*	*157*	*128*	*352*
	low pass filter	*g*	*73*	*260*	*156*	*116*	*340*
Braking distance block	*Model*	*m*	*0.11*	*0.10*	*0.23*	*0.31*	*0.14*
	Test	*m*	*0.24*	*0.23*	*0.28*	*0.36*	*0.16*
	(Video)	*m*	*0.16*	*0.19*	*0.2*	*0.42*	*0.17*
Maximum roof acceleration	*Model*	g	*4.5*	*5.8*	*6.5*	*8.6*	*51*
	measured	g	*-17*	*-75*	*-9*	*-16*	*-98*
	averaged	g	*-11*	*-12*	*-7*	*-12*	*-65*
	low pass filter	g	*-2*	*-26*	*-1*	*-12*	*-61*
Maximum roof velocity	*Model*	m/s	*0.41*	*0.81*	*1.17*	*2.23*	*3.33*
	Test	*m/s*	*-0.1*	*-0.3*	*-0.3*	*-0.5*	*-1.4*
Roof deflection	*Model*	*mm*	*8*	*102*	*25*	*60*	*78*
	Test	mm	*-1*	*-1*	*-2*	*-5*	*-11*

CONCLUSIONS

Field test as presented here and also performed in [2, 8] are important to predict the loads that act on gallery constructions due to rockfall impact. The model used in this contribution tends to overestimate the loads exerted on a gallery roof. I.e., the model stays on the safe side which is advantageous for a reliable design. To better predict limit loads of a gallery existing models can be improved as further described in [9].

REFERENCES

[1] ASTRA (2007) Einwirkungen infolge Lawinen auf Schutzgalerien. Bern: Eidgenössisches Departement für Umwelt, Verkehr, Energie und Kommunikation UVEK.
[2] SCHELLENBERG, K. (2009) On the Design of Rockfall Protection Galleries. PhD thesis, vdf Hochschulverlag AG, ETHZ, Zürich.
[3] FUJIKAKE, K. (2007) Response Analysis of RC Beams Subjected to Impact Loads, Proc. Structures under Extreme Loading (Protect 2007), Whistler, Canada, p. 22.
[4] SCHELLENBERG, K., VOLKWEIN, A., ROTH, A., VOGEL, T. (2006) Rockfall–Falling weight tests on galleries with special cushion layers. In Proc. 3rd International Conference on Protection of Structures against Hazards.
[5] GELLOZ, F. (2011) Dämpfender Steinschlagschutz. Die Baustellen, 03/2011.
[6] GHADIMI KHASRAGHY, S. (2011) Numerical simulation of rockfall protection galleries. PhD thesis, ETHZ.
[7] GERBER, W. (2001) Guideline for the approval of rockfall protection kits. Environment in practice. Swiss Agency for the Environment, Forests and Landscape (SAEFL), Swiss Federal Research Institute WSL. Bern.
[8] RÖTHLIN, C., KURIHASHI, Y., KONNO, H., KISHI, N., VOGEL, T. (2015) Drop weight tests on full-scale specimen of rockfall protection galleries. Institute of Structural Engineering, ETHZ.
[9] FERGG, D. (2016) Schutzwirkung von Galerieverbauungen bei Steinschlag. Bsc thesis, ZHAW.

EVALUATING EXISTING ROCKFALL PROTECTION EMBANKMENTS BASED ON THE CURRENT STATE OF KNOWLEDGE

Stéphane Lambert[1], Bernd Kister[2], Bernard Loup[3]

This article deals with the evaluation of large rockfall protection embankment parks, as observed in some countries. In this purpose, an expedient criterion for assessing the impact resistance of these structures and based on results from the literature is proposed. It is then applied to the Swiss park consisting in more than 250 structures.

Keywords: embankment, assessment, design, impact,

INTRODUCTION

Rockfall protection embankments (RPEs) have been widely used for now more than 30 years for protecting elements at risk against events with energies up to 150 MJ. As a result, large structure parks exist in some countries of the Alpine arch as for instance in Switzerland and France. Such structure parks are heterogeneous in terms of construction date, structure technology, constitutive materials, dimensions, and designed capacity. The vast majority of RPEs are owned by public owners.
In parallel, the improvement of the design of RPEs with respect to block impact has motivated various research works, based on experimental and numerical developments (see a review in [1]). In particular, real-scale impact experiments provide reliable data on the real response of RPEs to impact. Nevertheless, none of these works really benefited to commonly used design methods, except the rather recent Austrian standard (ONR 24810) that is based on small-scale experiments [2]. Besides, most of existing analytical methods, and thus easy to use for designing RPEs, have been shown to be unreliable [3].
In such a context, questions concerning the efficiency of existing RPEs occur, in particular due to the high heterogeneity of the parks. Such questions may rise when dealing with risk management as for instance revising natural risk prevention plans.
In order to get a better view of the Swiss RPE park, a survey was conducted under the supervision of the Federal Office for the Environment (FOEN) in the frame of the AERES project (Analysis of Existing Rockfall Embankments of Switzerland). The expected results were a quantified inventory of existing RPEs and a global vision of the design approaches in use in Switzerland. Based on the collected data, a global evaluation of the RPE park was conducted. In this purpose, an expedient criterion was developed in order to evaluate the ability of existing

1 Irstea, 2 rue de la papeterie, 38402 Saint Martin d'h7res cedex, France, + 33 4 76 76 27 94, stephane.lambert@irtsea.fr
2 Lucerne University of Applied Sciences and Arts, Technikumstrasse 21, CH – 6048 Horw, Switzerland, since 2017: kister - geotechnical engineering & research, Neckarsteinacher Str. 4 B, D – Neckargemünd, +49 6223 71363, kister-ger@t-online.de
3 Federal Office for the Environment (FOEN), 3003 Bern, Switzerland, +41 58 465 50 98, bernard.loup@bafu.admin.ch

RPEs in withstanding the impact by the design block. This criterion was developed based on results from real-scale experiments provided by the literature.
This article gives a general overview of the structure park, introduces the expedient criterion, and applies it to the Swiss rockfall protection embankment park.

PARK DESCRIPTION

The inventory revealed that the total number of RPEs in Switzerland by far exceeds 250 units. The study focused on 53 RPEs, very well documented and less than 20 years old and thus providing indications on the currently used design methods. The vast majority of these RPEs is made of compacted soil, with a rockery facing at the uphill slope. The dimensions range between 15 and 700 m in length and 1.5 and 13 m in height. Approximately 64% of the embankments have a height of 4 m or less, but only approximately 6% have a height larger than 7 m. The average values are 155 m in length and 4.3 m in height respectively.
These RPEs were designed considering reference blocks with a weight and a kinetic energy in very wide ranges: 15 to 1600 kN and 160 kJ to 50 MJ, respectively. About 40% and 64% of the embankments have been designed for stopping blocks with a kinetic energy less than or equal to 2000 and 4000 kJ respectively. 18% of the RPEs were designed for kinetic energies higher than 10 MJ.
When block impact resistance was considered, the design was based on equivalent static force methods as described in ONR 24810, FEDRO guideline for rock sheds, etc.. Obviously, such methods were only employed for recently built structures.

ASSESMENT CRITERION

The criterion was developed based on results from real-scale experiments proposed in the literature and with the aim of finding a simple relation between the downhill face displacement and the block kinetic energy. The downhill displacement is deemed relevant as it is related to the post-impact RPE stability. It is proposed to normalize both these parameters with respect to the structure dimensions, in order to allow comparison from one case to the other. As an initial approach, the kinetic energy is divided by the cross section of the structure. Indeed, the larger the cross section, the higher the energy dissipation capacity of the RPE. As for the downhill displacement, it is proposed to normalize this value by the mid-height structure width, which is representative of the structure dimension in the impact direction, irrespective of the cross sectional structure shape.

Fig. 1 plots the results presented in the literature in terms of these two normalized parameters. Data concerns various types of structures impacted under different conditions (see [1] for more details). It can be seen that there exists a limit in terms of kinetic energy beyond which the downhill displacement exceeds 25% of the structure width. This limit equals 250 kJ/m².
Considering this finding, the RPE is considered impact resistant if:

$$C_{25} = \frac{KE}{250 * A} < 1$$

where KE is the block kinetic energy (kJ), A is the structure cross section area along the vertical axis calculated from the ditch elevation (m²). The subscript 25 in C_{25} refers to the maximum allowable downhill deformation with respect to the structure width (here, 25%).

The validity domain of this expedient criterion is related to the experimental conditions:
- Reinforced structure;
- RPE with a height in the 3-4.2 m range, and a mid-height width in the 3-4.3 m range;
- Block with a 30° approx. downward incident trajectory;
- Impact point located at a significant distance from the crest (at least ¼ of the structure height).

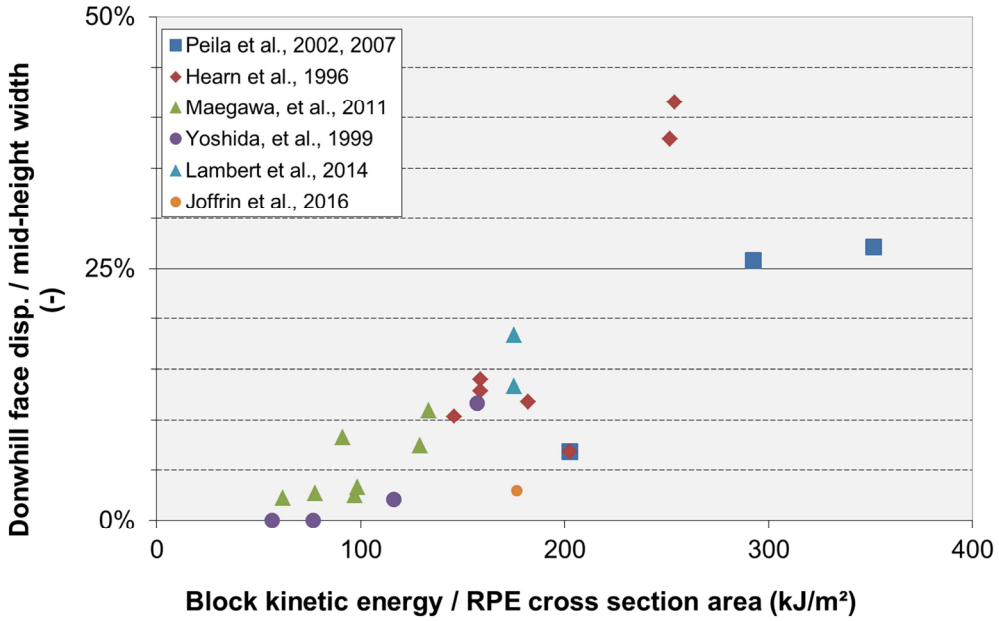

Fig. 1 Comparison of real-scale impact experiments on embankments (for precise references, see [1])

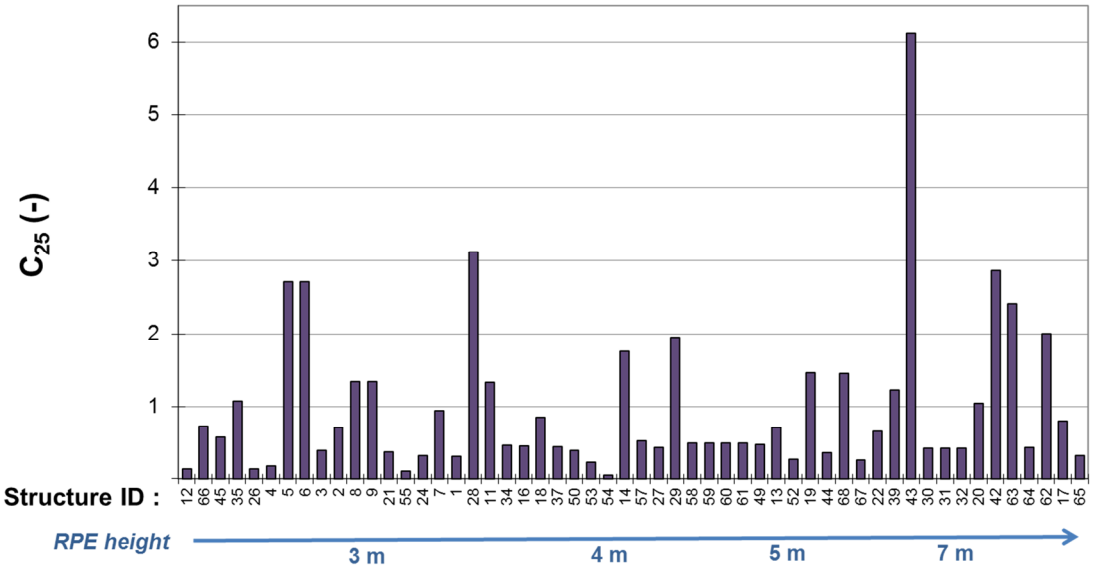

Fig. 2 Embankment Swiss park evaluation

Also, this expedient criterion was compared to data presented in the literature and concerning existing structures designed considering various complex approaches. None of the structure failed the criterion, suggesting the criterion to be consistent with these methods.

PARK EVALUATION

As most of the RPEs of the park are non-reinforced structures, and considering results from the literature, it was decided to divide the acceptable limit of C_{25} by 2.
When applied to the 53 RPEs, the efficiency criteria reveals that more than 50% of the RPEs have a C_{25} value less than 0.5 and thus may be considered able to withstand the impact by the block (Fig. 2). On the other hand, the C_{25} exceeds the value of 1 in 17 cases, among which 7 cases exceed the value of 2. It is worth highlighting that the criterion is used out of its validity domain for the 4 tallest ones out of these 17 cases, due to the RPE height and impact point location.
This expedient evaluation thus draws the attention on possibly critical structures. For these, complementary analysis may be required, depending on the protected elements at risk in particular. This concerns first, structures with a C_{25} higher than 2, and second structures with a C_{25} higher than 0.5. But prior to any detailed analysis, the relevance of using the C_{25} should be checked depending on the impact case vs. the experimental conditions. Also, the acceptability of the destruction of the RPE should be checked versus the return period of the event considered: destruction may be tolerated in case of a 300-year return period event but not for a 30-year one.

This park was also evaluated via criteria based on small and half-scale tests with rotating blocks [4]. This second evaluation complements the C_{25} approach and it is not detailed here.

CONCLUSION

Based on the AERES inventory more than 250 rockfall protection embankment structures exist in Switzerland. The vast majority are unreinforced structures with a rockery facing. Only a limited number of these structures were designed accounting for their block impact resistance. In such a context, an expedient criterion was proposed to allow the identification of possibly critical structures with respect to this design facet. When applied to the structure park, this criterion appeared to be fulfilled for the majority of the structures. On the opposite, this criterion draws the attention on about 20% of the structures for which complementary analysis could be conducted to assess their impact resistance.

REFERENCES

[1] LAMBERT, S, BOURRIER, F (2013) Design of rockfall protection embankments: a review. Engineering geology 154 (28), 77-88
[2] ONR (2013) ÖNORM 24810: Technischer Steinschlagschutz – Begriffe, Einwirkungen, Bemessung und konstruktive Durchbildung, Überwachung und Instandhaltung, Austrian Standards Institute
[3] KISTER, B, FONTANA, O (2011). On the evaluation of rockfall parameters and the design of protection embankments – a case study. Proc.of Rocexs 2011, Innsbruck, Austria, 31-32
[4] KISTER, B (2015) Development of basics for dimensioning rock fall protection embankments in experiment and theory (in German). FEDRO report 1524.

Development of Design Method for Rock Fall Attenuators

DUNCAN WYLLIE[1], TIM SHEVLIN[2], JAMES GLOVER[3], CORINNA WENDELER[4]

INTRODUCTION

A five year research program is nearing completion to develop improved rock fall protection structures that only absorb a portion of the impact energy, such that the net deflects the rock into the ground where the balance of the energy is absorbed. The structures are termed Attenuators and are recognised to require minimal maintenance [1]. The research has involved theoretical studies of impact mechanics, laboratory experiments, and full-scale testing in Canada where blocks of rock and concrete cubes weighing up to 950 kg were dropped down a 60 degree, 60 m high rock face. The performance of the structure was evaluated with an extensive instrumentation system.

Keywords: Rockfall, protection structures, testing, Attenuators, impact mechanics, instrumentation

ATTENUATOR PRINCIPLE

Figure 1 shows the typical features of Attenuators comprising a freely hanging, flexible but impact resistant steel net suspended from steel posts with hinged bases bolted to the rock face. Each post is supported with four support cables anchored to the rock face with cable loop anchors and cement grout [2]. The required capacity of all components has been established from the full-scale tests.

EXISTING ATTENUATOR INSTALLATIONS

A total of 24 Attenuators have been constructed in North America over the last 20 years approximately, and many of these have been impacted hundreds of times over their operational life (Figure 2). This experience has shown that virtually no maintenance is required, and that removal of the accumulated rock can readily be carried out.

[1] Wyllie & Norrish Rock Engineers, 1400 – 750 West Pender Street, Vancouver, BC V6H 2T8, Canada, dwyllie@wnrockeng.com
[2] Geobrugg North America, LLC 4676 Commercial Street SE, Salem, OR 97302, tim.shevlin@geobrugg.com
[3] Mountain Geohazards, Global Risk Forum GRF Davos, Obere Strasse 22B, CH-7270 Davos Platz, Switzerland, james.glover@grforum.org
[4] Geobrugg, AG Aachstrasse 11, CH-8590 Romanshorn, Switzerland, Corinna.wendeler@geobrugg.com

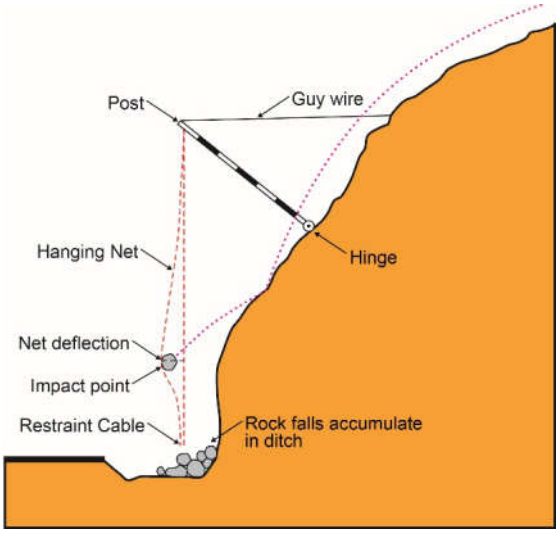

Figure 1. Typical Attenuator configuration

Figure 2. Attenuator installation showing series of hinged posts with support cables, and a freely hanging net.

FULL SCALE TESTING OF ATTENUATORS

Full scale testing for Attenuators described in this paper has been carried out to verify their performance during impact with respect to energy dissipation in the net, load transfer into the support cables, and net deflection (Figure 3). In order to make the testing as realistic as possible, the test blocks impacted the rock face as they fell so that they were translating and rotating when they impacted the net.

The test facility was constructed in a quarry where the test blocks could be dropped from heights up to 60 m down an irregular rock face at an overall slope angle of 60 degrees. The Attenuator was constructed with two, 8 m long steel beams attached to hinged bases bolted to the rock face.

Two types of blocks were used for the testing: initially 0.5 and 0.8 m blocks of rock, with masses up to 400 kg; secondly, heavily steel reinforced concrete cubic blocks, with dimensions of 0.75 m and a mass of 950 kg.

The instrumentation was designed to capture the mechanics of how the rock's impact momentum is transferred to the net, and the cables supporting the posts and net. The instrumentation included:

Cameras - rock fall motion was recorded with two video cameras, running at 60 fps (face view) and 250 fps (side view).

Figure 3. Construction of test Attenuator

Load cells - the load in each support cable was measured with a Z-type tension load cell, that were connected to a data acquisition system running at 2400 Hz.

Accelerometers and gyroscopes - a sensor incorporating 3-D accelerometers, 3-D gyroscopes (angular rate sensors), a data acquisition system running at 20,000 Hz and a programmable gravity trigger was used to record the translational and rotational motions of the concrete blocks.

RESULTS OF ATTENUATOR TESTING

In 2015 and 2016, a total of 46 tests was carried out in which the test blocks impacted the net and records were obtained by the video cameras and of the loads in the support cables [3]. The following is a brief description of the results.

Translational and rotational velocity - typical translational velocity behaviour was for a rapid decrease in velocity from the moment of impact (t = 0 seconds) to a time of about 0.2 seconds, which was the time at the maximum load was induced in the load cells (see Figure 4). During this 0.2 second time interval, the translational velocity decreased by about 50 per cent, and from this time the velocity remained approximately constant until impact with the ground occurred.

With respect to the rotational velocity, the videos clearly showed that the frictional contact between the rotating, irregular blocks and the openings in the wire mesh, caused the rotational velocity to be reduced to zero in a period of 0.15 to 0.2 seconds. Following this, rock's rotate in the opposite direction until they impacted the ground.

Loads in support cables - Figure 4 shows typical loads induced in the ten support cables during impact on the net. It was found that the peak load occurred at a time of about 0.2 seconds after impact, and that the duration of the peak loading is coincident with the most rapid reduction in translation velocity, and the loss of rotational velocity.

DESIGN METHOD FOR ATTENUATORS

The impact of rock falls with an Attenuator net system as shown in Figure 1 can be analyzed using momentum principles in which the translational and rotational momentum of the rock at impact is transferred to the net and the support cables. According to the conservation of momentum, the momentum lost by the impacting block as it is slowed by the net, is equal to the momentum gained by the movement of the net and the loads induced in the support cables. In addition, the frictional contact between the translating and rotating block and the net generates shear forces that are additional forces induced in the load cells.

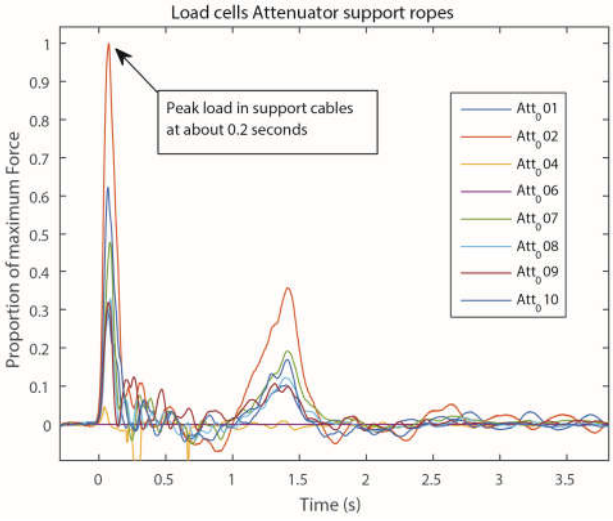

Figure 4. Typical forces in load cells during impact.

The data gathered from the cameras (velocity of block and net), load cells (forces in support cables) and accelerometers/gyroscopes

(acceleration changes and forces) provides values for the parameters in the conservation of momentum equations. These calculations show the mass of net that is required to reduce the velocity of the falling rock and redirect it into the ditch.

CONCLUSIONS

The integrated test information on the mass and shape of the test blocks along with the mass of the net, and data from the video cameras, load cells, accelerometers and gyroscopes has provided a unique insight into the performance of Attenuator net systems under full scale rock fall impact conditions. This information has demonstrated the following features of Attenuator performance:

- Nets fabricated with high strength steel wire and weighing 2 to 4 kg m^{-2} can withstand impact forces generated by translating and rotating blocks of rock and concrete with masses up to 1000 kg.
- The basis of Attenuator design is to use an appropriate ratio between the mass of the falling rock and the mass of the net.
- For blocks with velocities up to 25 m s^{-1}, the deflection of the net during impact was in the range of 1 to 2 m.
- The rotation of the blocks was reversed during impact with the net which helps to contain the rocks in the ditch.
- Because the velocity of the blocks is reduced by their impact with the net, only a portion of the impact momentum (and energy) is absorbed by the net and support system.
- The net is self-cleaning because the rocks fall out of the lower edge of the net into the ditch.

REFERENCES

[1] DESIGN CONSIDERATION FOR PASSIVE ROCKFALL PROTECTION STRUCTURE (2016). MBIE, New Zealand.
[2] WYLLIE. D. C. (2014). Rock Fall Engineering, CRC Press, Boca Raton, FL., 243 p.
[3] SHEVLIN, T., WYLLIE. D. C., GLOVER, J. (2016). Attenuators for controlling rockfall: result of a state-of-the-art full scale test program, HGS conference, Colorado Springs, USA.

IMPROVING THE DESIGN OF LOW-ENERGY ROCKFALL CATCH FENCES

Hassan Al-Budairi[1], Zhiwei Gao[1], Andrew Steel[2], Trevor Davies[1], Simon Wheeler[1]

Low-energy rockfall catch fences are widely used along railways and roads to mitigate rockfall hazards. A typical low-energy catch fence consists of double-twisted wire mesh, posts and ground anchors. Since there is no design guidance, numerical modelling is frequently used as an aid to their design. In this paper, three-dimensional finite element modelling of low-energy rock catch fences is presented, with special focus on the response of the wire mesh, which dissipates much of the impact energy. An accurate representation of the geometry of the double-twisted wires is used, which enables proper simulation of their deformation. The parameters for the constitutive model for the wire are determined from experimental tests. Using this approach, good agreement between the numerical simulations of catch fence response to boulder impact and experimental data have been obtained.

Keywords: low energy flexible barrier, double-twisted wire mesh, finite element modelling

INTRODUCTION

A typical low-energy and lightweight rockfall catch fence is shown in Fig. 1. This design is widely used to protect railway infrastructure in Scotland, where the energy of falling rocks is generally below 100 kJ. At present, these fences are primarily designed based on experience and engineering judgements, as there are no design guidance/codes. To improve the design of low-energy fences, numerical modelling using the finite element method is frequently used. Accurate modelling of the double-twisted wire mesh is particularly important because this element dissipates most of the impact energy. The wire mesh generally consists of symmetric hexagonal cells comprised of four sections of single wires and two sections of double-twisted wires. For example, the Maccaferri double-twisted hexagonal 2.7 mm diameter wire mesh with cell dimensions of 80 mm×100 mm, referred to as P8/2.7, is shown in Fig. 2.

Some earlier studies [1,2] simplify the mesh geometry to reduce the modelling complexities and to reduce computing time, but at the cost of reduced accuracy. In reality, mesh response is very complicated and cannot be satisfactorily modelled by over-simplification [3].

For example, the wires in double-twisted sections stretch and twist simultaneously. Impact energy is dissipated both by friction between the double-twisted wires and by elasto-plastic stretching of individual wires. At high loading levels, single wires may become damaged and cause unravelling of adjacent wires which degrades the response of nearby cells.

In this study, an accurate representation of the geometry of the double-twisted wires is adopted, which enables better simulation of interaction (friction) between the wires. Secondly, a constitutive model, which properly describes the failure of individual wires is employed, using the

[1] University of Glasgow, School of Engineering, Glasgow G12 8LT, UK, +44-141-330 3927, Zhiwei.Gao@glasgow.ac.uk
[2] QTS Group, Strathaven, Scotland ML10 6QJ, UK, +44-1357 440 222, AndrewSteel@qtsgroup.com

parameters obtained from experimental tests. All the simulations are carried out using the finite element code, Abaqus/Explicit [4].

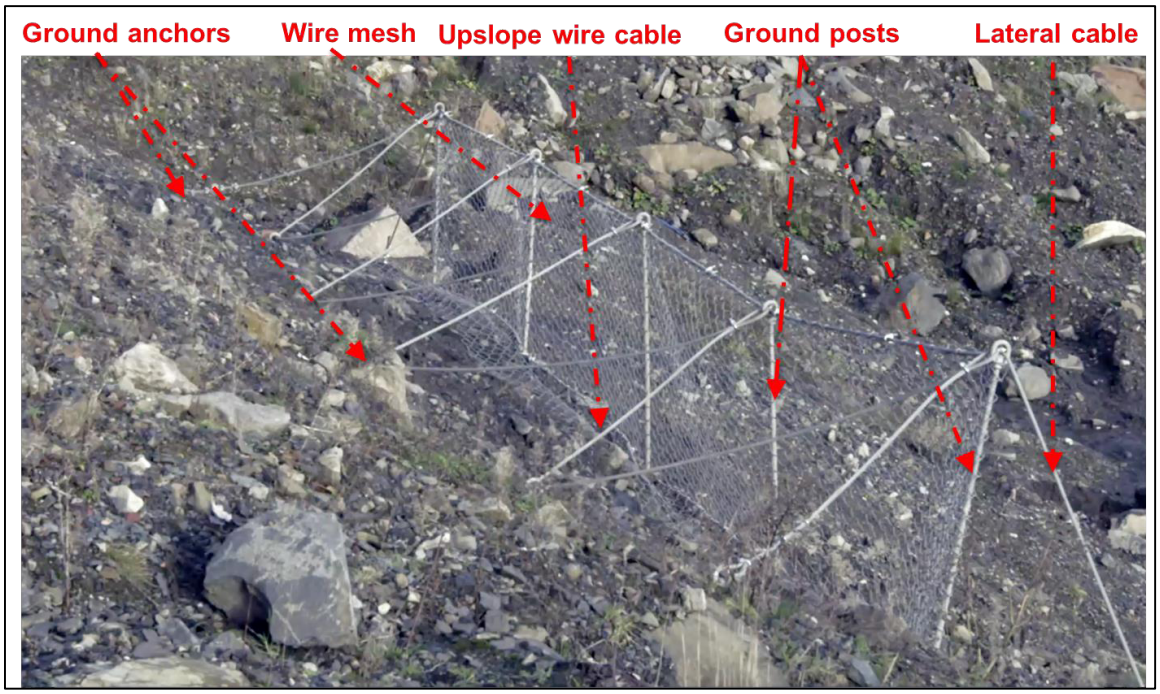

Fig. 1 A lightweight rockfall catch fence system.

NUMERICAL MODELLING

A general elasto-plastic constitutive model with progressive damage evolution model based on ductile damage initiation criteria was used in this study. To determine the parameters, uniaxial tensile tests were carried out on single wires, as shown in Fig. 2. A uniaxial tensile machine (Instron 3369) and a high speed video extensometer ((LIMESS RTSS) for optical strain measurements were used in these tests. A uniaxial loading rate of 2 mm/s was imposed as recommended by ETAG027 [5]. A number of uniaxial tensile tests were conducted and the average data where used to calculate the true stress-true plastic strain data required by Abaqus. A linear damage evolution model was employed to forestall any numerical instabilities arising from wire failure [4].

The geometrical model of the mesh was created in SolidWorks and then exported to Abaqus. The wire is discretised by using Timoshenko beam elements which allow the simulation of axial stretching, bending (change in curvature) and twisting in three-dimensional space. A discretized model of a double-twisted wire mesh panel is shown in Fig. 3.

In order to model the interaction between wires, Abaqus/Explicit provides a powerful beam-to-beam contact algorithm which simulates the real contact between the surfaces of beams rather than their centrelines [4].

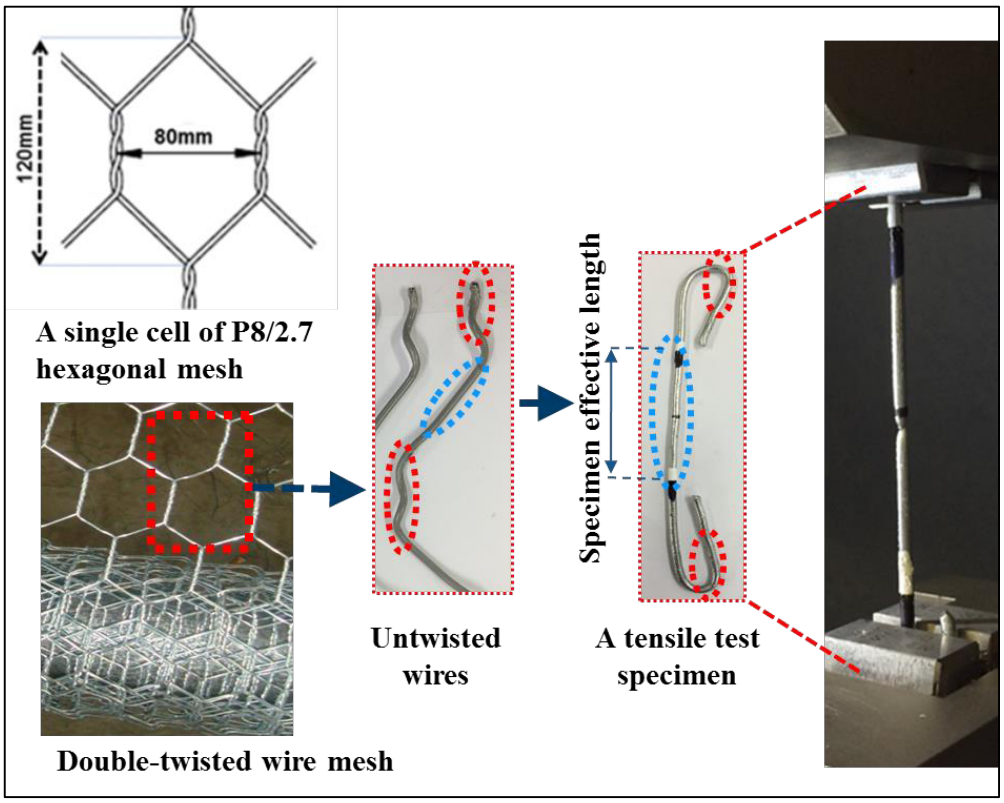

Fig. 2 Uniaxial tensile tests on single wires.

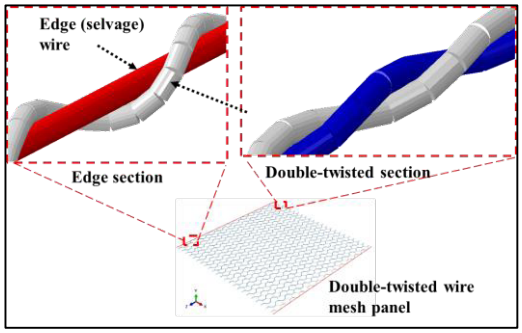

Fig. 3 A discretised model of a double-twisted hexagonal wire mesh panel.

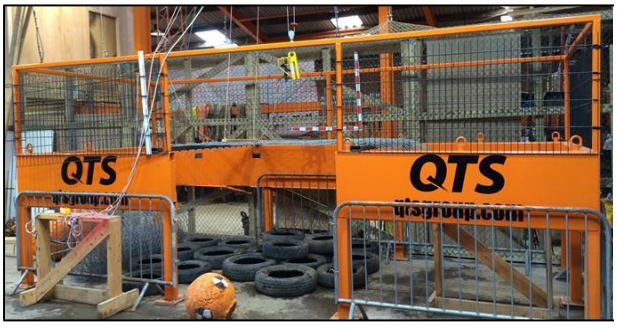

Fig. 4 Experimental impact tests on wire mesh samples.

MODEL VALIDATION AND RESULTS

An impact testing rig was fabricated to test laterally constrained wire mesh panels by dropping boulders from various heights as shown in Fig. 4. The test rig has two adjustable horizontal cross-beams which can support panels of various lengths. A high-speed camera (500 fps) was used to capture the boulder velocity and catch fence deformation. Two additional cameras were used to record the lateral deformation of the panel and the deflection of the supporting beams. Various boulder masses were employed in these tests with an impact velocity of 7 m/s.

The data from two impact tests using spherical concrete boulders of 100 kg (test 1) and 200 kg (test 2) masses on 2 m×2 m wire mesh panels are presented in Fig. 5. The vertical displacements of the boulders are measured after the impact and compared to the model predictions. The results show that the model reproduces the vertical response of the masses during the first impact

(from 0.1 s to 0.75 s) very well. The agreement between the experimental and modelling results for the subsequent impacts (i.e. after successive rebounds) is also very well captured.
The kinetic energy of the boulders during the tests are shown in Fig. 5: most of the impact energy is dissipated within the first 0.1 s (i.e., during the first impact).

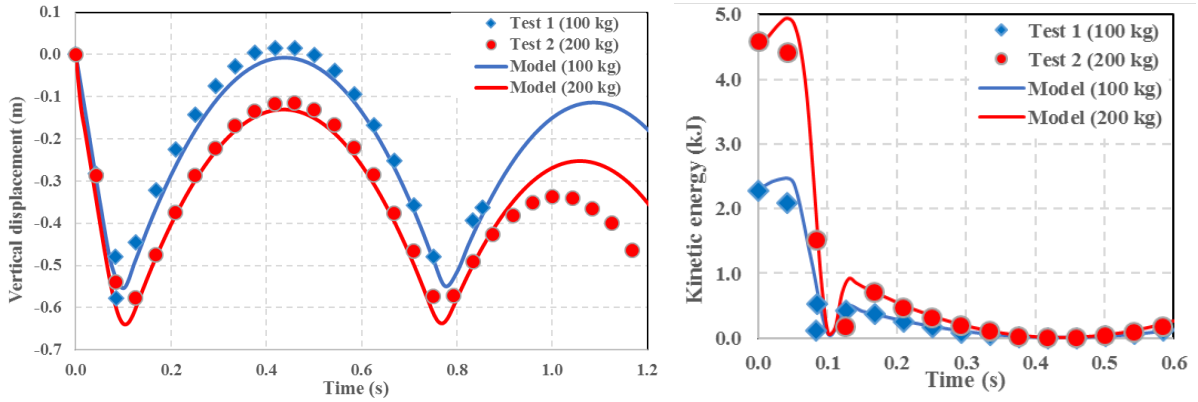

Fig. 5 Comparison between experimental data and numerical predictions for: (left) boulder vertical displacement, and, (right) boulder kinetic energy

CONCLUSIONS

An advanced 3D finite element model of boulder impact on catch fences has been developed. The good agreement between the model predictions and measured data from two full-scale impact tests lends confidence in the design method based on the finite element model.

AKNOWLEDGEMENT

This research is funded by the Knowledge Transfer partnerships (KTP) programme (Project No. 9980) and QTS Group Ltd., a leading railway infrastructure services company in the UK (http://www.qtsgroup.com/). We acknowledge the contribution of **Mr Mark Craig** of QTS and the use of laboratory and High Performance Computing facilities provided by the School of Engineering, University of Glasgow.

REFERENCES

[1] BERTRAND D, TRAD A, LIMAM A, SIVANI C (2012) Full-scale dynamic analysis of an innovative rockfall fence under impact using the discrete element method: from the local scale to the structure scale. Rock Mech Rock Eng. 45, pp 885–900.
[2] THOENI K, LAMBERT C, GIACOMINI A, SCOTT W (2013) Discrete modelling of hexagonal wire meshes with a stochastically distorted contact model. Comp Geotech 49, pp 158–169.
[3] AL-BUDAIRI H, GAO Z, STEEL A, WHEELER S, DAVIES T (2016) Modelling and optimising of a light-weight rockfall catch fence system. NAFEMS UK Conference, pp 129-132.
[4] ABAQUS ANALYSIS USER'S MANUAL (2014) Dassault Systems Simulia Corp, Providence, RI.
[5] EOTA ETAG 027 (2008) Guideline for European technical approval of falling rock protection kits. Eur Organisat Techn Appr.

UNUSUAL PREFABRICATED ROCKFALL GALLERY USING WIRE MESH AND GEOSYNTHETICS

Joëlle Arnaud[1], Magali Huteau[2], Philippe Robit[3], Nicolas Villard[3]

In the French Alps, a railway track frequently exposed to small rock falls has been protected thanks to an innovative method. Indeed, conventional mitigation options such as ETAG rock fall barriers were impossible to install because of the traffic intensity (high-speed trains, night-and-day freight). Moreover, risk assessment had concluded to high velocity trajectories with frequent small boulder falls so that it was quite problematic to safely set up protection for the staff.
Therefore, a prefabricated protection gallery using a light membrane over a steel structure was implemented by GTS after a design - build procedure with the SNCF authorities.

Keywords: prototype, gallery, railway, high velocity,

BACKGROUND

The section between Culoz and Modane is a high-speed train-track with a heavy traffic of passenger trains to ski resorts and of sensitive freight-trains. Along the 'lac du Bourget', the track follows a high and steep cliff of limestone subject to regular boulder falls (about 1 litre weekly). To protect the track, a warning system called DCR (in French: 'Détection de Chute de Rochers' [1]) was put into place in the sixties. Made of electrical wire ropes, it protects the trains from boulders larger than 10 litres. However, in 2016, a man was injured by a small boulder during a maintenance operation on the DCR. That's why an emergency complementary mitigation was set up on the upper cliff.

Fig. 1 Global view of the site, near Chambery, France

[1] SNCF Réseau, 235 Ch. de la Rotonde, 73000 CHAMBERY France, joelle.arnaud@reseau.sncf.fr
[2] SNCF Réseau, 6 Av. F. Mitterrand, 93210 SAINT DENIS France, magali.huteau@reseau.sncf.fr
[3] GTS, ZI 6 rue de la Métallurgie, 38420 DOMENE France, +33(0)685121732, nvillard@gts.fr

OBJECTIVES

The main issue was to protect both the rail infrastructure during mitigation works on the upper part of the cliff (anchoring…), and the staff involved on maintenance works.

Usually, hazards would have been solved by active protection using anchors associated to catch-barriers on the upper slope. However, external parameters made conventional installation strictly impossible due to staff exposure, residual risk of damage during works, traffic intensity, and the cost of traffic break-down - there was no scheduled time for works except for 2 hours on Sunday night.
Considering the emergency and so as to follow the natural risk management at SNCF [2], a consortium was developed with SNCF, GTS, SAGE INGENIERIE and ENGINEERISK,

The concept emerged from a passive protection pushed as closed as possible to the railway in order to be prebuilt ahead of time in a safe area, which was then put into place by heavy cranes with limited time-closure. Moreover, this option helps protect the staff during set up. The structure should remain temporary removable for service/maintenance work.

The reflections and studies of the working group resulted in the following results:

Reference hazard defined [3] :

- Boulders : 218 kg
- Velocity : 37 m/s
- Energy level (SEL) : 150 kJ
- High of cliff : 70 m high
- Length of cliff : 60 linear meters long

Three solutions under study [4]

- 1) “Sandwich structure” made of iron, wire mesh and sand bags
- 2) “Sheet metal gallery” like factory roof
- 3) “Gallery made of high-tensile wire mesh and high resistance geosynthetics”

After a full cost analysis of these results the SNCF Authorities opted for solutions 3.

DESIGN OF THE STRUCTURE AND INSTALLATION

The membrane is made of 2 layers including high-tensile wire mesh (170 kN/m), associated to high resistance geosynthetics (500 kN/m).
Dedicated connection systems have been developed in order to minimize the risk of perforation, as there is high boulder velocity on site.

The implementation geometry requires a strong metallic structure of 20 m high, 15 m width and 60 m long. The global weight is 33 tons, assembled in packs of 9 tons each using heavy cranes.

Fig. 2 Aerial view of the gallery.

FEEDBACK

This prototype shows a new way to protect the railway from natural hazards. The structure above the railway track was raised in 5 days with a 30-hour break. Then, the implementation of anchors - 3200 m² of steel wire mesh and various rock fall protection barriers - was undertaken with no impact on the train flow at the foot of the cliff. A little under 2 months of total closure of the traffic would have been necessary to treat the natural hazard. Even helicopter transports were facilitated.

Beyond the necessity of treating risks for the servicing team, the cost of such a tailor-made structure is rapidly counterbalanced, despite weeks of interruption of heavy traffic on an international railway track. This structure can be reused on other transport infrastructures after incidents or with limited intervention time on site. After we explored different scenarios in a few months, our team and partners tend to judge the solution as efficient and renewable.

This innovative process has improved the constant interactions between transporters, engineers, the coordinator of safety at work, and civil engineering firms. This project drove us to share technical and scientific information with dynamic team interactions. Communication has helped the team to be involved in the project from all levels from the operational team to the local authorities and the central decision organs of SNCF.

AKNOWLEDGEMENTS:
SNCF, SAGE INGÉNIERIE, ENGINEERISK, CITEM, the GTS team on the field

REFERENCES

[1] GRANDSERT P (2006) Les systèmes de détection sur le réseau ferré français, Actes des Journées Nationales de Géotechnique et de Géologie de l'Ingénieur, Lyon, France, pp 33-40.
[2] MIALI A, MIHAILOVITCH F, CHIROUZE F, TERPEREAU JM (2016) Management de la sécurité du système ferroviaire, International Railway Safety Council
[3] SAGE Ingénierie (2016) Etudes des risques de chutes de blocs, Versant de la Colombière, Gières, RP. 7220
[4] ENGINEERISK (2016) Protection pare-pierres – Falaise de la Colombière – Evaluation de différentes solutions au stade préliminaire, R&D36k

DISCRETE ELEMENT MODELLING OF PUNCH TESTS WITH A DOUBLE-TWIST HEXAGONAL WIRE MESH

Antonio Pol[1], Fabio Gabrieli[1], Klaus Thoeni[2], Nicola Mazzon[3]

Metallic wire meshes are commonly used for rockfall protection and rockfall mitigation. Their design is mostly based on empirical results and experience. Due to the significant importance of these structures their design needs to be more accurate and, therefore, numerical methods are nowadays used for improving and optimising the design. The most common approaches are the Finite Element Method (FEM) and the Discrete Element Method (DEM). The latter is used in this work as it is particularly well suited for studying discontinuous problems, including failure, with high accuracy. The study focuses on the validation of a numerical model of a double-twisted hexagonal wire mesh subject to punch tests. The numerical model is represented by a set of spherical particles at the physical nodes of the mesh. Remote interactions are implemented to represent the wires. The numerical predictions are compared to the results of experimental tests to calibrate and validate the model. In particular, the influence of the stress-strain curves of the single wire and double-twist on the punch tests are investigated by using deterministic and stochastic models.

Key words: Discrete Element Method, Wire Meshes, Punch Test, Rockfall Protection

INTRODUCTION

The detachment of small rock fragments or blocks from slopes represents one of the most significant hazard for people and infrastructures also in the context of quarries and mines. A common way to reduce this hazard is the installation of rockfall protective systems as drapery or cortical meshes and rockfall net barriers. In general, the design is based on engineering work experience, but in the last years the behaviour of structural protections has also been studied numerically and experimentally. Adequate numerical models to simulate wire meshes are still in development and several approaches have been proposed in the literature. The most common one is the Finite Element Method (FEM), where the wire meshes are modelled by using truss elements, beam elements, shell finite elements and special purpose finite elements. The FEM is well established for dynamic modelling of continuous problems with non-linear geometries, complex mechanical behaviour, and various contact conditions. A big issue occurs when the failure of the wire mesh needs to be considered, in this case computational demands become very high. Hence, the Discrete Element Method (DEM) represents a good alternative being particularly well suitable for dynamic problems that involve discontinuous materials and failure. In the DEM the material is represented by a discrete number of rigid particles which can overlap during collision. Particles interact with each other by a specific

[1] ICEA dpt., Univ. of Padova, via Ognissanti 39, 35129, Padova, Italy. +390498277994, fabio.gabrieli@unipd.it
[2] Centre for Geotechnical and Materials Modelling, University of Newcastle, Callaghan, NSW 2308, Australia.
[3] Maccaferri Innovation Center Srl, Via Werner Von Siemens 19-Siemensstrasse 19, 39100 Bozen (BZ), Italy.

contact or long-range interaction laws while contact detection algorithms and an explicit integration scheme of the equation of motion updates their position.
In this work, a numerical model of a double-twisted hexagonal wire mesh is used. Punch test results from the manufacturer are used in order to calibrate the model with particular attention on the choice of the constitutive law in the implementation of the wire mesh. The open-source framework Yade [6] is used in this study.

DISCRETE ELEMENT MODEL OF THE WIRE MESH

This study utilises the Maccaferri double-twisted hexagonal wire mesh of the type 8x10 with a wire diameter of 2.7 mm. The characteristics and size of the mesh considered in this study are summarized in Fig.1a.
The hexagonal honeycomb-like structure increases the overall strength of the wire mesh and the double-twist wires prevent that failure of a single wire compromise the entire panel.

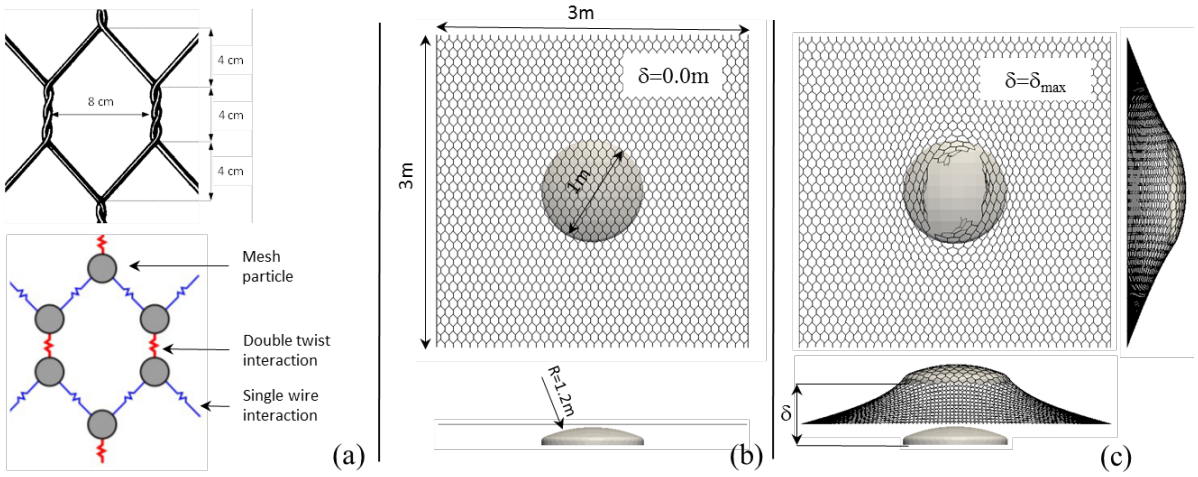

Fig. 1 (a) Sketch of a double-twisted hexagonal wire mesh with definition of the geometrical parameters and the corresponding remote interaction model. (b) Snapshots of punch test geometry at the beginning and (c) at failure.

The wire mesh is represented by a set of spherical particles located at the physical nodes of the mesh [1,2,3]. Physical contact between these particles is generally not allowed. The wires between the nodes are not discretised explicitly but they are substituted by remote interactions (Fig. 1a) with piece-wise linear force-displacement curves. The generation of the mesh follows the procedure outlined in [4]. Thereby, all particles have the same diameter which is equal to four times the diameter of a wire, and their density is adjusted so that the numerical mesh and the physical mesh have the same mass.
In this work, different constitutive laws are used in order to verify their validity, comparing numerical predictions with experimental data. In the first model, presented in [3], the force-displacement curve for a double-twisted wire is directly derived from the one of the single wire by using two local parameters λ_k and λ_ε: the first one acts on the initial stiffness of the double-twist, while λ_ε takes the strain reduction at failure into account.
The second model uses two distinct force-displacement curves for the single wire and the double twist [5]. Finally, the stochastically distorted model presented in [5] is applied. The latter takes into account the irregularity of the real wire mesh deriving from the difference of

the real length of the wire between nodes and the numerical length. For this aim, two parameters are introduced: the first parameter λ_u defines a horizontal shift for the force-displacement curve, the second parameter λ_F modifies the stiffness of the wire in the shifted part. This kind of irregularities are randomly distributed on the mesh panel according to a triangular distribution with the average value equal to $0.5\lambda_u L_0$, where L_0 is the undistorted length of the wire.

CALIBRATION OF THE PUNCH TESTS

Experimental results of punch tests conform to the conditions and the geometry given in UNI 11437-2012 have been used for the model calibration. The shape of the punching element is shown in Fig.1b. The mesh panel is 3 x 3 m with xyz displacement constraints at the four edge boundaries. The same conditions were reproduced in the numerical tests using a frictionless triangular mesh to describe the punching element, imposing the vertical displacement and measuring the force on the punching element.
In order to be able to compare the various models, the same laboratory stress-strain curves for wires are used with each model at the beginning. With the model 1 of [3], only the single wire curve is relevant and the best fitting parameters for the calibration of the double-twist interactions resulted $\lambda_k = 0.10$ and $\lambda_\varepsilon = 0.83$. For the deterministic model 2 of [5], both curves from experimental tensile tests (single wire and double-twist) are used. Instead, with the stochastic model 3 of [5], using the previous curves, the best fit of experimental data is obtained using $\lambda_u = 0.02$ and $\lambda_F = 0.80$. In Fig.2a the force-displacement curves obtained by using the above mentioned models are compared. A good agreement with the experimental results can be obtained using the different models.
With regards to the stochastic model, it is important to observe that the low value of λ_u, obtained in this calibration, suggests a negligible distortion and the model approximately behaves in a deterministic way. In Fig.2b a parametric study of the effect of λ_u is presented. It is possible to observe that δ_{max} decreases with decreasing λ_u value, whereas Force$_{max}$ initially decreases with decreasing λ_u and after a value of $\lambda_u = 0.2$ this parameter shows no more influence on the force at failure. In this case, neither the force nor the displacement values at failure are influenced by λ_F, due to the very low value of λ_u.

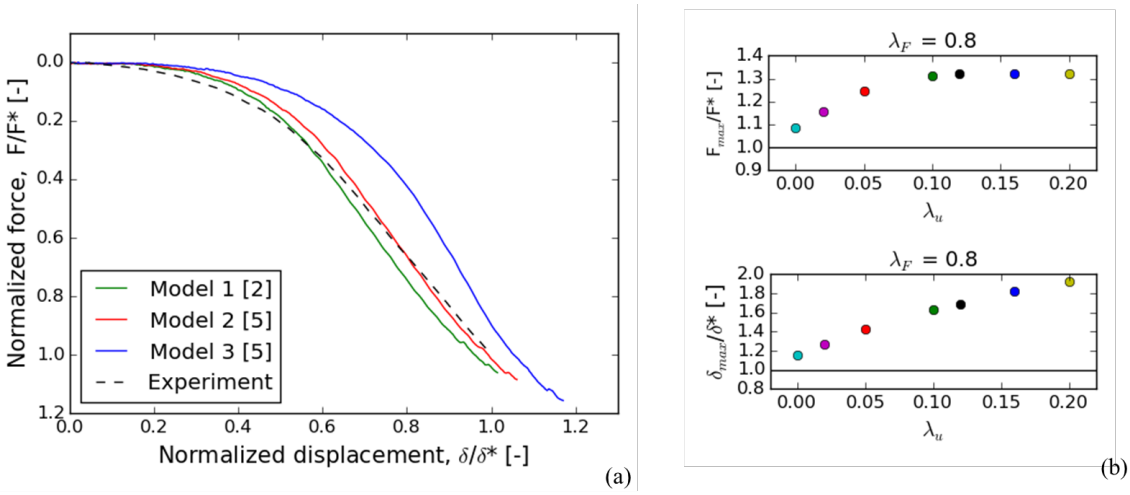

Fig. 2 (a) Comparison of experimental (1 test) and numerical (3 models) results of punch tests, the curves are normalized with the mean of maximum experimental values of force F* and displacement δ*; (b) influence of the stochastic parameter λ_u on force and displacement at failure (model 3).

Finally, the influence of adopting three different stress-strain curves obtained from a set of single wire and double twist laboratory tensile tests has been investigated. As shown in Fig.3, the choice of the stress-strain curve influences the numerical results in a non-negligible way. Moreover, using different stress-strain curves could be a way to assess the variability that is typical of laboratory tests.

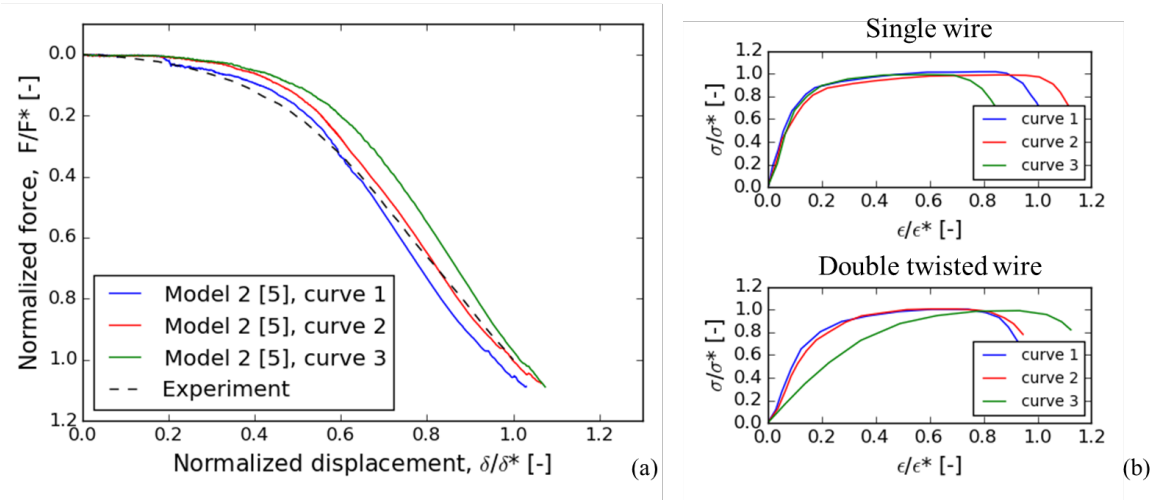

Fig. 3 (a) Mechanical response, curves are normalized as mentioned above, of punch tests (model 2) using curves from three repetitions of single wire and double-twist tensile tests; (b) experimental stress-strain curves, normalized with the mean of maximum experimental values of σ and ε, of single wire and double-twisted wire tensile tests [5].

CONCLUSIONS

Experimental results of punch tests are relevant for the assessment of the mechanical behaviour of wire meshes. The good agreement between discrete element simulations and experimental data confirms the effectiveness of this numerical tool to evaluate laboratory tests from small strains to failure conditions of the mesh.
Intrinsic variability of materials and mesh geometry seem to be important and can be effectively evaluated performing single wire and double-twist tensile tests on a set of samples and calibrating a stochastic model.

REFERENCES

[1] NICOT F, CAMBOU B, MAZZOLENI G (2001) Design of rockfall restraining nets from a discrete element modeling. Rock Mech Rock Eng 34, 99-118.
[2] BERTRAND D, NICOT F, GOTTELAND P, LAMBERT S (2005) Modelling a geo-composite cell using discrete analysis. Comput Geotech 32(8), 564-577.
[3] BERTRAND D, NICOT F, GOTTELAND P, LAMBERT S (2008) Discrete element method (DEM) numerical modelling of double-twist hexagonal mesh. Canadian Geotech J 45(8), 1104-1117.
[4] THOENI K, LAMBERT C, GIACOMINI A, SLOAN S.W (2011) Discrete modelling of a rockfall protective system. Oñate E, Owens D, editors. Particle-based methods II: Fundamentals and applications. II International conference on particle-based methods. CIMNE Internat Center for Numerical Methods in Engineering, 24-32.
[5] THOENI K, LAMBERT C, GIACOMINI A, SLOAN S.W (2013) Discrete modelling of hexagonal wire meshes with a stochastically distorted contact model. Comput Geotech 49, 158-169.
[6] ŠMILAUER V, CATALANO E, CHAREYRE B, DOROFENKO S, DURIEZ J, GLADKY A, ET AL (2010) Yade Documentation, 1st ed., The Yade Project <http://yade-dem.org/doc/>.

UPGRADING EFFECTS OF NEAR-SURFACE MOUNTING OF ARAMID FIBER REINFORCED POLYMER RODS ON IMPACT RESISTANT CAPACITY OF REIFORCED CONCRETE BEAMS

Norimitsu Kishi[1], Masato Komuro[2], Yusuke Kurihashi[3], Hiroshi Mikami[4]

In order to develop a rational strengthening method for upgrading impact resistant capacity of the reinforced concrete (RC) beams, proposing a near surface mounting (NSM) technique of Fiber Reinforced Polymer (FRP) rods, falling-weight impact tests of the RC beams were conducted. Here, Aramid FRP (AFRP) rod/sheet were used. From this study, it is seen that the AFRP rods NSM method may be more rational technique than the AFRP sheet boding method for upgrading impact resistant capacity of the RC beams.

Keywords: RC beam, Impact loading, AFRP rod, NSM method, Impact resistant capacity

INTRODUCTION

In Japan, many reinforced concrete rockfall galleries are constructed to protect the transportation network from disaster due to falling rocks. However, magnitude of falling energy of the rocks may be increased by big rocks being exposed on the ground due to long-term deterioration of the slope along the road and/or by big rocks being deteriorated due to freezing and thawing action. To keep structural safety of the galleries, absorbing performance of the cushion material and/or impact resistant capacity of the gallery components should be increased.

In order to upgrade impact resistant capacity of the RC members, concrete thickness increasing method, steel-plate jacketing method, and fiber reinforced polymer sheet bonding method are sometimes applied. Here, a NSM method of FRP rod was proposed and an applicability of the method was discussed comparing the experimental results with the case of applying FRP sheet bonding method for RC beams.

Figure 1 shows the concept of two methods: FRP sheet bonding method; and FRP rod NSM method. In this paper, Aramid FRP (AFRP) rod/sheet was applied which is light, flexural, and limp material and better impact resistant one. The AFRP rod was prepared by braiding bundles of the Aramid fiber to

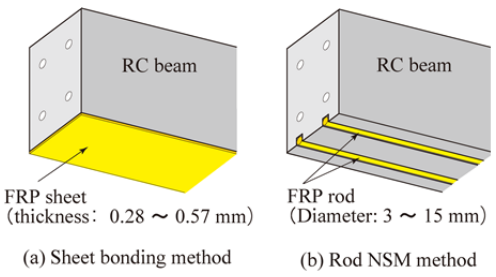

Fig.1 Flexural strengthening method for RC beams using FRP material.

[1] National Institute of Technology, Kushiro College, Kushiro 084-0916, Japan, kishi@kushiro-ct.ac.jp
[2] Muroran Institute of Technology, Muroran 050-8585, Japan, komuro@news3.ce.muroran-it.ac.jp
[3] Muroran Institute of Technology, Muroran 050-8585, Japan, kuri@news3.ce.muroran-it.ac.jp
[4] TRI of Sumitomo-Mitsui Construction Co. Ltd., Nagareyama , 270-0132, Japan, hiroshimikami@smcon.co.jp

be bar; after that impregnating with epoxy-polymer; and then being dried and hardened.

EXPERIMENTAL OVERVIEW

Specimens used in this experiment were listed in Tab. 1. In this table, the nominal name of specimen was designated in order of strengthening procedure (N: without strengthening, S: applying AFRP sheet bonding method, and R: applying AFRP rod NSM method) and set falling height H*n* (*n*: falling height in metric unit) of the weight. The estimated free falling height *H*' was evaluated using measured falling velocity of the weight just before impacting the upper surface of RC beam. In this experiment, the AFRP sheet and rods were debonded for the Beams S-H3.0 and R-H3.5, respectively.

Figure 2 shows dimensions of the beam, layouts of rebar and AFRP sheet/rod. The beams have a rectangular cross section of 250 × 200 mm (height × width) and a clear span length of 3.0 m. The AFRP sheet was bonded and AFRP rods were mounted onto the tension-side surface of the beams leaving 50 mm between the supporting point and the end of the sheet/rod as shown in Fig. 2.

The volumes of AFRP sheet and rods were determined for these total axial stiffnesses *EA* to be almost equal to each other as listed in Tab. 1. Calculated load-carrying capacity of each beam was listed in Tab. 1. The calculated capacity of the beam was estimated following Japanese concrete standard (Japan Society of Civil Engineers, 2005) and using material properties of concrete, and AFRP sheet/rod listed in Tab. 2.

Falling-weight impact tests were conducted by dropping the weight from a prescribed height onto the mid-span of the beam using the impact test apparatus as shown in Fig. 3. The weight is made of a solid steel cylinder and mass of the weight was 300 kg. The RC beams are placed on the supports equipped with load cells for measuring the reaction forces and are clamped at their ends using cross beams to prevent lifting off. The supports are able to rotate freely while restraining horizontal movement of the beam. The weight was vertically dropped via the guide rails at the mid-span of the beam.

Tab. 1 List of specimens

Beam	Strengthening method	Set falling height of weight *H* (m)	Measured falling height of weight *H*' (m)	Measured input impact energy E_r (kJ)	Axial stiffness of whole sheet/rod *EA* (MN)	Tensile capacity of whole sheet/rod (kN)	Compressive strength of concrete *f*'c (Mpa)	Calculated flexural capacity *P*usc (kN)	Calculated shear capacity *V*usc (kN)
N-H2.5	-	2.5	2.29	6.73	-	-	32.4	55.0	329.0
S-H1.0	sheet bonding method	1.0	1.12	3.29	13.5	235.7	35.4	102.1	331.6
S-H2.0		2.0	2.19	6.44					
S-H2.5		2.5	2.40	7.06					
S-H3.0		3.0	3.24	9.58					
R-H0.5	Rod near-surface mounting method	0.5	0.52	1.53	13	224	35.7	101.0	315.9
R-H1.0		1.0	1.08	3.18			35.4	98.6	331.6
R-H1.5		1.5	1.58	4.65			35.7	101.0	315.9
R-H2.0		2.0	2.19	6.44			35.4	98.6	331.6
R-H2.5		2.5	2.52	7.41					
R-H3.0		3.0	3.24	9.53					
R-H3.5		3.5	3.62	10.64					

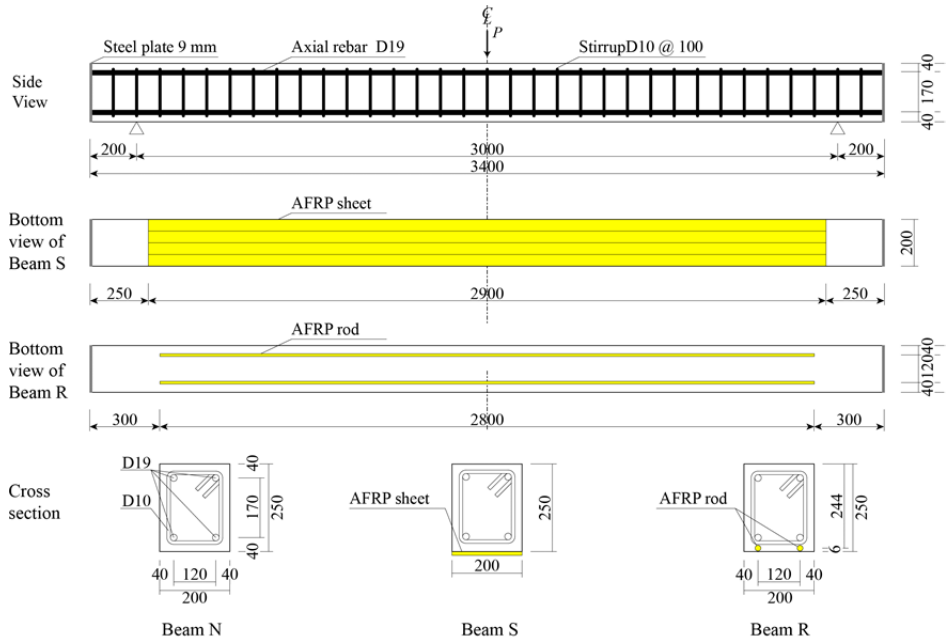

Fig. 2 Dimensions of test specimens

Tab. 2 Material properties of AFRP materials (nominal values)

AFRP material	Mass per unit (g/m^2)	Diameter of rod ϕ (mm)	Tensile strength (GPa)	Elastic modulus E (GPa)	Fracture strain (%)
Sheet	830	-	2.06	118	1.75
Rod	-	11	1.18	68.6	1.72

EXPERIMENTAL RESULTS AND DISCUSSIONS

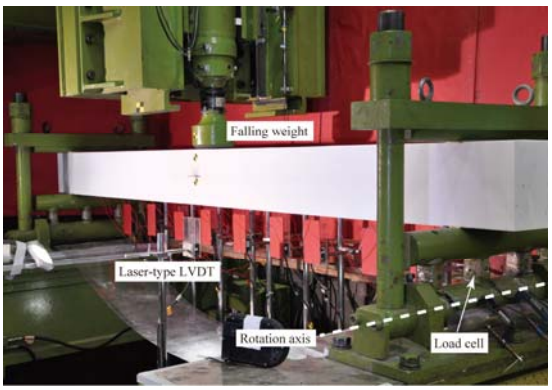

Fig. 3 Experimental setup

Figure 4 shows the time histories of the impact force P, the total reaction force R, and the mid-span deflection D for the beams. In these figures, an origin of the time axis is taken as the time when the weight impacts beam.

Figure 4(a) shows the impact force time histories P during a 20 ms time interval from the beginning of impact. From these figures, it is observed that the responses of all beams have a similar time history response and at the beginning of impact, the time history exhibits a triangular shape with high amplitude and short time duration of about 1 ms.

Figure 4(b) shows the total reaction force time histories R during a 80 ms time interval from the beginning of impact. From these figures, it is observed that all the beams behave similarly, i.e.: (1) a response with high amplitude is excited over 35 - 50 ms from the beginning of impact; and (2) the main response is composed of a triangular-shaped component and high-frequency components.

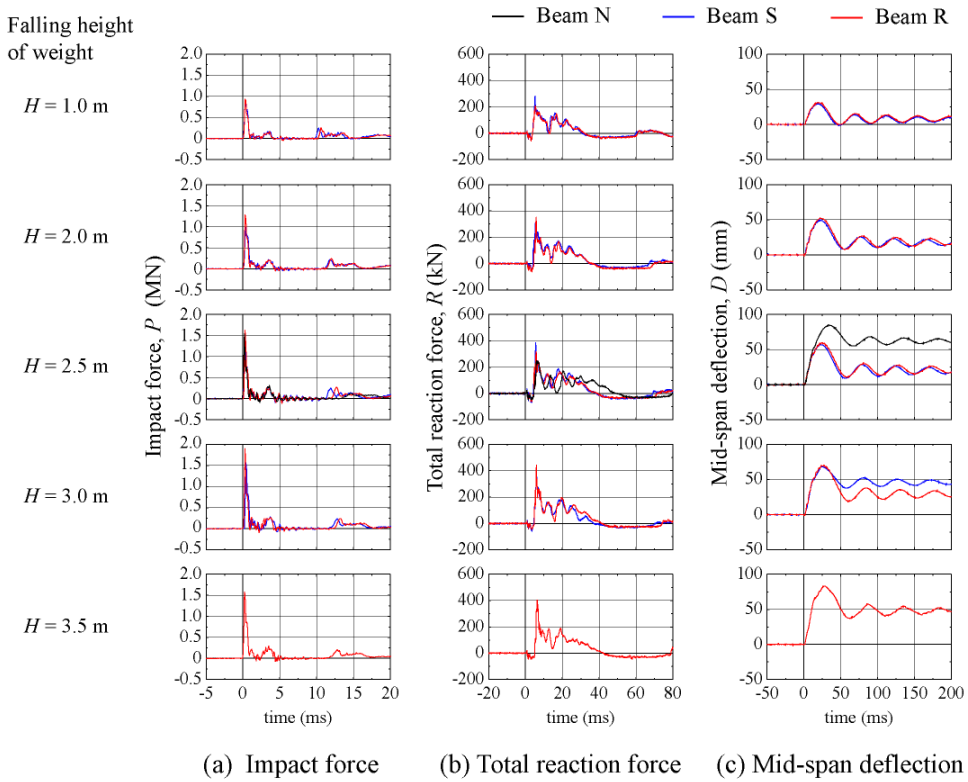

Fig. 4 Time histories of impact force *P*, total reaction force *R*, and mid-span deflection *D* of RC beams.

Figure 4(c) shows the mid-span deflection time histories *D* during 200 ms from the beginning of impact. From these figures, it is observed that: 1) shapes of the time history curves are similar for all the beams shown here; and 2) the main response exhibits a half-sine wave, after that the deflection is remained and the time history exhibits damped sinusoidal shapes.

Since time histories of the Beams S and R are almost similar in the cases of from H = 1 m through 2.5 m, it is seen that the upgrading effects of the AFRP material on impact resistant capacity of the beams are similar up to H = 2.5 m. However, at the case of H = 3.0 m, residual deflection of the Beam S was larger than that of the Beam R and AFRP sheet of the Beam S was debonded. In the case of Beam R, the deflections at the case of H = 3.5 m were larger than those at the case of H = 3.0 m, and the AFRP rods was debonded. Then, it is confirmed that the upgrading effects on impact resistant capacity of the RC beams due to applying AFRP rod NSM method may be greater than that due to applying AFRP sheet bonding method.

CONCLUSION

In order to rationally upgrade the impact resistant capacity of the RC beams, AFRP rod near-surface mounting (NSM) method was proposed and the applicability was experimentally discussed comparing with results in the case of applying AFRP sheet bonding method.

From this study, it is seen that the upgrading effects on impact resistant capacity due to applying the AFRP rod NSM method is greater than those due to applying AFRP sheet bonding method.

IMPACT TESTS ON SMALL SCALE EMBANKMENTS WITH ROCKERY – LESSONS LEARNED

Bernd Kister[1], Stéphane Lambert1[2], Bernard Loup[3]

In the project AERES (Analysis of Existing Rockfall Embankments of Switzerland) small-scale quasi-2D-experiments had been done with embankments with stones placed parallel to the slope and stones placed horizontally. The experiments showed that rotating cylinders acting as impactors may surmount an embankment with batter 2:1, even if the freeboard is chosen to 1.5 times the block diameter. So a slope with an inclination of about 60° and equipped with rockery in general does not guarantee that a freeboard of one block diameter will be sufficient as described by the Austrian standard. During the test series also a block with an octagonal cross section had been used. This block, with no or only very low rotation, on the other hand was not able to surmount an embankment with rockery and a freeboard of about 0.8 times the block diameter. The evaluation of test data showed additionally that the main part of energy dissipation occurs during the first 6 ms of the impact process. At least 75% to 85% of the block's total kinetic energy will be transformed into compression work, wave energy and heat when the block hits the embankment.

Keywords: rockfall protection embankment (RPE), impact, rockery, block shape, ratio rotational to translational energy, freeboard, energy dissipation

INTRODUCTION

A common measure used in Switzerland to stabilize steep slopes of rockfall protection embankments is the use of rockery. According to the interviews done with employees of cantonal administration as well as with design engineers the rockery used in the past at the uphill slope of an embankment was constructed with a batter between 60° to 80°. But in general only less attention had been paid on the behavior of such natural stone walls during the impact of a block. The main reasons to use rockery was to limit the area, which is necessary for embankment construction, and/or to stop rolling blocks.

To check the experimental results of [1] and to study the impact process of blocks impacting rockfall protection embankments (RPE) with a rockery cover at the uphill slope, small scale quasi-2D-experiments have been executed and analyzed at the Lucerne University of Applied Sciences and Arts (HSLU) during the project AERES [5].

[1] Lucerne University of Applied Sciences and Arts, Technikumstrasse 21, CH – 6048 Horw, Switzerland, since 2017: kister - geotechnical engineering & research, Neckarsteinacher Str. 4 B, D – 69151 Neckargemünd, +49 6223 71363, kister-ger@t-online.de
[2] irstea, 2 rue de la Papeterie – BP 76, 38402 Saint-Martin-d'Hères cedex, France, +33 (0)4 76 76 27 94, stephane.lambert@irstea.fr
[3] Federal Office for the Environment (FOEN), 3003 Bern, Switzerland, Tel. +41 58 465 50 98, bernard.loup@bafu.admin.ch

The load case "impact of a block onto an embankment" may be divided into two scenarios:

- The embankment is punched-through by the block and
- the embankment is surmounted by the block.

The first one is a question of stability of the construction itself while the second one concerns the fitness for purpose of a RPE. The most significant results of the tests done in the project AERES concerning the fitness for purpose of a RPE are shown below.

TEST CONDITIONS

Two types of rockery with different orientation of stones at the "uphill" slope had been studied. To create a relatively "smooth" rockery surface the stones had been placed parallel to the slope (Fig. 1a). For a "rough" rockery surface the stones had been placed horizontally, which resulted in a graded slope (Fig. 1b). Additional impact tests had been done on an embankment with a bi-linear slope with rockery at the lower part and soil at the upper part (Fig. 1c). The batter of the "rockery" was chosen to be 2:1, 5:2 and 5:1 in the tests.

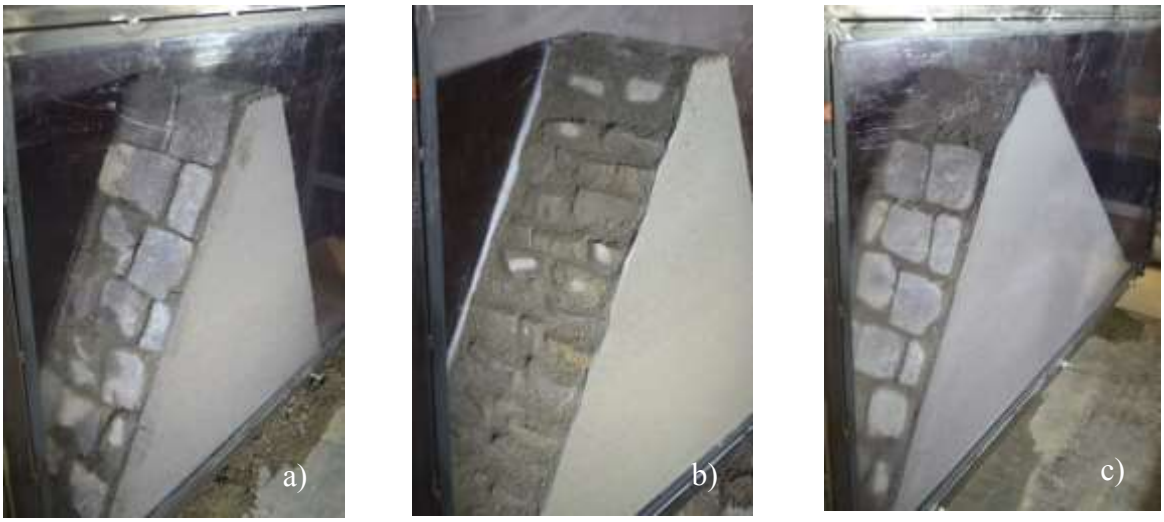

Fig. 1 Orientation of stones at the "uphill" slope: a) upright, b) horizontal, c) upright, upper slope without stones and reduced slope angle

Three types of impactors had been used: A concrete cylinder G with a ratio of rotational to translational energy > 0.3, a hollow cylinder GS with a triaxial acceleration sensor inside with a ratio of rotational to translational energy between 0.2 and 0.1 and a block OKT with an octagonal cross section with no or only very low rotation. The impactors had been accelerated via a down pipe. The ratio of rotational to translational energy of block GS corresponds very well with the results of in-situ tests done with natural blocks [4]. The impact translational velocity in most tests was between 6 m/s and 7 m/s. Transformed to a prototype embankment with height of approx. 7 m this will result in real world block velocities of about 18 m/s to 21 m/s taking into account a scaling factor of approx. 9 for the geometry [5].

FREEBOARD

The statements of Hofmann & Mölk [1] concerning the freeboard have been transferred to the Austrian technical guideline ONR 24810:2013 [2] and it is said that the freeboard for an embankment with riprap (resp. rockery) and a slope angle of 50° or more should be at least one block diameter. To determine the maximum climbing height of a block during an impact and

to get information about the influence of the roughness of the rockery surface, two impact tests on embankment models with a batter 2:1, but with different "rockery roughness" had been done. For these tests the freeboard was chosen to be approximately 1.9 times the block diameter. This value is a little bit less than the value of 2 times the block diameter specified in [2] for the freeboard of pure soil embankments, but significantly larger than the minimum value specified for embankments with rockery. The impact point was at a level, where the embankment thickness is larger than three times the block diameter (Fig. 2) and therefore according to [3] there was no risk that the embankment will be punched through.

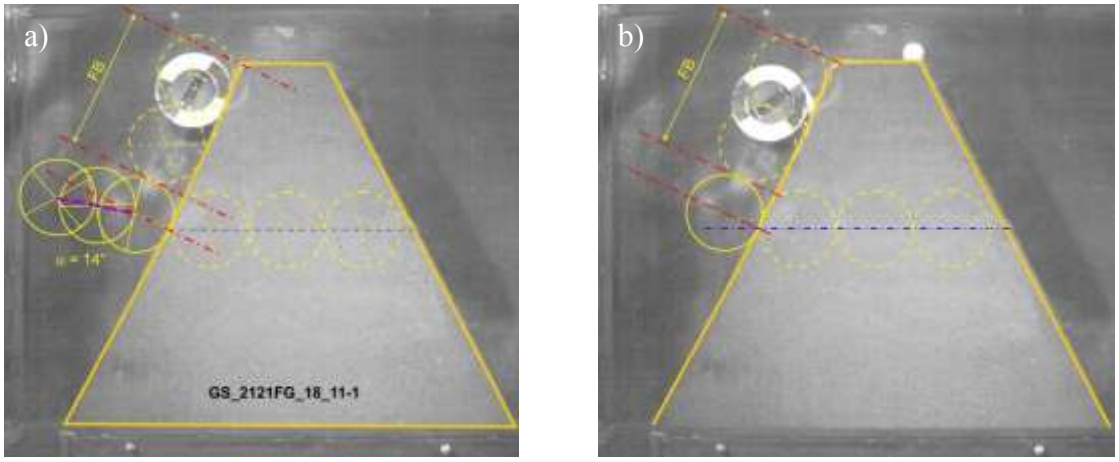

Fig. 2: Max. climbing height CH_{max} of impactor GS determined from high speed camera data, stones placed horizontally, freeboard FB = 1.9*2r: a) first impact: CH_{max} approx. 1.8*2r, b) second impact: CH_{max} approx. 1.55*2r, 2r = block diameter

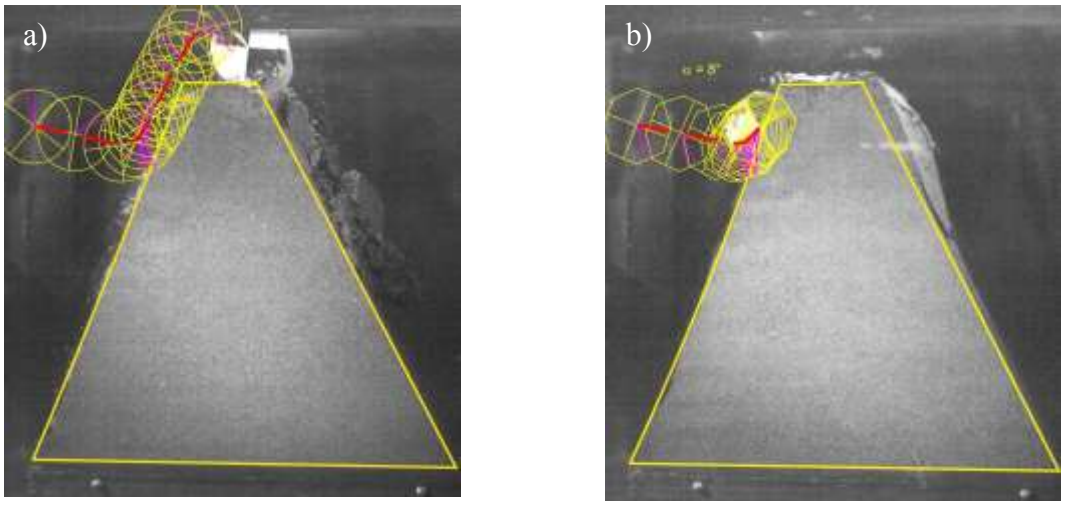

Fig. 3: Influence of block shape and block rotation: Trajectories of cylinder G (a) and block OKT (b), embankment with stones placed horizontally at the "uphill" slope, batter of rockery 5:2, determined from high speed camera data

For "rough" rockery surface the climbing height of block GS was 1.8 times the block diameter for the first impact and 1.55 times the block diameter for the second impact (Fig. 2). The "rough" surface of the rockery led to a larger climbing height for the block than the "smooth" surface, although the block velocities had been very similar. The first impact of the block resulted in a larger climbing height than the second impact for both surface roughness types.

The tests showed that a slope with an inclination of about 60° and equipped with rockery in general does not guarantee that a freeboard of approx. one block diameter will be sufficient as described by the Austrian standard.

BLOCK SHAPE AND BLOCK ROTATION

During the test series the block OKT with an octagonal cross section and with no or only very low rotation was not able to surmount an embankment with rockery, if a crest to block diameter ratio of approx. 1.1 was chosen, even so the freeboard was only about 0.8 times the block diameter. Fig. 3 shows the trajectories of the concrete cylinder G with rotation and the block OKT impacting an embankment with stones placed horizontally at the "uphill" slope, batter of rockery 5:2. The difference in the impact translational velocities of both blocks was about 7%, which is within the measurement error (G: 5.9 m/s, OKT: 6.3 m/s). So block shape and block rotation play a significant role in the impact process.

ENERGY DISSIPATION

The evaluation of test data received in the project AERES showed that the main part of energy dissipation occurs during the first 6 ms of the impact process. During this period the block translational velocity is reduced to less than the half value for all three types of impactors used in the project. Differences in loss of block velocity and block energy of the three used impactors mainly occur after the large drop of velocity and energy.

CONCLUSION

The following parameters had been found, which are dominating the impact process and led the embankment be either surmounted by a block or punched-through:

- The total block energy,
- the ratio of rotational to translational block energy,
- the impact angle, which is a function of block trajectory and slope inclination,
- the shape of the block,
- the embankment's thickness at the impact point.

These parameters are mainly responsible for the fitness for purpose of a rockfall protection embankment. The experiments have shown that there are some interactions between these parameters, which could not be solved in detail with the existing experimental set-up. Further research has to be done to determine the freeboard in case of blocks with a natural shape and with a ratio of rotational to translational energy between the limits 0.1 and 0.2.

REFERENCES

[1] HOFMANN, R.; MÖLK, M. (2012) Bemessungsvorschlag für Steinschlagschutzdämme. Geotechnik, Vol. 35, pp. 22-33
[2] ONR 24810 (2013) Technischer Steinschlagschutz – Begriffe, Einwirkungen, Bemessung und konstruktive Durchbildung, Überwachung und Instandhaltung, ASI Austrian Standards Institute (Österreichisches Normungsinstitut), Ausgabe 15.01.
[3] KISTER, B. (2015) Development of basics for dimensioning rock fall protection embankments in experiment and theory (in German), research project FEDRO 2012/003, FEDRO report 1524
[4] USIRO, T.; KUSUMOTO, M.; ONISHI, K.; KINOSHITA, K. (2006) An experimental study related to rockfall movement mechanism, Doboku Gakkai Ronbunshu FVOL. 62, No. 2, pp. 377-386
[5] KISTER, B., LAMBERT, S. (2016) Analysis of Existing Rockfall Embankments of Switzerland (AERES), research report part C, research project founded by the Federal Office for the Environment (FOEN)

AN EXAMINATION ON THE INFLUENCE OF CERTAIN PARAMETERS ON THREE-DIMENSIONAL DYNAMIC FRAME ANALYSIS FOR A ROCKFALL PROTECTION GALLERY

Fumio Yamasawa[1], Hisashi Konno[2], Hiroaki Nishi[3], Norimitsu Kishi[4], Masato Komuro[5] , Yusuke Kurihashi[6]

In this study on a rockfall protection gallery design method, the practical use of three-dimensional dynamic frame analysis was taken into consideration. The application of this relatively simple analytic method to the performance-based design of rockfall protection galleries was aimed at, and the analysis results were compared to experiment results to clarify the influence of various parameters on the analysis results. The comparison revealed the three-dimensional dynamic frame analysis to be a useful tool for practical designing, provided that the time histories of the weight impact force is used as the input load, the standard element length is set as 0.7 times the thickness of the member (0.5m), and the damping constant h is set within the range of 2.5% to 5.0%. The analysis was able to roughly reproduce the experiment results for maximum deflection, deflection distribution in the direction perpendicular to the longitudinal axis of the road, and deflection distribution near the loading point in the direction of the longitudinal axis of the road.

Keywords: rockfall protection galleries, falling-weight test, three-dimensional dynamic frame analysis, sand cushion

INTRODUCTION

For the purpose of accumulating data on the shock-resistant behaviors of existing structures, falling-weight impact experiments were carried out on a rockfall protection gallery that was constructed for these experiments. These experiments were conducted as a collaborative project between CERI and ETH Zürich. Many demonstration experiments have been performed in which the shock-absorbing material, the falling height of the weight and the input energy were used as variables.

[1] Civil Engineering Research Institute for Cold Region, Structural Team, Toyohira, Sapporo, 062-8602 Japan, +81 11 841 1698, yamasawa-f22aa@ceri.go.jp
[2] Civil Engineering Research Institute for Cold Region, Structural Team, Toyohira, Sapporo, 062-8602 Japan, +81 11 841 1698, konno@ceri.go.jp
[3] Civil Engineering Research Institute for Cold Region, Structural Team, Toyohira, Sapporo, 062-8602 Japan, +81 11 841 1698, h-nishi@ceri.go.jp
[4] Kushiro National College of Technology, Otanoshike, Kushiro, 084-0917 Japan, +81 154 57 8041, kishi@kushiro-ct.ac.jp
[5] Muroran Institute of Technology, Civil Engineering Research Unit, College of Environmental Engineering, Mizumoto, Muroran, 050-8585 Japan, +81 143 46 5228, komuro@news3.ce.muroran-it.ac.jp
[6] Muroran Institute of Technology, Civil Engineering Research Unit, College of Environmental Engineering, Mizumoto, Muroran, 050-8585 Japan, +81 143 46 5228, kuri@news3.ce.muroran-it.ac.jp

This study, which considered three-dimensional dynamic frame analysis in practical designing and which has the purpose of applying this analysis as a tool for the performance-based design of rockfall protection galleries, reports on the following. The examinations were done to clarify how various parameters affect the results of numerical analysis, with these being the parameters: element length, damping constant. The analysis results were compared with the results of the full-scale experiment. The comparison focused on the Time histories of deflection for the roof slab immediately below the loading point.

OUTLINE OF SPECIMEN

Photo 1 shows the experimental setup for this experiment. Figure 1 shows the dimensions of the gallery specimen. The gallery was designed for a 100 kJ input impact energy following the Japanese design guideline [1], which is based on the allowable stress design concept. The thickness of the cushion layer was 90 cm for both cushion material sand.

Photo 1 Experimental setup

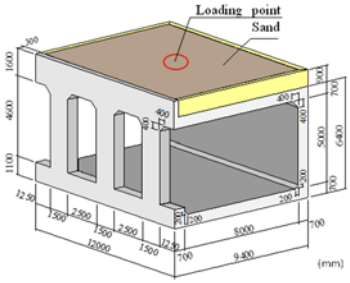

Fig. 1 Dimensions of gallery specimen

EXPERIMENTAL CASE AND ANALYSIS CASE

For the purpose of analysis and comparison, experiment was conducted by using input energy of 1,500kJ. Load was applied to the center of the rock-shed model in experiment. First, the time histories of the weight impact force of the experiment was used as the input load for the numerical analysis, and the experiment results were compared to the analysis results. The standard element length in this study was set as 0.7 times the thickness of the member (0.5m) so that the standard element length would be maintained within the length of subelement stated above and a relatively uniform division of the element would be possible. Use of a long element length is advantageous in creating analysis models and minimizing the analysis time. Therefore, the cases that used the standard element length of 1.4 times the thickness of the member (1.0m) and that used 2.8 times the thickness of the member (2.0m) were also done for the purpose of comparison with the case that used the standard element length of 0.5m. For the damping constant, four values of h (1.0%, 2.5%, 5.0%, 10.0%) were used in the numerical analyses. By using these values, the influence of the difference in the damping constant was examined.

THE NUMERICAL ANALYSIS MODEL AND THE MATERIAL PHYSICAL PROPERTIES MODEL

Fig. 2 shows the three-dimensional frame analysis model used for the analysis.
The fiber element was used in the frame model, in which the cross-sectional dimensions and the material constants were considered. The division of cells for the fiber element of the member whose axis was in the direction perpendicular to the axis of the road was set such that the

axial bar would be close to the center of each cell, as shown in Fig. 3. Engineer's Studio (Ver.1.07.00) was used for the numerical analysis.
Fig. 4 (a) and (b) show the material physical properties model of the concrete and that of the rebar used in this numerical analysis.

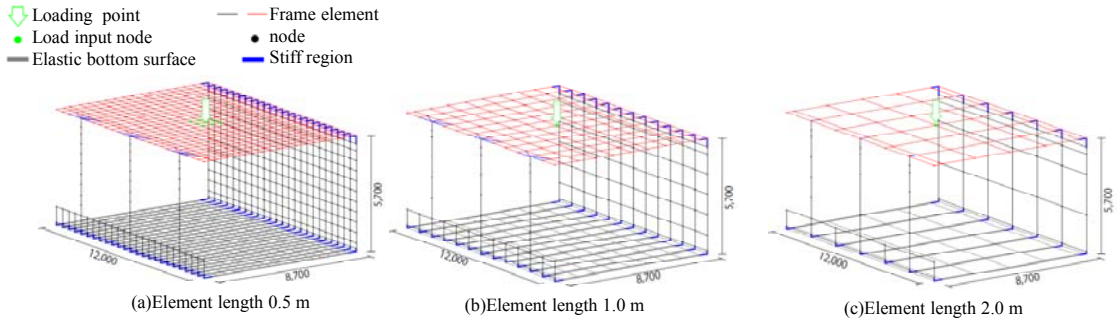

(a)Element length 0.5 m (b)Element length 1.0 m (c)Element length 2.0 m

Fig. 2 three-dimensional frame analysis model

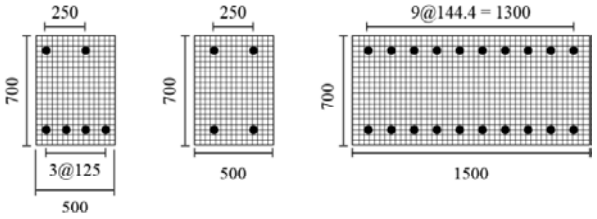

(a)roof slab (b)Sidewall / bottom surface (c)Pillar

Fig.3 fiber element model

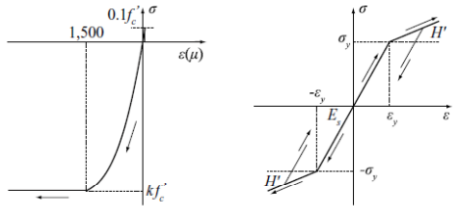

(a)Concrete (b)Rebar

Fig.4 material physical properties model

COMPARISON BETWEEN THE EXPERIMENT RESULTS AND THE NUMERICAL ANALYSIS RESULTS

Figs. 5 show the time histories of deflection of roof slab at the loading point for each element length when the time histories of the weight impact force (experiment result) was used as the input load. The time histories of deflection and the deflection, which were used for discussion in the latter parts of this report, were the results of analysis done for any given nodal point on the roof slab. When the time histories of deflection for each 0.5m standard element length shown in Fig. 5(a) is examined, it is understood that the deflection from the rising point to the maximum value for all of the damping constants show a similar shape. The maximum value shows a tendency to decrease with increase in the damping constant. For the damping constant h of 10.0%, the maximum value of the experiment results tended to be underestimated. The analysis results show different results from that of the experiment after the deflection have reached the maximum values. The experiment result shows small changes near the residual deflection value after t=150ms; however, the analysis result deflection show great changes. When the time histories of deflection for the standard element length of 1.0m in Fig. 5(b) are examined, it is understood that the deflections are roughly similar at the early stage of rising; however, none of the time histories of deflection for the four damping constants reach the experiment maximum value. In the analysis with the standard element length of 2.0m shown in Fig. 5(c), the analysis results underestimate the experiment results to an even greater extent.
Figs. 6 show the deflection distribution in the direction perpendicular to the longitudinal axis of the road at the time when the deflection at the loading point was the maximum in the analysis

results with the damping constant h of 2.5%. The results of the experiment are also shown in this figure.

As shown in Fig. 6, the deflection distribution in the direction perpendicular to the longitudinal axis of the road for all of the element lengths plot as smooth quadric curve-like curves with the maximum values being immediately below the loading point. The tendencies of the distribution curves are similar to those of the experiment results. As discussed above, the maximum deflection for the analysis increasingly underestimated the experiment results with increase in the element length from 1.0m to 2.0m. When the element length was 0.5m, the deflection near the side wall was slightly smaller than that of the experiment results; however, the analysis results other than the deflection near the side wall accurately reproduced the experiment results.

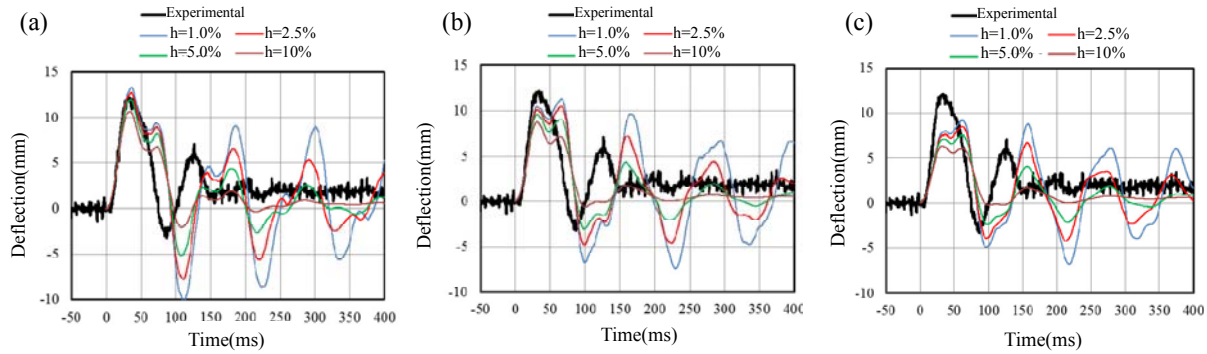

Fig.5 Time histories of deflection of roof slab at the loading point : (a) element length 0.5m ; (b) element length 1.0m ; and (c) element length 2.0m

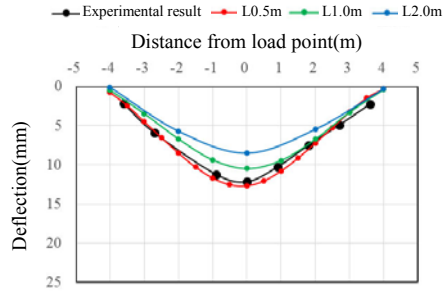

Fig.6 Distortion distribution in the direction perpendicular to the road axis at maximum strain occurrence

CONCLUSIONS

In three-dimensional dynamic frame analysis that used the time histories of the weight impact force as the input load, the time histories of deflection after the maximum response in four analysis cases were unable to reproduce the experiment results. However, by setting the standard element length as 0.7 times the thickness of the member (0.5m) and by setting the damping constant h between 2.5% and 5.0%, we were able to roughly reproduce the maximum deflection, the deflection distribution in the direction perpendicular to the longitudinal axis of the road. Based on these, the examined analysis method is thought to be satisfactorily applicable as an analysis tool for the practical designing of rockfall protection galleries.

REFERENCES

[1] Japan Road Association, Design guideline for anti-impact structures against falling rocks, 2000. In Japanese.

DESIGN AND VALIDATION OF ROCKFALL PROTECTION SYSTEMS BY NUMERICAL MODELING WITH DISCRETE ELEMENTS

Salvador Latorre[1], Miguel Ángel Celigueta[1], Joaquín Irazábal[1], Fernando Salazar[1], Eugenio Oñate[1]

Rockfall protection systems are installed in order to preserve civil infrastructures against landslides and falling rocks. For the evaluation of these systems, one of the main problems is the difficulty to develop laboratory tests, since landslides and falling rocks are unpredictable events that involve the movement of large masses of material over several meters or even kilometers. For this reason, the use of numerical methods, which allows reproducing full-scale situations without the need of laboratory devices or sliding materials, has become more popular. The study presented in this document shows the application of the Discrete Element Method (DEM) for the analysis of the behavior of one of the most popular rockfall protection systems, flexible metallic fences.
Keywords: Rockfall protection, Flexible metallic fences, Discrete element method, Numerical modeling

INTRODUCTION

Communication and supply needs of an increasing population, all around the world, force the construction of infrastructures in places threatened by natural hazards such as falling rocks. With the purpose of preserving these infrastructures, different containment systems, such as flexible metallic fences [1], drapery systems [7] and granular material embankments [5], are installed.

The difficulty to carry out full-scale laboratory tests, on account of the huge magnitude of the event [3], in addition to the uncertainties in the small-scale testing, due to the distortion in the contours (e.g. anchors of flexible metallic fences), has led to the use of numerical methods.

In this study, the Discrete Element Method (DEM) is used for the analysis of the behavior of flexible metallic fences for rockfall protection. The classic DEM is based on representing the material by rigid particles that interact with each other according to appropriate contact laws, defined by the material properties. It is a suitable numerical method for the problem under consideration, because: (a) it allows large deformations and displacements and (b) the contact detection is more computationally efficient than in other numerical methods, such as the Finite Element Method (FEM).

[1] International Center for Numerical Methods in Engineering (CIMNE), Barcelona, Spain
Polytechnic University of Catalonia (UPC), Barcelona, Spain
E-mail address: latorre@cimne.upc.edu (Salvador Latorre)

The flexible metallic fences are calculated using the bonded DEM, a modification of the classical DEM which assumes that bonds exist between particles, resisting their separation [2]. In this case, the net cables are represented using rigid spheres joined by bond elements that are deformed according to an elasto-plastic law.

Calculations were carried out using the DEMPack program, a specific software developed in CIMNE for modeling with the bonded DEM [4]. This software allows considering the interaction between discrete and finite elements [6], which can be useful to represent the boundaries of the domain, such as the surface of the slope.

Firstly, the code is validated reproducing two benchmark tests available in the literature [1] where the behavior of a small portion of a flexible metallic fence is evaluated. Finally, full-scale tests are reproduced in order to evaluate the energy dissipation capacity of the fence during a rockfall event.

VALIDATION

The validation tests were obtained from the work driven by Bertrand et al. [1] in 2012. Firstly, they performed a simple tensile test on a small portion of the net, composed of five meshes. The lower points of the specimen were fixed and a constant loading velocity of 4 mm/min was imposed to the upper points. The evolution of the force against the displacement was recorded.

Fig. 1 shows the net used in the laboratory test (diameter of the cable is 12 mm) and the corresponding numerical model composed of rigid spherical particles.

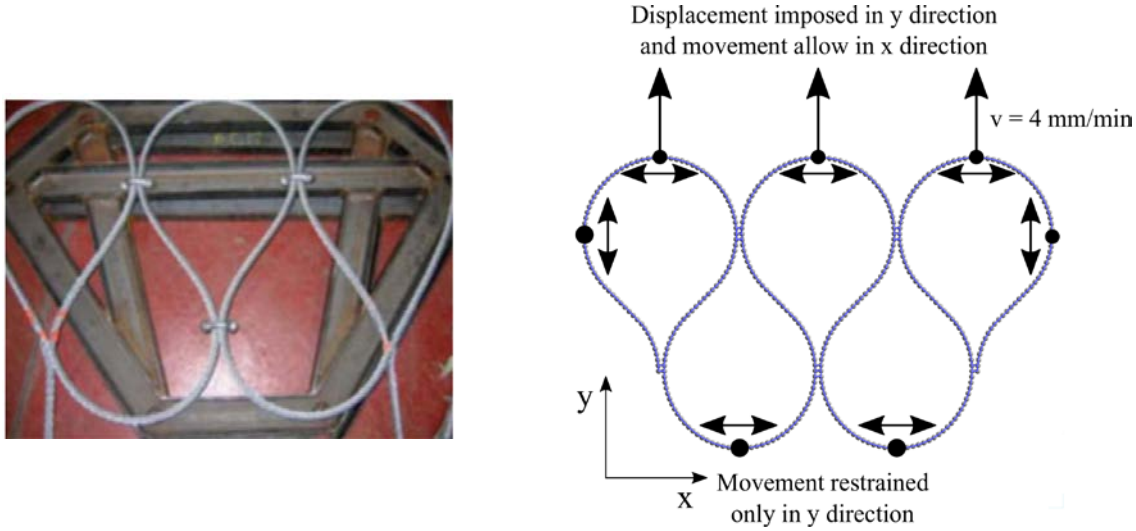

Fig. 1 Laboratory [1] (left) and numerical model (right) of the first validation test.

Fig. 2 exhibits the deformation of the net and the stresses to which it is subjected, during the calculation. It should be noted that this numerical model allows defining different constitutive laws in each bond. In this example, cables and clips are reproduced.

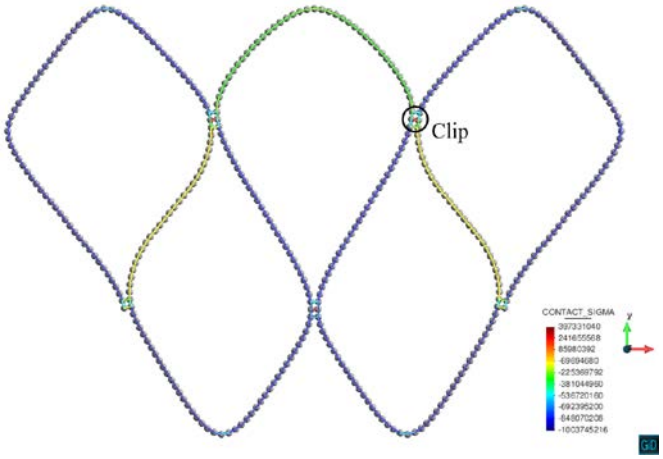

Fig. 2 Deformation of the net and stresses to which it is subjected during the first validation test.

The same authors also developed a punching test (see Fig. 3), aiming to analyze the net response under out-of-plane loading. Due to space restrains in the laboratory a half-scale model was tested, so the cable diameter in this case was 6 mm. A square net with dimensions 2 x 2 m was rigidly fixed to a framework allowing free rotations. A loading rate of 4 mm/min was applied by a cylinder (diameter 330 mm) along the normal direction of the net plane. Reaction forces and penetrations were measured.

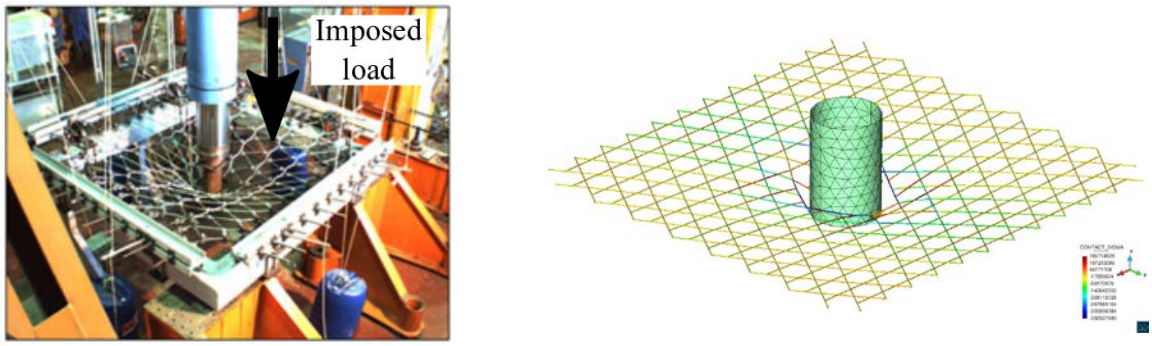

Fig. 3 Laboratory [1] (left) and numerical model (right) of the second validation test.

The two validation tests were calculated with the DEMPack code in order to evaluate its behavior and calibrate the model parameters. These tests allow to properly define the material characteristics of the full-scale test.

In the model presented, each cable is reproduced using several spheres, which increases the computational time of the calculation. However, the deformation of the net is represented in a more realistic way than using discrete elements only in the unions.

FULL-SCALE CALCULATIONS

Regarding full-scale tests, simplified scenarios were analyzed for demonstration purposes. Fig. 4 shows different scenarios, with variable number of falling rocks, shape and kinetic energy. The net geometry has also been modified from one calculation to another.

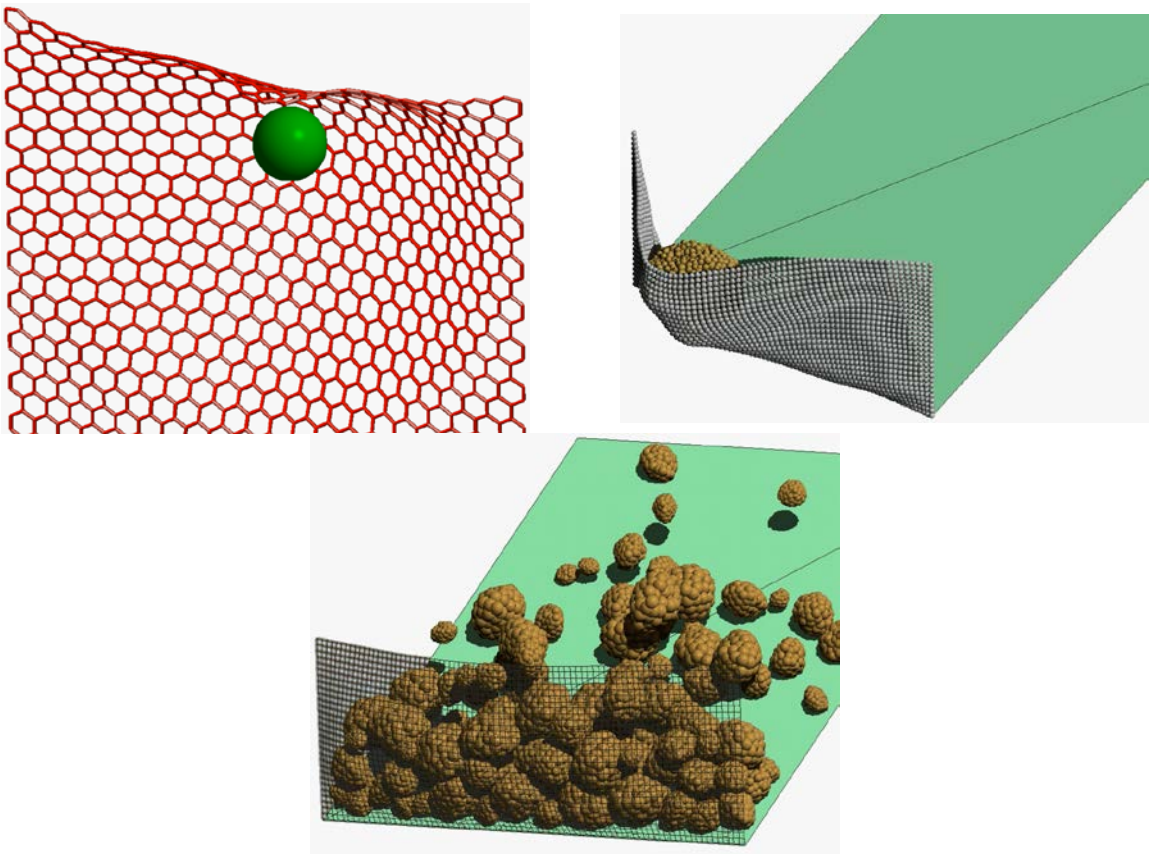

Fig. 4 Full-scale tests with variable nets and arbitrary rock shape.

With this numerical model, the energy and trajectories of the rocks can be accurately tracked. The energy absorbing capability of the net, the effect of the rock shape in the protection system behavior or the response of different net geometries, can be evaluated.

REFERENCES

[1] BERTRAND D, TRAD A., LIMAN A, SILVANI C (2012) Full-Scale Dynamic Analysis of an Innovative Rockfall Fence Under Impact Using the Discrete Element Method: from the Local Scale to the Structure Scale. Rock mechanics and rock engineering, 45(5), 885-900.
[2] BROWN N J, CHEN J F, OOI J. Y. (2014) A bond model for DEM simulation of cementitious materials and deformable structures. Granular Matter, 16(3), 299-311.
[3] CARDOSO D, ROMANA M, HILTUNEN D R (2013) Distancia recorrida por el material afectado por inestabilidades en taludes de carretera. VIII Simposio Nacional Sobre Taludes y Laderas Inestables.
[4] OÑATE E, ZÁRATE F, MIQUEL J, SANTASUSANA M, CELIGUETA M A, ARRUFAT F, RING L. (2015) A local constitutive model for the discrete element method. Application to geomaterials and concrete. Computational particle mechanics, 2(2), 139-160.
[5] PLASSIARD J P, DONZÉ F V (2010) Optimizing the design of rockfall embankments with a discrete element method. Engineering Structures 32 3817–3826.
[6] SANTASUSANA M, IRAZÁBAL J, CARBONELL J M, OÑATE E, (2016) The Double Hierarchy Method. A parallel 3D contact method for the interaction of spherical particles with rigid FE boundaries using the DEM. Computational Particle Mechanics 3(3): 407–428.
[7] THOENI K, GIACOMINI A, LAMBERT C, SLOAN S W, CARTER J P (2014) A 3D discrete element modelling approach for rockfall analysis with drapery systems. International Journal of Rock Mechanics & Mining Sciences 68 (2014) 107–119.

PRELIMINARY 3D MODELING OF CHAIN-LINK TECCO MESH FOR ROCKFALL PROTECTION

Soheil Tahmasbi[1], Anna Giacomini[1], Olivier Buzzi[1], Corinna Wendeler[2]

Full-scale experimentation has been used extensively in order to evaluate the behaviour of the rockfall protection systems. However, physical tests are quite expensive and time consuming and numerical methods are a useful and more economical alternative. Modelling the exact 3D geometry of a chain link mesh is quite complex and not very common in the literature although it allows capturing a realistic failure mechanism. This paper covers the validation of a numerical model reproducing the 3D chain-link and simulating its response under the impact of a block in free fall. ABAQUS finite element code was used for this simulation. The calibration was conducted using existing full-scale experiments performed on the Geobrugg TECCO mesh. The preliminary results show that this new model can accurately reproduce mesh perforation as well as block rebound.

Keywords: rockfall, numerical modelling, flexible barrier, chain-link, ABAQUS

INTRODUCTION

Rockfall can cause loss of lives and significant damages to infrastructure and it requires adequately designed protection structures to mitigate the risk. Flexible barriers are type of such protection systems. With the recent increase in computational power, numerical simulations are becoming a more economical and feasible alternative to traditional field experimentation [1-4]. The geometry of chain link mesh if often simplified [5] and it is only recently that Escallon and his co-workers have produced a full 3D model of a chain-link mesh [6]. The objective of this study is to develop a full 3D model of a chain-link mesh used in a drapery system. The advantage of a drapery system is the maintenance-free rockfall protection system for smaller energies (see figure 1). The first step of this research, presented in this paper, is to calibrate and validate a preliminary model of mesh subjected to free fall tests.

EXISTING EXPERIMENTAL DATA

The experimental data used in this study are the results of tests conducted at the Walenstadt test site where four different types of TECCO mesh, manufactured by Geobrugg, were impacted by free falling blocks (of ETAG [7] shape) having different sizes. High-speed cameras were used to record the block motion pre and post impact. More information on the experimental setup and data can be found in [8]. The model was calibrated using the data pertaining to a G65/4 TECCO mesh impacted by a 1140 kg ETAG block.

[1] The University of Newcastle, University Drive, Callaghan NSW 2308, Australia, Phone:+61 2 4921 5000, Email: soheil.tahmasbi@uon.edu.au, anna.giacomini@newcastle.edu.au, olivier.buzzi@newcastle.edu.au
[2] Geobrugg AG – Geohazard Solutions, Aachstrasse 11, CH-8590 Romanshorn, Switzerland, Phone: +41 71 466 81 79, Email: corinna.wendeler@geobrugg.com

Fig 1. TECCO drape installation in Vaduz, Switzerland-Geobrugg 2011

NUMERICAL SIMULATIONS

The exact 3D geometry of the TECCO mesh was modelled in Abaqus (See Figure 2a). The size of the mesh panel is 4200mm × 4200mm, the aperture diameter of each rhomboid is 65 mm and the wire diameter is 4 mm. The impacting block (mass of 1140 kg) was modelled as rigid. In order to adequately reproduce the test conditions, the shackles connecting the mesh to the peripheral cable were also simulated (as a rigid body) instead of fixing the outside nodes of the mesh. The mesh panel was discretised using 2-node linear beam elements. A total of 149382 elements were used for the mesh. The mesh material was assigned an elasto-plastic behaviour with a tensile strength of 1,770 MPa (as per high tensile steel wire) with a progressive damage requiring the definition of the plastic strain at the onset of damage (ε_0^{pl}), the equivalent plastic displacement (U_f) and the exponent (α_{damage}) defining the exponential relation between damage factor and equivalent plastic strain. These factors will be calibrated from experimental data.

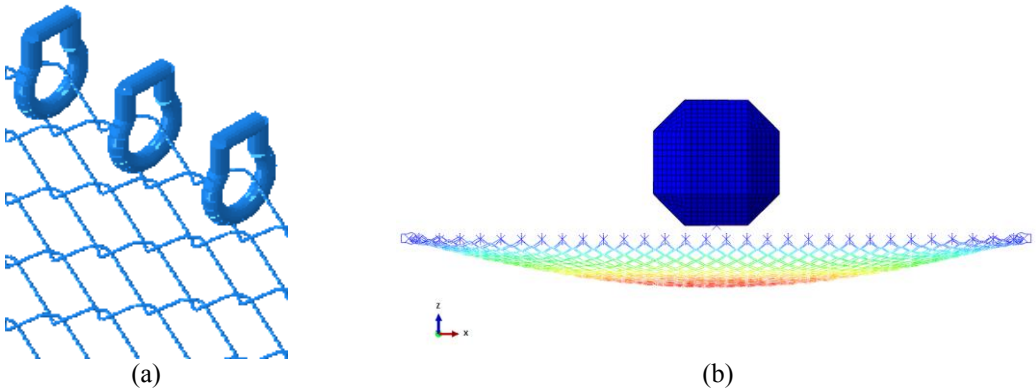

(a) (b)

Fig 2. (a) Views of the 3D model of the chain-link mesh and shackles. (b): Initial sag of the wire net under gravity. Maximum sag = 330 mm.

A general contact algorithm of ABAQUS/Explicit was used in this simulation. The tangential contact behaviour was modelled using a Coulomb friction model that calculates the maximum allowable frictional (shear) stress across an interface using the contact pressure between the contacting bodies [9]. Additionally, a damping factor was considered in the contact calculation in order to get more accurate results as well as reducing the solution noise. The analysis was conducted in two steps: a gravity step was first applied in order to achieve an initial sag (figure 2b) while the second step consists of the impact itself. In order to reduce the computational time, the free fall was not actually modelled but the block was initially placed close to the mesh and assigned an initial velocity, consistent with the testing conditions. Mass scaling was also used to control the computational time.

RESULTS AND DISCUSSION

The damage parameters of the steel (ε_0^{pl}, U_f and α_{damage}) were calibrated in order to obtain a correct evolution of block velocity post-impact. Figure 3a illustrates how the equivalent plastic displacement influences the block velocity following mesh perforation. A case of rebound was also modelled (Figure 3b) where a good agreement is found between model prediction and experimental results. In both cases, a slight delay (of 50ms) can be observed between numerical results and experimental data. This delay is still unexplained at this stage and research into this effect is currently on going. However, it is relatively small and unlikely to cause issues when modelling drapery systems where blocks interact with the mesh at relatively low speed.

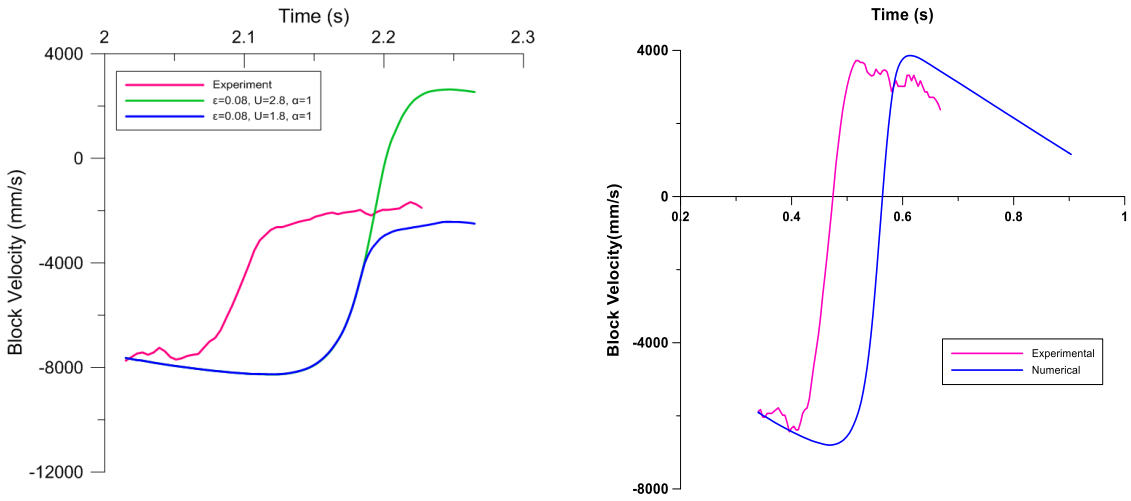

(a) (b)

Fig 3. (a) The results of the calibration jobs in comparison with the experimental results-effect of the equivalent plastic displacement. (b) The result of the validation job in comparison with the experimental one.

Figure 4 shows an example of mesh perforation with a detail of the failure pattern of the TECCO mesh. The model can clearly reproduce a realistic failure mechanism of the mesh, which brings confidence on the predictive capability of the model.

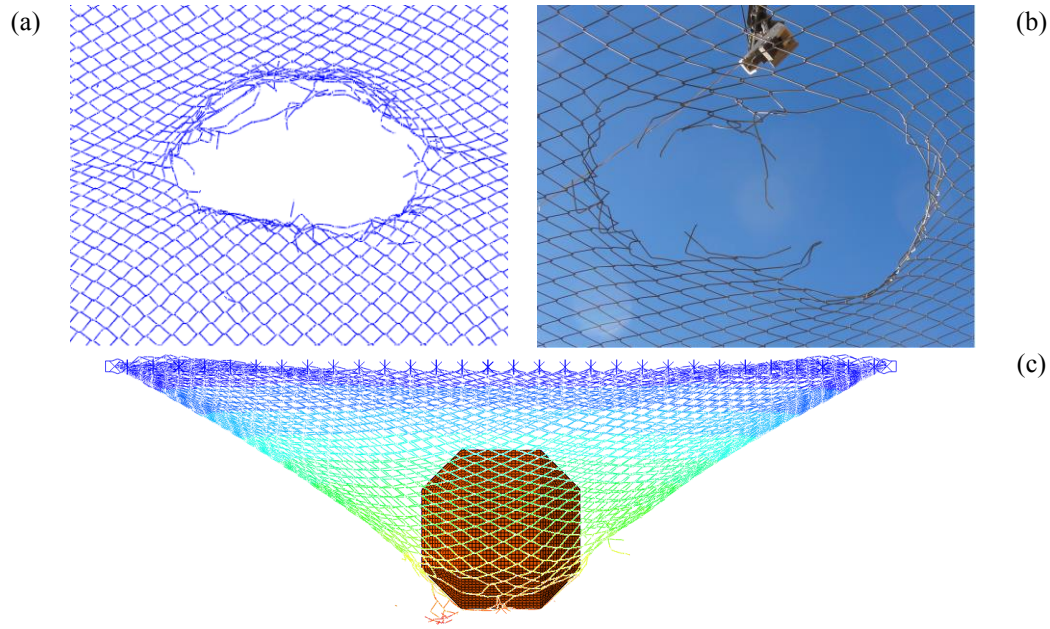

Fig 4. (a) Perforation pattern in the numerical model. (b) Perforation pattern in the Experiment (c) Wire net perforation from numerical model

CONCLUSIONS

A numerical model simulating the complete 3D chain-link mesh was developed using ABAQUS finite element code. The model was calibrated and validated by comparing the predictions to full-scale experiments. The model proved to be able to reproduce both mesh perforation and block rebound as well as the block displacement and velocity post impact. The failure mechanism of the TECCO mesh was also adequately captured which is in most of the existing models not the case. This study is the primary step of a long term plan to simulate chain-link drapery systems.

REFERENCES

[1] VOLKWEIN, A. (2005) Numerical simulation of flexible rockfall protection systems. Proc. of Int. Conf. on Computing in Civil Engineering, Cancun, Mexico pp 1-11.
[2] MENTANI A, GIACOMINI A, BUZZI O, GOVONI L, GOTTARDI G, FITYUS S (2016) Numerical modelling of a low-energy rockfall barrier: New insight into the bullet effect. Rock Mechanics and Rock Engineering 49, 1247-1262.
[3] GENTILINI, C., GOVONI, L., DE MIRANDA, S., GOTTARDI, G., & UBERTINI, F (2012) Three-dimensional numerical modelling of falling rock protection barriers. Computers and Geotechnics 44, 58-72.
[4] ALBRECHT G L VON BOETTICHER (2013) Flexible Hangmurenbarrieren: Eine numerische Modellierung des Tragwerks, der Hangmure und der Fluid-Struktur-Interaktion. Schriftenreihe des Lehrstuhls für Statik TU München. PhD thesis, 186 pp.
[5] SPADARI M., GIACOMINI A., BUZZI O., HAMBLETON J. (2012). Prediction of the bullet effect for rockfall barriers: a scaling approach. Rock Mechanics and Rock Engineering 45(2), 131-144.
[6] ESCALLON, J., BOETTICHER, V., WENDELER, C., CHATZI, E., & BARTELT, P (2015) Mechanics of chain-link wire nets with loose connections. Engineering Structures 101, 68-87.
[7] ETAG 027: guideline for European technical approval of falling rock protection kits; 06, 2013.
[8] BUZZI O, LEONARDUZZI E, KRUMMENACHER B, VOLKWEIN A, GIACOMINI A (2015) Performance of high strength rockfall mesh: effect of block size and mesh geometry. Rock Mech Rock 48(3), 1221–1231.
[9] Abaqus Analysis User's Manual, Version 6.13 Dassault Systmes Simulia Corp, Providence, RI.

GENERIC MODELING OF FLEXIBLE ROCKFALL BARRIERS: FROM COMPONENTS CHARACTERIZATION TO FULL-SCALE NUMERICAL SIMULATIONS

Jibril B. Coulibaly[1], Marie-Aurélie Chanut[1], Clément Galandrin[2], Ignacio Olmedo[3], Stéphane Lambert[4], François Nicot[4]

Numerical simulation is a powerful and cost-effective solution to investigate the complex dynamic behavior of flexible rockfall barriers. The mechanical modeling of such structures requires calibration and validation of the numerical model against experimental data. This document introduces a generic approach for modeling rockfall barriers and compares numerical simulation results to full-scale tests on a specifically designed rockfall barrier. The proposed model is first calibrated against experimental data from the extended testing of the barrier main components. Simulations of quasi-static and dynamic full-scale tests are then performed and numerical results compare greatly to experimental ones, proving the suitability of the generic approach to model flexible rockfall barriers.

Keywords: generic modeling, rockfall, barrier, numerical simulation

GENERIC APPROACH FOR MODELING ROCKFALL BARRIERS

Performances of rockfall barriers are determined by full-scale testing only, based on the ETAG 27 procedure [1]. Given the limitations in the ETAG27 testing conditions and the testing costs, numerical simulation has been used in order to facilitate the design of the barriers and to investigate their mechanical behavior under ETAG 27 and in situ loadings. Several modeling tools have been developed in this regard [2], [3], [4], [5]. Each one of these models was developed with one particular software to simulate the response of one particular technology and cannot be used to precisely model various structures, given the diversity in the technologies.

So that the modeling of different technologies can be harmonized, Chanut [6] developed a generic platform for modeling rockfall barriers. Based on the explicit dynamic Discrete Element Method (DEM), barriers are modeled as an abstract object made out of interacting nodes

[1] Cerema, 25 avenue François Mitterrand CS92803, 69674 BRON Cedex, France, jibril.coulibaly@cerema.fr
[2] CAN, Le Relut, 26270 Mirmande, France
[3] GTS, 27 rue des tâches, Saint-Priest 69800, France
[4] IRSTEA, 2 rue de la Papeterie-BP 76, F-38402 St-Martin-d'Hères, France

and solids, arranged in a way to represent the constitutive elements of the barrier: nets, cables, posts, energy dissipating devices and anchors.

A non-linear mechanical model for 4-contact interlaced ring nets (Fig. 1) has been developed [7]. This model provides a good mechanical response both at the local scale of the ring and at global scale of the net. It accounts for complex irreversible processes with use of a limited number of elements that ensures computational efficiency. A specific numerical procedure permits the calibration of the model parameters from experimental data. A new sliding cable model has also been developed [8]. This model expands many existing previous models and consists of a multi-node sliding cable accounting for friction, with a general dynamic formulation, an effective numerical implementation and applicability to various material behavior. This model is capable of reproducing the sliding of the net on the cables known as "curtain effect" (Fig. 2). Posts and energy dissipating devices are modeled respectively as rigid solids and as 1-dimensional elements with an appropriate constitutive behavior depending on their technology. Anchors form the boundary conditions of the problem (fixed points).

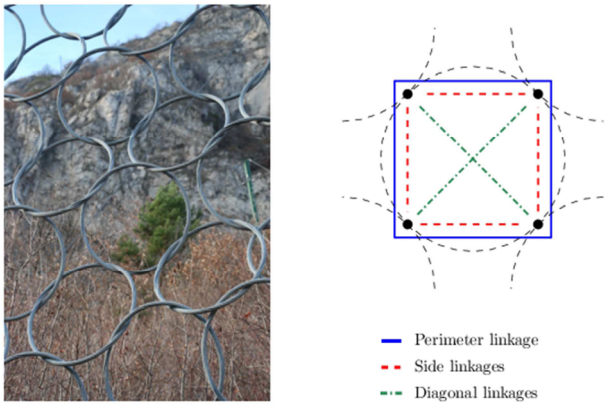

Fig. 1 4-contact ring net (left) and ring model (right)

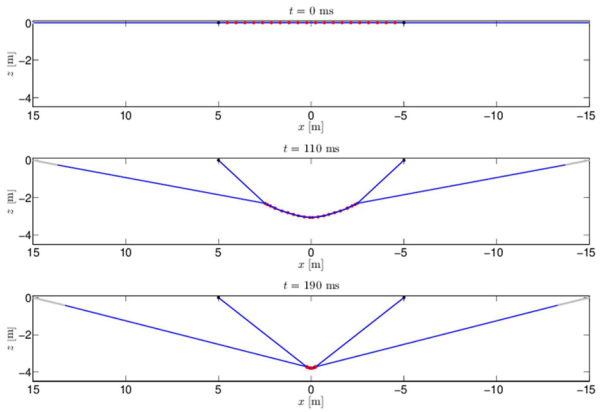

Fig. 2 Modeling of the curtain effect on a system of 2 sliding cables

DEM models of the main components of the structure are then assembled to form a multi-scale model of the flexible barrier. The mechanical models offer a general description of components of rockfall barriers and may adapt to variations in the technologies through their input parameters and assembly.

DEFINITION OF THE PROTOTYPE BARRIER

Calibration and validation of the barrier model is made thanks to a rockfall barrier prototype specifically designed for that purpose. Development and testing of a dedicated prototype has been made possible in the framework of the French National Project C2ROP. This C2ROP barrier prototype has been designed for a 350 kJ maximum energy level. This kit is made of 3 modules, 5 meters long and 2.75 meters of nominal height, spanned by a ring net and with energy dissipating devices distributed throughout the structure. Detailed presentation of the C2ROP 350 kJ structure can be found in the RocExs 2017 extended abstract entitled “Extended experimental studies on rockfall flexible fences”.

Tensile tests have been performed on isolated rings from the ring net of the C2ROP barrier and the numerical calibration method is applied to obtain the model parameters for this given ring technology. Similar tests are performed on the energy dissipating devices of the barrier in order to determine their elastoplastic constitutive behavior. Cables are given an elastic linear constitutive relation calibrated thanks to the supplier's data.

Well instrumented full-scale tests have been performed on the C2ROP barrier. A quasi-static test has been performed. Dynamic full-scale tests will be performed in February 2017 to pursue further validation of the generic numerical approach. ETAG 27 and other impact conditions will also be addressed.

NUMERICAL SIMULATION OF FULL-SCALE TESTS AND MODEL VALIDATION

Numerical simulations of the quasi-static full-scale test on the C2ROP barrier have been performed thanks to the generic model. The calibrated ring model and energy dissipating devices model are used in the simulation. Geometry of the tested barrier and weaving patterns of the rings on the supporting cables are carefully respected. The block is displaced into the net at constant speed of 0.2 m/s to reach a maximum deflection of 5 meters (Fig. 3). The simulation results for the quasi-static loading agree very well with the experimental measurements. The global force-displacement response of the barrier matches perfectly the experimental measurements of the traction force and of the central deflection (Fig. 4), showing that the model properly assesses the global behavior of the structure in terms of force and energy.

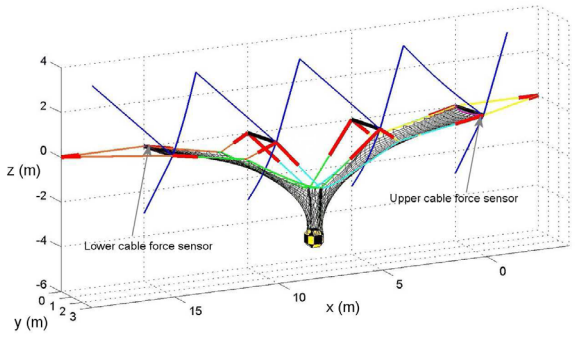

Fig. 3 Simulation of the full-scale quasi-static test

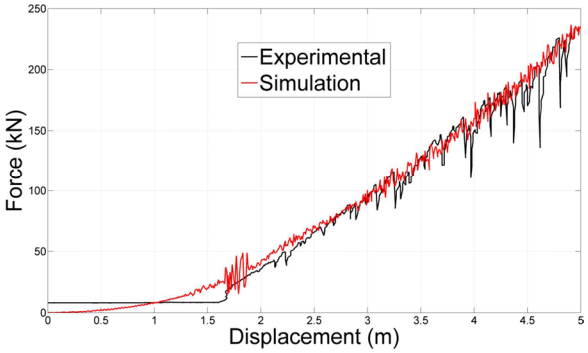

Fig. 4 Quasi-static force - displacement response of the barrier

The local behavior and force distribution are also studied. Tension in lower and upper longitudinal supporting cables are properly captured by the model in terms of intensity and trend (Fig. 5). Qualitative results regarding the deformation kinematics of the structures is also in good accordance with experimental observations. The capacity of the model to finely replicate the behavior of the C2ROP 350 kJ barrier validates the relevance of the mechanical models of the barrier components as well as their assembly into a complete rockfall protection barrier. These results also underline the suitability of the multi-scale approach and of the calibration methods on isolated components in assessing the response of the entire structure.

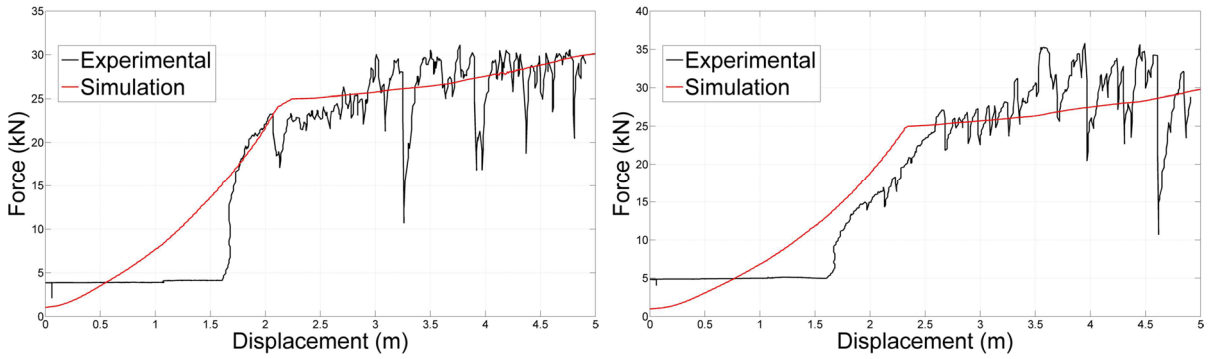

Fig. 5 Quasi-static force – displacement response: (left) lower longitudinal cable; (right) upper longitudinal cable

CONCLUSION

The generic model provides a powerful and unified tool to study the behavior of flexible rockfall barriers. The model is first calibrated thanks to characterization tests on isolated components. Then, comparison between numerical simulations and full-scale tests under quasi-static loading shows great accordance, validating the model capabilities to assess the behavior of these protection structures. Further developments of this generic modeling approach will contribute to a better understanding of the structural response of the barriers. Manufacturers may also use the generic modeling tool for design and numerical prototyping purposes before performing full-scale tests.

REFERENCES

[1] EOTA (2008) Guideline for European Technical approval of falling rock protection kits ETAG 27.
[2] NICOT F, CAMBOU B, MAZZOLENI G (2001) Design of rockfall restraining nets from a discrete element modelling. Rock Mechanics and Rock Engineering, 34 (2), 99-118.
[3] ESCALLON J P, WENDELER C, CHATZI E, BARTELT P (2014) Parameter identification of rockfall protection barrier components through an inverse formulation. Engineering Structures, 77, 1–16.
[4] TRAD A, (2011) Analyse du comportement et modélisation de structures souples de protection : le cas des écrans de filets pare-pierres sous sollicitations statique et dynamique. PhD Thesis, INSA de Lyon, Villeurbanne
[5] GENTILINI C, GOTTARDI G, GOVONI L, MENTANI A, UBERTINI F (2013), Design of falling rock protection barriers using numerical models, Engineering Structures, 50, 96-106.
[6] CHANUT M-A, DUBOIS L, NICOT F (2014) Dynamic behavior of rock fall protection net fences: a parametric study, IAEG 2014, Turin.
[7] COULIBALY J B, CHANUT M-A, LAMBERT S, NICOT F (2016) Non-linear discrete mechanical model of steel rings. Journal of Engineering Mechanics.
[8] COULIBALY J B, CHANUT M-A, LAMBERT S, NICOT F (2017) Sliding cable modeling : an attempt of unified formulation. (to be published)

PREDICTIONS AND CONCLUSIONS OF FE-SIMULATIONS FOR FULLSCALE IMPACT TEST ON PROTECTION GALLERY

Yusuke Kurihashi [1], Masato Komuro [1], Norimitsu Kishi [2], Kristian Schellenberg [3] and Tomoki Kawarai [1]

In order to develop an appropriate prediction method for the impact resistant behavior of rockfall protection galleries, finite element simulations were conducted by means of LS-DYNA and compare with experimental results of full-scale impact loading tests. Readjustment of material properties for post analyses and a comparison of the impact forces with the results of an independent model as well as with both worldwide existing design guidelines give confidence for the application of the FE Model for the assessment of similar existing structures.

Keywords: rockfall protection gallery, full-scale impact test, FE-simulation, SMDF

INTRODUCTION

Today, a large number of existing rockfall protection galleries need to rehabilitated and cost depend on whether the structures have to be strengthened or not. The assessment of existing structures by the current guidelines [1, 2] often results in recommendations for costly measures. Based on research results of the last 10 years [3, 4], some potential savings can be expected. The planned demolishion of the protection gallery Parde on the Oberalp pass between Sedrun and Andermatt in Switzerland in 2016 allowed for carrying out falling weight tests accepting even severely damage to the structure. The test results were reported in detail [5] and have been valuable for improving the evaluation approach to predict impact resistant behavior of the gallery.

In order to investigate the applicability of Finite Element (FE)-simulations for predicting impact resistant behavior of rockfall protection gallery, test predictions were carried out by means of LS-DYNA[6]. After the test post analyses were conducted in order evaluate readjustments in the material properties. Additional comparison of impact forces with a System of Multiple Degrees of Freedom model (SMDF) and with the corresponding Japanese and Swiss design guidelines are presented.

EXPERIMENTAL OVERVIEW

Gallery Parde (Fig. 1) was built in 1940 in order to protect the road from avalanches and was demolished in 2016 after having reached its design lifetime. Boulders of 800 to 3200 kg were hoisted up to heights up to 25 m by using track crane, then released and dropped to the central

[1] Muroran Institute of Technology, Muroran 050-8585, Japan, kuri@news3.ce.muroran-it.ac.jp
[2] National Institute of Technology, Kushiro College, Kushiro 084-0916, Japan, kishi@kushiro-ct.ac.jp
[3] Road Office of Grisons (TBA GR), Chur 7001, Switzerland, kristian.schellenberg@tba.gr.ch

point of the gallery. The impact force and the penetration depth of the boulder into the galleries cushion layer were measured. After the test, samples have been taken from the gallery, in order to evaluate the effective material properties, revealing an average concrete compressive strength of 41 MPa and a rebar yield strength of 290 MPa.

Fig. 1 Gallery Parde

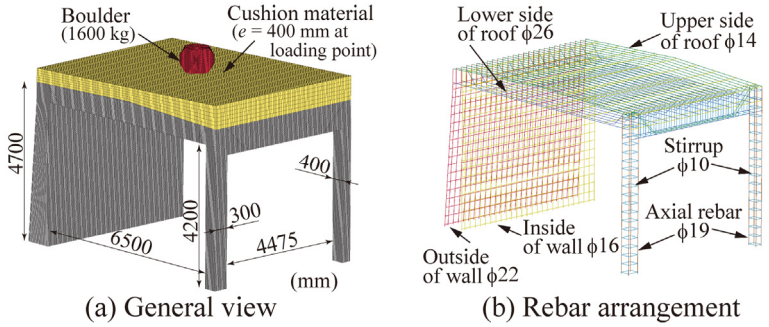

Fig. 2 General view and rebar arrangement for FE model

DESCRIPTION OF FE MODEL

One-span of the gallery has been modelled with a standard mesh size of approx. 50 mm (see mesh geometry in Fig.2). The rebars were modelled using beam elements with two nodes. For the concrete and cushion material eight-node solid elements were used. Contact surface elements were defined to take into account the interaction between the cushion layer and surface of roof slab, allowing to cope for contact, detachment, and sliding of two adjacent elements. The bottom surface of side wall and of the columns were completely fixed with the ground. In the analysis for the prediction of the test (hereinafter pre-analysis), the cushion material was assumed as compacted gravel. These analyses were conducted for the impact of the 1600 kg boulder and falling from 25 m height.

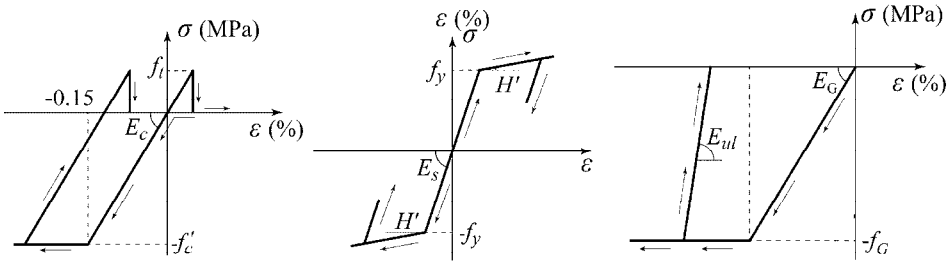

Fig. 3 Stress-strain relations

For the material properties (stress-strain relationship) of concrete, a perfect elastic-plastic bilinear model is adopted by using Drucker-Prager's yield criterion (Fig. 3a). Concrete yielding was assumed at a strain of 1500μ. For tension, a linear model is used with a cut off at 10% of the compressive strength. For the rebar a bilinear isotropic hardening rule as shown in Fig. 3b is used. The plastic hardening coefficient H' is 1% of the Young's modulus Es (= 206 GPa). For the cushion layer, a bilinear model is applied using a crushable foam model with tension cut-off (Fig. 3c). The elastic modulus was assumed as 200 MPa [7] in pre-analysis.

COMPARISON BETWEEN ANALYTICAL AND EXPERIMENTAL RESULTS

Figure 4 compares the time histories of the impact force, the penetration depth, and the deflection of roof slab. It can be observed that impact force estimated from the pre-analysis is approx. double than the experimental result. The impact time duration estimated in the analysis is with 10 ms about 30% of test results and the penetration depth estimated from analytical results is also approx. one-third of the penetration obtained from the experimental results (see Fig. 4b). Therefore, the assumed cushion layer in the pre-analysis was significantly overestimated.

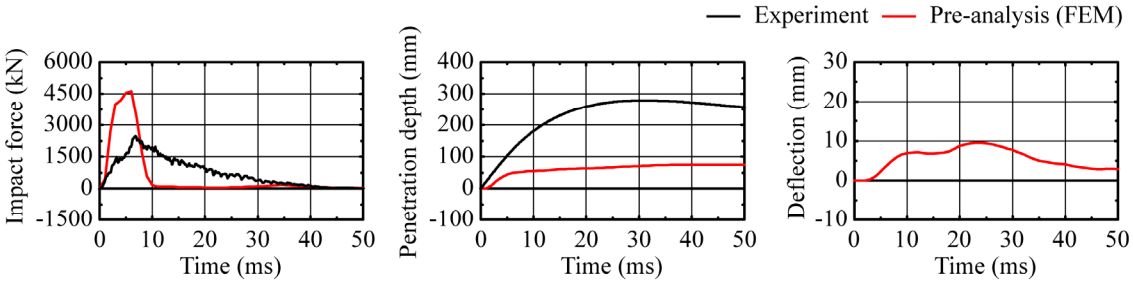

Fig. 4 Comparison between pre-analytical and experimental results for time histories

The post-analysis was carried out by adjusting the stiffness of the cushion layer until impact force and penetration depth related to the test results. The elastic modulus of cushion layer was changed from 200 to 8.8 MPa.

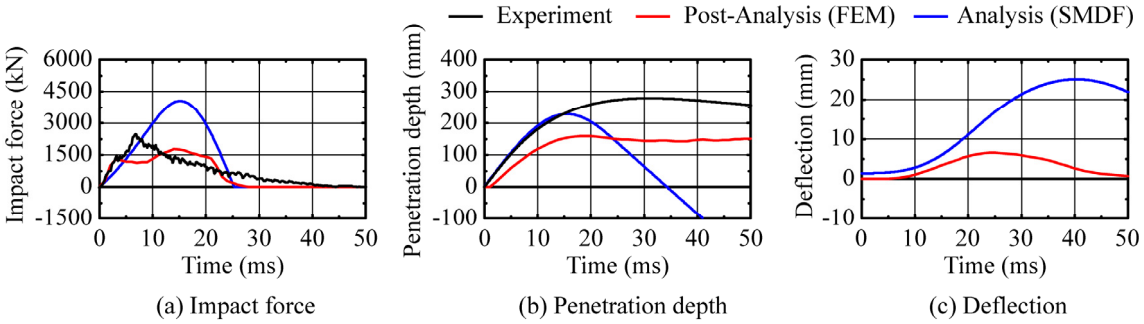

Fig. 5 Comparison between post-analytical and experimental results for time histories

Figure 5 shows the time histories for post-analysis as well as for the SMDF-model proposed by Schellenberg [4], where the parameters are described in the test report [5]. The impact duration time for all cases are almost similar and the maximum impact force by FEM is significantly smaller than the case of pre-analysis. The maximum impact force estimated by the SMDF-model is two times larger than the test result. Both, penetration depth and deflection evaluated by SMDF are larger than those by post-analysis of FE-simulation, concluding that also that SMDF was conservatively estimating the actual impact resistant capacity.

The results of pro-analysis of FE-simulation showed fine bending cracks in the bottom surface of the roof slab. At the test site, however, no cracks were observed after impact test of this case. This means that FE simulation gives conservative evaluation.

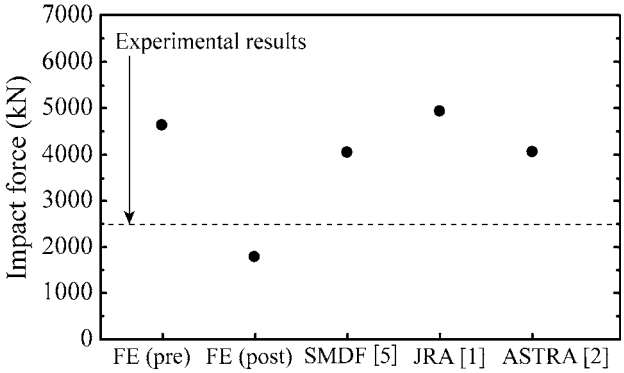

Fig. 6 Predicted impact force

Figure 6 shows a summary of the impact forces by pre-/post-analysis of FE-simulation, SMDF [5], and evaluated by the design guidelines of Japan Road Association (JRA) [1], and Switzerland (ASTRA) [2], comparing them with experimental result. For the design guideline of JRA, Lame's constant of the cushion layer was taken as 8,000 kN/m^2 and from the ASTRA guideline, soil modulus was set as 10,000 kN/m^2. The evaluated impact forces by pre-analysis of FE simulation, SMDF, guidelines of JRA and ASTRA are greater than actual impact force. Also, impact force estimated from JRA is the biggest among those values.

CONCLUSIONS

1) In the case of the pre-analysis of FE-simulation, the impact force is two times larger than that of experimental results, because the cushion layer was assumed as compacted gravel overestimating its stiffness.
2) In the case of post-analysis, elastic modulus of cushion layer was reduced until the impact force wave is in good agreement with experimental results.
3) Evaluated impact forces by pre-analysis of FE simulation, SMDF, guidelines of JRA and ASTRA are greater than experimental results of impact force. This means those evaluation method give conservative values.

REFERENCES

[1] JAPAN ROAD ASSOCIATION (2000) Manual for anti-impact structures against falling rocks (in Japanese).
[2] ASTRA (2008) Einwirkungen infolge Steinschlags auf Schutzgalerien, Richtlinie, Bundesamt für Strassen, Baudirektion SBB, Eidgenössische Drucksachen- und Materialzentrale, Bern.
[3] KISHI N, OKADA S, KONNO H (2009) Numerical Impact Response Analysis of Rockfall Protection Galleries, Structural Engineering International, 19(3), 313-320.
[4] VOGEL T, SCHELLENBERG K, GHADIMI KHASRAGHY S (2015) Dynamic structural capacity of reinforced concrete slabs due to rockfall: AGB-Report 673, pp 249.
[5] VOLKWEIN A. (2016) Durchführung und Auswertung von Steinschlagversuchen auf eine Stahlbetongalerie. Testing report, WSL, Switzerland.
[6] HALLQUIST J O (2017) LS-DYNA Version 971 User's Manual, Livermore Software Technology Corporation.
[7] HIRATA T, KOMURO M, YAMAGUCHI S, KISHI N (2015) Numerical simulation on impact resistant behavior of full-scale RC rock protection gallery with gravel cushion, Proceedings of JCI Annual convention, 37(2), 601-606 (In Japanese).

IMPACT OF ROCK FALLS AND ROCK SLIDES ON PROTECTIVE BARRIERS: COMPARATIVE CALCULATIONS USING DISTINCT ELEMENT METHOD (DEM)

Alexander Preh[1], Mariella Illeditsch[1], Mathias Schmidt[1], Peter Pamminger[1]

Dimensioning of protective barriers for falling rock represents a very important task to minimize risk to human life and infrastructure. Current approaches for the estimation of the dynamic impact of rock falls are providing static equivalent forces and are limited to the analyses of single block impacts (e.g. [1]). Two DEM-programs, PFC and UDEC of Itasca Consulting Group, have been used to analyze the different effects of action (max impact forces) from single rock fall compared to rock mass fall by means of simple numerical models. Moreover, the models have been used in order to get a better understanding of the mechanics of rock falls, rock mass falls and rock slides.

Keywords: rock fall, rock fall embankment, impact forces, rock mass fall, rock slide

INTRODUCTION

The estimation of the effects of action as a result of the dynamic impact of rock falls and rock slides is essential for the dimensioning of protective barriers, such as rock fall embankments. In order to realistically calculate impact forces, knowledge of the velocity, the incident angle and the mass of the rock fragment, as well as the interaction between rock fragment and embankment (penetration depths and damping) are of importance. Current approaches providing static equivalent forces are based on empirical relationships [1]. Those approaches are limited to the analyses of single block impacts; the dynamic impact of small rock mass falls or rock slides is not considered. In reality, dynamic impact is not always caused by single blocks, but often by (sliding or falling) fragmented rock mass.
Until now, there is no satisfying reference if and how the impact of rock mass differs from the impact of a single block. Using simple numerical models based on Distinct Element Method (DEM), the (significant) differences between the impact of a single block and the impact of fragmented rock mass have been analyzed and evaluated. For this purpose, the programs UDEC and PFC of Itasca Consulting Group have been applied.

ANALYSIS 1: SLIDING BLOCK VS. ROCK SLIDE

Objective of Analysis 1 was the estimation of the maximum impact force (both, dynamic and static) of a rock slide onto a protective barrier, depending on the number of blocks and their joint spacing. The DEM-codes UDEC and PFC (Itasca Consulting Group) have been applied using strongly idealized model geometry, as shown in Figure 1a. The sliding plane (bedrock) was chosen at a constant angle of 30° and the impact plane (stiff barrier) was defined perpendicular to the sliding plane, at all times (Fig. 1a). Comparative calculations have been conducted

[1]Institute of Geotechnics, Research Center of Engineering Geology, Vienna University of Technology, Austria

using rigid blocks, at which elastic and plastic deformations are represented by means of contact models. Elastic deformations were modeled by means of a linear contact model, whereas plastic deformations were simulated by means of an appropriate damping model, accordingly. With PFC, the viscous damping model was used, whereas with UDEC, the Rayleigh damping proportional to the joint stiffness was used for the simulation of the plastic deformations. The default local damping, proportional to acceleration, was deactivated for all kinds of block movements. The damping factors used for this comparison have been calibrated equal to a restitution coefficient of 0.2 by means of simulated drop tests.

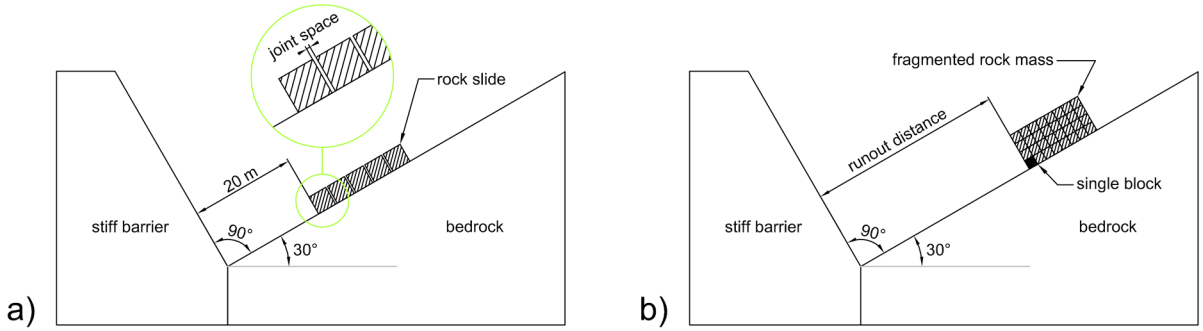

Figure 1: a) Model used for Analysis 1; b) Model used for Analysis 2

The initial state of the model is shown in Figure 1a. A chain of a given number of cubic shaped blocks of 1 m³ volume each was released at a constant distance of 20 m from a stiff barrier, which was placed perpendicular to the sliding plane. The number of modeled blocks was varied between 1 and 30 and the joint spacing between the adjoining blocks was varied between 0 and 20 mm. Figure 2 shows the relation of the maximum total impact force to the number of adjoining blocks of the rock slide.

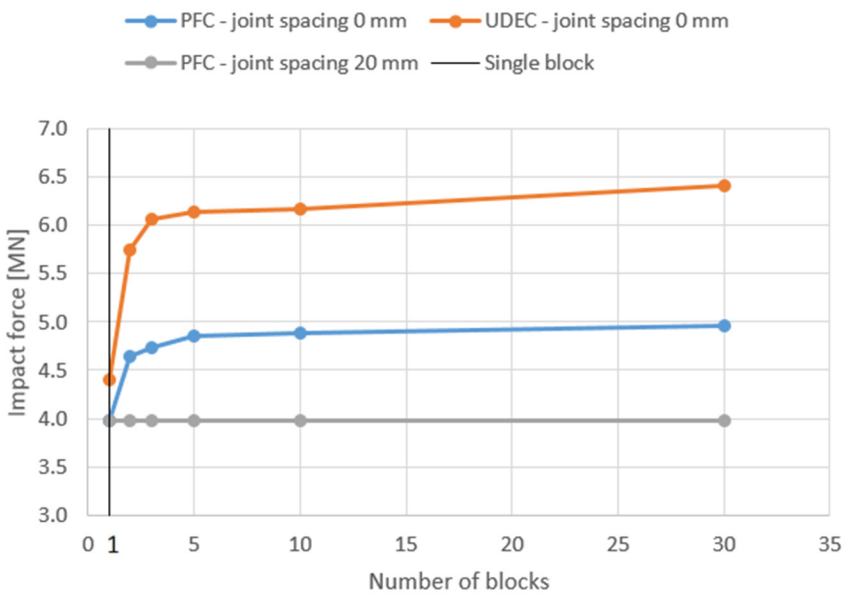

Figure 2: Maximum impact force vs number of blocks

For the case of directly adjoining blocks (joint spacing 0 mm) both, PFC and UDEC show an increase of the maximum impact force with an increasing number of blocks. However, the increase of the impact force is significantly high between the single block and the five-block-chain. With an increasing number of blocks beyond five the increase of the impact force is insignificant. For assemblies with a joint spacing greater than zero, the maximum impact force is identical to that of a single block. However, UDEC and PFC show slightly different results in terms of the amount of the max. impact force. The reason could be the different damping models used with PFC and UDEC. Both damping models have been calibrated by means of simulated drop tests, however, this procedure may not be sufficient for the calibration of the Rayleigh damping used with UDEC.

ANALYSIS 2: ROCK FALL VS. ROCK MASS FALL

Objective of Analysis 2 was the investigation of the ratio of the maximum impact force generated by rock mass fall to the maximum impact force generated by comparative single rock fall. The model setup used for the analysis is shown in Figure 1b. Both, the geometry and the damping and material parameters are as defined in Analysis 1. An assembly of discrete equally sized blocks was released at varying runout distances of 20 m, 50 m and 100 m from a stiff barrier. The number of released blocks was kept constant with 1000 blocks. The volume of the modeled equally sized blocks was varied between 0.1 and 10 m³.The black colored block in Figure 1b represents the block position, which was used for the comparative simulations of single rock fall.
Figure 3 shows the impact force ratio (ratio of the maximum impact force generated by rock mass fall to the maximum impact force generated by single rock fall) as a function of the block volume. Two extreme scenarios have been investigated in terms of rotational velocity, fixed spin and free spin.

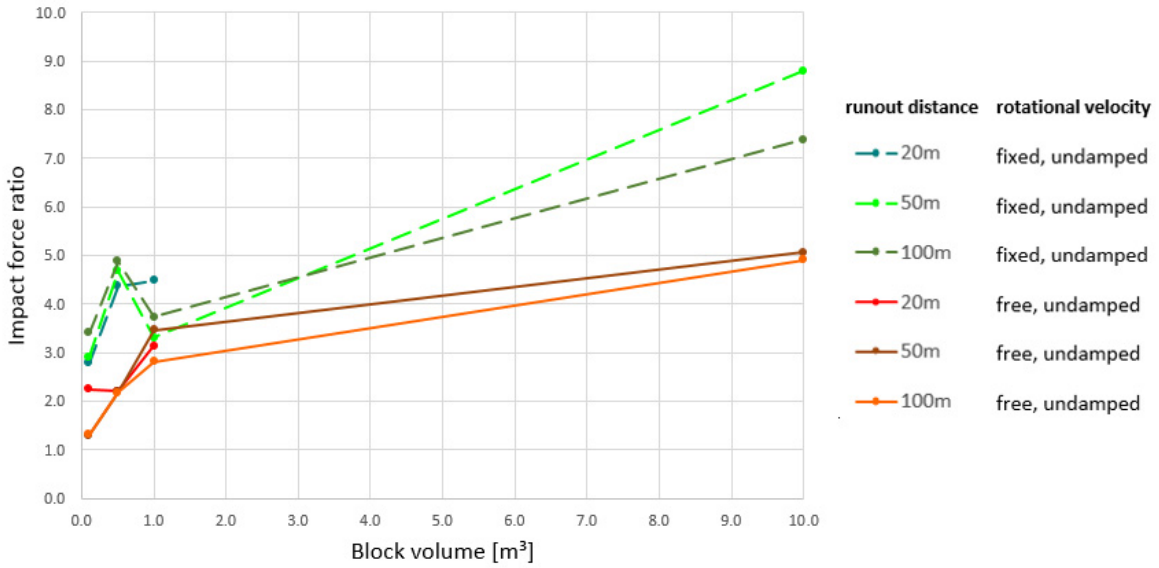

Figure 3: Ratio of the maximum impact force generated by single rock fall and rock mass fall (impact force ratio) for single block volumes of 0.1, 0.5, 1.0 and 10.0 m³.

The analysis shows a dependency of the calculated impact force ratio (rock mass fall / single rock fall) on the block volume and on the rotational damping (fixed spin and free spin). Compared to these parameters, the runout distance has minor influence on the impact force ratio.
Figure 4 shows the course of the impact force and the accumulated material at the barrier for a simulated rock mass fall with a single block volume of 1 m³ and a runout distance of 50 m (Fig. 1b).

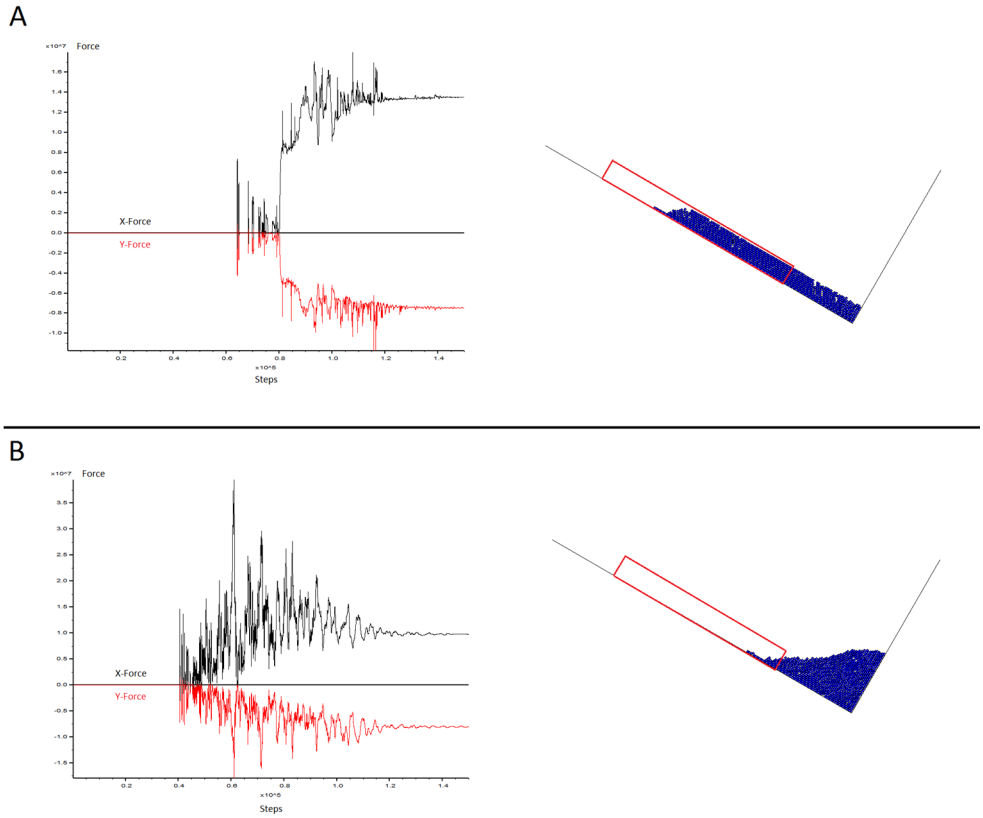

Figure 4: Impact force vs. calculation steps (left) and end position of the released blocks (right) for a runout distance of 50 m and a block volume of 1 m³. The red rectangle indicates the release position of the simulated 1000 rock blocks. A) rotational velocity fixed, B) rotational velocity free

CONCLUSIONS

This study provides first results of an extensive study with regards to the dynamic interaction of rock slide and rock fall onto protective barriers.
The results of Analysis 1 indicate that the front part (i.e. the first five blocks) of a rock slide generates 90-98% of the maximum impact force. The effect of the following sliding blocks (beyond five) is negligible. An explanation could be that the first few blocks, after their impact, are acting as a barrier themselves, taking up most impact force of the following blocks.
The results of Analysis 2 indicate that there is a relationship between single rock fall and rock mass fall, which predominantly depends on block volume and rotational damping.

REFERENCES

[1] HOFMANN R, MÖLK M (2012) Bemessungsvorschlag für Steinschlagschutzdämme / Design proposal for rock fall embankments. Geotechnik, Volume 35, Issue 1, pp 22-33

EXTENDED EXPERIMENTAL STUDIES ON ROCKFALL FLEXIBLE FENCES

Ignacio Olmedo[1], Philippe Robit[1], David Bertrand[2], Clément Galandrin[3], Jibril Coulibaly[4], Marie-Aurélie Chanut[4]

The development of new rockfall protection structures and their validation by experimental tests [1] demand a significant economical investment. Thus, numerical modeling becomes a useful tool to investigate the physical processes involved in the impact of a block on a flexible fence. Moreover, numerical models allow simulating particular impact conditions, difficult to test experimentally. For this, the development of consistent numerical models of rock impacts on flexible fences is a priority for manufacturers to optimize their barriers and for the scientific community given the particularities of these complex dynamic interactions.

A specific working group of the French National Project C2ROP has been organized to cluster the different French researchers and manufacturers in this domain. The aim of this project is to assess the numerical models in the calibration and validation tasks. Thus, a rockfall flexible fence has been specifically designed and tested under different loading conditions. In particular, all the components of this structure have been tested and characterized in order to perform the models calibration. Moreover, real scale field tests have been performed in different loading conditions to guarantee an accurate model validation. In this paper, all the experimental campaigns done and foreseen are described and the results presented.

Keywords: Rockfall, protection fence, experiments, impact

INTRODUCTION

Different numerical models to simulate the impact of rockfall on a flexible fence have been and are being developed or improved following different approaches [2], [3], [4]. However, numerical tools still need experimental data to characterize the physical process involved and to validate the numerical results. For this, in the French National Project C2ROP, a specific device has been designed without commercial purposes. This structure is representative of any rockfall fence and presents similar characteristics. In particular, the C2ROP fence is a 350kJ model including the main components found in any commercialized structure: net, posts, energy dissipating device and anchors (see Fig.1). Constitutive components are a combination of products of the two industrials participating to this project: CAN and GTS. The designed structure is composed of 3 functional modules of 5 meters long each and 2.75 meters of nominal height.

[1] GTS, 27 rue des tâches, Saint-Priest 69800, France, iolmedo@gts.fr
[2] INSA-Lyon, 20 Avenue Albert Einstein, 69100 Villeurbanne, France
[3] CAN, Le Relut, 26270 Mirmande, France
[4] CEREMA, 5 allée Général Benoist, Bron 69500, France

Fig. 1 C2ROP 350kJ rockfall flexible fence under study

COMPONENT'S CARACTERIZATION

The first stage of this experimental study has been to characterize all the components of the structure. Thus, laboratory tests have been carried out on the ring-net and on the energy dissipating devices. Experiments have been carried out on the CAN and GTS tensile quasi-static (QS) testing devices.

3 different types of ring-nets have been analyzed and characterize from the tests. In particular, the 6, 7.5 and 9 mm diameter ring nets have been tested at two different scales: single-ring samples and multi-ring net samples (see Fig.2 and 3). The former aimed to characterize the deformation of a single ring under different loading depending on the number of points applying the tensile effort: 2, 3 and 4 points (see Fig. 2). These tests provide precious data to assess the numerical modeling of rings, in particular, the first stages of their deformation [5].

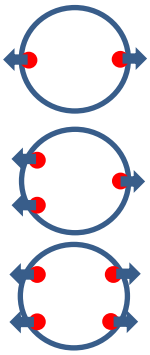

Fig. 2 2, 3 and 4 points single-ring tensile tests.

In a second stage of the analysis, tests on 3x3 rings nets have been carried out. 3 sides of the squared net were blocked and an imposed displacement was applied to the fourth. Tests were carried out until the rupture of the net and load-unload cycles were also carried out to characterize the elasto-plastic behavior of nets [4].

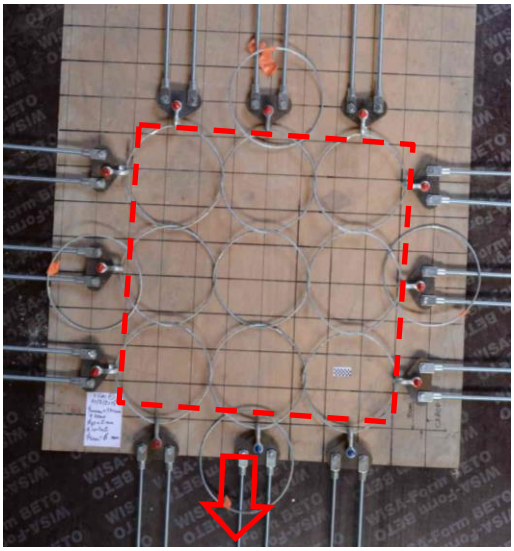

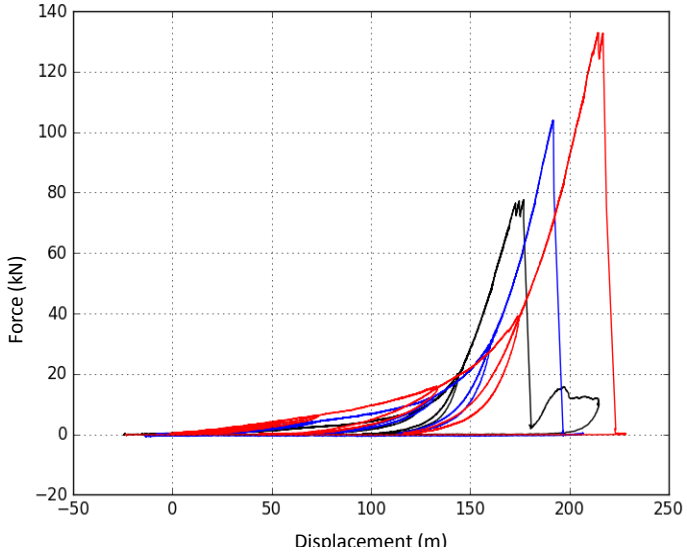

Fig. 3 Tensile test on 3x3rings net (left) and the force-displacement curves for the 6 (black), 7.5 (blue) and 9mm(red) diameter rings.

The GTS energy dissipating devices used on the C2ROP 350kJ fence uses the friction between a wire-rope and rigid steel elements as energy dissipating process. An experimental campaign of more than 30 tests has been carried out in order to adjust the geometrical characteristics of this component to achieve a trigger load value of 25kN and an optimal energy dissipation (see Fig.4). The final configuration shows a good repeatability of results in terms of triggering value and load-displacement behavior after the triggering.

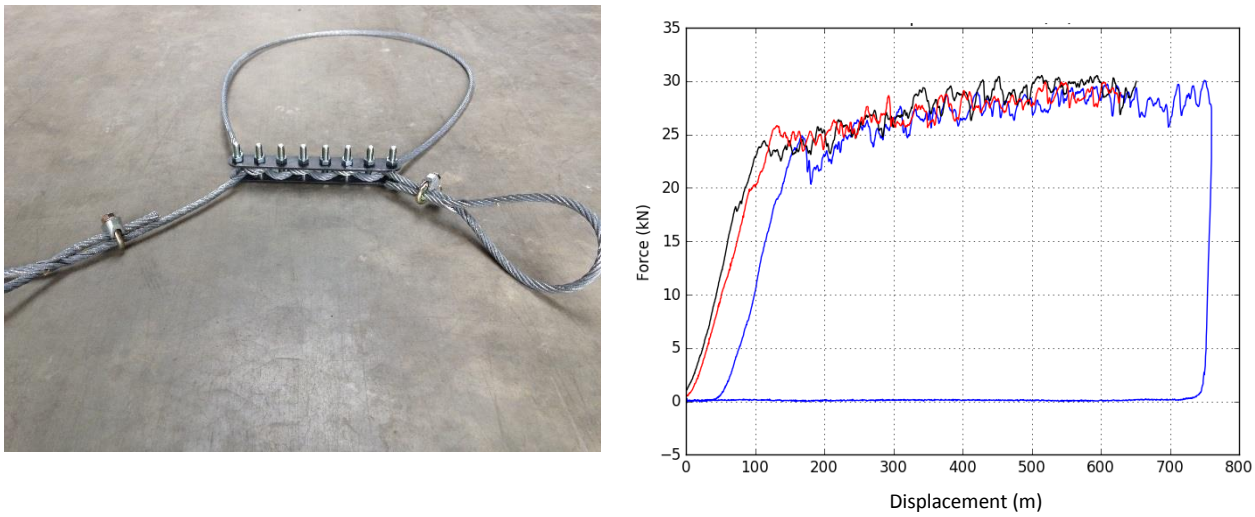

Fig. 4 GTS energy dissipating device and force-displacement results of the QS tensile tests.

FULL SCALE STRUCTURE EXPERIMENTS

In order to provide experimental data to validate the numerical models, two full scale tests on a C2ROP fence are carried out. The first experiment consisted of a QS loading of central module of the fence. The aim of this experimentation was to progressively load the structure to evaluate the charges distribution on the whole device without the contribution of the dynamic effects. For this, a winch device was installed under the central module allowing to pull down a block previously placed on the structure. Force sensors were installed on the loading device and on different locations on the structure. The displacement of the block was measured from high resolution images taken along the test.

Force – displacement results allowed identifying the energy dissipating devices triggering at the expected force value. Moreover, the evolution of the tensions on the longitudinal upper and lower cables as well as on the upstream side cables can be compared to the applied winch loading and the net deflection.

The last part of this extended experimental study consist of impact test following the ETAG027 [1] guideline. This experimental campaign took place in February 2017 and consisted in 2 maximal (MEL) and 3 service (SEL) energy level impacts. Moreover, complementary tests as multiple impacts on lateral modules or impacts while a permanent loading is applied on contiguous modules are foreseen to simulate real scenarii which are not considered in the ETAG027.

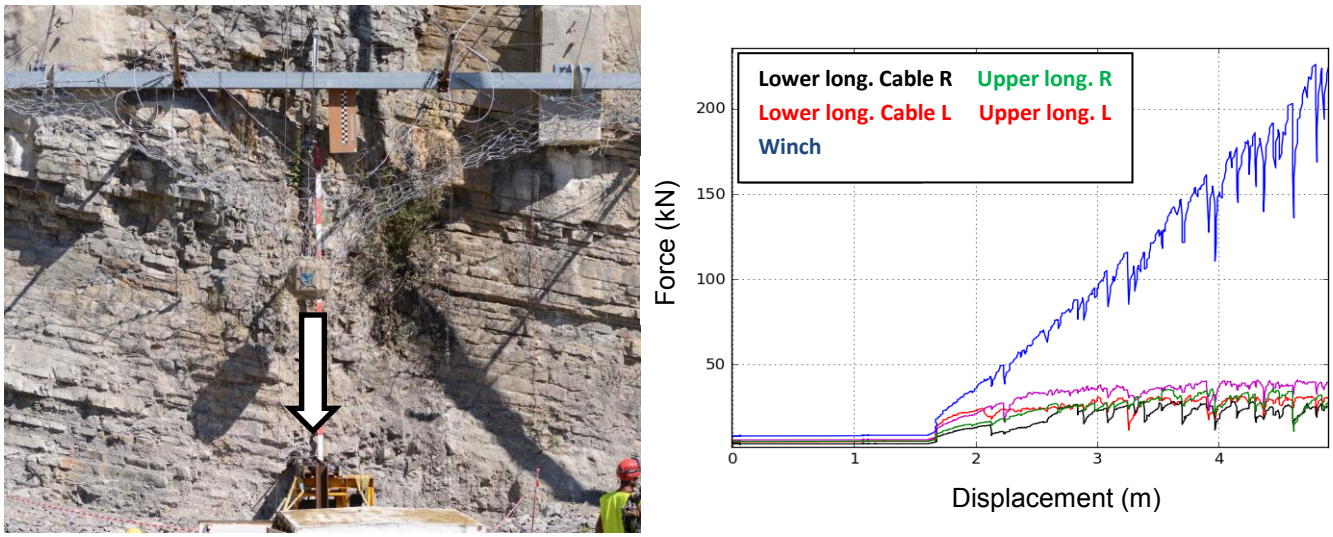

Fig. 5 Quasi-static real scale test configuration (left) and force-displacement results measured at the winch and at the extremities of the longitudinal lower cable (right).

CONCLUSIONS

Preliminary analysis allowed verifying that the behavior of the energy dissipating devices installed on the structure are the same that those observed in laboratory studies. Moreover, it has been observed that the distribution of efforts on the structures during the dynamic impact is similar than under a QS solicitation. In the case of multiple SEL impacts on the same structure a significant and progressive increase of the efforts has been observed. Further analysis of the recently obtained experimental data is carried out.

REFERENCES

[1] ETAG 27 (2008) Guideline for European Technical approval of falling rock protection kits
[2] BERTRAND, D.; TRAD, A.; CHAUVEL, R. & LIMAM, A. Discrete element simulation of an innovative metallic net dedicated to rockfall protection : a multi-scale approach, Euro-mediterranean symposium on Advances in Geomaterials and Structure, 2010, 399-406
[3] NICOT, F.; CAMBOU, B. & MAZZOLENI, G. Design of Rockfall Restraining Nets from a Discrete Element Modelling, Rock Mechanics Rock Engineering, 2001, 34 (2), 99-118
[4] ESCALLÓN J.P., WENDELER C., CHATZI E., AND BARTELT P. (2014) Parameter identification of rockfall protection barrier components through an inverse formulation. Engineering Structures, 77:1–16.
[4] VOLKWEIN A. (2004) Numerical simulation of flexible rockfall protection systems PhD thesis, Swiss Federal Institute of Technology, Zurich, Switzerland.
[5] COULIBALY J.B., CHANUT M-A., LAMBERT S., NICOT F., (2016), Non-linear Discrete Mechanical Model of Steel Rings, Journal of Engineering Mechanics,
[6] TRAD A. Analyse du comportement et modélisation de structures souples de protection : le cas des écrans de filets pare-pierres sous sollicitations statique et dynamique. Thèse de l'INSA de Lyon, Ecole Doctorale MEGA, 2011

NUMERICAL SIMULATION ON IMPACT RESISTANT BEHAVIOR OF FULL-SCALE POCKET-TYPE ROCKFALL PROTECTION NETS

Masato Komuro[1], Hiroaki Nishi[2], Hisashi Konno[3]

In order to establish a numerical analysis method for appropriately evaluating dynamic response characteristics of full-scale pocket-type rockfall protection nets, 3D impact response analysis was conducted taking impact velocity of the striker as variable. An applicability of the proposed analysis method was discussed comparing with the experimental results. From this study, it is seen that the horizontal displacement at the loading point can be appropriately predicted irrespective of the magnitude of input impact energy.

Keywords: rockfall protection nets, impact loading test, finite element analysis

INTRODUCTION

In the mountainous areas and/or coastlines in Japan, many rockfall protection structures have been constructed along and/or over the highways to protect transportation networks and human lives from falling rocks. One type of these rockfall protection structures called as a pocket-type rockfall protection net is made combining with hunger rope, H-shaped steel struts, diamond-shaped wire net, and wire ropes. This kind of net is designed based on the absorbing capacity of each member, and difference of kinetic energy of the rock between before and after collision [1]. However, the dynamic response characteristics and energy balance based on intake energy due to collision of rocks and the consumed energy due to each structural member have not been clearly verified yet. In order to verify these, it is necessary to be experimentally and numerically investigated.

From this point of view, in order to establish a numerical analysis method for appropriately evaluating dynamic response characteristics of the full-scale pocket-type rockfall protection nets, 3D impact response analysis was conducted taking impact velocity of the striker as variable. An applicability of the proposed method was discussed comparing with the experimental results. Here, LS-DYNA code [2] was used for this numerical analysis.

OUTLINE OF EXPERIMENT

Photo 1(a) shows a view of the full-scale rockfall protection net used in this experiment, and Fig. 1 shows the dimensions of net specimen. The model was designed against a 150 kJ input impact energy due to collision of a rock following Japanese design guideline [1]. Height and

[1] Muroran Institute of Technology, Mizumoto, Muroran 050-8585, Japan, +81 143 46 5228, komuro@news3.muroran-it.ac.jp
[2] Civil Engineering Research Institute for Cold Region, Structural Team, Toyohira, Sapporo 062-8602 Japan, +81 11 841 1698, h-nishi@ceri.go.jp
[3] Civil Engineering Research Institute for Cold Region, Structural Team, Toyohira, Sapporo 062-8602 Japan, +81 11 841 1698, konno@ceri.go.jp

arranging interval of the strut were 3.5 m and 3.0 m, respectively. Diameter of the diamond-shaped wire is 5 mm, and area of the wire net was 10×15 m wide. Main horizontal and vertical wire ropes was 3×7 G/O φ18, and diameter and anchoring length for wire rope were D32 and 1 m, respectively. The wire ropes and net were connected using the coupling coil (φ4) as shown in Photo 1(b).

Full-scale falling-weight impact tests were conducted to investigate dynamic response behavior of the wire net varying input energy due to collision of a striker. Experimental cases were listed in Tab. 1. Axial strains of a total of 16 turnbuckles were measured to evaluate the tensile force applied in the wire ropes. All responses were measured by using a digital data recorder with sampling time of 0.1 ms. Here, two sets of high-speed cameras located in front of the net, were used to precisely measure the 3D deformation of the wire net. One of high-speed cameras located in the side of wire net, was used to evaluate the input energy due to the striker and maximum deformation of the wire net.

A total of 72 target marks was set on the wire net for high-speed camera as shown in Fig. 1. The striker (mass: 1 ton) was used (See, Photo 1c), and was collided by sliding along the guide rail at the center of the horizontal rope.

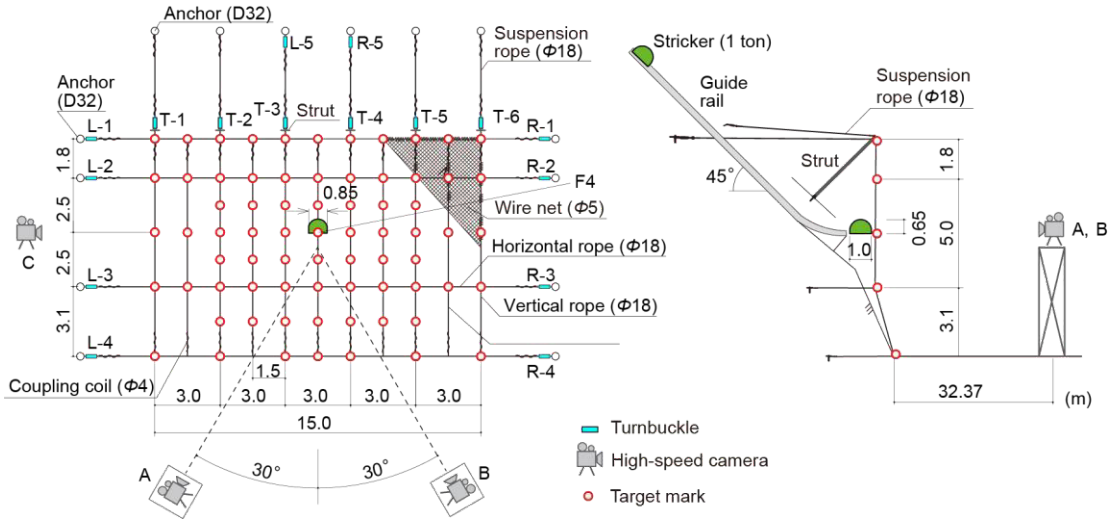

Fig. 1 Dimension and measuring items of pocket-type rockfall protection net

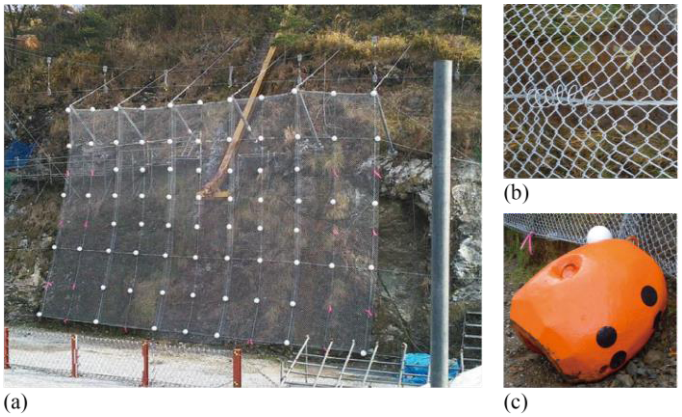

(a)

Photo 1 View of specimen
(a: panorama view, b: coupling coil, c: striker)

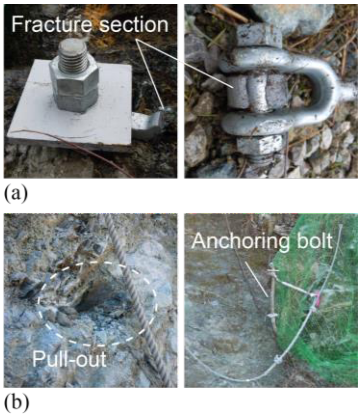

(a) (b)

Photo 2 Failure of anchoring device
(a: fracture, b: pull-out failure)

Tab. 1 Experimental cases

Specimen	Falling height (m)	Input energy (kJ)		Remark
		Design	Actual#	
S1	6	53	50	Unmeasurable of tensile force of horizontal rope (L-3)
S2	12	106	95	Fracture of anchoring device (L-3)
S3	18	159	142	Pull-out failure of anchoring bolt (R-3)

Actual input energy E was calculated by using actual impact velocity v ($E = 0.5\ mv^2$).

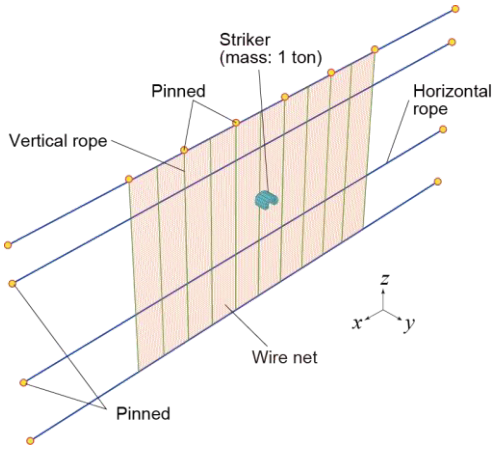

Fig. 2 FE model

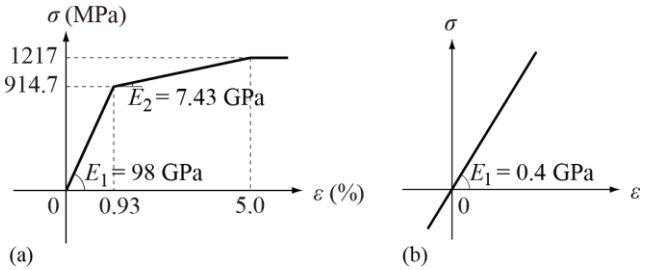

Fig. 3 Stress-strain relations (a: wire rope, b: wire net)

OUTLINE OF FINITE ELEMENT ANALYSIS

Since the actual specimen was three-dimensional and had a complicate shape, it is very difficult to precisely consider these shapes in the FE model. Here, simplifying the wire net, a 2D plane model was used as shown in Fig. 2. Length of horizontal rope and area of wire net were 27 m, 10×15 m, respectively. Wire net was modeled by using shell elements. Vertical and horizontal ropes were modeled using cable elements in which the compressive stress occurred in those elements was ignored. The ends of each wire rope were pinned, and each wire rope and net was assumed to be perfectly bonded to each other. Contact surface model was introduced for interaction between striker and wire net. Friction of the contact surface and damping effect were not considered.

Figure 3 shows the stress-strain relation applied for wire rope and wire net. Here, a tri-linear model was applied as the relation of the wire ropes following Japanese design standard [1]. Wire net was assumed to be elastic material having an elastic modulus of 0.4 GPa following the previous report. Striker was also assumed to be elastic with material properties of steel and its density was given to be equal to the actual mass.

NUMERICAL RESULTS AND DISCUSSION

Figure 4 shows the comparison of the time history of the horizontal displacement at the loading point between numerical analysis and experimental results. From these figures, it is observed that maximum displacements obtained from the numerical analysis were almost similar to those obtained from the experimental results. However, in cases of S2 and S3, configuration of the time histories after peak obtained from numerical analysis were larger than those from the

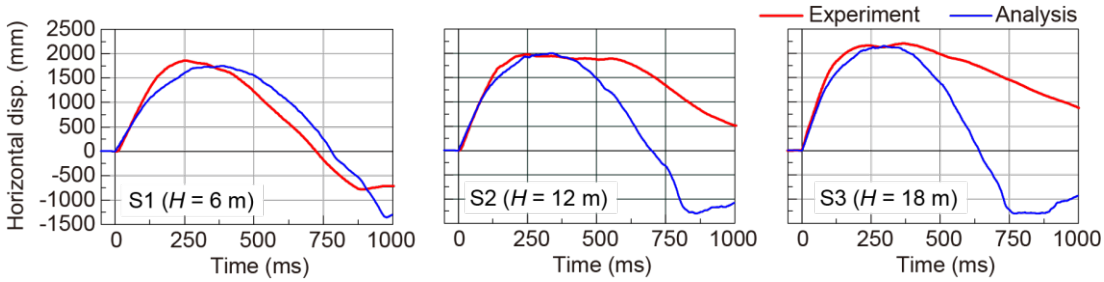

Fig. 4 Time history of horizontal displacement at loading point (F4)

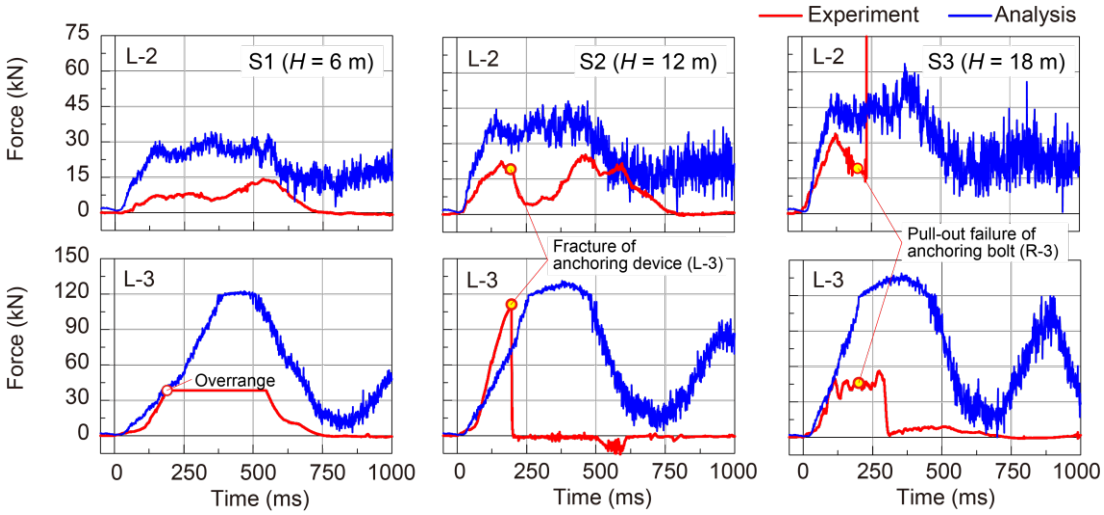

Fig. 5 Time history of force applied in horizontal ropes near loading point (upper: L-2, lower: L-3)

experimental results. Because in these cases, anchoring devices have been fractured and pull-out as shown in Photo 2.

Figure 5 shows the time history of the forces applied in the horizontal ropes near the loading point. Regarding tension force applied in the rope L-2 located above the loading point, results obtained from the numerical analysis overestimated the experimental results. In the case of the rope L-3 located bellow the loading point, incremental rate of the force obtained from the numerical analysis tends to be similar to that of the experimental result until the supporting device was fractured.

CONCLUSIONS

1) Displacement of the wire net at the loading point can be appropriately predicted by using proposed FE analysis method irrespective of the magnitude of the input energy; and
2) On the other hand, tensile force applied in the upper horizontal rope above the loading point tends to overestimate the experimental result.

REFERENCES

[1] JAPAN ROAD ASSOCIATION (2000) Design guideline for anti-impact structures against falling rocks, Maruzen, pp 132-146. in Japanese.
[2] HALLQUIST JO (2012) LS-DYNA Version 971 User's Manual, Livermore Software Technology Corporation.

CALIBRATION OF AN EQUIVALENT SHELL MODEL FOR A CHAIN-LINK MESH

Alessio Mentani[1], Laura Govoni[2], Anna Giacomini[2], Olivier Buzzi[1], Guido Gottardi[2]

In recent years, there has been an up surging interest toward the investigation of the response of low energy rockfall barriers. The mechanical response of these structures largely depends on the interception structure. In this short note, the response of a chain-link mesh, typically used for this barrier type, is explored, by means of dynamic and static tests on panel portions at different scale. Based on the experimental data, an approach to develop an accurate and computationally effective FE model of the net is then described.

Keywords: FEM, shell elements, chain-link, numerical strategy

INTRODUCTION

Finite Elements numerical models, calibrated and validated on the base of experimental evidences, are a valid tool to numerically predict the response of rockfall protection countermeasures [1, 2]. An appropriate modelling of the interception structure of a rockfall barrier plays a crucial role on the effective simulation of the whole structure [3]. In fact, the response of a rockfall barrier is strictly correlated to the efficiency of the metallic mesh installed, in particular for low to medium energy absorption capacity barriers [4]. Several meshwork configuration exist in the field of rockfall protection devices, among which a common system is the chain-link type (Fig. 1a). Experimental tests in both quasi-static and dynamic conditions have been performed on this mesh [5, 6], the latter proving its dependency on the boundary conditions. Thus, modelling a chain-link mesh represents a specific challenge since its behavior is influenced by the particular construction at the nodes (intertwined steel wires, Fig. 1a). Usually beam or truss elements are implemented to model a metallic net in FEM simulations, but they would not be sufficient to replicate the mesh response without recurring to specific adjustments at the nodes. Alternatively, shell elements can be used to numerically reproduce a mesh. Few solutions to reproduce the response of the chain-link with shell elements were proposed [5, 7]. However, most constitutive laws adopted simply model for the plastic phase without taking into account the anisotropic behavior of the net, as well as the potential failure of the elements constituting the mesh. Recently, an efficient method to model the chain-link net by using two-nodes beam elements was developed by [8]. The approach is reliable but complex with a specific attention given to simulate the link nodes, which imply a high-computational cost of the model. Based on this background, this study intends to present a numerical strategy to identify an equivalent shell model of a mesh while reducing the computational cost of the model. The

[1] University of Bologna, Department of Civil, Chemical, Environmental and Materials Engineering, Viale Risorgimento 2, Bologna 40136, Italy, 051 2093521, alessio.mentani2@unibo.it
[2] The University of Newcastle, ARC Centre of Excellence for Geotechnical Science and Engineering Discipline of Civil, Surveying and Environmental Engineering, 2308 Callaghan, Australia, +61249215454, anna.giacomini@newcastle.edu.au

method is here proposed for the chain-link TECCO® G65/3 mesh manufactured by Geobrugg, but could be similarly applied to other mesh. The approach defines an anisotropic behavior of the shell elements in terms of both elastic and plastic mechanical properties, using experimental evidences to calibrate the material parameters. Results of full-scale impact tests are used to define the material failure criterion and to assess the reliability of the model, with specific attention given to the mesh size dependency and to the computational cost effectiveness.

SHELL ELEMENTS FOR A CHAIN-LINK MESH

The TECCO chain-link is a 3 mm high-tensile steel wire mesh, protected by a zinc-alum coating. Each steel chain is interlaced with each other to form a diamond pattern with openings of 83x143 mm (Fig. 1a). The numerical analyses described in the identification procedure are performed with the commercial code ABAQUS [9], both quasi-static standard and dynamic explicit operators are used to run the simulations.
The numerical mesh was built with 3-nodes small membrane strains shell elements with reduced integration control (S3RS). The triangular elements constitute a robust solution for impact dynamic problems where small in-plane strains but large rotations and bending are expected [9]. The reduced integration option implies a lower-order of integration points needed to form the element stiffness, thus decreasing the running time. In fact, from a computational cost point of view, a reduced number of integration points offers the advantage to decrease the CPU time and storage requirements without decreasing the reliability of the solution, especially in 3D problems [9]. The disadvantage is that the reduced integration procedure can admits deformation modes that produce no straining at the integration points. This is the so-called hourglassing phenomenon, for which zero-energy deformation modes propagate through the mesh leading to inaccurate solutions. To prevent this effect, an artificial stiffness is added to the element by the operator, but a mesh size control is then required. In order to check the mesh dependency of the model, the ratio R between the surface area of a triangle of the rhomboidal pattern (A_{tri}, Fig. 1a) and the area a triangular shell elements ($A_{tri,FEM}$) was checked to obtain a final stable solution (i.e. $R = A_{tri} / A_{tri,FEM}$).

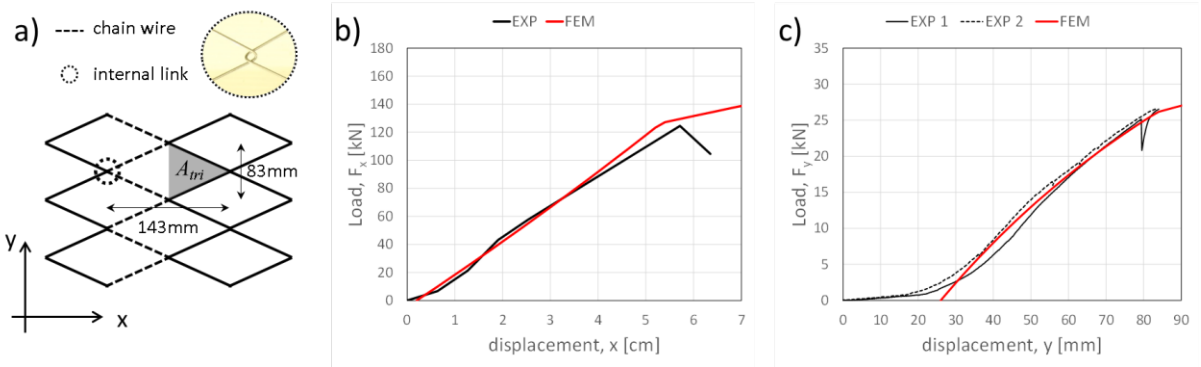

Fig. 1 a) Configuration of a chain-link system and EXP vs FEM results of in-plane tensile tests: b) in x direction and c) in y directions

CALIBRATION OF THE SHELL MECHANICAL PROPERTIES

Experimental tensile tests performed on chain-link panels in quasi-static conditions have shown that its in-plane behavior is not isotropic (Fig. 1b and c). Experimental results are illustrated in

terms of forces recorded at the fastened nodes and mesh elongation. The initial dimensions of the panel were 858x996 mm for the test in x-direction [6], while a panel of 429x249 mm was tested in y-direction.
Based on these results, the elastic stiffness matrix assigned to the shell elements was defined with an orthotropic material in the mesh plane, while neglecting the properties in the normal direction (i.e. membrane behavior). The numerical mesh was built according to the experiments and with a ratio R equal to 1 (no mesh dependency was shown in static conditions). The two tests were reproduced to calibrate the elastic modulus in the principal directions (E_x and E_y). Similarly, the yielding stresses ($\sigma_{y,x}$ and $\sigma_{y,y}$) were calibrated based on the experimental data and the Hill stress potential was implemented to consider the anisotropic behavior of the material [11]. The numerical results obtained from the calibration of the two tensile tests are reported in Fig. 1b and c. Values of 650 MPa and 120 MPa were used for the elastic modulus and yield stresses of 35 MPa and 25MPa in x and y-direction, respectively.

MODELLING OF NET FAILURE AND VALIDATION

First the elasto-plastic properties of the material were defined. The procedure of calibration of the equivalent shell model was then finalized by defining the conditions at failure. Experimental results of two impact tests on squared panel of 2 m size were considered for this purpose (Fig. 2a). In the test, a polyhedral shaped block of 650 mm size and 440 kg mass was released to impact the mesh vertically. In the first test the block impacted the mesh with a velocity of 4.384 m/s without reaching failure (test T01), while in the second test the velocity increased to 5.436 m/s and a mesh failure was observed (test T02 in Fig. 3a). These data were used to define failure properties in dynamic condition, to verify the mesh size sensitivity and to validate the model. In order to define the material failure, a damage function was introduced. The equivalent plastic strain ($\varepsilon_{pl,u}$), which represents the plastic deformation produced at the onset of the damage was first calibrated. The behavior of the chain-link is almost fragile, hence the definition of a damage evolution law was neglected and a value of $\varepsilon_{pl,u}$ equal to 10% was determined.

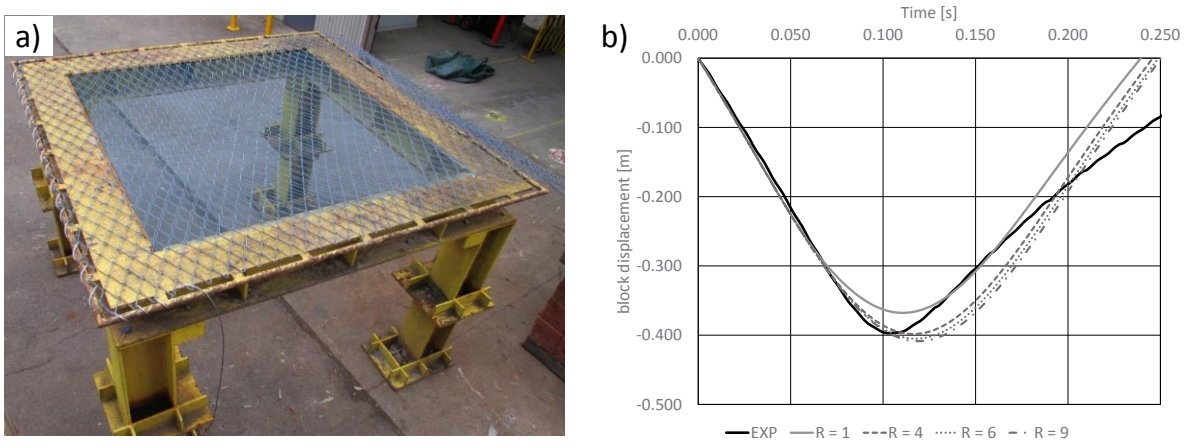

Fig. 2 a) Frame used for the out-of-plane impact tests; b) EXP vs FEM results of T01 for different values of *R*

The results of test T01 showed a susceptibility of the model to the mesh size. Stability in the solution was reached by increasing the value of *R* till a convergence of the solution for a ratio larger or equal to 6 (Fig. 2b). Finally, a qualitative comparison between experimental and FE results of test T02 shows the ability of the model to adequately reproduce the experimental

evidences also in terms of mode of failure. In Figure 3a, the area of the mesh which undergone failure in the experiment is highlighted with a dashed line. It can be observed that the simulation produced a similar response, confirming an appropriate calibration of the model (Fig 3b).

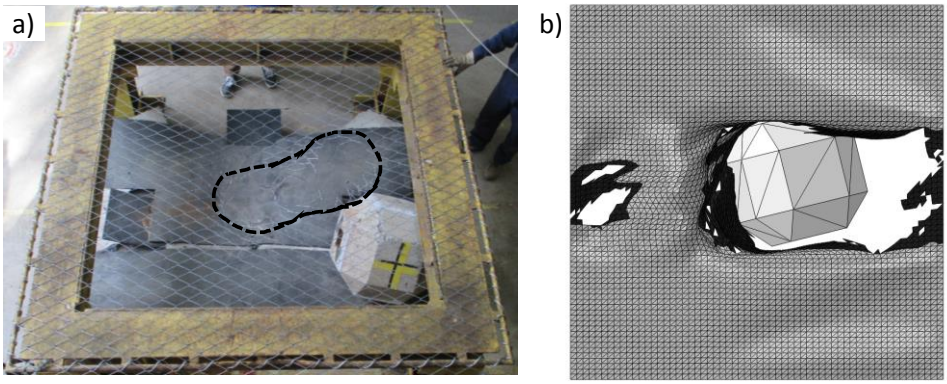

Fig. 3 Impact tests in failure conditions (T02): a) EXP with failed area highlighted by dashed line and b) FEM.

CONCLUSION

In this note, the mechanical response of a chain-link mesh, typically used as interception structure for low energy barriers, is explored, based on the results of dynamic and static tests on panel portions. The experimental data have been used to develop a new approach to devise effective FE models of the net. Results of preliminary analyses are promising as the model, which make use of shell elements, was shown able to capture the essential features of the experimentally observed response.

REFERENCES

[1] VOLKWEIN A, SCHELLENBERG K, LABIOUSE V, AGLIARDI F, BERGER F, BOURRIER F, DORREN LKA, GERBER W, JABOYEDOFF M (2011) Rockfall characterisation and structural protection – a review. Natural Hazards and Earth System Sciences 11, 2617-2651
[2] GENTILINI C, GOTTARDI G, GOVONI L, MENTANI A, UBERTINI F (2013) Design of falling rock protection barriers using numerical models. Engineering Structures 50, 96-106
[3] MENTANI A, GIACOMINI A, BUZZI O, GOTTARDI G, GOCONI L, FITYUS S (2016) Numerical modelling of a low-energy rockfall barrier: new insight into the bullet effect. Rock Mechanics and Rock Engineering 49, 1247-1262
[4] DE MIRANDA S, GENTILINI C, GOTTARDI G, GOVONI L, MENTANI A, UBERTINI F (2015) Virtual testing of existing semi-rigid rockfall protection barriers. Engineering Structures 85, 83-94
[5] SASIHARAN N, MUHUTHAN B, BADGER TC, SHU S, CARRADINE DM (2006) Numerical analysis of the performance of wire mesh and cable net rockfall protection systems. Engineering Geology 88, 121-132
[6] BUZZI O, LEONARDUZZI E, KRUMMENACHER B, VOLKWEIN A, GIACOMINI A (2015) Performance of high strength rock fall meshes: effect of block size and mesh geometry. Rock Mechanics and Rock Engineering 48, 1221-1231
[7] DHAKHAL S, BHANDARY NP, YATABE R, KINOSHITA R (2011) Experimental, numerical and analytical modelling of a newly developed rockfall protective cable-net structure. Natural Hazards and Earth System Sciences 11, 3197-3212
[8] ESCALLON JP, BOETTICHER V, WENDELER C, CHATZI E, BARTELT P (2015) Mechanics of chain-link wire nets with loose connections. Engineering Structures 101, 68-87
[9] Abaqus Analysis User's Manual, Version 6.13 Dassault Systmes Simulia Corp, Providence, RI.
[10] HILL R (1948) A Theory of the yielding and plastic flow of anisotropic metals. Proc. of the Royal Society of London. Series A, Mathematical and Physical Sciences, 193(1033), pp 281-297.

THE COST-EFFECTIVENESS OF MEASURES MITIGATING THE RISK CAUSED BY THE FORMER QUARRY OF SPITZ (AUSTRIA)

Rainer Poisel[1], Nikolaus Hödlmoser[1], Bernhard Grasemann[2]

In the former quarry near Spitz many rockslides have occurred during operation as well as after closure. They have endangered a railway, the Wachau - bicycle route, an important road and the left Danube river bank. To clarify the need for risk reduction measures, the hazard caused by the former quarry near Spitz was investigated by analysing weather– and occurrence statistics in order to assess the probability of future rock slides. Simulations of possible future rock slides were performed using 3DEC to estimate the damage caused by these slides. Cost-benefit-calculations show that mitigation measures would be highly profitable.

Keywords: rockslide, failure probability, 3DEC, damage, cost-benefit-analysis

INTRODUCTION

The former quarry of Spitz is situated approximately 1,5 km southsouthwestward of the township of Spitz an der Donau at the left Danube river bank. The quarry often changed hands and many rockslides occurred (Fig. 1). The present situation poses a hazard of undetermined intensity to a railway, the Wachau bicycle route, an important road as well as the left Danube river bank. Several proposals for reducing the risk caused by the present situation were made. However, the costs for the realization of these proposals would be considerable [1], [2].

Fig. 1 Current state of the former quarry of Spitz

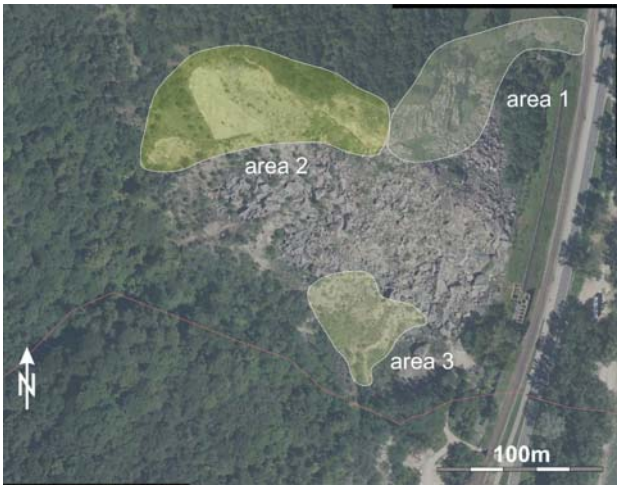

Fig. 2 Areas of homogenous geological structure (aerial photo from 2014; from: www.atlas.noe.gv.at).

[1] Vienna University of Technology, Karlsplatz 13, 1040 Vienna, Austria, +43 664 2772771, rainer.poisel@tuwien.ac.at
[2] University of Vienna, Universitätsring 1, 1010 Vienna, Austria, +43-1-4277-0, bernhard.grasemann@univie.ac.at

The dominating lithology in the quarry consists of coarse grained massif marbles with calcsilicate layers, which have been deformed under high grade metamorphic conditions. The metamorphic layering dips consistently towards SE. Cm- to m-thick amphibolite layers, oriented parallel to the metamorphic layering, contain more than 50% biotite. The foliation cleavage has very high persistence and served as sliding planes for the rockslides.

Based on the structural measurements, which were complemented by a drone surveying flight and the application of Shape MetriX3D [3] in inaccessible places, three different areas can be distinguished within the quarry (Fig.2): Area-1 is mainly characterized by drag folds parallel to the strike of the slope. Area-2 contains the major sliding surface and the NW-SE striking lateral bordering face. Area-3 neither contains folds nor shear bands and records only uniformly SE dipping layering.

ROCKSLIDES SINCE 1961

Table 1 lists the rockslides in the former quarry of Spitz since 1961. The rockslide shaping the present state occurred on October 11th, 2002 (Fig. 1). The rock mass most probably slid down on the same foliation plane, on which the 1984 slide occurred, with relatively low velocity. Thus, the main part of the sliding mass did not reach the railway.

Tab. 1 Rockslides in the former quarry Spitz since 1961.

Date [dd.mm.yyyy]	Volume [m³]	Cause
12.03.1961	70.000	inappropriate excavation
1975	many blocks (estimated 1.000 m³)	precipitation
04.10.1984	10.000	inappropriate excavation
23.04.1996	100	?
11.10.2002	60.000 - 85.000	precipitation
16.04.2006	2.500 – 5.000	?
2012-2015	several times some m³	?

The question arises, why the whole rock mass lying on an amphibolite layer did not slide down in 2002, but only the SW part of it. The geological investigations revealed that in the NE area (area 1) the foliation is folded strongly (Fig. 2). The upper fold flanks clearly dip more gently than the foliation in the SW area, where the 2002 rockslide took place. Thus, sliding is possible only, if

1. either the folds are sheared through or if
2. the rock in area 1 slides on the flat (i.e. horizontal) fold flanks.

The influence of the folds in area 1 on the stability of the rock masses NE of the lateral boundary of the rockslide 2002 was assessed using calculations based on the hypothesis of limit equilibrium.

- Using the values of the cohesion and of the angle of friction of the foliation planes back calculated from the rockslide 2002 and
- assuming the strength of the marble clearly below the real strength,

the calculations showed that

- NE of the lateral border plane of the rockslide 2002 the safety against sliding is higher than 1 and
- it is increasing in NE direction.

PROBABILITY OF FUTURE ROCKSLIDES

Whereas the rockslide in 1961 was caused predominantly by excavation, the 2002 event with high probability was caused by extreme precipitation (Table 2), as excavation stopped in 1996. Due to the high persistence of the foliation cleavage of the amphibolite layers it must be assumed that primarily water filling of cleavage planes induced the rockslide 2002. Assuming that the rockslide occurred only after a cleavage plane was filled with water to the downmost point, the permeability coefficient amounts to 10^{-6} m/s which seems to be a plausible value for a mica-rich amphibolite with cleavage planes of high persistence.

In 2009 and 2010 the sums of precipitation were like the one in 2002, but no rockslides occurred. The return periods (annualities) of the 7-, 30-, 60- and 90-days precipitation sums were found using statistic methods [4].

Tab. 2 Extreme precipitation events.

Precipitation event				Return period
Duration [days]	**Start [dd.mm.yyyy]**	**End [dd.mm.yyyy]**	**Sum [mm]**	**[Years]**
7	6.8.2002	12.8.2002	256,8	> 1.000
30	14.7.2002	12.8.2002	338,9	400
60	3.7.2002	31.8.2002	398,0	80
90	6.6.2002	3.9.2002	467,1	35
90	10.5.2010	7.8.2010	507,6	

It seems to be unlikely that solely the 7-day precipitation two months before the event caused the rockslide. Moreover, the 90-day precipitation (507,6 mm) from May 10th to August 7th, 2010, was higher than the one (467,1 mm) from June 6th to September 3rd, 2002 (Table 2). However, no rockslides occurred. The 90-day precipitation therefore seems to be irrelevant. Thus, a return period of a precipitation event causing a rockslide in the 2002 dimension between 80 and 400 years seems to be probable.

POSSIBLE FUTURE ROCK DETACHMENTS

The possible damage caused by future rockslides is influenced significantly by their volumes. At the moment, however, there is no evidence for determining them such as cracks, larger displacements of particular areas etc. Assessments of possible scenarios are possible only on the basis of knowledge of the place and experience. Thus experts, who have already been engaged with the former quarry, were invited to a meeting, where a detachment scenario in the northeast of the event 2002 with a volume of 70 000 m³ was defined. Determinations, which are not possible on the basis of objective data, by expert-panels („Delphi-panels“) are an approach chosen more and more often [5]. The run out of the detachment scenario described above were investigated using 3DEC [6] because of the blocky structure of the debris. The model parameters were calibrated by a back calculation of the 2002 run out. Using these parameters, the run out of the scenario determined in the expert panel was simulated. The calculations showed that the run out would not reach the existing rockfall protection dam, which has been modelled as part of the bedrock and which – in the model - was therefore indestructible. However, the run out of the scenario determined in the expert panel would push the 2002 debris against the dam. The maximum horizontal deceleration of the debris blocks caused by the contact with the dam and calculated during this process was 9 m/s².

COST – BENEFIT ANALYSIS

Human lives will not be in danger, because a signal system controlled by a monitoring system closes the traffic routes in case of large rock displacements. Thus, cost – benefit analyses [7] can be reduced to amounts of money. Taking a cubical block with edge lengths of 10 m yields a horizontal force of 10^3 m³ · 2.700 kg/m³ · 9 m/s² = 24,3 MN exerted on a barrier by a single block. Preh et al. [8] showed that the impact of a mass of blocks exerted on a barrier is a series of forces of individual blocks with a maximum of 6,5/4 times the force of the first block. This results in a maximum force of 39,5 MN, which only a massive retaining structure fixed to the ground by bored piles can resist. A rough estimate of the costs for such a structure gives about two Mio €, the life cycle of such a structure is estimated to be about 100 years. Therefore, yearly costs of a barrier stopping the rock slide from burying the railway, the bicycle route as well as the road would be 20.000 € (capitalisation costs not considered).

On the other hand, a rough estimate of direct consequences of a massive barrier not being constructed (e.g. removal of the debris, repair of the traffic infrastructure) gives a damage of about 3 Mio €. In the case of Spitz indirect consequences mainly consist of the reduction of tourism for two years and detours of domestic people and of enterprises for the same period, because removal of the debris would take two years at least. The reduction of tourism has been derived from the decrease of overnight stays caused by a highwater event in 2013 and amounts to a damage of about 46 Mio € in two years (hindrances of the rest of economic activities not included). The cost of detours is estimated based on the average daily traffic of about 8 000 vehicles. Taking 2.000 vehicles with detours of 15 km each into account amounts to a damage of 9,2 Mio €. Thus, rough estimates of direct and indirect consequences lead to a damage of 3 + 46 + 9,2 = 58,2 Mio €. Considering the results of the limit equilibrium calculations giving a safety factor above 1 against sliding of the areas northeast of the 2002 event and maximum return periods of precipitation events leading to the 2002 run out of 400 years, the probability of occurrence is estimated to be 1/300 years and therefore the risk to be 58,2 Mio € · 1/300 years = 194.000 € per year.

Thus, according to the above rough estimates yearly costs for mitigation measures of about 20 000 € stand opposed to a risk of about 194.000 € per year. Therefore, mitigation measures seem to be highly economical. More exact cost-benefit analyses and the final decision how to proceed, however, is left to the authorities.

REFERENCES

[1] ALPINFRA (2006) Felssturz Spitz a.d. Donau - Technischer Bericht an die ÖBB zur Variantenuntersuchung.
[2] WAGNER H (2006) Sanierungskonzept für den Steinbruch Fehringer in Spitz a.d. Donau
[3] 3GSM GmbH (2016) Bericht ShapeMetrix3D. ehem. Steinbruch Spitz/Donau 3D Luftbilddokumentation für eine geologische Bewertung.
[4] G, VIGLIONE A (2016) Ermittlung der Wiederkehrzeiten der 7-, 30-, 60- und 90- Tagessummen der Station Mühldorf bei Spitz. Unpublished report.
[5] FELL R (2016) Human induced landslides. Proc. 12th Int. Symp. Landslides. Neapel 2016. Vol. I, 171-199
[6] ITASCA (2016) 3DEC: 3-dimensional Distinct Element Code.
[7] POISEL R, ANGERER H, POELLINGER M, KALCHER T, KITTL H (2006) Assessment of the Risks caused by the Landslide Laerchberg – Galgenwald (Austria). Felsbau 24, 42-49
[8] PREH A, ILLEDITSCH M, SCHMIDT M, PAMMINGER P (2017) Impact of rock falls and rock slides on protective barriers: comparative calculations using the DEM. Proc. RocExs 2017, Barcelona, Spain. In press

CE MARKING OF FALLING ROCK PROTECTION KITS BASED ON THE CONSTRUCTION PRODUCTS REGULATION (EU) NO 305/2011

Dr Georg Kohlmaier[1]

In the Regulation (EU) No 305/2011 [1] the European Assessment Document (EAD) is defined as harmonized technical specification, adopted by EOTA (European Organisation for Technical Assessment). The EAD forms the basis for issuing the European Technical Assessment (ETA), issued by a Technical Assessment Body (TAB), designated for this product area by its Member State. In agreement with the European Commission the EOTA Guideline ETAG 027 [2] may be used as European Assessment Document till its replacement by an EAD. The Regulation (EU) No 305/2011 entered into force by 1 July 2013. European Technical Approvals issued in accordance with the Directive 89/106/EEC [3] before 1 July 2013 according to ETAG 027 may be used by the manufacturer as European Technical Assessments throughout the period of validity of those approvals.

Keywords: Regulation (EU) No 305/2011, European Assessment Document EAD, European Technical Assessment ETA, Declaration of Performance DoP, CE marking

INTRODUCTION

By consideration of the EAD as the harmonized technical specification, and not the ETA any more, an essential change in the legal situation has been made: The ETA is now the tool for implementation of the harmonized technical specification for the individual product. The ETA applies, together with the EAD or the ETAG 027 used as EAD, as reference for the Declaration of Performance (DoP) to be drawn up by the manufacturer in order to CE mark a falling rock protection kit.

According to Art. 4 of the Regulation (EU) No 305/2011 for a construction product for which an ETA has been issued it is obligatory to draw up a Declaration of Performance (DoP) and to CE mark the product when it is placed on the market. The DoP has to follow the Commission Delegated Regulation (EU) No 574/2014 [4]. It is drawn up by the manufacturer for falling rock protection kit on basis of a certificate of constancy of performance of the product due to the AVCP system 1. This certificate is to be issued by a notified product certification body who undertakes an initial inspection of the manufacturing plant and of the factory production control. During production it undertakes continuous surveillance and assessment and evaluation of the factory production control, carried out by the manufacturer. Of course, the notified product certification body may subcontract another body for the continuous surveillance of the factory production control.

[1] EOTA Technical Board Chairman 2013-2017, Austrian Institute of Construction Engineering (OIB), Schenkenstraße 4, 1010 Vienna, Austria, Phone: 0043 1 533 65 50, Email: kohlmaier@oib.or.at

All essential characteristics (e.g. energy level and related observations during impact, residual height, maximum elongation, resulting gaps between net and the lateral posts, maximum anchor forces, durability) given in the EAD or ETAG 027 used as EAD shall be quoted in the ETA and in the DoP by addressing the achieved performances. If the manufacturer is deciding not to assess all of them, even those for which no performance has been assessed shall be addressed. In the ETA those shall be indicated with "No performance assessed", in the DoP by "No performance determined" (NPD). Differentiation made between "assessed" and determined" is due to terminology of the Regulation (EU) No 305/2011.

On the contrary, the availability of ETAG 027 or of an EAD as such do not require issuing an ETA for products covered by them. Therefore, the availability of an EAD or ETAG as such do not lead to obligatory CE marking of products covered by them.

THE EUROPEAN ASSESSMENT DOCUMENT (EAD)

Article 19 of the Regulation (EU) No 305/2011 is laying down the cases where an EAD applies due to the lack of an appropriate harmonized standard. In addition, Article 21 is determining the use of an already existing EAD for issuing an ETA, if a product is covered by it. As long as ETAG 027 is not superseded by an EAD, this Article applies for the availability of ETAG 027 used as EAD as well.

The content of the EAD is following a format agreed between the European Commission and EOTA. The key elements are:

- Description of the product, intended use and working life/durability
- Specific terminology (if not covered by the Regulation (EU) No 305/2011 itself)
- Essential characteristics of the product (may be related to specific intended uses), expressed by means of level (e.g. residual height as percentage of nominal height), classes (e.g. classes A, B, C for residual height after MEL in ETAG 027) and description (e.g. "durable")
- Methods and criteria for assessing the performance of the product
- Assessment and verification of constancy of performance (AVCP), including information on system to be applied, cornerstones of tasks to be undertaken by the manufacturer for the factory production control and by the notified body.

For the DoP it is important to take into account: It only can include information on the performance of the product in relation to the essential characteristics as defined in the harmonized technical specification (EAD, ETAG 027 used as EAD).

The Regulation (EU) No 305/2011 is referring to the development of an EAD based on a request of a manufacturer. Products not (fully) covered by an already available EAD are going to be dealt with either by a separate EAD or by an amendment of an existing EAD. Mainly it depends on whether the deviations relevant are to be considered as of general relevance (amendment of EAD for product family) or rather as individual product-related issues (separate EAD). Reasons may be divergences in the scope or different designs of products and, therefore, not possible to assess this product according to the available EAD(s) and the methods therein, but also due to additional performances claimed by a manufacturer for his product. The same principles apply in case a product is not covered by or deviating essentially

from ETAG 027. The philosophy of the Regulation is much more oriented to tailor-made EADs due to the idea that the manufacturer should be free in placing products on the market.

EUROPEAN ASSESSMENT DOCUMENT (EAD) AS SUCCESSOR OF ETAG 027

The EOTA Guideline ETAG 027, for the first time published in 2008 and revised in 2013, is well known amongst manufacturers in and outside of the EU, as well as on the level of administrations and authorities. Even it is addressed to the TABs for issuing ETAs from formal point of view, it is one of the documents which are used as reference document for demonstration of the state-of-the art, even outside of the EU.

So, the question is "Why to transfer this document into an EAD"? Based on an agreement of the European Commission with EOTA, EOTA is currently developing all ETAGs, elaborated and published under the Directive 89/106/EEC, into EADs within an agreed time horizon. This also applies for ETAG 027, whereas the agreed time horizon for its transfer into an EAD is defined by end of 2018. According to the position of the European Commission an ETAG shall not be used any more after citation of the reference of the EAD in the Official Journal of the European Union (OJEU) and superseding the ETAG.

In general, this approach is related to the fact that the ETAGs, even ETAG 027, do contain aspects not relevant for the assessment of the product but expressing conditions for the use of products covered by ETAs. Some of the chapters in ETAG do not apply when using it as EAD now. Especially the conditions for installation, maintenance and repair are not of relevance as the ETA is, simply said, the documented assessment of the product at is production. Even terminology and the way of expressing the assessment results is to be considered according to the Regulation. Furthermore, according to the concept of the Regulation (EU) No 305/2011 it is the manufacturer who decides for which essential characteristics he is going to carry out the assessment of their performances and to introduce them in the DoP. This means, the set of essential characteristics given in an EAD (even in an ETAG used as EAD) is not obligatory to follow in total in the individual ETA. It is not possible to introduce on this level a "No-Go" for NPD options for certain essential characteristics.

It has been agreed in EOTA that this conversion of ETAGs into EADs is considered as formal issue in order to cope with the Regulation (EU) No 305/2011. In other words: It is not focusing on a change of the technical content of the document. Beside others, this is also related to the question of possible repercussion on already issued ETAs and drawn up DoPs once the EAD is cited in the OJEU. Therefore, on EOTA level criteria for this kind of transfer have been established. A further development of an EAD, including technical changes in the assessment methods and criteria etc., may take place at a later stage.

The EAD is following another numbering route than the ETAGs did: EOTA is coding the EAD number "ECNNNN-ED-PGSG" according to the following principles:

- product area according to Annex IV of the CPR (**EC**NNNN-ED-PGSG)
- subsequent number in that product area (EC**NNNN**-ED-PGSG)
- edition (ECNNNN-**ED**-PGSG)
- EOTA classification related to intended use (ECNNNN-ED-**PGSG**)

This also applies for the conversion of ETAG 027. The final adopted EAD, once cited in the OJEU, will be made available on the EOTA Website (www.eota.eu) for Download. At the same time, in the list of ETAGs on EOTA Website information will be included that ETAG 027 is superseded by EAD ECNNNN-ED-PGSG.

EUROPEAN TECHNICAL ASSESSMENT (ETA)

There are several reasons for the manufacturer to apply for an ETA: To demonstrate compliance of the product with the regulatory requirements in the Members States where he is going to place the product on the market, for innovative products the ETA is also an appropriate tool in comparison to CE marked standardized products.
The ETA is following a strict format [5] laid down by the European Commission. The ETA consists of a general part (Indication of trade name, manufacturer, manufacturing plant, issuing date, reference to EAD or ETAG 027 used as EAD, etc.) and of specific parts (product description, working life, performances achieved, AVCP system). Focus shall be given on a correct and comprehensive product description in order to know the product for which the assessment has been carried out and the performances achieved do apply. Regarding the results, expressed in the ETA: The European Technical Assessment does not include an "evaluation" of the performances achieved, it is rather a "statement". It does not contain an expiry date!

CONCLUSIONS

The ETA according to the Regulation (EU) No 305/2011, issued on basis of an EAD or on basis of ETAG 027 used as EAD, is the documented assessment of the product but it is not an approval. Therefore, conditions for its use or maintenance and repair are no longer a matter of the ETA! It is important to consider that the ETA based on the Regulation (EU) No 305/2011 does not constitute any warranty as to the use of the product. The use of the product depends on the performances expressed and whether they do meet the requirements for the works in the Member States. As an example of how to implement this, e.g. the Austrian Service for Torrent and Avalanche Control is informing the "community" on such issues regularly, for example published in its Journal "From Practice to Practice" [6].

REFERENCES

[1] REGULATION (EU) No 305/2011 of the European Parliament and of the Council of 9 March 2011 laying down harmonized conditions for the marketing of construction products and repealing Council Directive 89/106/EEC.
[2] ETAG 027 Guideline for European Technical Approval of Falling Rock Protection Kits, edition February 2008; Amended April 2013.
[3] 89/106/EEC: COUNCIL DIRECTIVE of 21 December 1988 on the approximation of laws, regulations and administrative provisions of the Member States relating to construction products, including amendment 93/68/EEC.
[4] COMMISSION DELEGATED REGULATION (EU) No 574/2014 of 21 February 2014 amending Annex III to Regulation (EU) No 305/2011 of the European Parliament and of the Council on the model to be used for drawing up a declaration of performance on construction products.
[5] COMMISSION IMPLEMENTING REGULATION (EU) No 1062/2013 of 30 October 2013 on the format of the European Technical Assessment for construction products.
[6] KOHLMAIER G, MÖLK M (2015) Practical implications of the "Regulation on Construction Products" for the application of ETAG 027 for Rock-Fall Protection Kits – Expert discussion. Journal for Torrent, Avalanche, Landslide and Rock Fall, Austria, Volume No 176, 79th year of journal, 166-173.

MAINTENANCE OF ROCKFALL NET FENCES

Andrea Luciani[1], Daniele Peila[2]

The efficiency of rockfall protection net fences is affected during their lifetime by damages and ageing phenomena. To identify the main issues that can affect the durability of rockfall protection net fences a site survey campaign has been performed in the North-west of Italy. This campaign aims to point out to the main aspects to focus on for maintenance management.

Keywords: rockfall protection net fence, maintenance, damages, corrosion

INTRODUCTION

The design of rockfall net fences had a big development in the last decades. However, little attention has been paid to the management and maintenance of rockfall protection devices during their lifetime. This is a big concern for public administrations that have to know the state of the protection devices to correctly plan the maintenance and to identify the loss in efficiency to ensure risk mitigation [1]. The rockfall protection devices nowadays present in Italy are a very heterogeneous ensemble of models and types, installed in the last 50 years. The long time span also implies a big variation in standards of design and installation. Therefore, for the public administrations it is a major issue to understand how the rockfall protection devices degrade with time, how to guarantee that the risk mitigation is still effective and when these devices have to be changed with new ones.
In this paper the results of a site survey on 62 net fences in North-west of Italy and a numerical model to simulate the ageing effect on a net fence will be presented. The aim is to point out the main aspects that affect the efficiency of rockfall net fences, in order to give clear indication to the local administrations for maintenance needs and guidelines for design and installation.

CHECKLIST DEVELOPEMENT

A site survey checklist has been developed based on available installation and maintenance guidelines, on standards [2, 3] and on site experience. This checklist aims to be a tool for local administrations for periodical checking of the products. The checklist has been improved by testing on site and has been implemented on an app for mobile devices. This tool has been used for the site survey of the rockfall protection net fences to identify the damages and problems of installation. The checklist is fulfilled with information about the type, geometry and deterioration of the barrier, but also with GPS coordinates of post position and with photos of the damages. This allows to input all the data from the survey on a GIS model and to compare the state of the barrier during different surveying times.

[1] Department of Environment, Land and Infrastructure Engineering, Politecnico di Torino, Corso Duca degli Abruzzi 24, Torino – 10129, Italy, +39 011 0907723, andrea.luciani@polito.it
[2] Department of Environment, Land and Infrastructure Engineering, Politecnico di Torino, Corso Duca degli Abruzzi 24, Torino – 10129, Italy, +39 011 0907607, daniele.peila@polito.it

Fig. 1 - Slid clamps

Fig. 2 - Short upstream rope

Fig. 3 - Long upstream ropes

ROCKFALL PROTECTION NET FENCES SITE SURVEY

During the site survey campaign 62 rockfall protection net fences have been analyzed. The observed defects can be summarized as installation issues (90 %), maintenance issues (19 %) and corrosion (58 %). Hereinafter, the main issues observed during the survey campaign are discussed synthetically. In Dimasi et al. [4] the complete review of the data and the collected check-list have been presented.

INSTALLATION ISSUES

Problems related to installation and design are the most frequent. In several situations, the rockfall protection barriers checked during the survey campaign are not installed in accordance with the installation guidelines. It must be observed that for works installed before the promulgation of ETAG 027 [2], the installation manual was not required. In any case, some discrepancies had been detected between the installed configuration and the available construction drawings.
Moreover, problems related to the quality of the connections using clamps. During the survey campaign the clamps were often found not installed in accordance with the regulations in force [5] in terms of number, distance and closure. The clamp connection shown in Fig. 1 has not worked and the clamps have get close to each other letting the rope slide during the impact. This phenomenon may be connected to an incorrect torque applied to the fastener. Therefore, during the campaign, the torque applied to the clamps was recorded using a torque wrench. These measures show a different behavior of clamps installed on tensioned ropes and on loose ropes. The first ones maintain the prescribed torque in the 95% of the recorded samples while the latter ones have only the 80% of the prescribed torque, even in clamps installed in the last 5 years. This seems to be a key aspect to focus on in order to guarantee the correct behavior of the connection structures during all the life span of a rockfall protection barrier and more studies are needed to analyze the behavior of clamps on net fences.
Furthermore, ETAG 027 [2] prescribes to indicate, in the installation manual, the tolerances and imposes to the designer to perform specific evaluation reports in the case the barrier is installed disregarding those tolerances. Nevertheless, during the survey campaign several barriers have shown a configuration not compliant with the available installation manual. For example, in Fig. 2 one of the upstream ropes is installed sub-horizontal and shorter than all the other due to the presence of a rock slope immediately behind the post. On the contrary, in Fig. 3, the upstream ropes are much longer than what required by the installation manual due to the slope conformation.

MAINTENANCE ISSUES

Several net fences were found filled with material (rock and vegetation) in the net. This highlights a clear lack in the maintenance procedures, also due to the difficulty to reach the rockfall protection devices. This situation obviously reduces the efficiency of the net fence and thus the risk mitigation. During the survey campaign in some barriers, already subjected to maintenance, some problems have been recorded due to maintenance works that have not restored the original configuration of the barrier.

CORROSION OF METALIC ELEMENTS

Even if the barriers detected during the survey campaign reflect a sample of works installed just in the last 12 years and all in mountain environment, corrosion issues have been detected in some of the components. Ropes do not show significant corrosion phenomena; posts and ring nets have corrosion only in the impacted zones while wire rope clamps are sometimes corroded. The elements that more often result subjected to corrosion are the clamps, even in works installed in the last 5 years. The corroded clamps are often randomly diffused on the barrier and corroded and not corroded clamps can be found on the same rope. No clear indication on the trigger event of corrosion has been detected. Therefore, producers should put specific attention and analyses on the corrosion resistance of clamps in order to ensure the duration of the connections.

NUMERICAL SIMULATION

In order to evaluate the influence of the different problems found during the site survey campaign, a numerical simulation of these damages has been performed. A complete presentation of the results of these simulations are reported in Luciani et al. [6]. In these analyses, a numerical simulation of a commercial net fence has been developed and set using the data of real scale tests reported by Gottardi and Govoni [7]. The numerical model has been modified to simulate the damages or ageing phenomena observed during the surveys. Specifically, six modified models were considered to simulate damages to the upstream ropes or to the clamp connections, damages to the anchorages and different installation geometries.
On the modified models an impact test was simulated following the ETAG 027 [2] and the energy withstood by the aged net fence was evaluated (Fig. 4). Thank to these simulations, it was possible to assess define the influence of the different damages and ageing on the efficiency of the net fence.

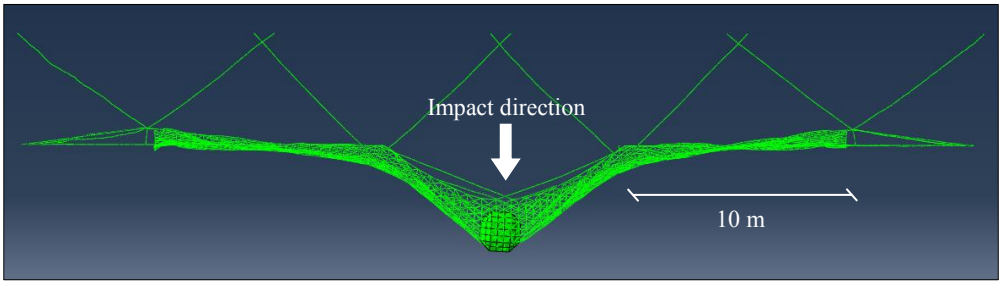

Fig. 4 - Numerical model of the net fence during an impact. It is possible to see that a barrier of 4 posts has been studied.

Tab. 1 – Main results of the simulations expressed in residual efficiency

Problem simulated	Residual efficiency [%]
Failure of one clip connection or of one central upstream rope	100
Failure of one clip connection or of one lateral upstream rope	100
Failure of two clip connection or of the central anchorage	97
Failure of two clip connection or of a lateral anchorage	100
Short and horizontal upstream ropes	80
Long upstream ropes	87

The most important results obtained by the numerical simulation are reported in Tab. 1 where the effect of ageing is represented by the residual efficiency value defined as the ratio between the energy withstood by the aged model and the nominal energy of the barrier.

CONCLUSION

A site survey campaign on rockfall protection net fences in North-west of Italy allowed to assess the main damages and ageing processes on net fences. Many of these damages can be avoided with a careful design and installation of the device. Furthermore, a proper maintenance plan and a timely refurbishment after impact can avoid the reduction of efficiency of the net fence. Particularly the clamps appears to be a weak link in the system, both for their installation and for their durability against corrosion and further studies are needed to analyze this aspect. A numerical simulation of the main damages has been performed to analyze their influence on the efficiency of the net fence and an assessment of the residual efficiency is presented.

AKNOWLEDGMENTS

The project has been financed by Italian national research program PRIN n°201572YTLA_008, research unit of Politecnico di Torino.

REFERENCES

[1] GERBER W, MEYER M (2009) Endurance of rockfall protection fences. [Abstract] Geophys. Res. Abstr. 11: EGU2009-12409
[2] EOTA (2013) Guideline for European Technical approval of falling rock protection kits (ETAG 027). https://www.eota.eu/en-GB/content/etags-used-as-ead/26/ (last access, 30/01/2017)
[3] UNI 11211-4 (2012) Opere di difesa dalla caduta massi – Parte 4: Progetto definitivo ed esecutivo. (in Italian)
[4] DIMASI C, LUCIANI A, MARTINELLI D, PAGANONE M, PEILA D (2015) Controllo delle barriere paramassi a rete per la loro gestione e manutenzione. Geoingegneria Ambientale e Mineraria 146, 65-73. (in Italian)
[5] UNI EN 13411-5 (2003) Terminations for steel wire ropes - Safety - Part 5: U-bolt wire rope grips.
[6] LUCIANI A, BARBERO M, MARTINELLI D, PEILA D Maintenance and risk management of rockfall protection net fences through numerical study of damage influence. Journal of rock mechanics and geotechnical engineering. (accepted)
[7] GOTTARDI G, GOVONI L (2010) Full-scale modelling of falling rock protection barriers. Rock mechanics and rock engineering 43, 261-274.

USING UNMANNED AERIAL SYSTEMS (UAS) FOR THE MONITORING OF PROTECTIVE CONSTRUCTIONS IN STEEP, INACCESSIBLE TERRAIN, PASS LUEG, AUSTRIA

Andreas Schober[1], Robert Delleske[2], Ingo Hartmeyer[2], Markus Keuschnig[2]

Protective structures against natural hazards are essential for individual and infrastructure safety in steep terrain. However, protective structure inventories are frequently not up-to-date and information on their structural conditions are lacking, representing an underrated risk factor.
In this contribution we address the need for quick and cost-effective inspections of protective structures by presenting a monitoring approach that centers on the use of consumer-grade unmanned aerial systems (UAS). All UAS flights were carried out at Pass Lueg, a narrow section of the Salzach valley characterized by a high density of critical infrastructure. Based on photogrammetric data acquired with UAS in December 2016 an orthophoto was generated. High ground resolution of 0.1 m and absence of snow and leafy vegetation enabled an excellent representation of the terrain surface and the existing protective structures. The quality of the UAS-derived orthophoto clearly surpasses conventional orthophotos, which display dense vegetation and extensive shading effects that obstruct the representation of most protective structures.
Based on the newly generated orthophoto 70 rockfall protection nets and one rockfall/avalanche dam were mapped and assessed. These results were consistent with the results of a conventional inspection campaign, underlining the applicability of UAS for the monitoring of protective structures.

Keywords: Unmanned Aerial Systems (UAS), 3D-Photogrammetry, Critical Infrastructure, Natural Hazards, Protective Structures

INTRODUCTION

Protective structures against natural hazards such as rockfall or avalanches are essential for individual and infrastructure safety in steep terrain. Due to their exposed locations, protective structures are impacted by destructive forces at irregular intervals. Damaged protective structures represent a severe hazard, which emphasizes the necessity of regular inspections that include assessments of their structural conditions. However, as protective structures are generally situated in inaccessible and steep locations, conventional inspections are dangerous and time-consuming procedures that require highly qualified personnel and involve high costs. Conventional remote sensing products, such as orthophotos derived from large heights above ground (e.g. airplanes) are often inadequate due to shading effects and insufficient ground resolution. For these reasons, protective structure inventories are frequently not up-to-date and information on their structural conditions are lacking, representing an underrated risk factor.

[1] Geoconsult ZT GmbH, Hölzlstraße 5, 5071 Wals, Austria, office@geoconsult.eu, +4366265965-271
[2] Georesearch, Hölzlstraße 5, 5071 Wals, Austria

In this contribution we address the need for detailed, yet quick and cost-effective, inspections of protective structures and present an approach that centers on the use of consumer-grade aerial systems (UAS). The presented methodology is consistent with the Austrian standard rule "Permanent Technical Protection against Rockfall" (ONR 24810) [1] and allows the updating and optimization of the present protective structure inventory.

STUDY SITE

The study site comprises a deeply incised section of the Salzach valley, situated in the federal province of Salzburg, Austria. The investigated rockwalls cover an elevational difference of up to 700 m and are mainly made up of banked limestone. In the narrow valley air space is limited and light conditions change rapidly, creating a challenging setting, ideal to test the limits of consumer-grade UAS for protective structure inspection.
The study area is characterized by a high density of critical infrastructure as railways, motorways, federal main roads and high-voltage power lines pass through the site. Rockfall events and avalanches represent a recurring a problem within the study area. Road maintenance and associated protective structure management lie within the responsibility of the federal province of Salzburg. In order to reduce risks stemming from natural hazards, a large number of protective structures was installed. Some structures are up to 40 years old and no longer correspond with state-of-the-art technology.

METHODS

Photogrammetric data taken during multiple UAS flights was used to generate a comprehensive, high-resolution orthophoto of the study area. All UAS flights were carried out in mid-December 2016 during a largely snow-free stretch of the season.

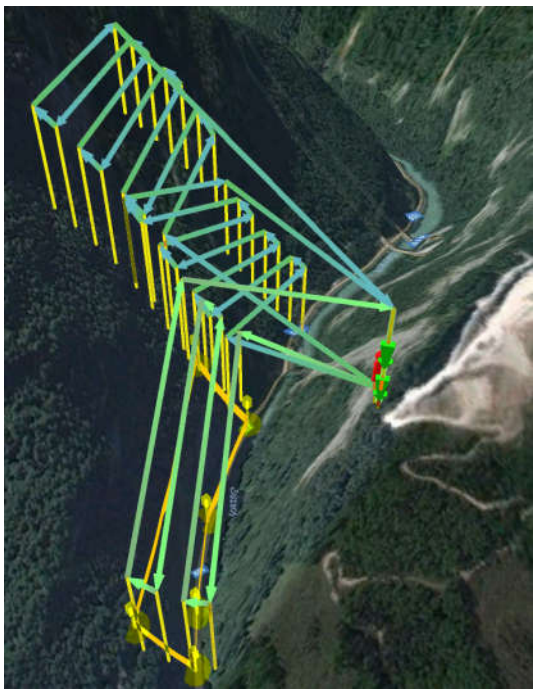

Fig. 1: Cascade-like flight pattern used for UAS data acquisition at Pass Lueg.

For data acquisition the commercially available UAS "DJI Phantom 3 Advanced" was used. Due to the complex terrain solid flight planning was of particular importance. In order to reduce battery-consuming elevation gain during flights to a minimum, a cascade-like flight pattern was chosen that involved long phases of horizontal movement (Fig. 1). To keep a constant line-of-sight connection between the UAS and the control unit, a position on the opposite slope, approximately 400 m above the valley floor, was picked as departure and landing point. Flight planning and flight operation was carried out with the ground station software "UGCS".
Prior to data acquisition ground control points were measured with a differential GPS system. The flying height was 150 m above ground level, the total flight distance covered 14 km. For photogrammetric overlap and airspeed different parameters were tested. To ensure excellent data quality a conservative forward and lateral overlap of 90%

was selected, corresponding to a 50m-distance between flight paths. Low sunlight intensities caused long exposure times, airspeed was therefore restricted to 5 m/s to enable the acquisition of clear images while using standard ISO sensitivity values. Data post-processing, including structure-from-motion analysis, was performed with the software package Pix4D.
In addition to UAS-based data acquisition and analysis, a conventional inspection campaign was carried out to allow direct comparisons. Existing protective structures were inventoried and assessed on-site according to ONR 24810 [1]. GPS-based registration of protective structures was partially inadequate due to topographic shading effects.

RESULTS

The orthophoto generated from UAS photogrammetry data displays a high ground resolution of 0.1 m. The absence of snow and leafy vegetation, together with the high resolution, make for an excellent representation of the terrain surface and the existing protective structures (Fig. 2). Based on the newly generated orthophoto 70 rockfall protection nets and one rockfall/avalanche dam were mapped and assessed. The results were consistent with the results of the conventional inspection campaign, underlining the applicability of UAS for the assessment of protective structures. Structural damages, filling level and major corrosion damages were identified based on single shot oblique images. Minor damages such as slight corrosion, small inclination changes or small-sized rockfall impact marks could not be detected.
The direct comparison of the UAS-derived orthophoto with the conventional orthophoto generated from large-scale, high-altitude flights (Fig. 3) offered substantial differences. The conventional orthophoto, acquired during the summer season, displays dense vegetation, that obstructs the representation of most protective structures, emphasizing the advantages of data acquisition during early winter season. Moreover, extensive shading effects exacerbate the recognition of small-scale features, rendering it unusable for protective structure inspection.


Fig. 2 (left): High-resolution orthophoto from UAS photogrammetry data acquired in December 2016
Fig. 3 (right): Conventional orthophoto generated from high-altitude flight (Source: Government of Salzburg)

In a further step that went beyond the inspection and assessment of the existing protective structures, information from the UAS-derived orthophoto was integrated into a 3D rockfall modeling (Rockyfor3D) [2]. Here, the newly generated orthophoto provided key advantages for the exact definition of the rockfall release areas (Fig. 4), which represents an essential prerequisite for rockfall modeling. Aside from UAS-derived data, observations from field inspections, data from previous investigations [1], [4], [5], [6] and a DTM with a resolution of 2 m were used.

The rockfall modeling yielded energies of up to 5000 kJ and jump heights of several decameters. In order to cope with these energies several rows of rockfall protection nets (3000 to 5000 kJ) and the enlargement of an existing dam were recommended.

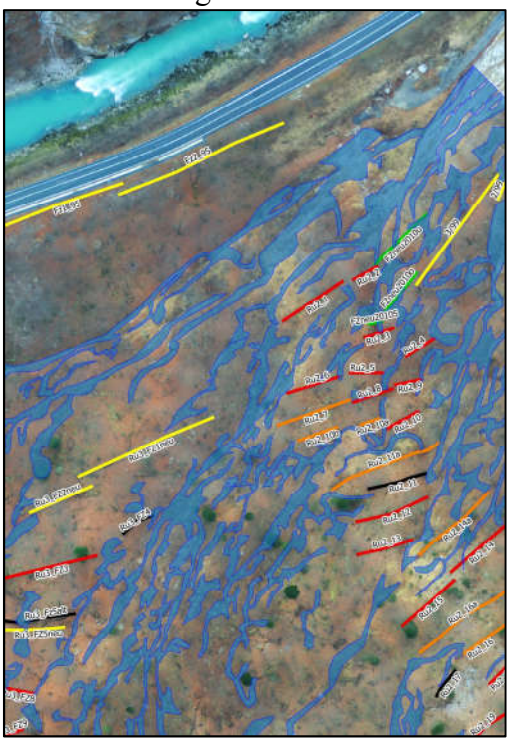

Fig. 4: Identification of rockfall release zones based on terrain information derived from UAS flights.

CONCLUSIONS

The presented results demonstrate the suitability of photogrammetric data acquired with UAS for the monitoring of protective structures in steep, inaccessible terrain. Despite complex terrain, dense vegetation and adverse lighting conditions, the existing protective structure inventory was updated and structural conditions were assessed. The selection of large overlaps and low airspeeds during data acquisition proved to be key for high data quality.
Constant improvement of UAS hard- and software may allow simultaneous and automatic operation of several UAS in the near future, enabling quicker data acquisition and higher ground resolutions. This may give rise to improved DTM generation from photogrammetric data and automatic extraction of protective structures based on OBIA (Object-Based Image Analysis).

REFERENCES

[1] ONR 24810 (2013) Permanent Technical Protection against Rockfall – Terms and definitions, effects of actions, design, monitoring and maintenance.
[2] DORREN L K A (2015) Rockyfor3D (V5.2.5) revealed – Transparent description of the complete 3D rockfall model. ecorisQ paper (www.ecorisq.com): 32 p.
[3] GEOTEST (2014) Risk analyses Pass Lueg, Salzburg, Austria.
[4] GEOCONSULT ZT GMBH (2013) Bestandsbegutachtung Schutzbauten Pass Lueg, Salzburg, Austria.
[5] GEOCONSULT ZT GMBH (2015) Bestandsbegutachtung Schutzbauten Pass Lueg, Salzburg, Austria.
[6] GEOCONSULT ZT GMBH (2016) Schutzbautenservices Pass Lueg, Salzburg, Austria.

SURVEILLANCE OF ROCKFALL PROTECTION SYSTEMS ON THE ROADS OF *SERRA DE TRAMUNTANA* RANGE IN MALLORCA

Joan M. Rius Gibert [1], Raül Aguiló González [1]

The local government of Mallorca has developed a surveillance and inventory tool to evaluate the maintenance status of rockfall protection systems installed on the roads of the Tramuntana mountain range to protect them against rockfall events. These events, closely related to high intensity rainfall episodes of Mediterranean climate are quite frequent. The inventory and its evaluation shows a wide range of maintenance status and, in addition to recent rockfall events, indicate that several maintenance works have to be undertaken.

Keywords: rockfall, protection system, surveillance, inventory

INTRODUCTION

Serra de Tramuntana is the main mountain range of the island of Mallorca. It is oriented from the northeast to the southeast in the northern part of the island. Its maximum heights is almost 1500 m in the middle part. Although its geology is relatively heterogeneous, throughout the range arise limestone masses of Jurassic age that form great cliffs. The rock wheatehering and its fractures allow the rocky masses to detach from these cliffs. Its typical Mediterranean climate, with hot summers, temperate winters and heavy rainfall events, makes the range a very prone area to rock and soil instabilities, mainly rockfall events.

Along the range there are several towns and villages, urbanizations and country houses scattered. A network of communications with roads and paths crosses its valleys (figure 1). These facilities are systematically affected by different geological processes, the most recurrent of which are rockfalls.

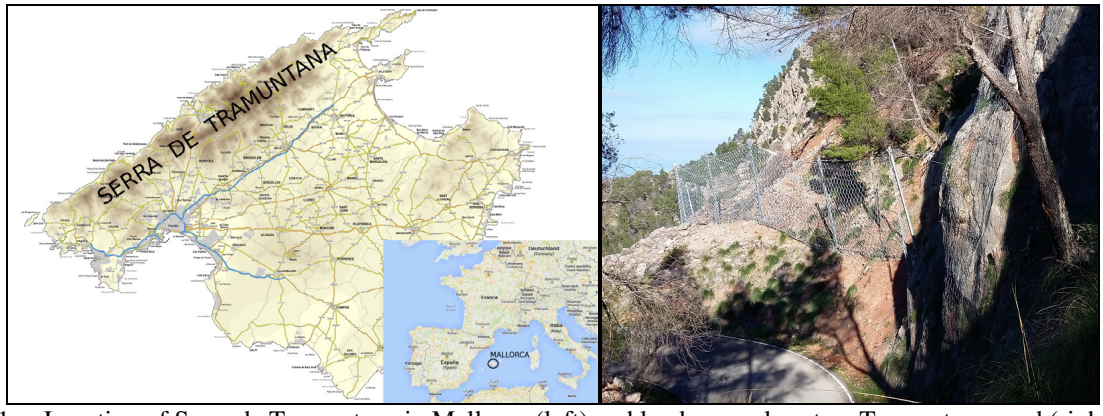

Fig. 1 Location of Serra de Tramuntana in Mallorca (left) and landscape close to a Tramuntana road (right)

[1] Direcció Insular d'Infraestructures i Mobilitat. Consell de Mallorca, General Riera 113, Palma de Mallorca 07010, (Illes Balears) Spain, +34971219960, jmrius@conselldemallorca.net

The local goverment of the island, Consell de Mallorca, has been managing the island's road network of up to 500 km since the beginning of the 21st century and, consequently, has been investing in the protection and correction against rockfall events and others. Different models have been applied to design protection systems [1], [2].In recent times, with the rise of tourism and the declaration of the Serra de Tramuntana as Unesco Heritage, investment has grown and, therefore, the road network has a large number of protection systems to maintain. Thus, there are a large number of passive protection systems (about 80,000 m2 of meshes and cable networks) and active protection systems (some 2,500 m of static and dynamic barriers) with long periods of service that require verification of their status functional. Besides that, some of these protection systems have been actuated by rockfall events and, in some cases, their system capacity has been exceeded.

SURVEILLANCE TASKS

A first phase of the work consisted in inventorying the existing protection systems. From this phase it should be pointed out that the oldest protection systems date back to the early 1990s and the most modern ones are of recent installation, being at one-year warranty period at the end of 2016. In this sense, a first distinction has been made between systems whose warranty period is in force and those that do not (table 1). Inspection tasks have focused on this first phase in installations whose warranty period is no longer in force. The fieldwork of this inventory has been made by the company Georisk International during the last months of 2016.

Tab. 1 Inventory of rockfall protection systems

System	In force warranty period	Off-warranty period
Surface meshes (m^2)	58153	21457
Static barriers (m)	1286	-
Dyanmic barriers (m)	750	542

As regards off-warranty systems, which are the subject of this abstract, there are two main types of installations: direct slope protection meshes and dynamic barriers. In the first group of meshes there are different typologies: triple torsion mesh, steel wire netting, steel ring netting, meshes with funnels, etc. In the group of dynamic barriers there are also different typologies. In this case they are distinguished by the protection energy, with values between 100 kJ and 3000 kJ and by the height of the barrier between 3 and 6 m.

PROTOCOL FOR EVALUATION AND DIAGNOSIS OF PROTECTION SYSTEMS

In order to make a diagnosis of the different elements in a homogeneous way, it was decided to apply the Austrian regulation ONR24810 [3]. This regulation establishes a maintenance strategy that is governed by the requirements of security and effectiveness of the protection, the number of protection structures, the category of the structures and the available financial resources. Thus, different strategies are established depending on the urgency of the action to maintain the facility under conditions: Forecast and maintenance, prevention due to wear, medium to long term correction and short-term correction.

The diagnosis is established differently if it is a mesh of direct protection of slopes or of dynamic barriers. For direct protection meshes, a protocol of elements to be controlled and

aspects to be verified is established. The elements to be controlled are: cables, meshes, cable ties and shackles, bolts, slings and anchors. The aspects to be taken into account are: stresses, oxidations and alterations, as well as condition of the nuts in cable ties and shackles, and nominal load in bolts and anchors.

For the case of dynamic barriers, besides a control and verification protocol similar to the previous one, it establishes a temporary program for the determination of the practical functionality of the barrier in its concrete location. Thus, an initial registration as well as continuous inspection and supervision is established to determine the evolution of the barrier (loss of functionality by impact or disappearance of elements, for example). In addition, further control actions may be carried out to evaluate their maintenance status, extraordinary control or an additional examination to evaluate the condition of all the elements of a barrier by specialized personnel.

Once the initial diagnosis has been made and the different phases of the temporary inspection program have been established, all facilities have been rated according to a maintenance status level ranging from 1 (very good) to 5 (very bad). Each state has associated a number of possible typified damages. For example, for state 4 there are: anchors or bolts torn or bent, bent or inclined supports, cable breaks, broken meshes or fastening elements and braking elements very deformed. The diagnosis for dynamic barriers and for the direct protection meshes is presented in table 2 and some examples of status and damages are shown in figures 2 and 3. For the case of figure 3 some comments have to be made. Its status as bad implied their almost immediate repair. A rockfall event in January 31st 2017, with blocs between 1 – 3 m^3, and a total amount of 50 tones of mass detached provoked their collapse. Thus, its protection energy of 1000 kJ (diminished by its poor maintenance status) was not enough.

Tab. 2 Practical status of Tramuntana rockfall protection systems (off-warranty period)

	Level	**State**	**Security / practical utility**	**Lapse**	**Dynamic barriers (m)**	**Pasive protection (m^2)**
1	Very good	No restrictions	Proper	Long term	-	-
2	Good	Few restrictions	Proper	Long term	-	4430
3	Acceptable	Small damages	Proper	1 year	250	4229
4	Poor / bad	Significant / several damages – restricted functionality	Restricted	1 month	172	6800
5	Very bad / Destruction	Non-existant functionality	Non-existant	Immediate	120	1046

Fig. 2 Pictures of proper elements of a barrier (left) and usual small damages in protection systems (right)

Fig. 3 Pictures of a barrier stated at level 4, installed in 1999, before in 2016 (left) and after it collapsed caused by a rockfall event of 2017-01-31 (mid and right).

The diagnosis indicates that there are a series of repair and restitution actions that should be undertaken in the short term. On the other hand, the varied casuistry obtained, along with several important detachments and incidents in protection elements in the last winter 2016-2017 with various periods of intense rains and storms, has involved the rethinking of some of the actions performed. The incidences in this last period have affected both old and out-of-warranty facilities, as well as some that are under warranty. For these new barriers, installed under the European regulations ETAG027 [4], a new aspect to review has appeared, i. e. verification of compliance with project requirements. This work is under development.

CONCLUSIONS

A very useful tool is available for the diagnosis and evaluation of the temporal evolution of maintenances status of the slope protection systems and barriers designed and intalled by the Insular Direction of Roads of the Consell de Mallorca, for the permanent management of its conservation. With the present diagnosis there are a number of important investments to be undertaken to have the slope protection systems in a correct state of conservation and maintenance status.

Finally, it should be pointed out that, as different performing situations have arisen in recent years with very different magnitude rockfall events, all these maintenance and managing activities of the slope protection systems on the roads of Serra de Tramuntana range of Mallorca are considered as tasks in constant and permanent updating.

REFERENCES

[1] Mateos, R.M.; García-Moreno, I., Herrera, G.; Reichenbach, P.; Sarro, R.; Rius, J.; Aguiló, R. & Fiorucci, F. (2015). Calibration and validation of Rockfall Modeling: Mallorca (Spain). Case Study. Landslides. Springer-Verlag, Berlin Heidelberg, Germany, 13 pp. Doi 10.1007/s10346-015-0602-5

[2] Rius Gibert, J.M; Aguiló, R. & Massanet, C. (2016) Rockfall risk mitigation in the Tramuntana range of Mallorca (Spain). Proceedings of the 12th international symposium on landslides, Napoli, Italy. pp 1715-1722.

[3] ONR24810, Technical protection against rockfall - Terms and definitions, effects of action, design, monitoring and maintenance (2013), 112 pp. Austrian standards.

[4] ETAG027: Guideline for European Technical Approval of Falling Rock Protection Kits (2008), 53 pp. http://www.eota.eu/.

INTEGRATING DESIGN APPROACHES AND RISK EVALUATION TO MITIGATE ROCKFALL FROM A MINE HIGHWALL

Wesley Ashwood[1] and Paul Schlotfeldt[1],

A coal mine in Canada experienced a rockfall event that damaged infrastructure and narrowly missed injuring workers. The open pit mine was transitioning from above ground works to underground operations. Four access portals had been constructed at the toe of a 200 m high headwall in layered sedimentary units. Differential weathering of a thin shale unit underlying a more competent sandstone unit at the crest of the highwall undermined the overlying sandstone unit allowing for relaxation and eventual failure from the top of the highwall. A site inspection provided insight into the failure mechanism and alternatives for rockfall mitigation were conceptualized. A qualitative risk approach was used to show that mitigation at the toe of the headwall, as opposed to at the bench below the failure, was safer to construct and addressed rockfall from the entire slope. The selected mitigation option chosen by the mine included buried steel portal extensions and a flexible rockfall fence at the outside edge. The mitigation measures where designed to protect workers entering the underground works within the small footprint at the pit floor. Rockfall modelling was used to provide a target rockfall retention while minimizing impact on mine operations.

Keywords: runout analysis, impact load, energy dissipation, flexible barrier, risk analysis

INTRODUCTION

A rockfall hazard and risk assessment was performed for a mine in Canada and used as input for design of a mitigation scheme. The mine has requested to stay anonymous as they continue operation and development. The rockfall occurred from the crest of a highwall of an open pit impacting infrastructure at the base of the wall 200 m below. The base of the highwall included four portals used to access underground operations. This contribution outlines the nature of the rockfall as observed during a field inspection, an overview of the risk analysis and the resulting mitigation design.

The pit was excavated through a series of thick sedimentary units following a series of metallurgical coal seams. Sedimentary units included interbedded shales, siltstones, sandstones, and coal. The bottom of the pit is approximately 1,780 masl, and the top of the highwall is near 1,950 masl. The pit was excavated in 30 m high benches resulting in an overall slope angle of roughly 56°.

[1] Golder Associates Inc., 37702 3rd Avenue, Squamish, BC, Canada, 604-815-0768, Wesley_Ashwood@golder.com, Paul_Schlotfeldt@golder.com

Bedding is sub-horizontal dipping gently into the slope. Typical spacing in the more competent sandstone units varied from 1 to 3 m with units up to 15 m thick. The weaker, more friable siltstone and shale units varied in thickness from a 2 to 3 m with bedding spacing between 0.1 and 10 cm. Two systematic sub-vertical and orthogonal joint sets were observed throughout the rock mass resulting in a blocky structure. Overhangs up to 1.5 m deep were observed at the crest of the highwall where the sandstone unit was underlain by weaker shale and siltstone units. This upper sandstone unit was the source of recent rockfall.

Prior to transitioning to underground work the mine installed drape mesh in two different sections over the highwall. The upper section extended from the crest of the slope to a bench near elevation 1870 masl. The second extended from the 1870 bench to the pit floor. A light 2 mm gauge wire mesh was used throughout, and was only attached to top cables and supports. The design drawings for this mesh provided little information regarding design other than the target rockfall event were blocks up to 0.8 m in diameter.

ROCKFALL EVENTS

In late winter of 2015 a rockfall event occurred above the uppermost bench of the highwall. The upper drape mesh did not contain the fall, which rolled off the 1870 bench, over the lower mesh, and impacted the pit floor. It was estimated that 72 m^3 of rock was released with individual blocks up to 13.5 m^3 (Fig. 1). The rockfall impacted the pit floor in multiple locations damaging mine infrastructure and nearly impacting a worker.

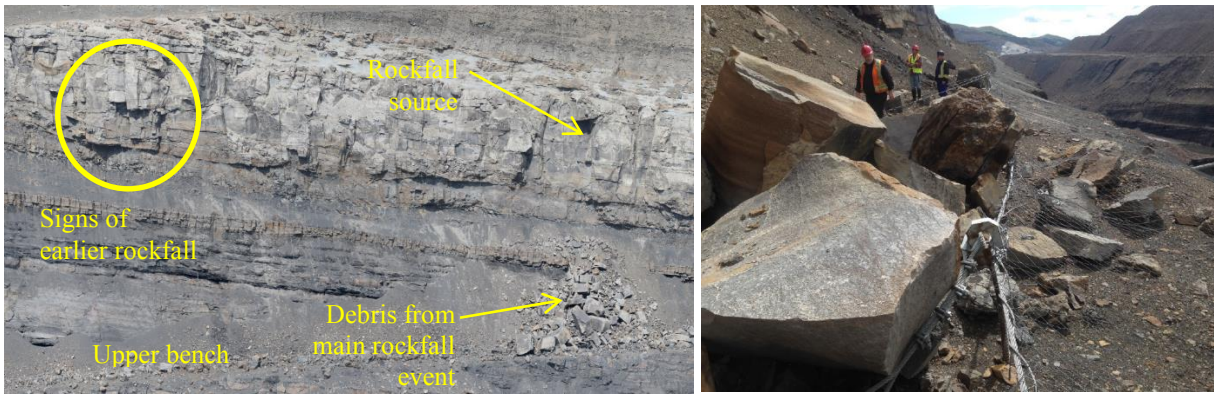

Fig. 1 View of the upper bench where the rockfall occurred. Note the shadowed overhangs resulting from differential weathering between the weaker shales and more competent sandstone above. Rockfall debris accumulated on the bench.

A site inspection determined that the rockfall was the result of differential weathering. At the crest of the highwall a discrete 2 to 3 m thick shale layer exists below the more competent, and blocky sandstone. The weaker lithology is more susceptible to erosion due to accelerated weathering (slake durability), and mechanical breakage during bench excavation. The continual raveling of the shale results in undercutting of upper most the sandstone. Where through cutting joints exist in the sandstone, individual blocks can release as the center of gravity extends over the raveling surface below. In areas of more intact rock, the tensile strength of the sandstone rock mass is periodically exceeded resulting in larger failures. This is an ongoing process. During the site inspection multiple smaller failures were observed along the upper bench. Later in

the design process another rockfall occurred at the same bench towards the west which was estimated to be 54 m^3.

MITIGATION OPTIONS ASSESSMENT

Prior to the rockfall the mine had begun construction of four portals that would serve as access to underground room and pillar mining. The mine required a rockfall mitigation program over and above that already installed in order to access the portals safety.

The mine had a 2,000 kJ flexible rockfall fence available on site, leftover from previous mitigation programs. They wanted to install the fence on the upper 1870 bench immediately below the sandstone unit where the rockfall occurred. However, after assessing the hazard, it was deemed necessary for any solution to also address rockfall from behind the lower mesh, which had been extensively damaged by rockfall.

Four options were considered: (1) cut back the upper part of slope to a more stable angle, (2) a rockfall fence on the upper bench and mesh rehabilitation below the bench, (3) an attenuator type systems where new mesh would be suspended from the fence frame installed on the upper bench, and (4) install mitigation measures at the pit floor. Options (1) through (3) would have required prolonged exposure to rockfall hazard while clearing the narrow 1870 bench to install the superstructure, as well as extensive time using roped access to address the lower drape mesh. Mitigation at the pit floor had the advantage that it would not require the upper benches to be cleared from multiple rockfall events, required no access onto the highwall, and much of the construction work to build the mitigation measures could be completed remotely using cranes at the base of the pit.

RISK ASSESSMENT

The decision to install mitigation at the pit floor as opposed to on the highwall was evaluated using a risk-based analysis [1]. The mine and regulatory agencies requested numeric calculations of risk for all the options, however the data required for such an analysis was limited. Therefore the analysis was considered to be semi-quantitative as assumptions were made regarding factors required to calculate the Probability of Individual Risk (PIR).

The following risk parameters were defined and quantfied:

1. *Probability that a hazardous event occurs, P_h* – four major rockfalls occurred from the upper sandstone unit over ten years of the mines operational records resulting in a 40% probability of failure annually.
2. *Probability that a rockfall would impact the construction area, P_i* – varies depending on the installed location of the chosen mitigation measure.
3. *Temporal probability that the workers are present, P_t* – estimated that construction on the bench would take 1.5 months working 12 hours a day due to limited space and large volume of rockfall debris, while construction at the pit floor would only take a month.
4. *Spatial probability that workers and rockfall are coincident, P_s* – includes two independent variables: (the space that workers and equipment occupy / total length of the working area) x (space that rockfall occupies / total length of the working area). The total length of

the working area was assumed to be 150 m for both construction approaches, as well as the normal working area for a baseline risk calculation.

5. *Vulnerability, V* –assumed a constant 90% probability that impact from the upper source area would cause serious injury or a fatality.

Calculation of the PIR is shown in Table 1. In the baseline scenario workers are exposed to rockfall 12 months of the year, but only for approximetely an hour a day total while entering the underground. During construction, workers are exposed throughout the work day (12 hours), but only for truncated part of the year. As a result, the time exposed to rockfall, P_t, is comparable for the baseline risk and construction at the toe of the headwall. In the baseline scenario workers are also spread throughout a larger area at the toe of the slope.

Tab. 1 Comparison of Probability of Individual Risk for two construction methodologies against baseline risk for rockfall event impacting an individual at the toe of the headwall.

Scenario	P_h	P_i	P_t	*Working Width (m)*	*Rockfall Width (m)*	P_s	V	PIR
Baseline risk	0.4	0.5	0.042	*48*	*30*	0.064	0.9	4.8E-04
Construction on the upper bench	0.4	1.0	0.063	*30*	*20*	0.027	0.9	6.0E-04
Construction at the toe of the headwall	0.4	0.5	0.042	*20*	*30*	0.027	0.9	2.0E-04

The analysis suggested that mitigation on the upper bench was more risk prone during construction compared to construction at the toe.This is because of the extended time wokers would be exposed to rockfall on thespaced constrained 1870 bench.The PIR for construction on the bench is also higher than the estimated baseline risk because of the exposure on the 1870 bench, and more than double that for construction at the pit floor.

The PIR values were compared to commonly accepted levels of risk[2,3], and recalculated for anticipated long term conditions after construction.

MITIGATION DESIGN

The mitigation design required a small footprint that was capable of meeting a target rockfall retention rate of 95% for the anticipated design block established during review of the recent rockfall events. The solution included steel portal extension structures (prefabricated corrugated bridge plates) (Fig. 2). The entire structure could be mostly constructed remotely using a crane located a sufficient distance away from the highwall to reduce worker exposure. The extensions were designed to be covered with mine waste rock, which would be placed loosely and act as a cushion layer similar to gravel fill on top of roadway galleries [4]. The length of the portals were reduced by including the flexible rockfall barrier at the outside edge of the fill running parallel to the highwall. The fence was designed be founded on independent support structures fabricated from spare haul truck tires backfilled with reinforced concrete. These would be lowered into place using a crane.

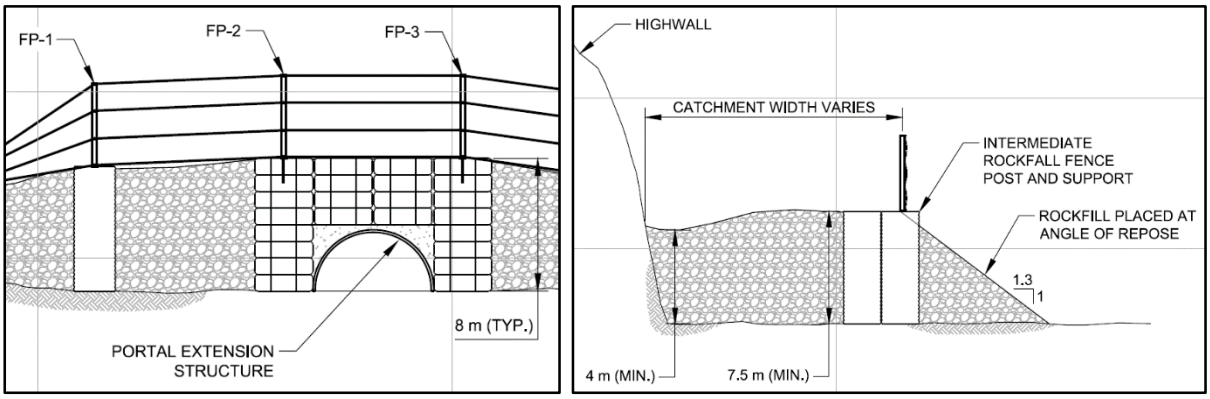

Fig. 2 Select details from the rockfall mitigation design showing an elevation view of the portal extensions with fence on top and section view of the intermediate fence post supports.

The length of the portal extensions, and depth of the rockfall cushion layer, were determined through rockfall modelling using RocScience Rocfall 5.0. Four sections were cut along each portal. Based on observations of the largest blocks that reached the toe of the headwall during the 2015 event, a typical, yet conservative, design block of 1.5 m^3 (4,000 kg) was used for back analysis and predictive modelling. Each section was modelled with four different slope parameters based on the nature of the material (exposed rock or colluvium), and the anticipated angle of incidence [5]. The parameters were calibrated to mimic the distribution of blocks at the toe of the slope after the 2015 failure, then applied to the mitigation design (Fig. 3).

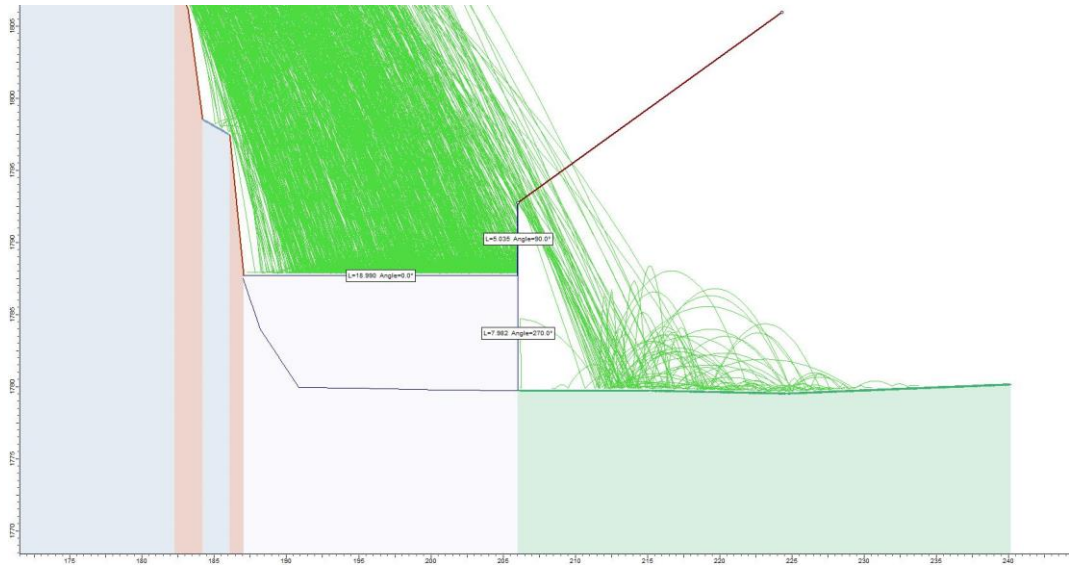

Fig. 3 Example results for final rockfall modelling showing the portal extension structure and flexible rockfall fence. Length of the extension was adjusted until 95% of the 1,000 blocks released were retained behind the barrier.

The length of each portal was set using an iterative approach until roughly 95% of the simulated blocks were retained behind the fence while accounting for expected randomness in the slope profile, material parameters and block itself (Fig. 3).

The depth of the cushion layer on top of the portal extension was based on the allowable design load provided by the bridge plate manufacturer. The design block and rockfall kinematics were

understood from the rockfall simulation. A relationship developed by the Swiss Federal Roads Office [6,7] was used to translate the impact energy into a pseudo-static force. The impact load, F_k, was initially calculated as:

$$F_k = 2.8 \cdot e^{-0.5} \cdot r^{0.7} \cdot M_{e,k}^{0.4} \cdot \tan \varphi_k \left(\frac{m_k \cdot v_k^2}{2} \right)^{0.6}$$

Where e is the thickness of the cushion layer (varied iteratively in the analysis), r is the radius of an equivalent sphere for the anticipated rockfall, $M_{E,k}$ is the soil modulus of the cushion layer based on case studies of embankment and rockfill [8], φ_k is the internal friction of the cushion layer, m_k is the block mass and v_k is the impact velocity. The impact load is converted to static equivalent force, A_d, according to:

$$A_d = C \cdot F_k$$

Here C is a factor to account for ductile or brittle failure. As the bridge plates are ductile steel a value of 0.4 was applied for C. Using this relationship we determined that a minimum of 2.0 m of loose cover was required to properly insulate the structure.

CONCLUSION

The rockfall was the result of failure of a thick sandstone unit at the crest of the highwall. Differential weathering in a weak shale unit at the base of the sandstone unit resulted an over-hanging rock mass and associated failure, which will likely continue to progress with time. Future rockfall could also include smaller failures from below the upper bench. The mitigation scheme developed for the mine addresses rockfall from the full height of the highwall. Conceptually, the approach minimizes risk during construction by limiting the exposure time to the rockfall hazard. The mitigation has yet to be constructed, but is expected to be constructed in the near future, and will reduce the overall risk of rockfall for workers entering the mine underground to acceptable levels.

REFERENCES

[1] COROMINAS J, COPONS R, MOYA J, VILAPLANA JM, ALTIMIR J, AMIGO J (2005) Quantitative assessment of the residual risk in a rockfall protected area. Landslide, 2, pp 343-357.

[2] GEO (GEOTECHNICAL ENGINEERING OFFICE) (1998) Landslides and boulder falls from natural terrain: interim risk guidelines. GEO Report 75, Gov. of Hong Kong SAR.

[3] LACASSE S (2011) Risk assessment and management of geohazards. International Journal of Geo-Engineering, 3(2), pp 5-25.

[4] YOSHIDA H, NOMURA T, WYLLIE DC, MORRIS AJ (2007) Rock fall sheds – application of Japanese design in North America. Proc. 1st. North American Landslide Conference, Vail, CO., AEG Special Publication No. 22, pp 179-196.

[5] WYLLIE DC (2014) Calibration of rock fall modeling parameters. International Journal of Rock Mechanics & Mining Sciences, 67, pp 170-180.

[6] ASTRA (2008). Einwirkungen infolge Steinschlags auf Schutzgalerien, Richtlinie, Bundesamt für Strassen, Baudirektion SBB, Eidgenössische Drucksachen- und Materialzentrale, Bern (in German).

[7] RODUNER A, MOOR R, WYRSCH R (2013) New damping system for rockfall protection galleries. Proc. 1st. International Conference on Rock Dynamics and Application, Lausanne, Switzerland, pp 531-536.

[8] HUNTER G, FELL R (2002) The deformation behavior of rockfill. UNICIV Report R-405, The University of New South Wales, Sydney, Australia.

INDEX AUTHORS

RocExs 2017

6th Interdisciplinary Workshop on Rockfall Protection

Field trip

Rockfall risk management in the Montserrat Massif

24 May 2017, Montserrat Mountain (Barcelona)

Annex

ROCEXS 2017 FIELD TRIP: ROCKFALL RISK MANAGEMENT IN THE MONTSERRAT MASSIF

Marc Janeras[1], Jordi Corominas[2], José A. Jara[3], Marta Guinau[4], A. Aguasca[5], Xabier Blanch[3], David Paret[6], Anna Ferré[5], Pere Buxó[1]

This field trip has been devised as the closure of this sixth edition of the RocExs workshop, on the Wednesday May 24th. According to the purposes of this interdisciplinary meeting, most of the suggested topics for the workshop are tried to be present during the field trip: Rockfall characterization, inventory and mapping; testing and modeling; hazard and risk analyses; monitoring; large rockfall cases; protective measures; risk mitigation and management.

We hope that you will enjoy this trip, both from technical point of view and leisure, because Montserrat Mountain is a special place where earth and heaven meet configuring captivating scenery. The rockfall risk in Montserrat must be managed properly in order to keep on enjoying this cultural and natural heritage.

Keywords: risk mitigation, monitoring, hazard analysis, rockfall protection

INTRODUCTION

The technical contents of this field trip are mainly related to the geological risk mitigation plan in Montserrat (PMRGM) that is funded by the Catalan Government, promoted by the Board of Montserrat Mountain (Patronat de la Muntanya de Montserrat, PMM) and managed by the Geographical and Geological Survey of Catalonia (Institut Cartogràfic i Geològic de Catalunya, ICGC). There are also many works done in rockfall protection for the rack railway by the Railway Catalan Agency (Ferrocarrils de la Generalitat de Catalunya, FGC).

This guide consists on the collection of all the posters that have been used to illustrate the explanations on the field by the lecturers. They are attached following this abstract. For more details on each issue, this abstract contains a large list of references of published and academic works centered in Montserrat and the rockfall risk.

[1] Institut Cartogràfic i Geològic de Catalunya (ICGC), Department of geotechnics and georisk prevention
Parc de Montjuïc, Barcelona 08038, Spain, +34935671500, marc.janeras@icgc.cat
[2] Universitat Politècnica de Catalunya, Department of Civil and Environmental Engineering (DECA)
[3] Institut Cartogràfic i Geològic de Catalunya (ICGC), Department of geophysics and seismology
[4] Universitat de Barcelona, Department of Geodynamics and Geophysics, RiskNat research team
[5] Universitat Politècnica de Catalunya (UPC), Remote Sensing Laboratory (RSLab)
[6] Ferrocarrils de la Generalitat de Catalunya (FGC), Department of Infrastructure

Fig. 1 Panoramic view of the Montserrat Monastery at the south-eastern part of the Montserrat Mountain.

FIELD TRIP CONTENTS

During the first stop at the rack railway station in Monistrol Vila, a village at the bottom of the mountain, the geological context is presented. From this place we have a nice point of view of the massif, crowned by the Cavall Bernat tower and the Aeri wall, which are emblematic rock faces for climbers coming from all around the world. The ascent to the Sanctuary area is done by rack railway, and just before, it is shortly presented the intense risk mitigation work carried out since its beginning in 2003.

Tab. 1 Contents in the Stop 1 at Monistrol Vila rack railway station

Title	Subtitle	Lecturers	Posters
Presentation	Location and field trip planning	ICGC (M. Janeras)	101
Geological context	Regional context	UPC (J. Corominas)	102
	Genessis of the massif		103
	Rock mass and mountanin morphology		104
	Geohazards: rockfall and landslides		105
Rack railway	History and Route	ICGC (M. Janeras) & FGC (D. Paret & A. Ferré)	106
	Rockfall risk mitigation		107

The second stop is placed on the terraces of the upper railway station and Santa Cova funicular that are faced to the Sanctuary and Monastery scenery. The ongoing mitigation plan (PMRGM) for this buildings area and its access infrastructures is exposed. The monitoring works take a relevant role according to the risk configuration, derived from the hazard characteristics, high level of exposure and vulnerability of the 2.5 million visitors that yearly reach this touristic spot of first order.

Fig. 2 Protective works for both building area and terrestrial access infrastructures.

Tab. 2 Contents in the Stop 2 at the funicular terrace faced to the Montserrat Sanctuary.

Title	Subtitle	Lecturers	Posters
Risk management in building area	Reference events	ICGC (M. Janeras)	2.01
	Rockfall hazard and mechanisms		2.02
	Rockfall risk mitigation plan		2.03
Rock face monitoring	Monitoring strategy	ICGC (M. Janeras) & UPC (J.A. Gili)	2.04
	Surveying Total Station, STS		2.05
Block joint monitoring	Instrumentation	ICGC (J.A. Jara & M. Janeras)	2.06
	Wireless sensor network & ZigBeeLoggers		2.07
	Wireless sensor network, WSN		2.08
	Data collecting and managing		2.09
	Results of contact sensors instrumentation		2.10

After a coffee break, the next stop is placed at the entrance of the parking area. Here, the Degotalls wall with several recent rockfalls revealed the critical section of the terrestrial accessibility, because both road and railway are simultaneously exposed to the same hazard focuses. Since these events, new knowledge was born about the precursory signs before the detachment of large blocks. At this stop the main monitoring experiences with remote sensing techniques and its results are presented.

Tab. 3 Contents in the Stop 3 at the parking at the bottom of Degotalls wall.

Title	Subtitle	Lecturers	Posters
Risk mitigation for the accessibility	Reference events	ICGC (M. Janeras)	3.01
	Rupture propagation		3.02
	Protective works		3.03
LiDAR monitoring	Methodology	UB (M. Guinau)	3.04
	Rockfall detection and analysis: Degotalls N		3.05
	Rockfall detection and analysis: Degotalls E		3.06
	Precursory movements: Block displacement		3.07
GbSAR monitoring	Results of 5 months measurement campaign	UPC (A. Aguasca)	3.08

The visit also includes free time for a short visit to the Sanctuary before lunch and later for a light walk in the Natural Park. It is just a taste of the natural and cultural assets that are treasured within the Montserrat Mountain.

Tab. 4 Contents in the Stop 4 at upper station of the Sant Joan funicular.

Title	Subtitle	Lecturers	Posters
Rock mass joint analysis	Introduction, Degotalls and Monestir cliffs	UB (X. Blanch)	401
	Collbató cliff and Conclusions		402
Overview on the massif	Rockfall hazard and runout	ICGC (P. Buxó & M. Janeras)	403
	Regional cartography: MPRG25k		404
Rockfall gallery for the funicular	Hazard conditions	ICGC (M. Janeras) & FGC (D. Paret & A. Ferré)	405
	Mesh test		406
	Structure design		407

CONCLUSIONS

After its first phase during 2014-16 consisting on pilot tests, strategy design and first priorities in protective works, the mitigation plan in Montserrat (PMRGM) carries on with the second phase. From now on, this strategy for the rockfall risk mitigation must be deeply developed and expanded. We hope to be able to report new interesting results from our rockfall research in Montserrat at the next RocExs event, expected for 2020. See you soon, and keep in contact!

ACKNOWLEDGMENTS

The organizing committee wants to acknowledge all the colleagues that have contributed to the field trip organization and guidance. Likewise, we want to highlight the gratitude to the partners that have contributed to make possible this field trip: the Board of Montserrat Mountain (Patronat de la Muntanya de Montserrat, PMM), the Railway Catalan Agency (Ferrocarrils de la Generalitat de Catalunya, FGC) and the touristic and security responsible services of the Sanctuary and Monastery.

REFERENCES

ALSAKER E, GABRIELSEN RH, ROCA E (1996) The significance of the fracture pattern of the Late-Eocene Montserrat fan-delta, Catalan Coastal Ranges (NE Spain). *Tectonophysics* 266, 465-491.

BLANCH X (2016) *Anàlisi estructural i detecció de despreniments rocosos a partir de dades LiDAR a la Muntanya de Montserrat*. Degree Thesis, Guinau & Royán (Adv.) Universitat de Barcelona.

BLANCH X, GUINAU M, ROYÁN MJ (2017) Caracterización geomorfológica y estructural de zonas de salida de bloques en una pared rocosa afectada por desprendimientos. *IX Simposio Nacional sobre Taludes y Laderas Inestables*, Santander, *in press*.

BUXÓ P, JANERAS M, DOMÈNECH G, PONS J, PRAT E, LÓPEZ F (2017). Development of a Rockfall Risk Mitigation Plan in the Montserrat Massif (Central Catalonia, Spain). In: Mikos *et al*. (Editors), *Advancing Culture of Living with Landslides*. Springer, Ljubljana, in press.

CABRANES FJ (2015) *Estudio geomecánico de la estabilidad de la Cadireta d'Agulles (Montserrat)*. Degree Thesis, Gili & Janeras (Adv.) Universitat Politècnica de Catalunya.

CARMONA A (2015) *Sectorización y zonificación de la peligrosidad por caída de rocas, aplicación en Montserrat*. Master Thesis, Vilaplana & Janeras (Adv.) Universitat de Barcelona.

FONTQUERNI S, VILAPLANA JM, GUINAU M, ROYÁN MJ, BARBERÀ M, JANERAS M (2011) Los elementos vulnerables expuestos a los desprendimientos de rocas en Montserrat. *VIII Congreso Geológico de España*, Oviedo: Sociedad Geológica de España, 4 pp.

FONTQUERNI S, VILAPLANA JM, GUINAU M, ROYÁN MJ (2013) El factor exposición en el análisis del riesgo geológico. Aplicación a los desprendimientos de roca en la Montaña de Montserrat. *Seguridad y Medioambiente*, 131, 8-25.

FONTQUERNI S, VILAPLANA JM, GUINAU M, ROYÁN MJ (2013) Exposición a los desprendimientos de roca en Montserrat. In Alonso, Corominas, Hürlimann (Eds.) *VIII Simposio Nacional sobre Taludes y Laderas Inestables*, Palma de Mallorca, 554-565

GABARRÓ X (1996) Propagació de despreniments en roca: Influència de les característiques del vessant i dels incendis forestals: aplicació a Montserrat. Degree Thesis, Corominas (Adv.) Universitat Politècnica de Catalunya.

GALLACH X (2012) *Estudi de susceptibilitat de caiguda de roques a la paret del Monestir de Montserrat a partir de la inspecció d'indicadors d'inestabilitat i d'anàlisi SIG*. Master Thesis, Vilaplana (Adv.) Universitat de Barcelona.

GASCÓN B (1997) *Estudi evolutiu de les àrees cremades durant els incendis de 1986 i 1994 a la zona de Montserrat*. Degree Thesis, Calvet (Adv.) Universitat de Barcelona.

GRAU F (2003) *Efecte dels obstacles i característiques dels vessants sobre l'abast dels despreniments. Aplicació al mètode de l'angle d'abast*. Degree Thesis, Corominas (Adv.) Universitat Politècnica de Catalunya.

GONZÁLEZ M, PINYOL J, OLLER P (2016) The geological multi-hazard map of Catalonia. A user-friendly tool for land use planning and management risk. In: Aversa *et al*. (Eds.) *Landslides and Engineered Slopes. Experience, Theory and Practice*, Associazione Geotecnica Italiana, Rome, ISBN 978-1-138-02988-0, 999-1002

ICGC (2002) Olesa de Montserrat – 392-1-2 (71-30). *GeoTreball I – Mapa Geològic de Catalunya 1:25,000*

ICGC (2003) Monistrol de Montserrat – 392-1-1 (71-29). *GeoTreball I – Mapa Geològic de Catalunya 1:25,000*

ICGC (2011) Olesa de Montserrat – 392-1-2 (71-30). *GeoTreball IV – Mapa per a la Prevenció dels Riscos Geològics de Catalunya 1:25,000*

ICGC (2012) Monistrol de Montserrat – 392-1-1 (71-29). *GeoTreball IV – Mapa per a la Prevenció dels Riscos Geològics de Catalunya 1:25,000*

ICGC (2013) Castellolí –392-1-2 (71-30). *GeoTreball I – Mapa Geològic de Catalunya 1:25,000*

JANERAS M, PALAU J, PRAT E, RIPOLL J (2011) Montserrat: on a long way to rock fall risk mitigation. First experiences, some lessons and future perspectives. *Interdisciplinary Rockfall Workshop RocExs 2011*, Innsbruck – Igls, poster sesion.

JANERAS M, PALAU J, PRAT E, PONS J, RODRÍGUEZ H, MARTÍNEZ P, COMELLAS J (2013) Valoración de 10 años de mitigación del riesgo de caída de rocas en el Cremallera de Montserrat. In Alonso, Corominas, Hürlimann (Eds.) *VIII Simposio Nacional sobre Taludes y Laderas Inestables*, Palma de Mallorca, 624-636

JANERAS M, JARA JA, LÓPEZ F, MARTURIÀ J, ROYÁN MJ, VILAPLANA JM, AGUASCA A, FÀBREGAS X, CABRANES F, GILI JA (2015) Using several monitoring techniques to measure the rock mass deformation in the Montserrat Massif. *International Symposium on Geohazards and Geomechanics ISGG 2015*, IOP Conf. Series: *Earth and Environmental Science* 26 (2015) 012030, DOI:10.1088/1755-1315/26/1/012030

JANERAS M, DOMÈNECH G, PONS J, PRAT E, BUXÓ P (2016) Rockfall hazard assessment by means of the magnitude-frequency curves in the Montserrat Massif (central Catalonia, Spain): first insights. *EGU General Assembly 2016*, Vienna, *Geophysical Research Abstracts Vol. 18, EGU2016-13341-2, 2016*.

JANERAS M, JARA JA, LÓPEZ F, MARCÈ A, CARBONELL T, ELVIRA A (2016) Development of a wireless sensor network for rock mass deformation monitoring in the Montserrat Massif. *3rd Rock Slope Stability conference*, Lyon, 131-132.

JANERAS M, JARA JA, ROYÁN MJ, VILAPLANA JM, AGUASCA A, FÀBREGAS X, GILI JA, BUXÓ P (2017) Multi-technique approach to rockfal monitoring in the Montserat massif (Catalonia, NE Spain). *Engineering Geology* 219 (2017), 4-20, DOI: 10.1016/j.enggeo.2016.12.010.

JANERAS M (2017) ¿Qué nos enseña la pared de Degotalls en Montserrat sobre los desprendimientos de roca? *IX Simposio Nacional sobre Taludes y Laderas Inestables*, Santander, *in press*.

LÓPEZ-BLANCO M (1996) Estratigrafía secuencial de sistemas deltaicos en cuencas de antepaís: ejemplos de Sant Llorenç del Munt, Montserrat y Roda (Paleógeno, cuenca de Antepaís surpirenaica). *Acta Geologica Hispanica* 31, no 4, p. 91-95

LÓPEZ-BLANCO M, MARZO M, BURBANK DW, VERGÉS J, ROCA E, ANADÓN P, PIÑA J (2000) Tectonic and climatic controls on the development of foreland fan deltas: Montserrat and Sant Llorenç del Munt systems (Middle Eocene, Ebro Basin, NE Spain). *Sedimentary Geology* 138(1-4), 17–39, DOI:10.1016/S0037-0738(00)00142-1

LÓPEZ-BLANCO M, MARZO M, PIÑA J (2000) Transgressive-regressive sequence hierarchy of foreland, fan-delta clastic wedges (Montserrat and Sant Llorenç del Munt, Middle Eocene, Ebro Basin, NE Spain). *Sedimentary Geology* 138(1-4), 41–69. DOI:10.1016/S0037-0738(00)00143-3

LÓPEZ-BLANCO (2006) Stratigraphic and tectonosedimentary development of the Eocene Sant Llorenç del Munt and Montserrat fan-delta complexes (Southeast Ebro basin margin, Northeast Spain). *Contributions to Science* 3(2), 125–148. Institut d'Estudis Catalans. DOI: 10.2436/20.7010.01.1

MAESTRO E, POCH J. Montserrat. *Geocamp* (web resource by UAB, UdG, UPC).

MARGALEF A (2008) *Anàlisi d'un mètode d'ajuda a la cartografia regional de perillositat en base a l'angle d'abast de despreniments*. Master Thesis, Furdada & Janeras (Adv.) Universitat de Barcelona.

MARQUÈS MA (2001) Impacto en el medio físico de unas lluvias extremas en el macizo de Montserrat. *Tecnología del agua* 213, 42-50.

MARTÍN DÍAZ E (2002). *Anàlisi de susceptibilitat a moviments de massa superficials al Parc Natural de Montserrat*. Degree Thesis, Marquès (Adv.) Universitat de Barcelona, 84 pp.

MARTÍNEZ RIUS A (2006) Aproximació a la geología de Montserrat. *Muntanya* 864, 32-37.

OMS O, BIOSA J. La Muntanya de Sal de Cardona i la vall del Cardener. *Geocamp* (web resource by UAB, UdG, UPC).

PALAU J, JANERAS M, PRAT E, PONS J, RIPOLL J, MARTÍNEZ P, COMELLAS J (2011) Preliminary assessment of rockfall risk mitigation in access infrastructures to Montserrat. *Second World Landslide Forum*, Rome.

PINYOL J, GONZÁLEZ M, OLLER P (2016)A regional methodology for rockfall hazard assessment in the hazard prevention map of Catalonia 1:25,000. A geomorphological approach. In: Aversa *et al*. (Eds.) *Landslides and Engineered Slopes. Experience, Theory and Practice*, Associazione Geotecnica Italiana, Rome, ISBN 978-1-138-02988-0, 1631-1636.

RASET J (2016) *Anàlisi geomorfológica del Serrat de Garrigoses (Montserrat). Avaluació de la perillositat a l'accés a la Cova del Salnitre i a la carretera B-112*. Degree Thesis, Furdada & Guinau (Adv.) Universitat de Barcelona.

REQUENA G (2010) *Caracterització de les zones de sortida de despreniments de la paret de Degotalls (Montserrat)*. Degree Thesis in Engineering Geology, Vilaplana & Guinau (Adv.) Universitat de Barcelona

ROYÁN MJ (2010) *Los desprendimientos de rocas en la montaña de Montserrat*. Master Thesis, Vilaplana (Adv.) Universitat de Barcelona. 26 pp.

ROYÁN MJ, VILAPLANA JM (2012) Distribución espacio-temporal de los desprendimientos de rocas en la Montaña de Montserrat. *Cuaternario y Geomorfología* (2012), 26 (1-2), 151-170.

ROYÁN M J, GUINAU M, VILAPLANA J M, ABELLÁN A (2013) Análisis y seguimiento de las laderas del Monasterio de Montserrat mediante LiDAR Terrestre. In: Alonso, Corominas, Hürlimann (Eds.) *VIII Simposio Nacional sobre Taludes y Laderas Inestables*, Palma de Mallorca, 751-762.

ROYÁN MJ (2015) *Caracterización y predicción de desprendimientos de rocas mediante LiDAR terrestre*. PhD Thesis, Vilaplana (Adv.) Universitat de Barcelona.
(http://diposit.ub.edu/dspace/bitstream/2445/68667/1/MJRC_TESIS.pdf)

ROYÁN MJ, VILAPLANA JM, JANERAS M, ABELLÁN, A (2016) Detección e inventario de desprendimientos de rocas mediante el seguimiento con LiDAR Terrestre en la Montaña de Montserrat (Catalunya, España). *XIV Reunión Nacional de Geomorfología*, Málaga.

SORIANO D (2009) *Identificación y análisis de corrientes de derrubios en el macizo de Montserrat mediante Google Earth y SIG*. Degree Thesis, Hürlimann & Lantada (Adv.) Universitat Politècnica de Catalunya.

VASQUEZ S (2015) *Grado de exposición a los desprendimientos de rocas en vehículos en la montaña de Montserrat*. Degree Thesis, Vilaplana & Fontquerni (Adv.) Universitat de Barcelona.

VILAJOSANA I, SURIÑACH E, ABELLÁN A, KHAZARADZE G, GARCIA-SELLES D, LLOSA J (2008) Rockfall induced seismic signals: case study in Montserrat, Catalonia. *Natural Hazards and Earth System Science*, 8(4), 805–812. DOI:10.5194/nhess-8-805-2008

VILAPLANA JM, ROYÁN MJ, FONTQUERNI S, JANERAS M, GONZÁLEZ M (2016) Los desprendimientos de rocas en la montaña de Montserrat. Un riesgo geológico relevante. In: Oms, Climent & González (Eds.) *Excursiones geológicas por la Cataluña Central*, monografía técnica 6, ICGC, 196 pp.

Rockfall risk management in the Montserrat massif

Field trip

Wednesday, 24 May 2017

1.01 Presentation

Location and field trip planning

Stop 1 (Village)
M. Janeras (ICGC)

Timetable

8:15 Meeting in UPC

9:15 Arrival to Monistrol Vila railway station

9:20

0:30	STOP 1	Monistrol Village
0:05	Welcome	ICGC
0:15	Geological context	UPC / ICGC
0:10	Rack railway	FGC / ICGC

9:55 Rack railway ascent to Montserrat

10:20

0:40	STOP 2	Sanctuary
0:15	Risk mitigation plan	ICGC
0:10	Rock face monitoring	ICGC
0:15	Block joint monitoring WSN	ICGC

11:00 Coffee break

11:40

0:50	STOP 3	Degotalls wall
0:15	Risk mitigation in terrestrial access	ICGC
0:10	LiDAR monitoring	UB
0:15	GbSAR monitoring	UPC

12:40 Free time for touristic visit

13:40 Lunch

15:00 Funicular ascent to Sant Joan

15:35

0:45	STOP 4	Sant Joan funicular
0:15	LiDAR analysis of rock mass structure	UB
0:10	Massif overview and MPRG	ICGC
0:10	Protection shed for funicular	FGC / ICGC
0:10	Closure	UPC / ICGC

16:20 Free time for park visit

17:12 Funicular descent back

17:45 Bus meeting

18:30 Arrival to Barcelona

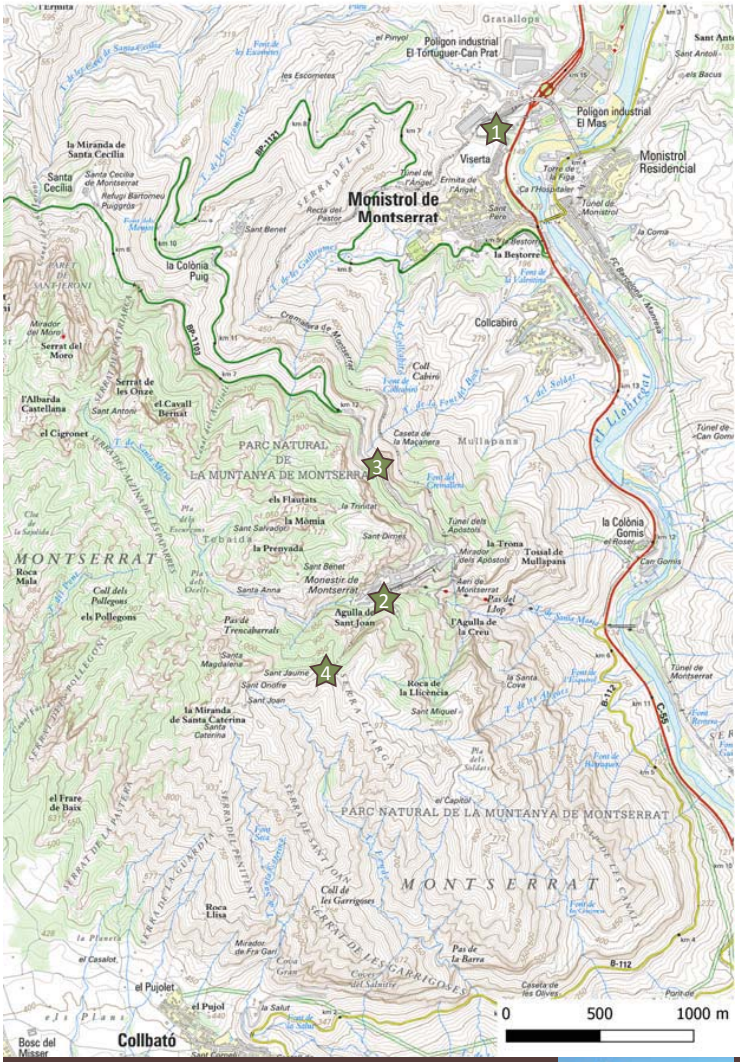

Field trip

Wednesday, 24 May 2017

1.02

Geological context

Regional context

Stop 1 (Village)

J. Corominas (UPC)

M. Janeras (ICGC)

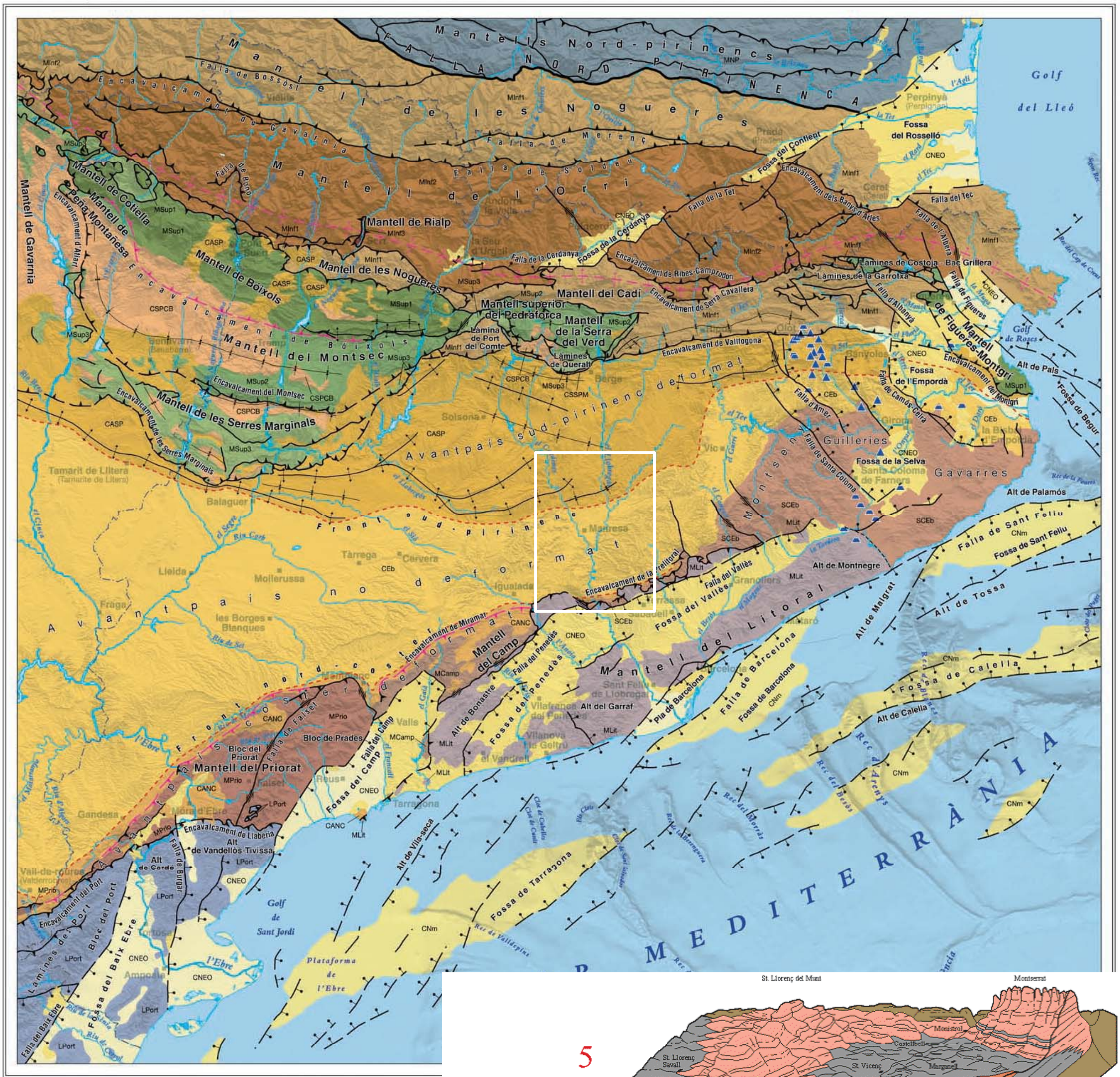

Generalitat de Catalunya
Departament de Territori i Sostenibilitat

Map of the major structural units of Catalonia, ICGC
Original scale: 1:1,000,000
Edition: 2014

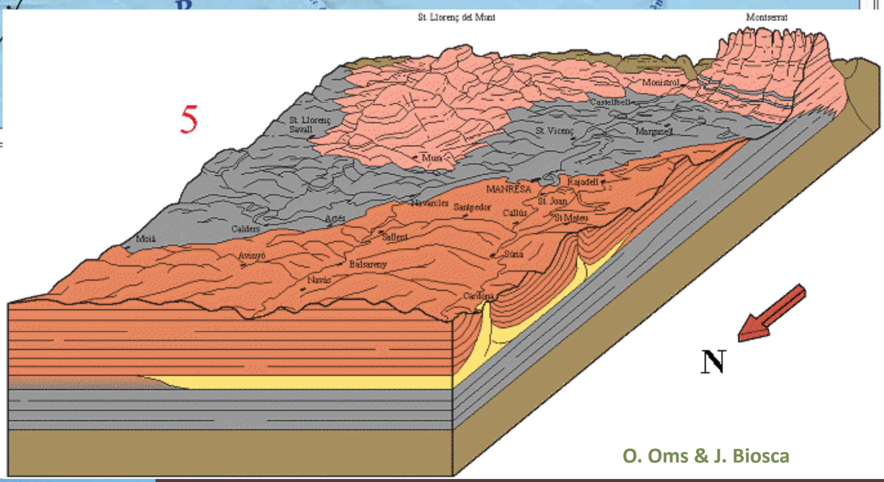

O. Oms & J. Biosca

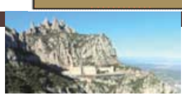

1.03

Geological context

Genesis of the massif

Stop 1 (Village)

J. Corominas (UPC)
M. Janeras (ICGC)

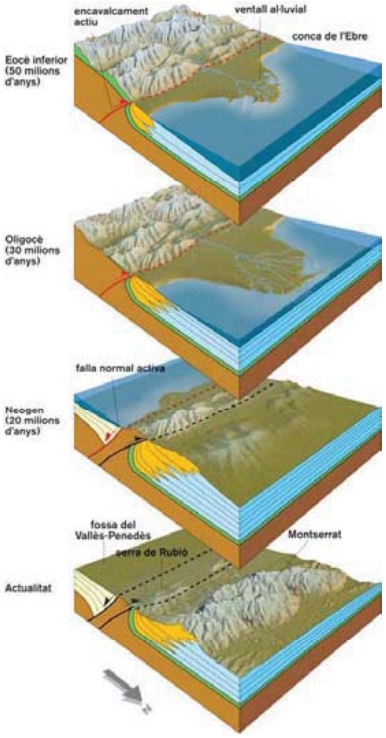

Martínez-Rius, 2006

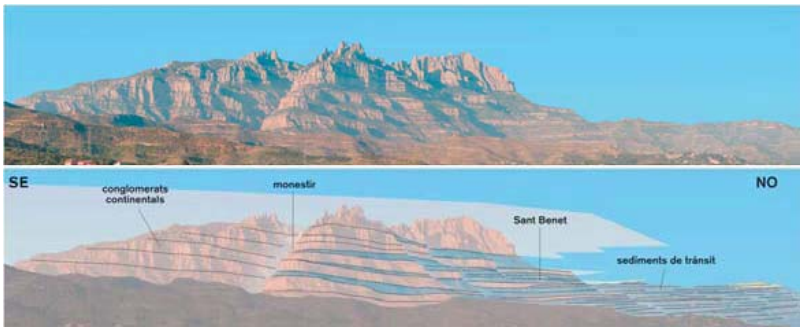

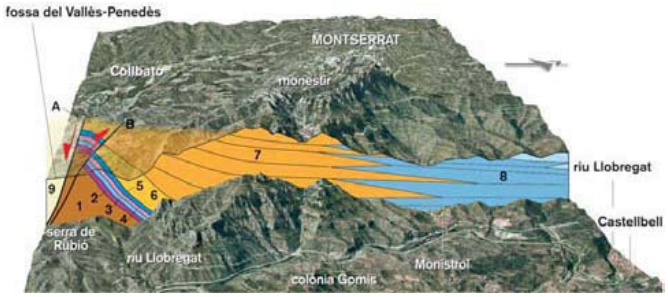

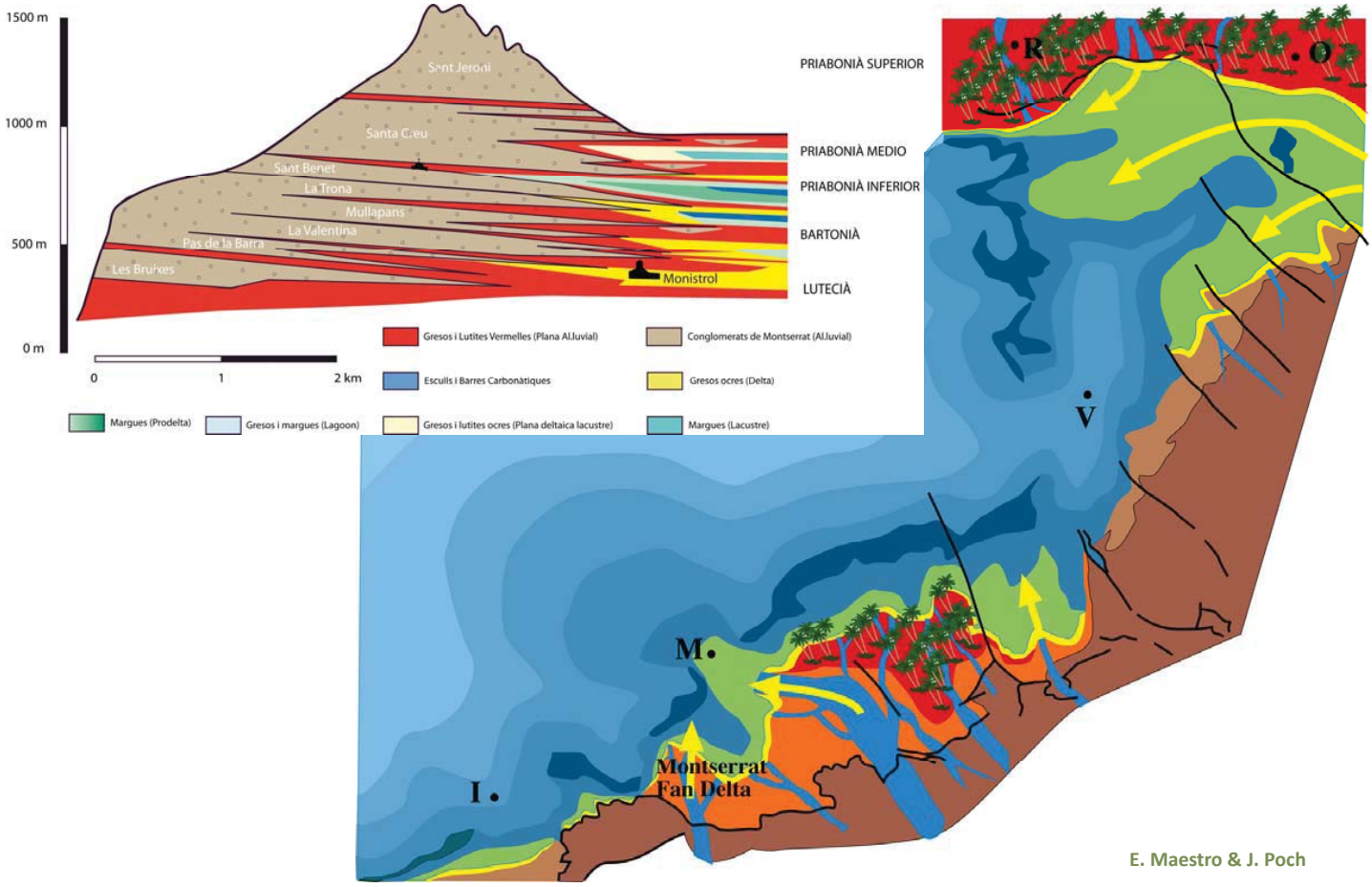

E. Maestro & J. Poch

Rockfall risk management in the Montserrat massif

Field trip

Wednesday, 24 May 2017

1.04

Geological context

Rock mass and mountain morphology

Stop 1 (Village)
J. Corominas (UPC)
M. Janeras (ICGC)

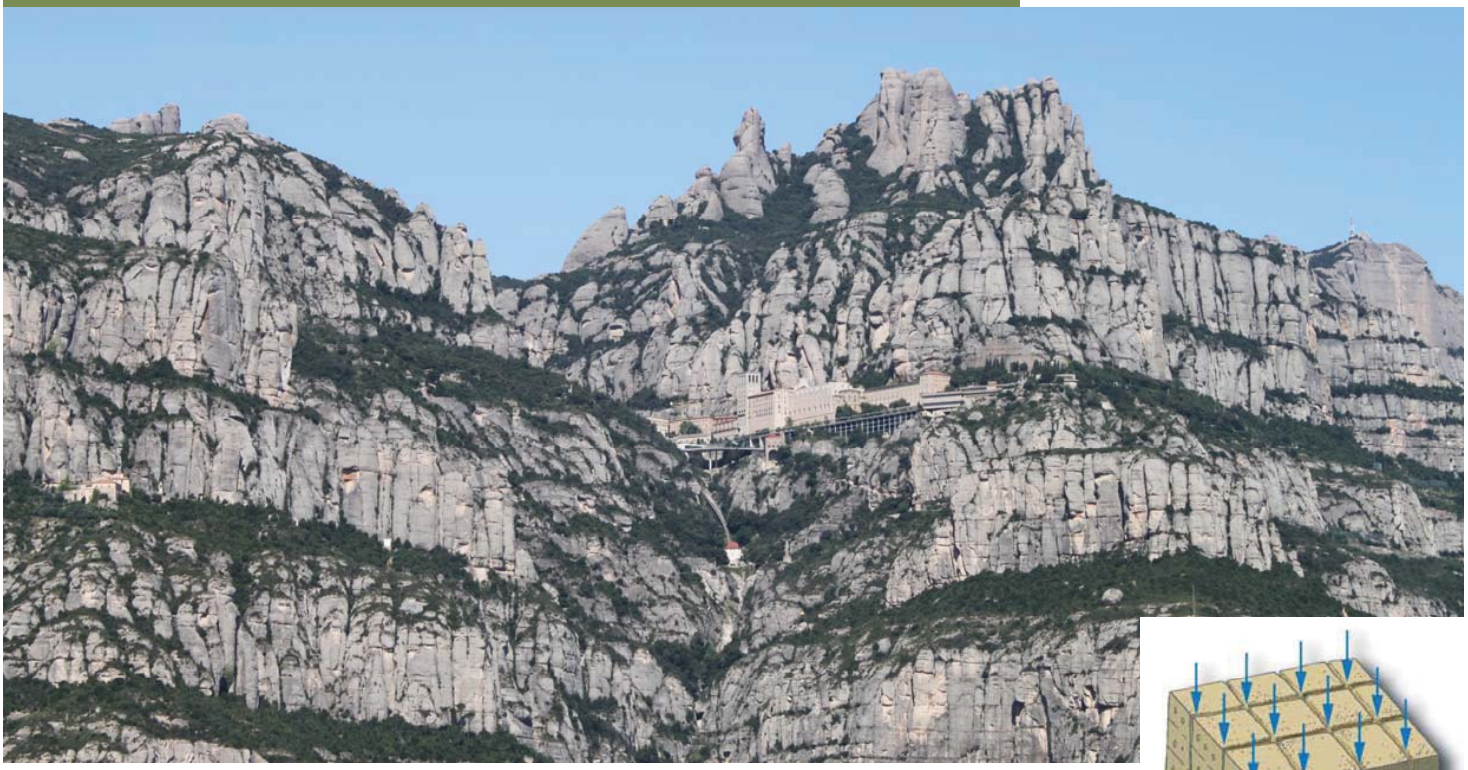

Martínez-Rius, 2006

Rockfall risk management in the Montserrat massif

Field trip

Wednesday, 24 May 2017

1.05

Geological context

Geohazards: rockfall and landslides

Stop 1 (Village)

J. Corominas (UPC)
M. Janeras (ICGC)

Debris flood
(hyperconcentrated flow)

10/06/2000 event

Regió7, 2000

Superficial landslides
Colluviums slide / flow

03/11/2015 event

Rockfall risk management in the Montserrat massif

Field trip

Wednesday, 24 May 2017

1.06

Rack railway

History and Route

Stop 1 (Rack Railway)

D. Paret & A. Ferré (FGC)
M. Janeras (ICGC)

FGC Ferrocarrils de la Generalitat de Catalunya

Cremallera i funiculars de Montserrat

History of the rack railway

1881: Constitution of the company Ferrocarriles de Montaña a Grandes Pendientes
1892: The rack railway was inaugurated (steam train)
1947: During celebrations for the enthronement of the Mare de Déu, its highest number of passengers: a total of almost 274,000
1953: Serious accident and start of decline
1957: Closure of the railway
1991: The drawing up of a project that would form the basis of the current railway
2000: Project updated following the serious torrential floods of June 10th
2001: Beginning of the works for the new rackrailway
2003: The new rackrailway was opened on June 11th

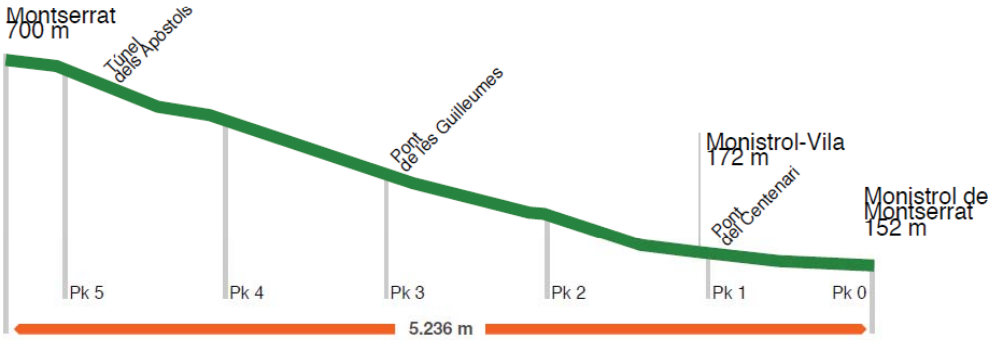

Route of the rack railway

Ascent: 550m
Length: 5200m
Slope: up to 18%
Structures: 3 tunnels, 3 bridges

Rockfall risk management in the Montserrat massif

Field trip

Wednesday, 24 May 2017

1.07 Rack railway

Rockfall risk mitigation

Stop 1 (Rack Railway)

D. Paret & A. Ferré (FGC)
M. Janeras (ICGC)

FGC Ferrocarrils de la Generalitat de Catalunya

Cremallera i funiculars de Montserrat

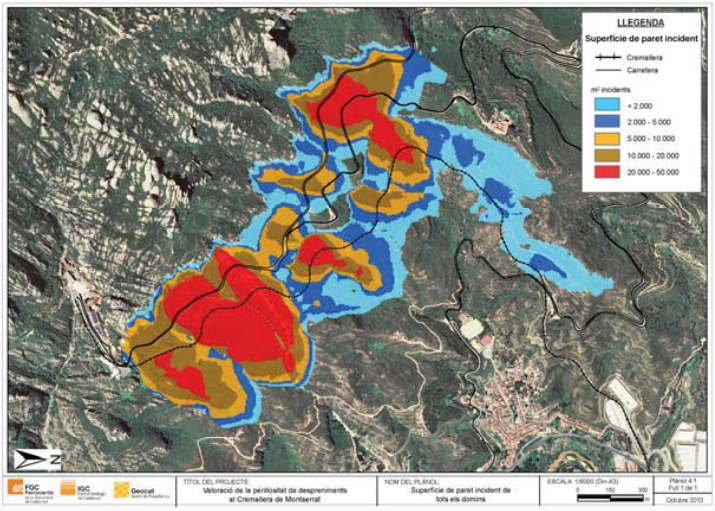

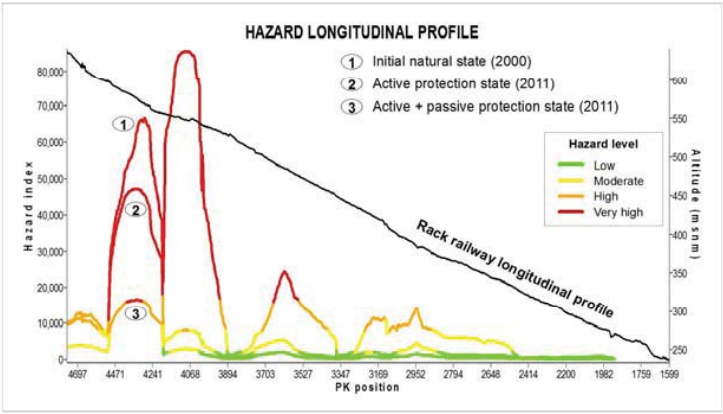

Hazard level at present (2011) with protection (active and passive) along rack railway

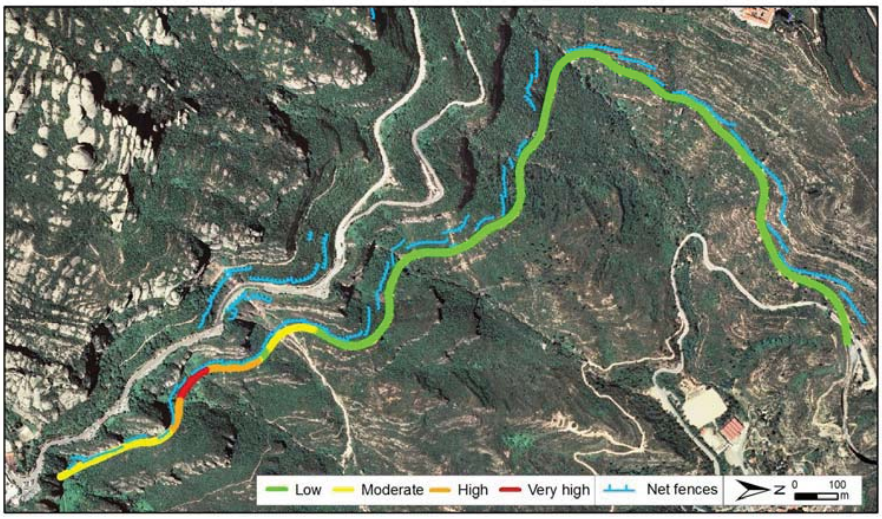

Investment: 4.1 M€ (half at the beginning + half according to surveillance)

Active & passive protection:

- 2800m fences (500 – 5000 kJ)
- 8200m steel rod anchors
- 2000m² steel grid

J. Palau, M. Janeras, E. Prat, J. Pons, J. Ripoll, P. Martínez, J. Comellas (2011) "Preliminary assessment of rockfall risk mitigation in access infrastructures to Montserrat". Second World Landslide Forum, Rome.

M. Janeras, J. Palau, E. Prat, J. Pons, H. Rodríguez, P. Martínez, J. Comellas (2013) "Valoración de 10 años de mitigación del riesgo de caída de rocas en el Cremallera de Montserrat". In: E. Alonso, J. Corominas y M. Hürlimann (Eds.) VIII Simposio Nacional sobre Taludes y Laderas Inestables, Palma de Mallorca, Junio 2013, pag. 624-635.

Detaching hazard level by domains at initial natural state (2000) without protection

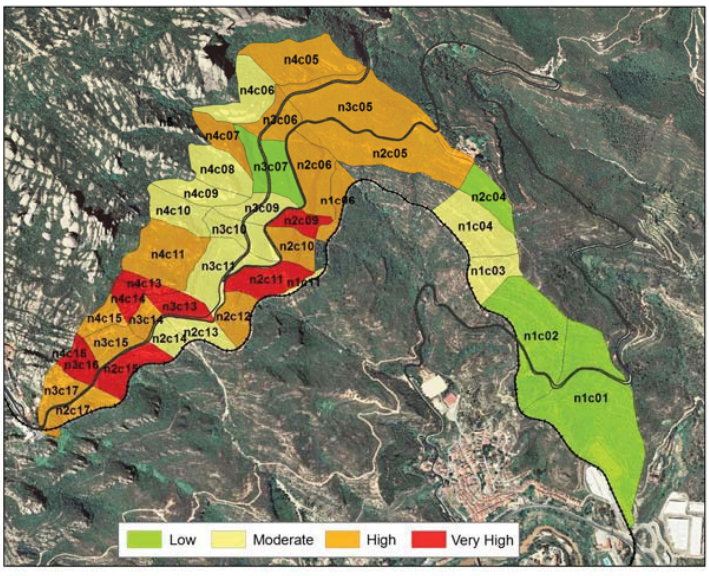

Detaching hazard level by domains at present (2011) considering active protection (stabilization)

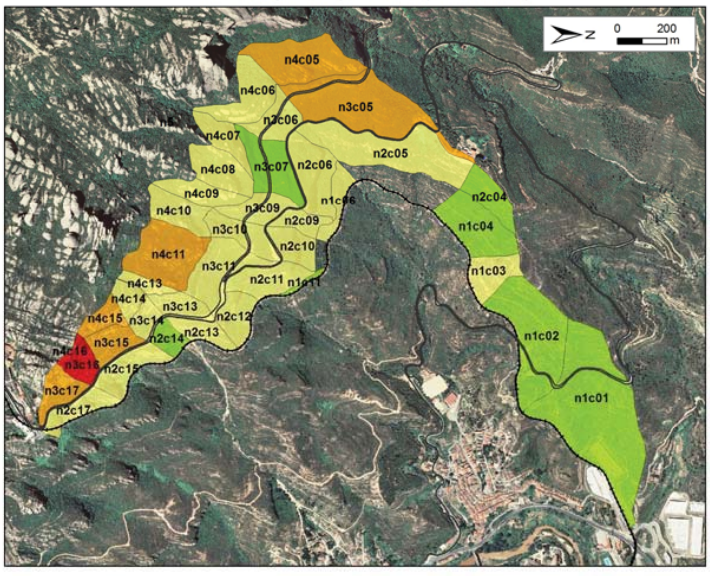

Rockfall risk management in the Montserrat massif

Field trip

Wednesday, 24 May 2017

2.01 Risk management in building area

Reference events

Stop 2 (Sanctuary)

M. Janeras (ICGC)

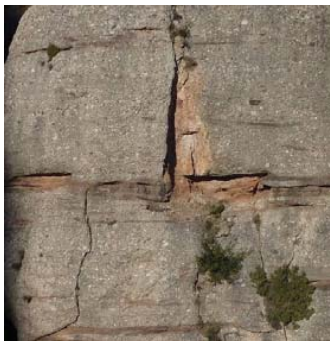

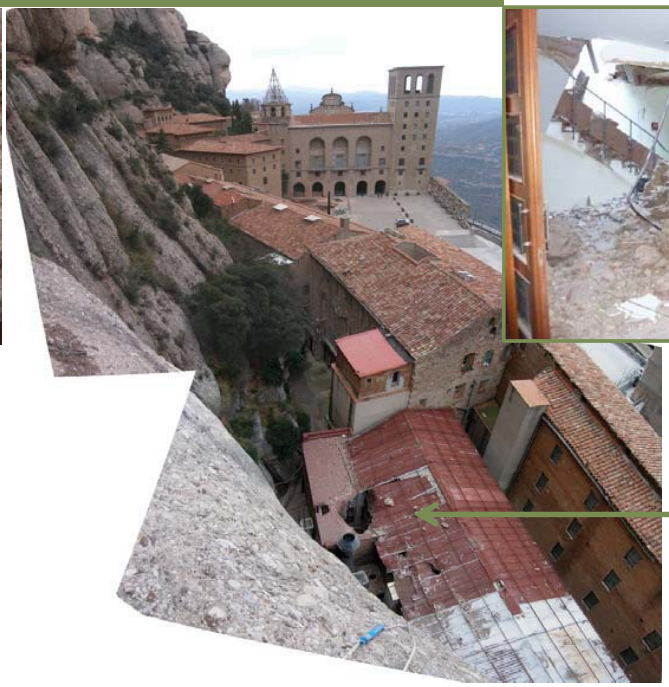

Hotel Cisneros: Volume=4m^3

Monastery: 4monks dead in the nursery

15/12/2010 event

March 1546 event

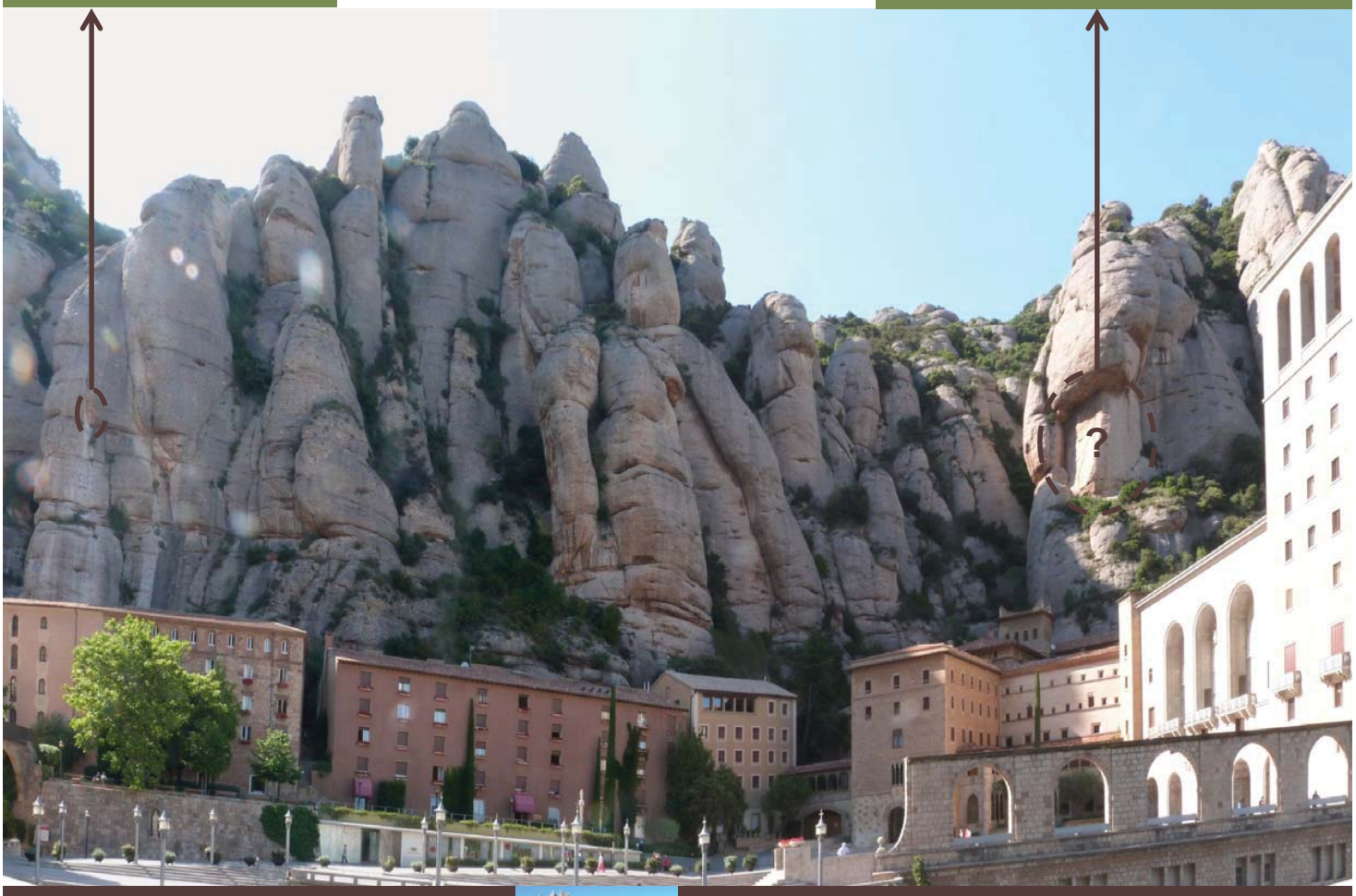

Rockfall risk management in the Montserrat massif

Field trip

Wednesday, 24 May 2017

2.02 Risk management in building area

Rockfall hazard and mechanisms

Stop 2 (Sanctuary)

M. Janeras (ICGC)

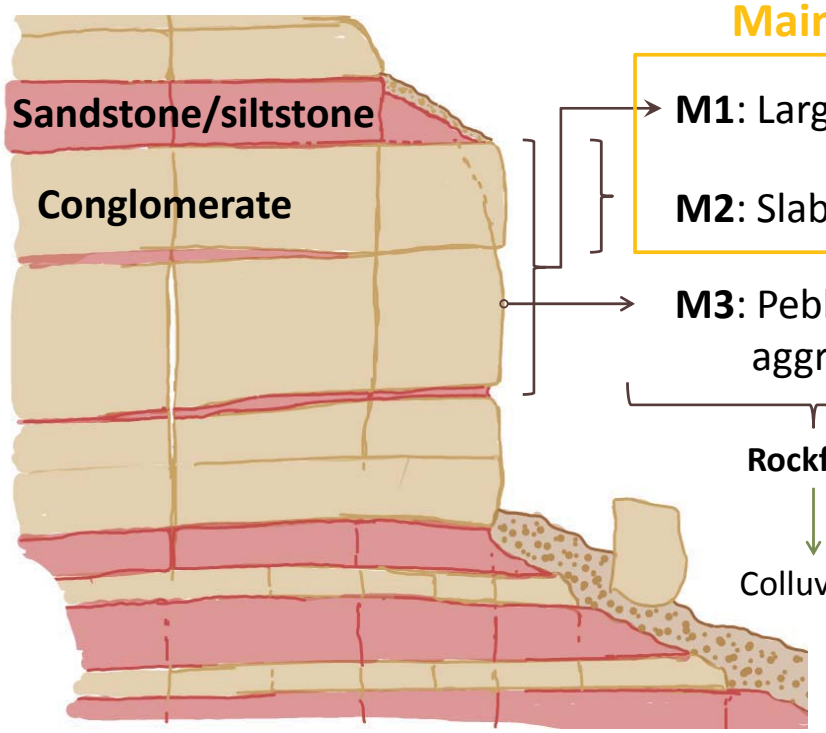

Main goal

M1: Large blocks

M2: Slabs, sheets

M3: Pebbles and aggregates

Rockfalls

Colluvium

Shallow landslides
Torrential floods

Rockfall mechanisms

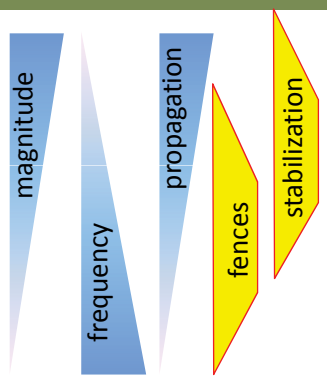

Protection efficiency

	Block typology	Detachment mechanism	Modal volume	Typical Shape
M1	Large blocks, spires and singular	Stability controlled by the discontinuities (vertical joints and bedding planes)	30 m^3 – 1000 m^3	Prims
M2	Slabs, plates or sheets	Plastic deformation due to weathering-induced stress (thermic effect)	0.3 m^3 – 10 m^3	Plate
M3	Pebbles and aggregates	Physical and chemical weathering of the matrix	0.001 m^3 – 0.03 m^3	Oval

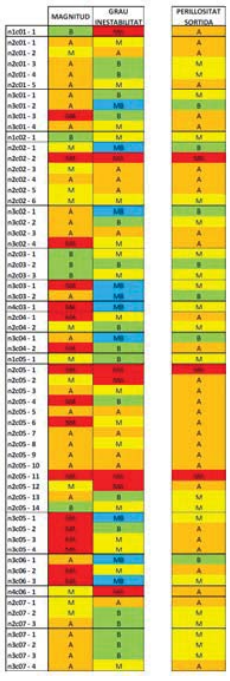

M1 inventory

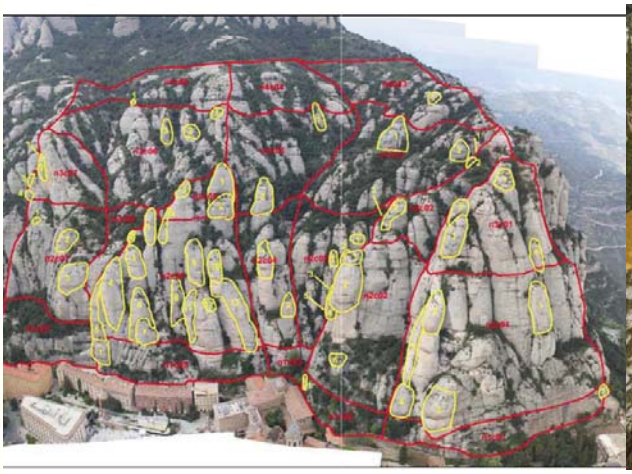

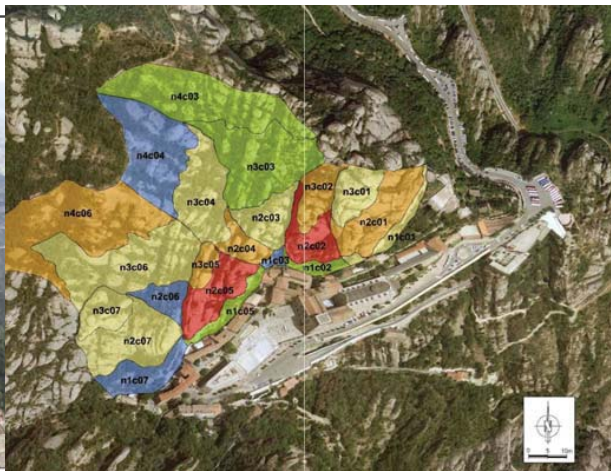

Preliminary inventory of potentially unstable masses (2011)
Priorities based on interpretation of visual signs and qualitative assessment of hazard

M. Janeras, J. Palau, E. Prat, J. Ripoll (2011) "Montserrat: on a long way to rock fall risk mitigation. First experiences, some lessons and future perspectives" *4th Interdisciplinary Rockfall Workshop RocExs-2011*, Innsbruck.

Rockfall risk management in the Montserrat massif

Field trip

Wednesday, 24 May 2017

2.03 Risk management in building area

Rockfall risk mitigation plan

Stop 2 (Sanctuary)

M. Janeras (ICGC)

Risk Management

PMRG 2013 (georisk mitigation plan)

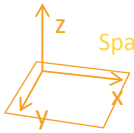

t
Time prediction

Risk management

Land planning and Infrastructures authorities

Civil protection and Emergency authorities

Mitigation

Prevention for the future

Recovering from the past

Response

Preparedness

- Magnitude +

Incident

Disaster

- Damage +

Resilience

PEMONT 2009 (emergency protocol)

Risk Mitigation

Protection alternatives

work package 1

work package 2

Study Stage

Identification, characterization, hazard zoning , risk assessment

Project Stage

Analysis of alternatives, sizing calculation , structural design

Planning

Reconsidering

Risk management

Implementing

Maintaining

Operation Stage

Forecast, inspection surveys, monitoring, crisis analysis

Construction Stage

Countermeasures, active and passive protection, quality control

Monitoring

Optimization *cost / benefit*

Risk Mitigation

P. Buxó, M. Janeras, G. Domènech, J. Pons, E. Prat, F. López (2017) "Development of a Risk Mitigation Plan in the Montserrat Massif (Central Catalonia, Spain)". In: Mikos *et al.* (Editors), *Advancing Culture of Living with Landslides*. Springer, *4th World Landslide Forum*, Ljubljana, in press.

Rockfall risk management in the Montserrat massif

2.04 Rock face monitoring

Monitoring strategy

Field trip

Wednesday, 24 May 2017

Stop 2 (Sanctuary)

M. Janeras (ICGC)
J.A. Gili (UPC)

Overview of the 4 monitoring techniques used in the pilot tests

		Temporal domain: Continuous	Temporal domain: Discontinuous
Spatial domain	Continuous	Ground Based Syntethic Aperture Radar (Gb-InSAR)	Terrestrial Laser Scanner (TLS)
	Scattered	Rock joint instrumentation	Surveying Total Station

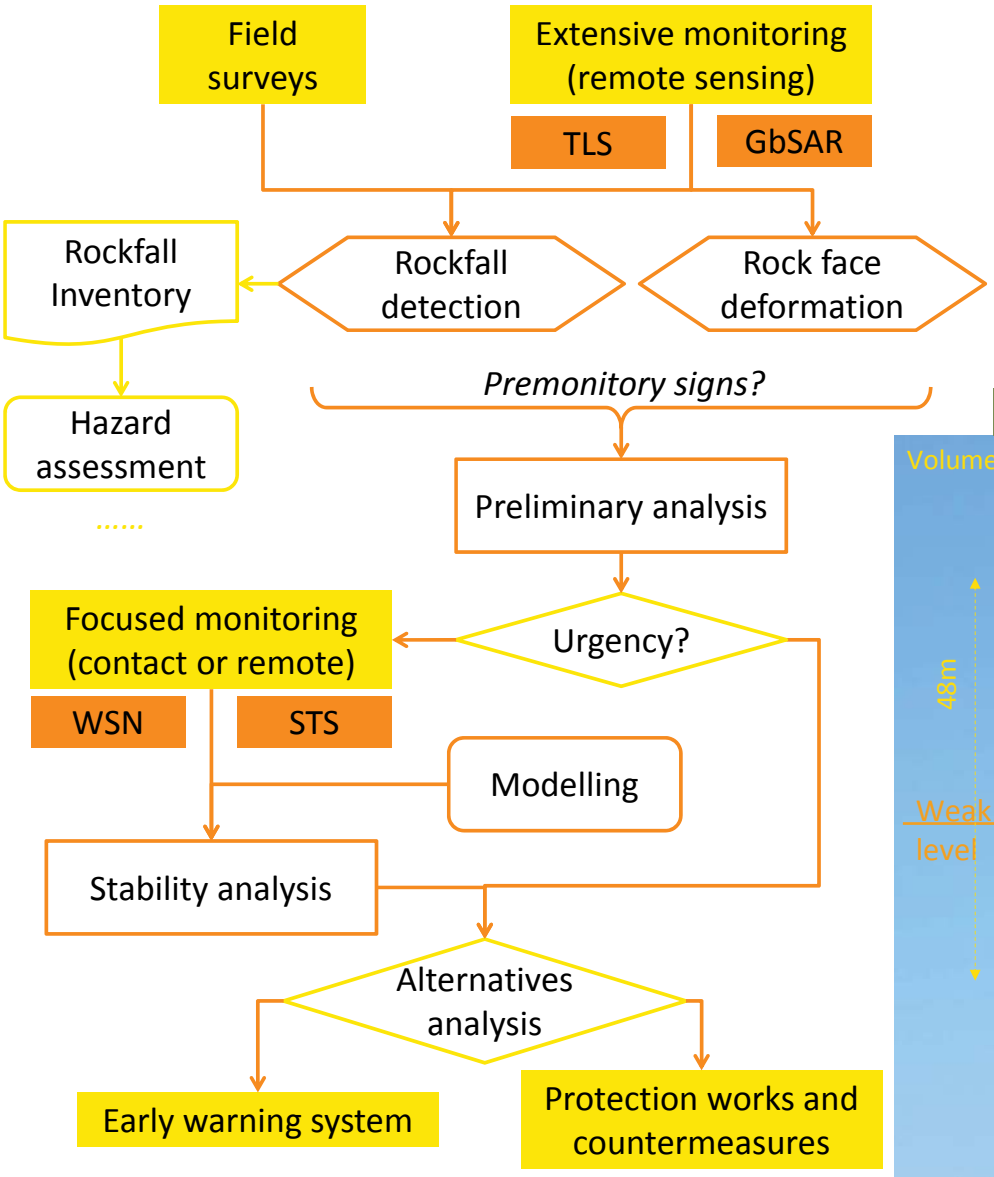

M. Janeras, J.A. Jara, F. López, J. Marturià, M.J. Royán, J.M. Vilaplana, A. Aguasca, X. Fàbregas, F. Cabranes, J.A. Gili (2015) "Using several monitoring techniques to measure the rock mass deformation in the Montserrat Massif" *International Symposium on Geohazards and Geomechanics ISGG-2015,* Warwick, IOP Conf. Series: *Earth and Environmental Science* 26 (2015) 012030, DOI:10.1088/1755-1315/26/1/012030.

Cadireta rock needle / tower

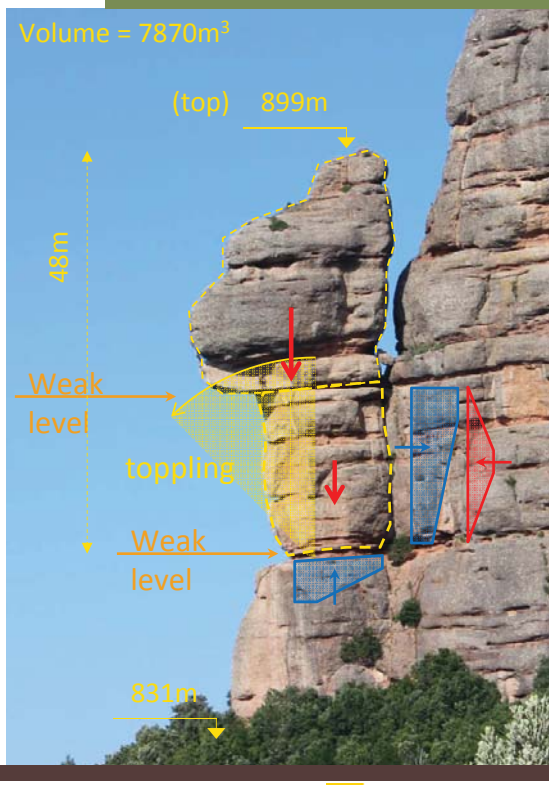

Rockfall risk management in the Montserrat massif

Field trip

Wednesday, 24 May 2017

2.05 Rock face monitoring

Surveying Total Station, STS

Stop 2 (Sanctuary)
M. Janeras (ICGC)
J.A. Gili (UPC)

M. Janeras, J.A. Jara, M.J. Royán, J.M. Vilaplana, A. Aguasca, X. Fàbregas, J.A. Gili, P. Buxó (2017) "Multi-technique approach to rockfall monitoring in the Montserrat massif (Catalonia, NE Spain)" *Engineering Geology* 219 (2017) 4–20.

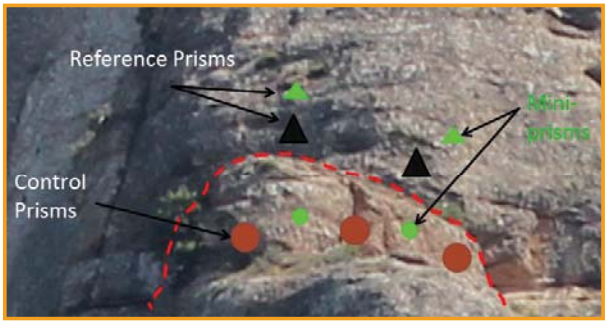

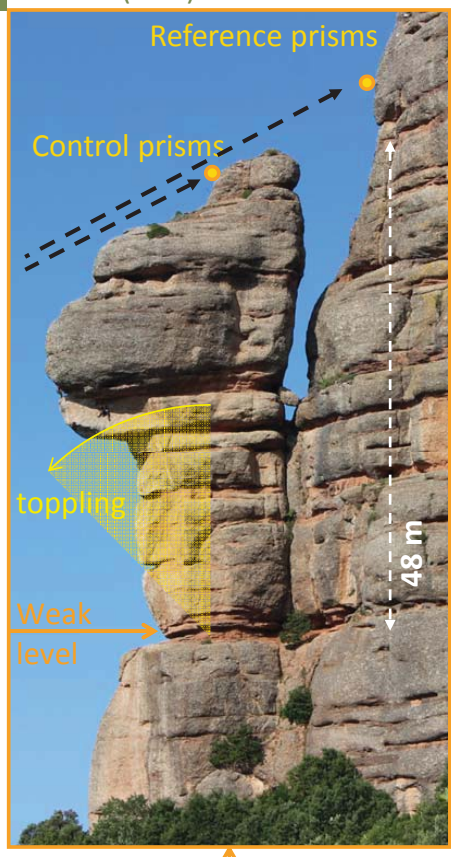

Survey: Seasonal measurement (4/year)

Results: Oscillation amplitude = 8 mm

More year cycles are needed to determine if this displacement is fully retrievable or not.

Measurement of the relative distance between prisms along main trajectory

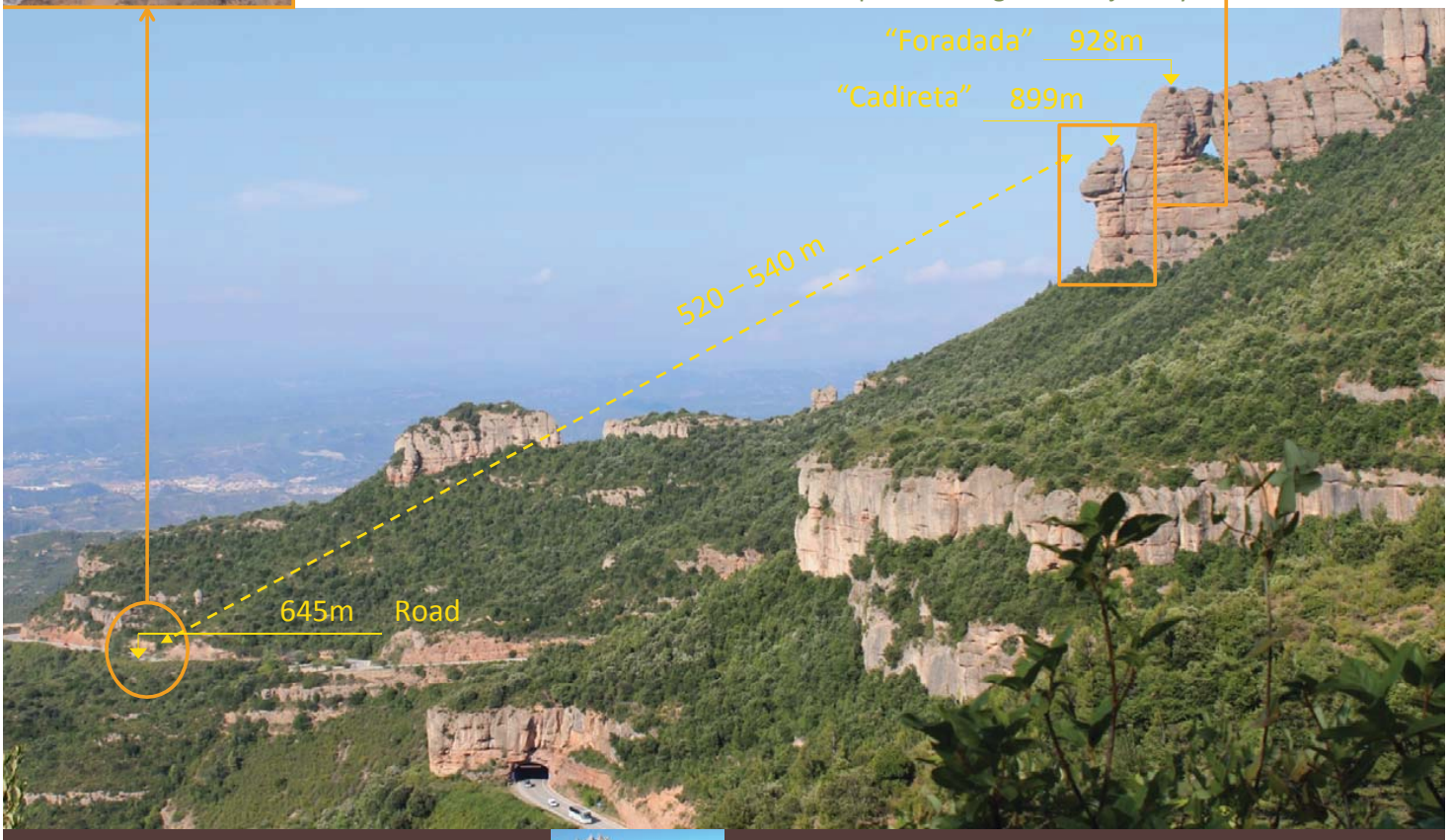

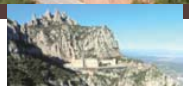

Rockfall risk management in the Montserrat massif

Block joint monitoring

2.06

Instrumentation

Field trip

Wednesday, 24 May 2017

Stop 2 (Sanctuary)

M. Janeras & J.A. Jara (ICGC)

Installation and equipment

Constraints:

- Several blocks to monitor
- Proximity of each other and to buildings
- Difficulty of access
- Minimizing the visual impact

Wireless network

2.07

Block joint monitoring

Wireless sensor network & ZigBeeLoggers

Stop 2 (Sanctuary)

J.A. Jara & M. Janeras (ICGC)

ZBLogger characteristics

General

- Based on ZigBee protocol (IEEE 802.15.4)
- Low power device (sleep mode ~ 95% of time)
- ICGC own design and production
- Low cost device (~ 110 €/unit)

Enclosure

- Waterproof (IP67) 120x120x80 mm

Power

- Solar cell 0.96W
- 8 LR6 1.5V (AA) rechargeable batteries
- Power consumption: ~1-10µA (passive sensors)
  ~1-10mA (active sensors)

Measurement:

- Input channels: 3 single ended or 1 differential + 1 single ended
- Sensor output: voltage, current (4-20mA), resistance
- Active / passive sensors
- 16 bits sigma-delta A/D converter
- State of health (SOH): battery voltage

Communication:

- Up to 250 kbps
- Transmit power: +18 dBm E.I.R.P (max)
- Working distance: up to 1.6 km outdoor line-of-sight
- Various Antenna Options: Dipole 1/3/5 dBi
- Radio Frequency Range: 2.410 ~2.475 GHz
- Number of frequency channels: 14
- Transmission Method: Direct Sequence Spread Spectrum
- Modulation Method: O-QPSK

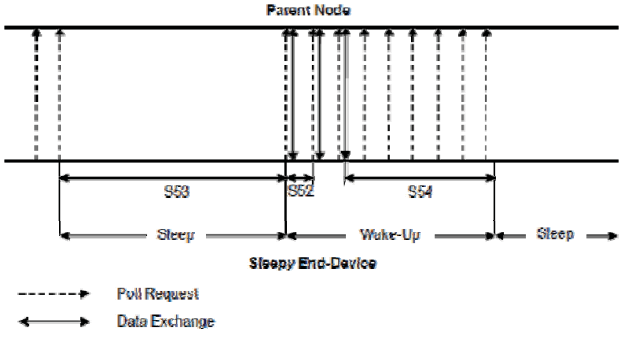

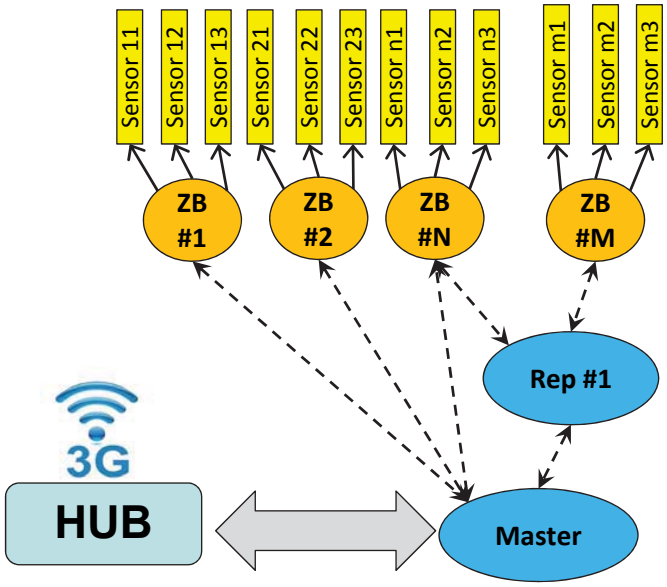

Dynamic topology for every path (best route for connectivity)

Rockfall risk management in the Montserrat massif

Block joint monitoring

2.08

Wireless sensor network WSN

Field trip

Wednesday, 24 May 2017

Stop 2 (Sanctuary)

J.A. Jara & M. Janeras (ICGC)

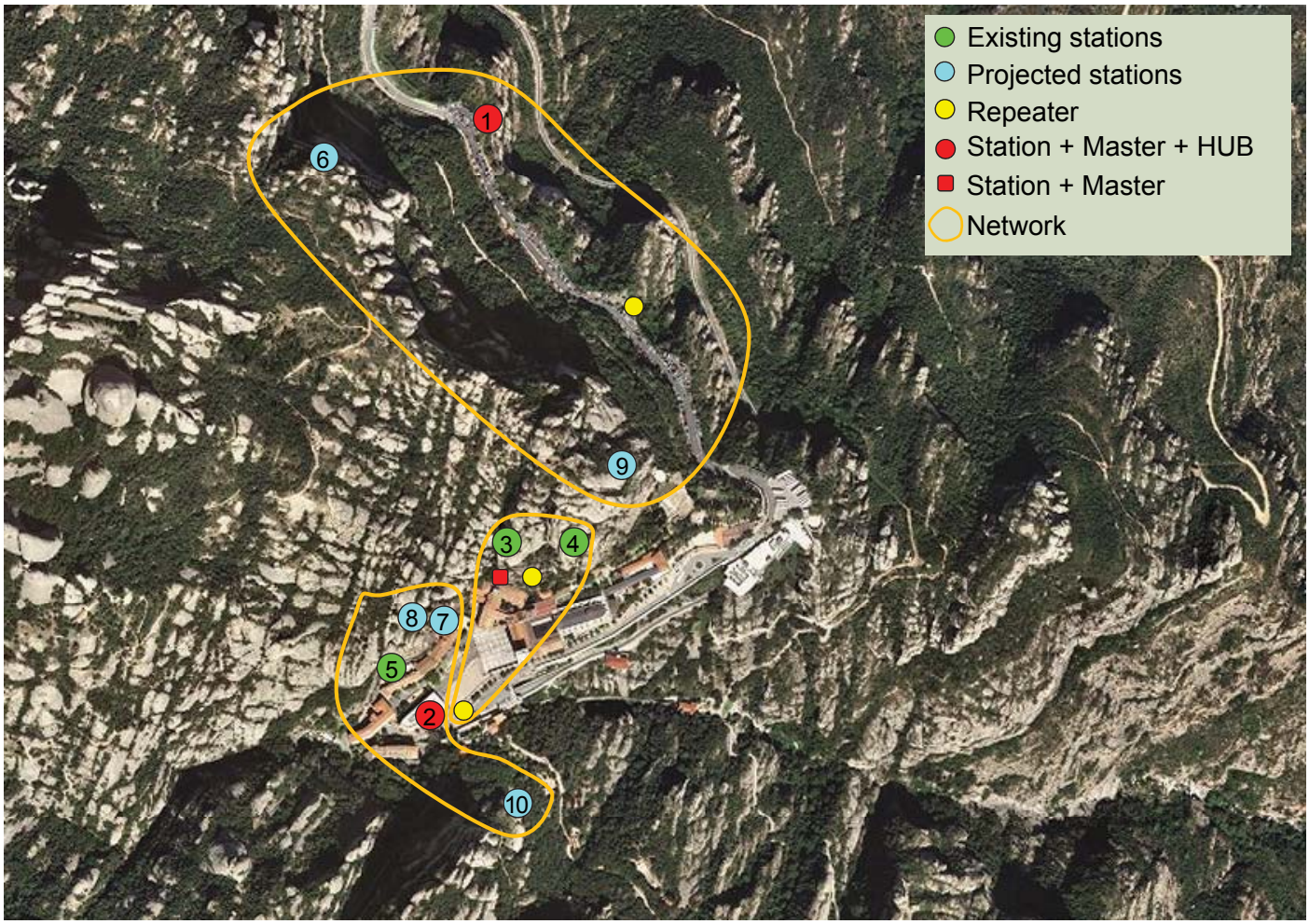

	Station	Risk zone
1	Block A3-6	Railway
2	Nostra Senyora	Meteorological station and HUB
3	Castell del Diable	Monastery
4	Berruga	Sanctuary
5	Esperó Cisneros	Hotel
6	Degotalls wall	Parking
7	N2c05b11 column	Hotel
8	N2c05b1 needle	Hotel
9	Dipòsit slab	Tank of water
10	Viacrucis	Funicular & path

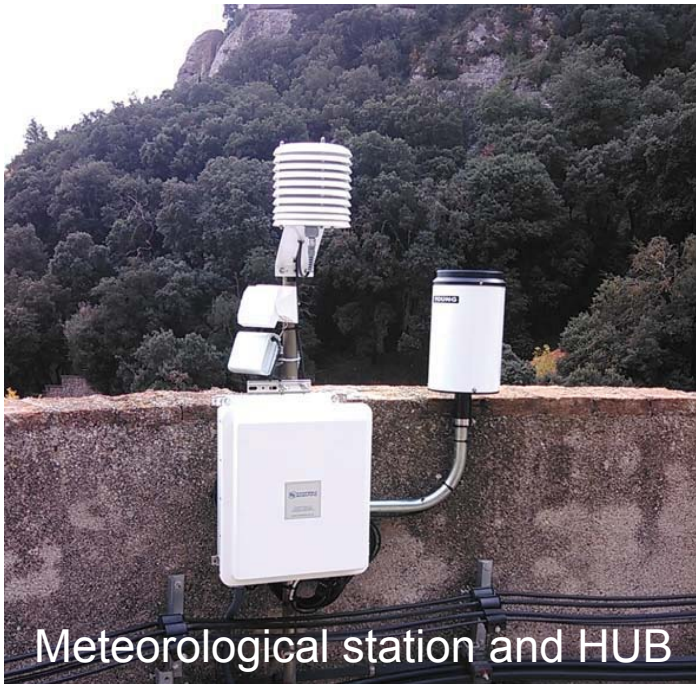

2.09 Block joint monitoring

Data collecting and managing

Stop 2 (Sanctuary)

J.A. Jara & M. Janeras (ICGC)

NETMON ©ICGC

Unified and homogeneous management of all the monitoring projects in ICGC

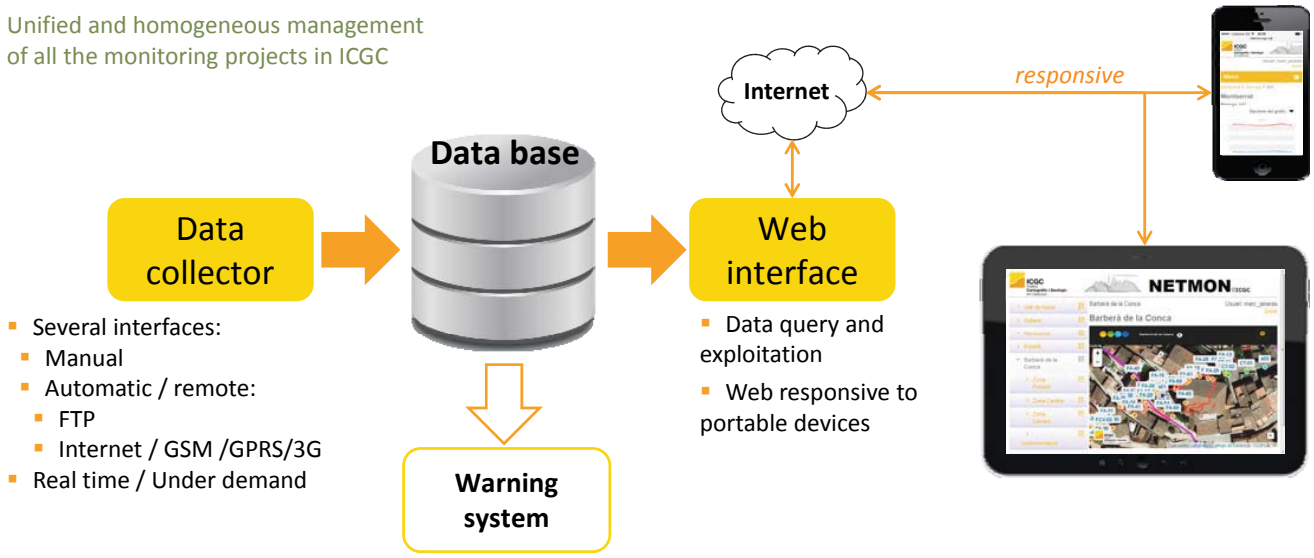

- Several interfaces:
  - Manual
  - Automatic / remote:
    - FTP
    - Internet / GSM /GPRS/3G
- Real time / Under demand

- Data query and exploitation
- Web responsive to portable devices

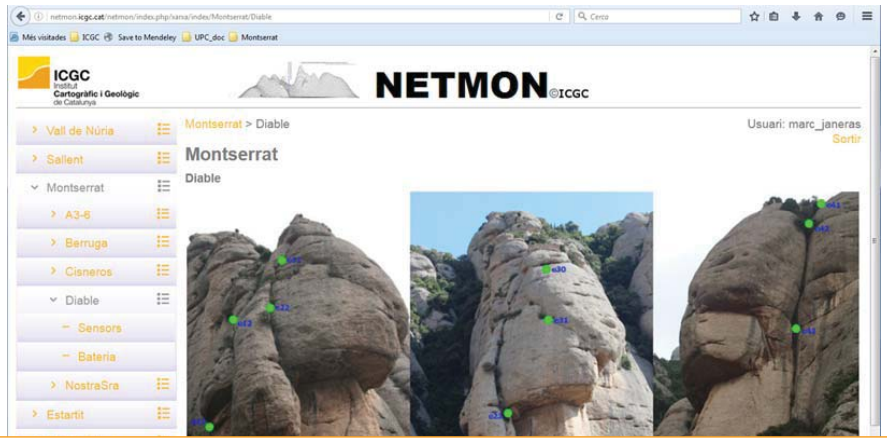

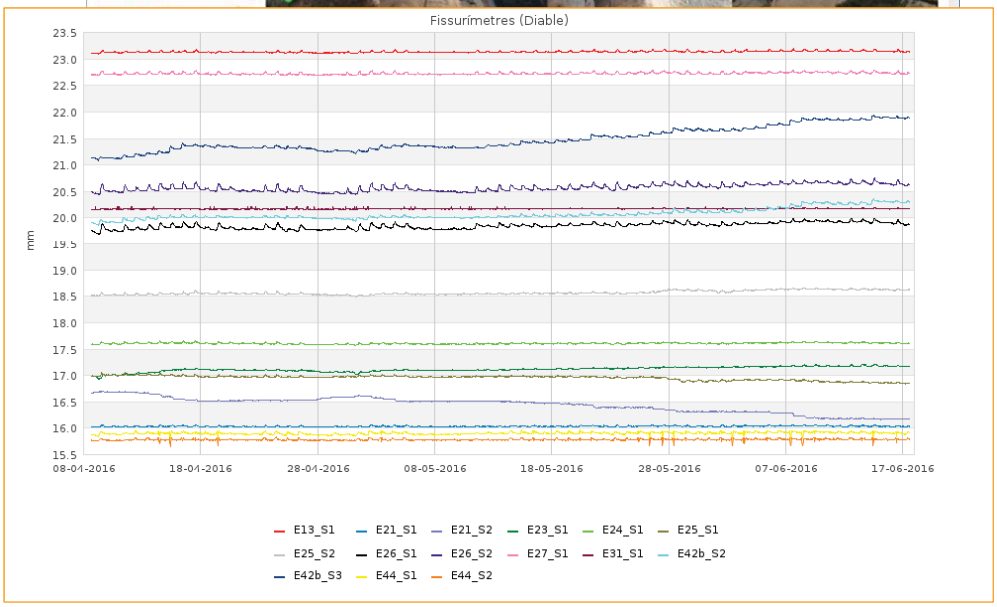

M. Janeras, J.A. Jara, F. López, A. Marcè, T. Carbonell, A. Elvira (2016) "Development of a wireless sensor network for rock mass deformation monitoring in the Montserrat Massif" *3rd Rock Slope Stability conference*, Lyon.

Rockfall risk management in the Montserrat massif

Field trip

Wednesday, 24 May 2017

2.10 Block joint monitoring

Results of contact sensors instrumentation

Stop 2 (Sanctuary)

M. Janeras & J.A. Jara (ICGC)

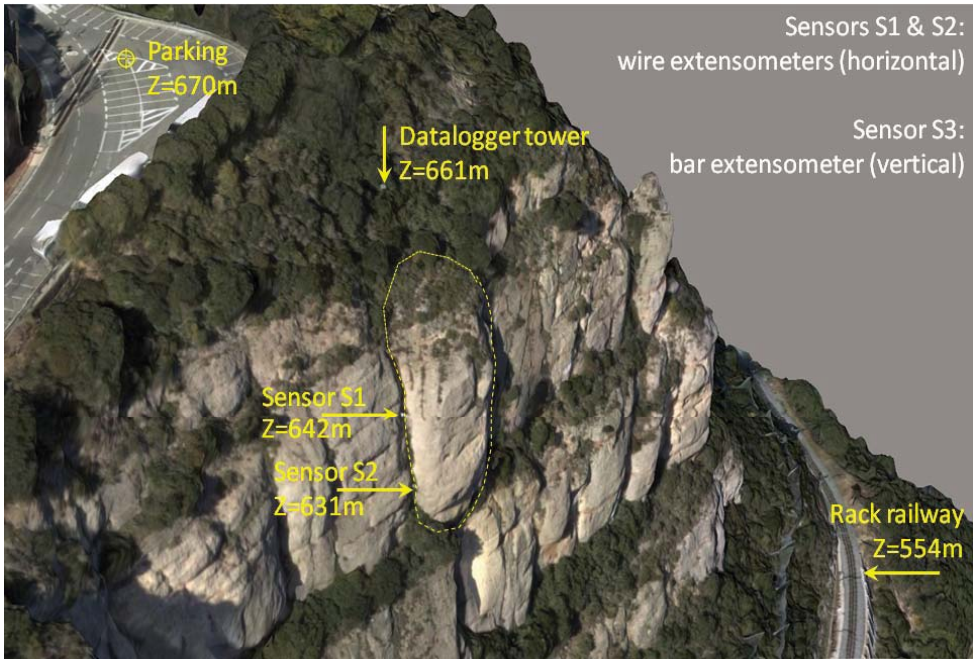

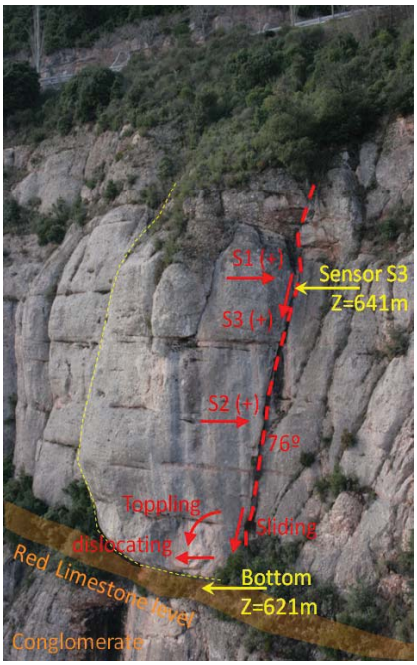

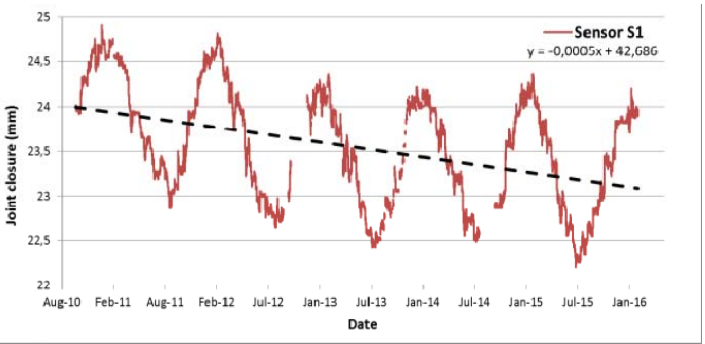

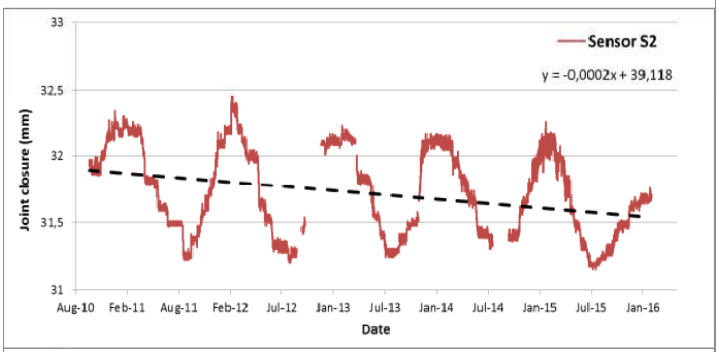

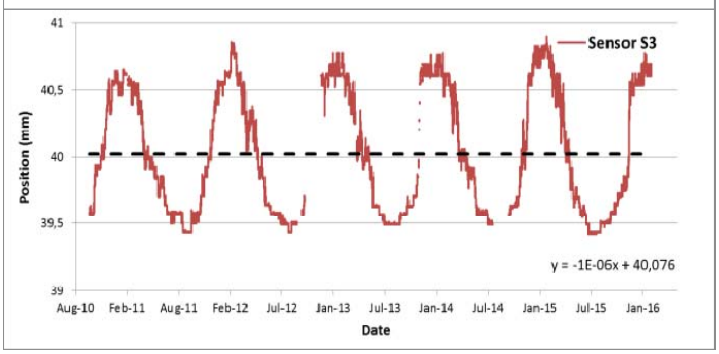

Sensor	amplitude of annual oscillation	Accumulated displacement	Proportion
Sensor 1	2.0 mm	-0.17 mm/year	8.5%
Sensor 2	1.0 mm	-0.065 mm/year	6.5%
Sensor 3	1.3 mm	0.000 mm/year	0.0%
Air Temp.	36.7 ºC	---	

Toppling rate: 1E-5 rad/year

Block A3-6:

- First monitoring station
- Since October 2010
- Longest time series
- Wired (sensors – datalogger)

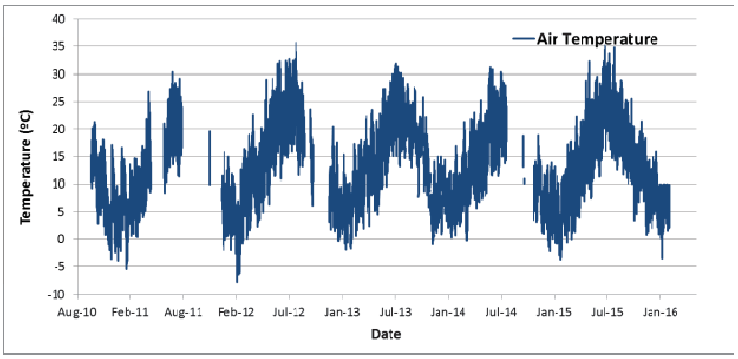

M. Janeras, J.A. Jara, M.J. Royán, J.M. Vilaplana, A. Aguasca, X. Fàbregas, J.A. Gili, P. Buxó (2017) "Multi-technique approach to rockfall monitoring in the Montserrat massif (Catalonia, NE Spain)" *Engineering Geology* 219 (2017) 4–20.

Rockfall risk management in the Montserrat massif

Field trip

Wednesday, 24 May 2017

3.01 Risk mitigation for the accessibility

Reference events

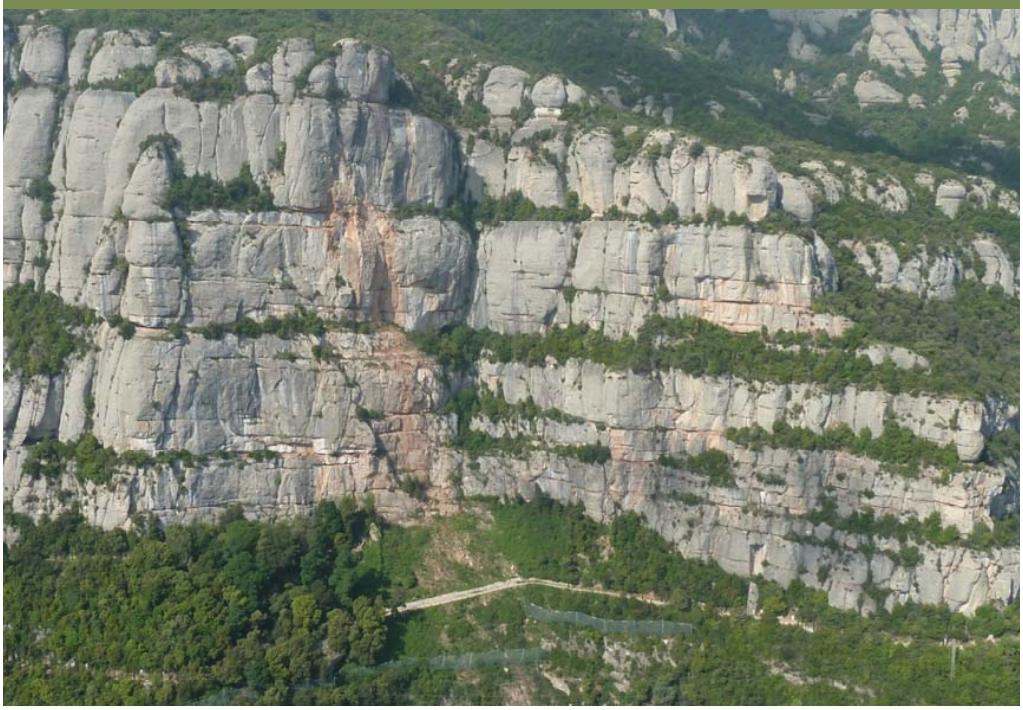

Stop 3 (Degotalls)

M. Janeras (ICGC)

02/01/2007 event

Time: 6:45
Volume: 300 m^3
Effects:
Road & railway blocked

28/12/2008 event

Time: 13:45
Volume: 900 m^3
Effects:
1800 people to be evacuated by cable car (finish at 21:30)
213 cars & 7 buses blocked
Recovery:
14Feb: emergency path by road
13March: railway service
27March: road without limitations

Rockfall risk management in the Montserrat massif

3.02 Risk mitigation for the accessibility

Rupture propagation

Field trip

Wednesday, 24 May 2017

Stop 3 (Degotalls)

M. Janeras (ICGC)

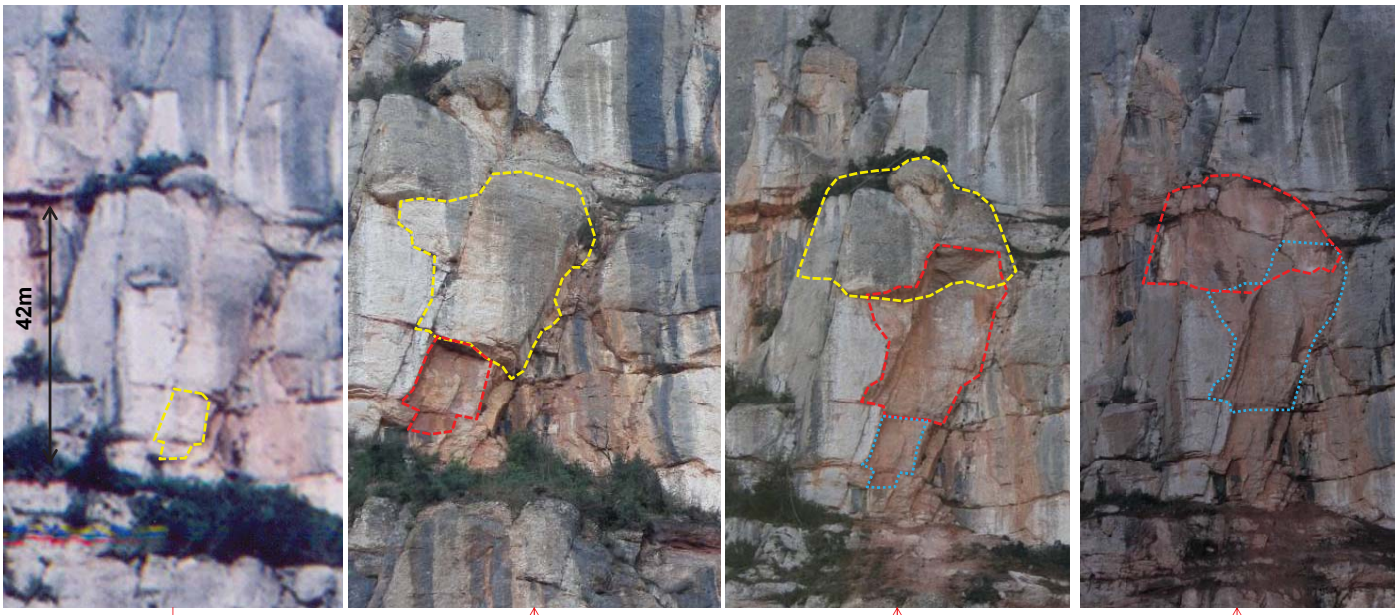

Photo date:	2001	30/01/2006	02/01/2007	19/01/2009
Event date:	dd/mm/2001	02/01/2007	28/12/2008	
Rockfall volume:	20 m^3	300 m^3	900 m^3	
Chronologic order	Previous event	Present event	Next event	

03/11/2008 episode (rainfall and several rockfalls)

Retrospective (after 2008):
Precursory displacements?
Signs of instability evolution?

Photos: L. Baciero (19/05/2008)

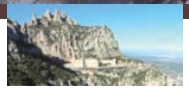

Rockfall risk management in the Montserrat massif

Risk mitigation for the accessibility

3.03

Protective works

Field trip

Wednesday, 24 May 2017

Stop 3 (Degotalls)

M. Janeras (ICGC)

3.04

LiDAR monitoring
Methodology

Stop 3 (Degotalls) RISKNAT

M. J. Royán; M. Guinau; J.M. Vilaplana ; A. Abellán; D. Garcia (Universitat de Barcelona)

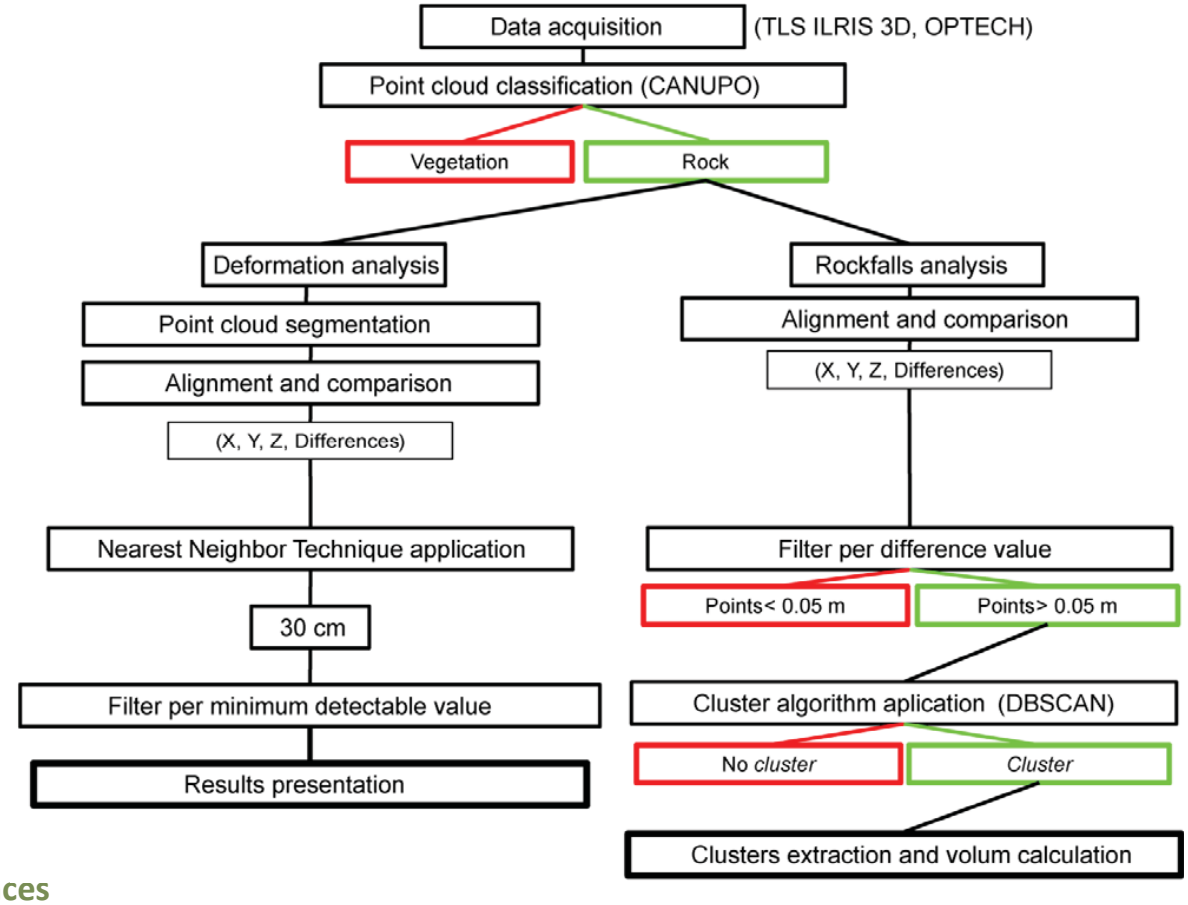

References

Royán, M. J. (2015). Caracterización y predicción de desprendimientos de rocas mediante LiDAR Terrestre. PhD Thesis, Universitat de Barcelona, 2015. http://diposit.ub.edu/dspace/bitstream/2445/68667/1/MJRC_TESIS.pdf

Janeras, M., Jara, J.A., Royán, M.J., Vilaplana, J.M., Aguasca, A., Fàbregas, X., Gili, J.A., Buxó, P. 2017. Multi-technique approach to rockfall monitoring in the Montserrat massif (Catalonia, NE Spain). Eng. Geol., 219, 4-20.

Rockfall risk management in the Montserrat massif

Field trip

Wednesday, 24 May 2017

3.05 LiDAR monitoring

Rockfall detection and analysis: Degotalls N

Stop 3 (Degotalls) RISKNAT
M. J. Royán; M. Guinau; J.M. Vilaplana ; A. Abellán; D. Garcia (Universitat de Barcelona)

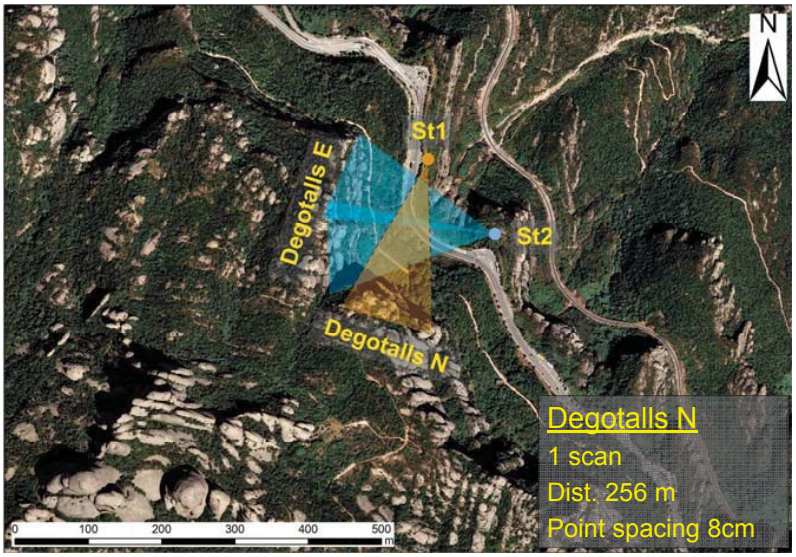

Monitoring Period 2007.05 – 2017.01

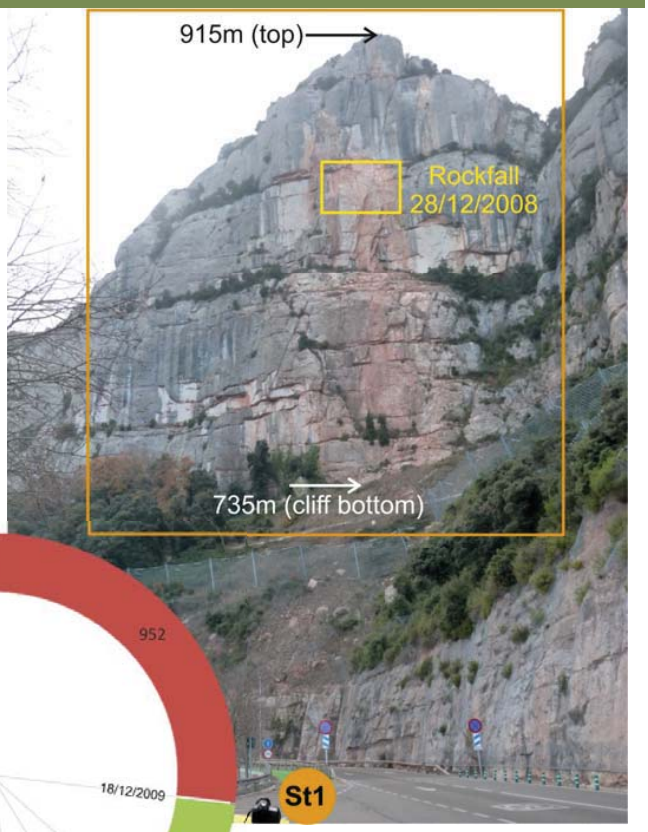

Rockfall inventory

3.538 monitoring days

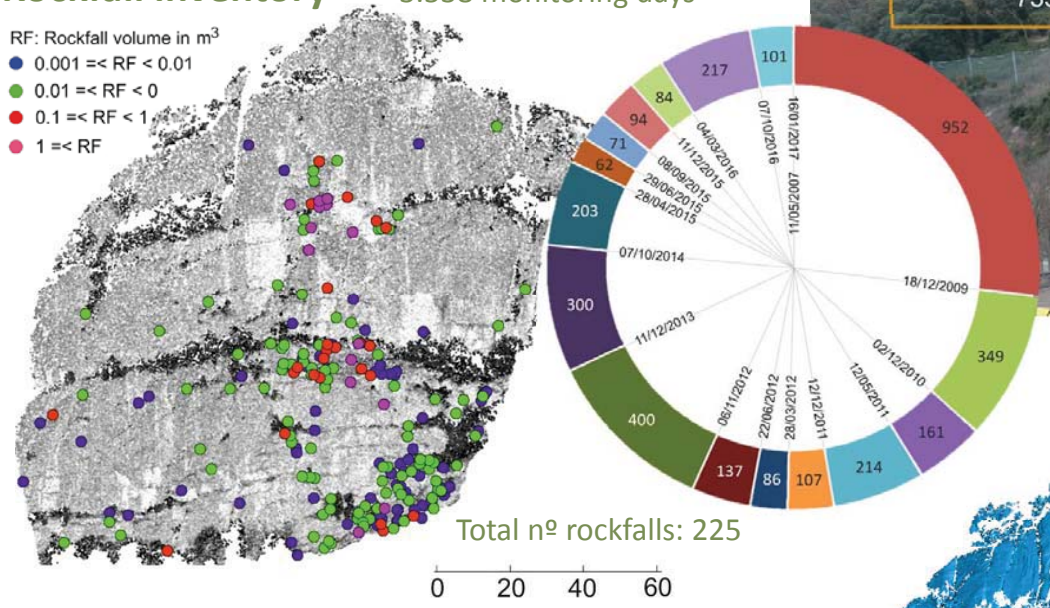

Total nº rockfalls: 225

0 20 40 60

Rockfall density

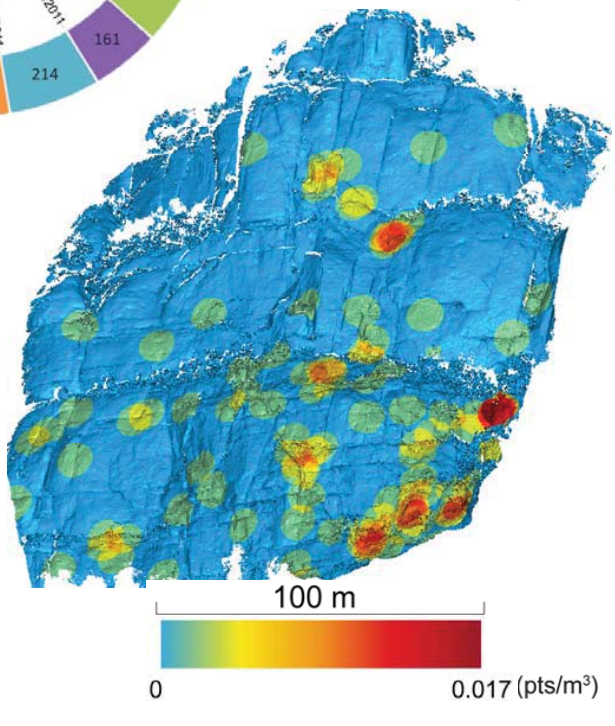

Accumulated nº of rockfalls vs Time

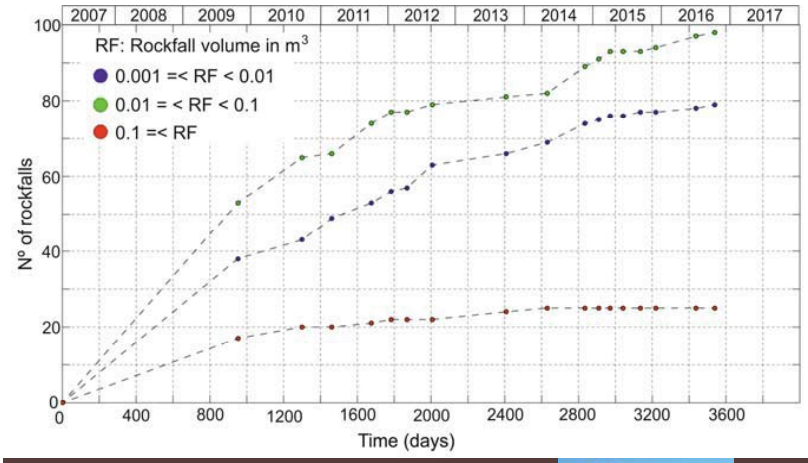

Rockfall risk management in the Montserrat massif

Field trip

Wednesday, 24 May 2017

3.06 LiDAR monitoring

Rockfall detection and analysis: Degotalls E

Stop 3 (Degotalls) RISKNAT

M. J. Royán; M. Guinau; J.M. Vilaplana ; A. Abellán; D. Garcia (Universitat de Barcelona)

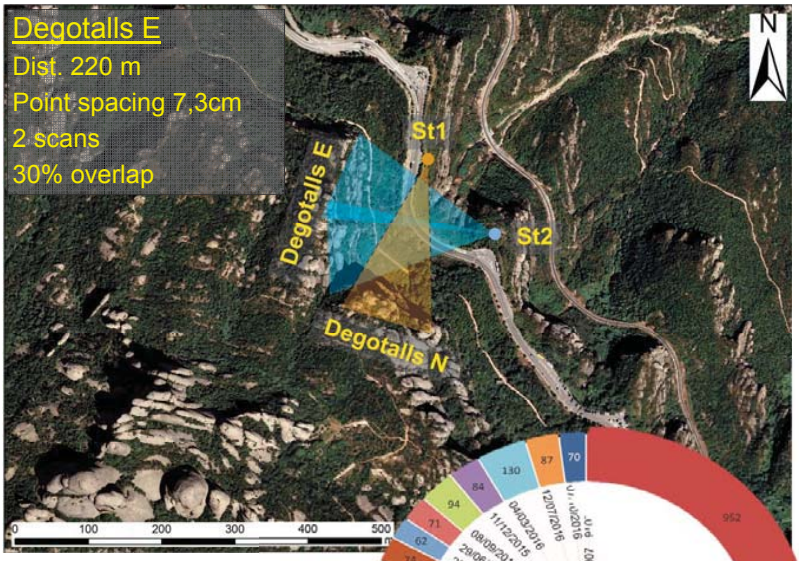

Monitoring Period 2007.05 – 2016.12

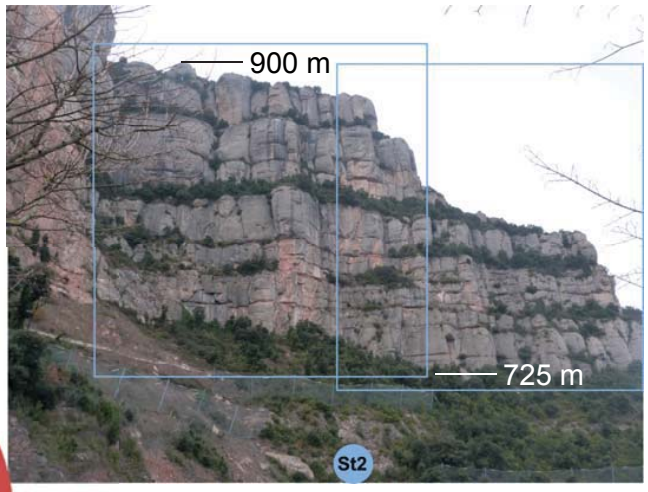

Rockfall inventory

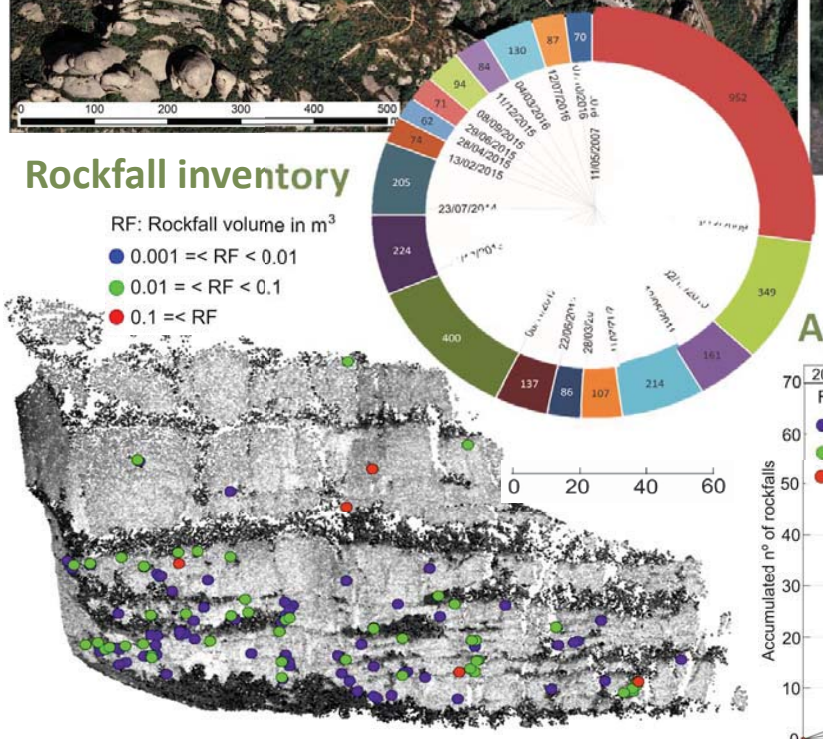

3.507 monitoring days

Total nº rockfalls: 126

Accumulated nº of Rockfalls vs Time

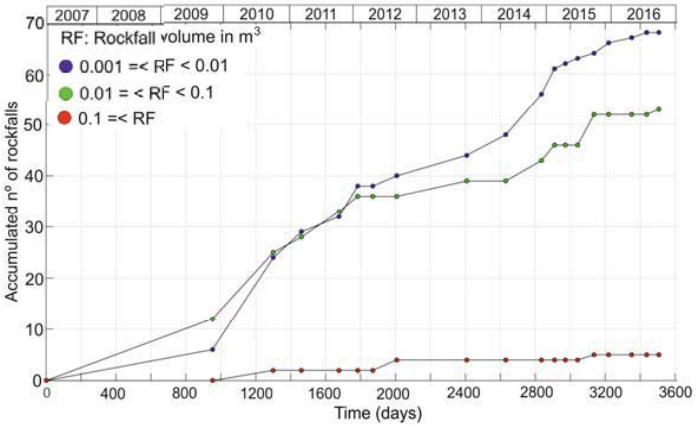

Rockfall density

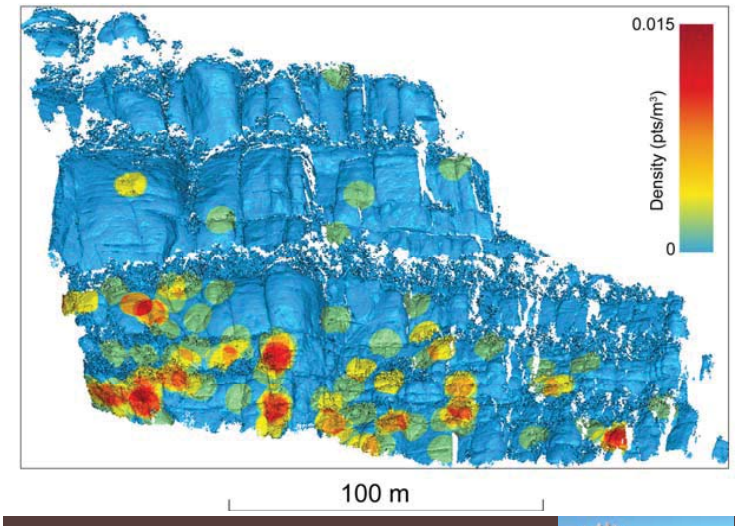

Magnitude-Frequency relationship

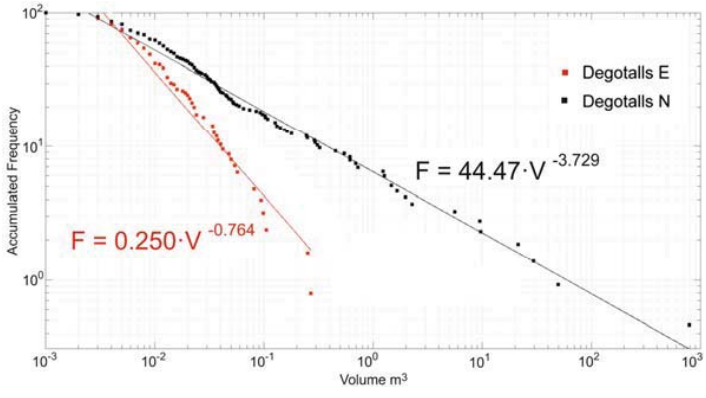

Rockfall risk management in the Montserrat massif

3.07 LiDAR monitoring

Precursory movements: Block displacement

Field trip

Wednesday, 24 May 2017

Stop 3 (Degotalls) RISKNAT

M. J. Royán; M. Guinau; J.M. Vilaplana ; A. Abellán; D. Garcia (Universitat de Barcelona)

Monitoring period: **2007.05 – 2017.01**

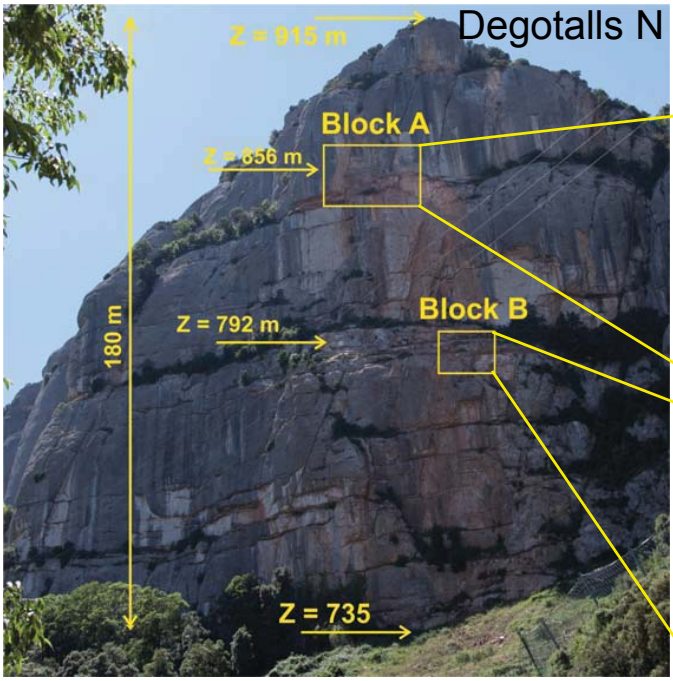

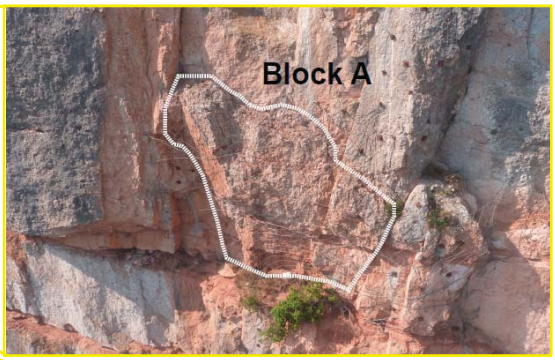

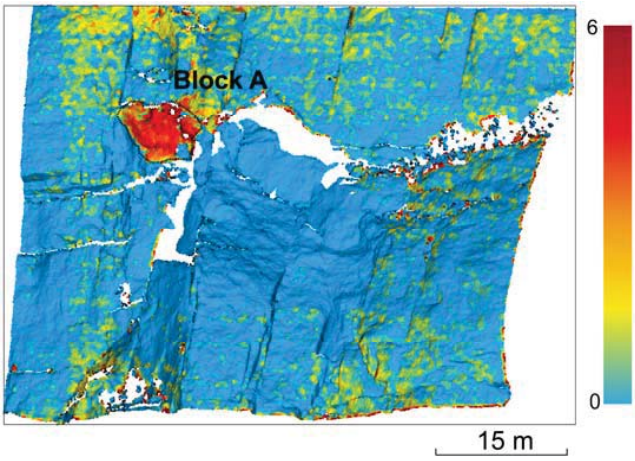

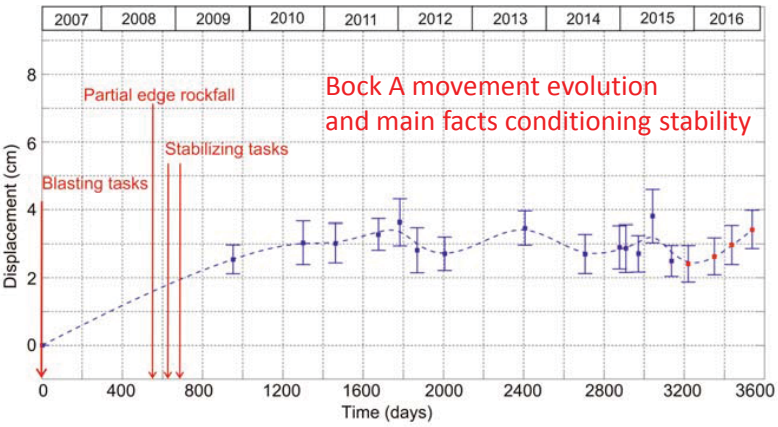

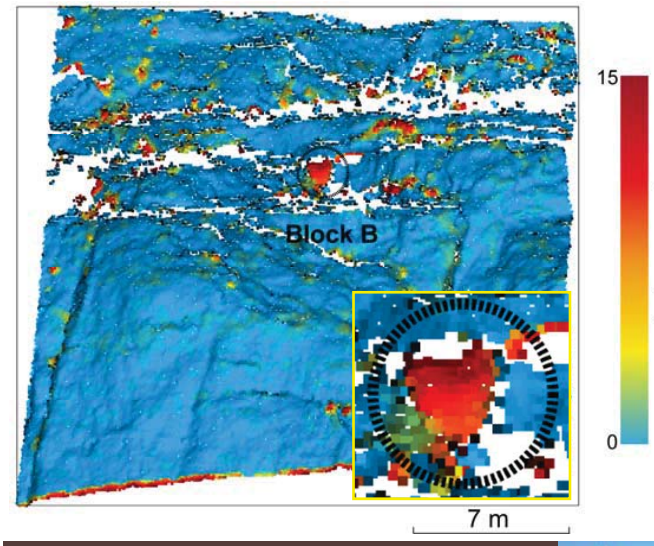

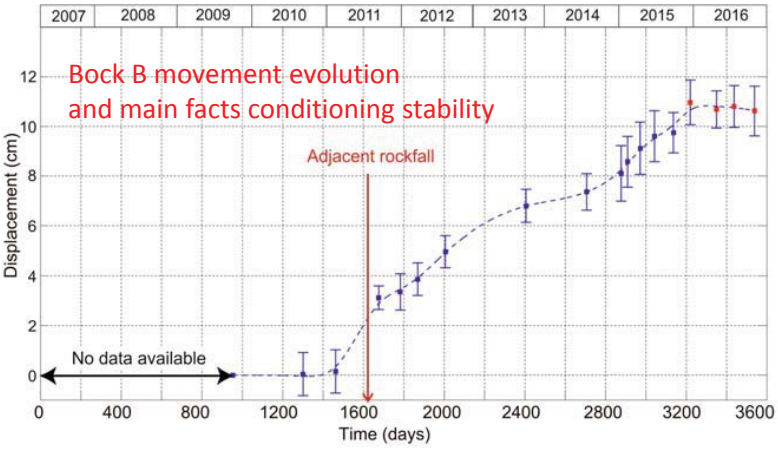

Rockfall risk management in the Montserrat massif

Field trip

Wednesday, 24 May 2017

3.08 Monitoring with GB-SAR system

Results of 5 months measurement campaign

Stop 3 (Degotalls wall)
A. Aguasca & X. Fàbregas
(RS-LAB, UPC)

DIn-SAR *(Differential Interferometric Synthetic Aperture Radar)*

DIn-SAR provides a differential interferogram from two acquisitions, representing the ground motion occurring between the acquisitions with a sub-centimetric accuracy. **GB** = Ground Based.

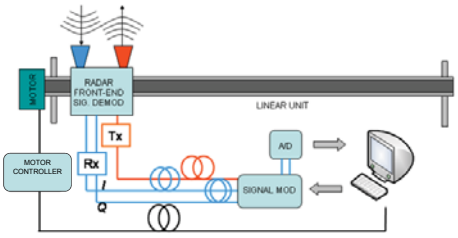

From Reflectivity maps (Complex data) to Coherence Map & Differential Interferogram

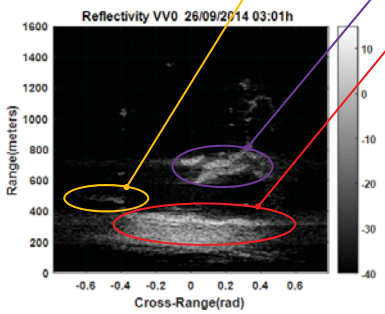

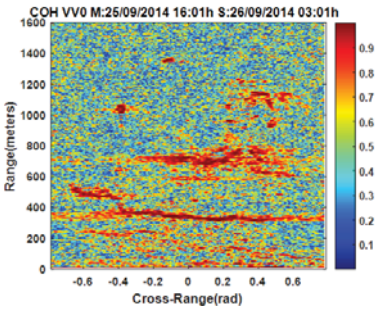

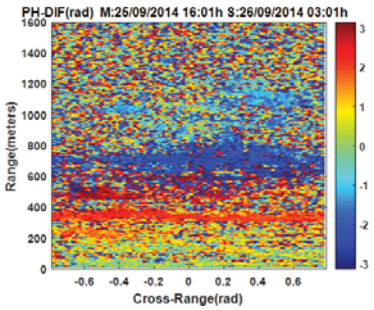

Atmospheric Artifact compensation , pixel selection & parameter extraction

Example of different atmospheric profiles

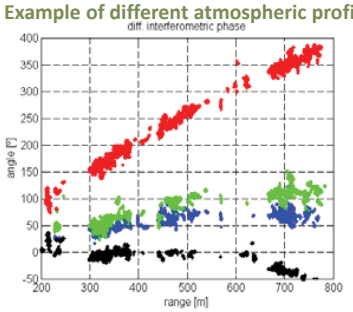

Linear velocity estimation

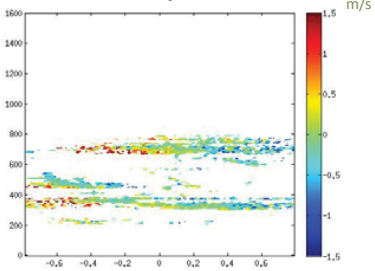

Maximum Linear displacement

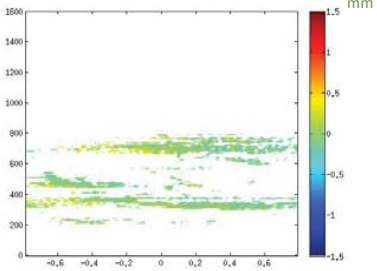

Conclusions

- GB-SAR system working at 9,65GHz. Range resolution of 1.5m, azimuth resolution of 10 mrad (eq. of 5m @ 500m range), sub-centimetric sensibility.
- 5 months of remote controlled, unattended service.
- Geometry of stepped slopes and atmospheric artifacts are a big issue.
- No movement was detected. Further campaigns to be developed
- New areas to explore: Monestir and Degotalls

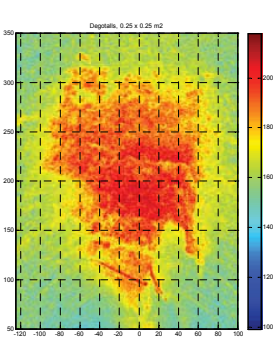

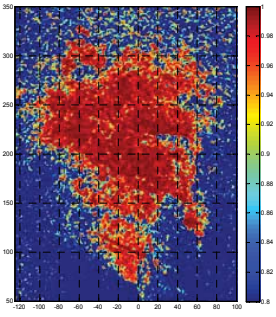

Rockfall risk management in the Montserrat massif

Field trip

Wednesday, 24 May 2017

4.01

Joint Analysis

Introduction, Degotalls and Monestir cliffs

Stop 4 (Sant Joan) RISKNAT
X. Blanch. M. Guinau, M.J. Royán. F. Sàbat, D. García-Sellés (Universitat de Barcelona)

Situation

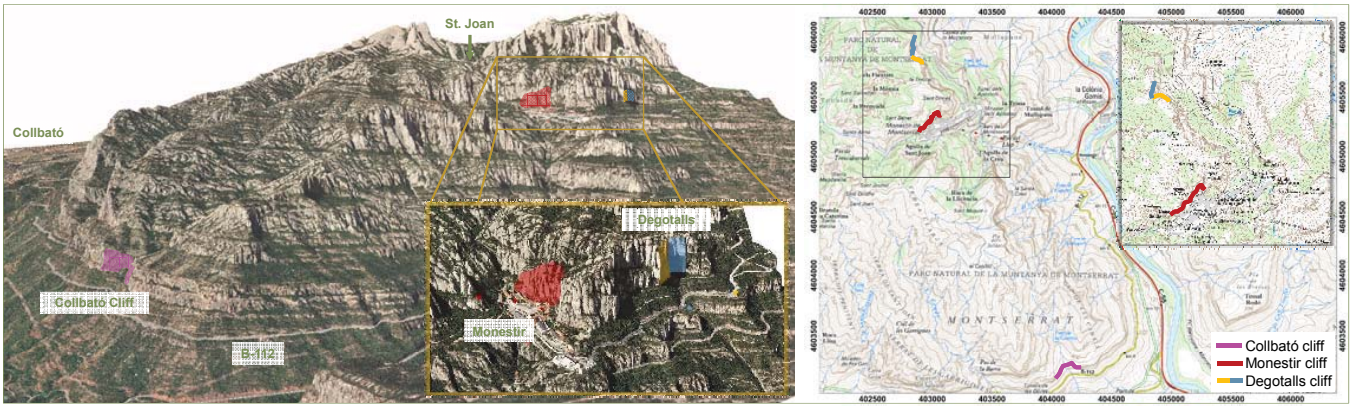

Methodology

LiDAR acquisition → Planar Regression → Classification

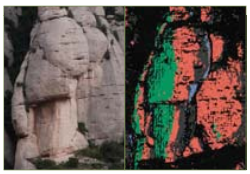

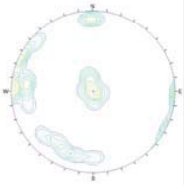

García-Sellés, D. et al., 2009

Massif joint sets

Alsaker, E. et al., 1996

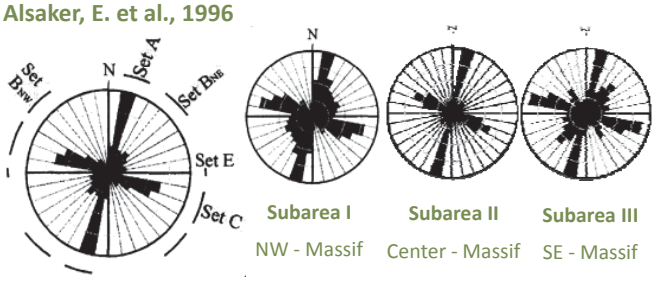

Subarea I — NW - Massif
Subarea II — Center - Massif
Subarea III — SE - Massif

Degotalls cliff

Sàbat F. 2011

Field measurements

Outcrop 1 | Outcrop 2 | Outcrop 3

LiDAR data

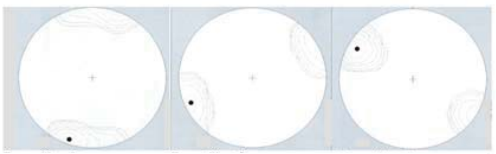

Set 1 86/014 | Set 3 85/065 | Set 5 80/120

Set 2 85/038 | Set 4 78/096 | Set 6 83/1411

Monestir cliff

Royán, M.J. et al., 2013

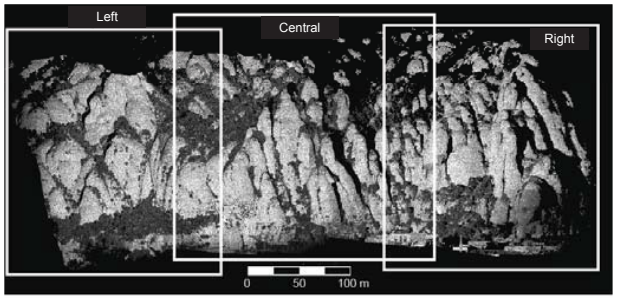

Bedding 17/339 | Set 1 71/182 | Set 2 81/225 | Set 3 83/254

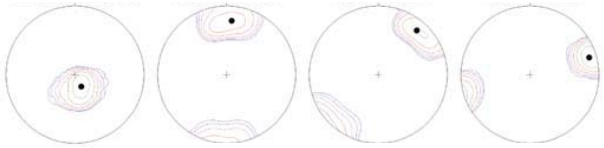

Set 4 73/103 | Set 5 70/122 | Set 6 72/144

Field trip

Wednesday, 24 May 2017

4.02

Joint Analysis

Collbató cliff and Conclusions

Stop 4 (Sant Joan) RISKNAT

X. Blanch. M. Guinau, M.J. Royán. F. Sàbat, D. García-Sellés (Universitat de Barcelona)

Collbató cliff

Blanch et al., 2017

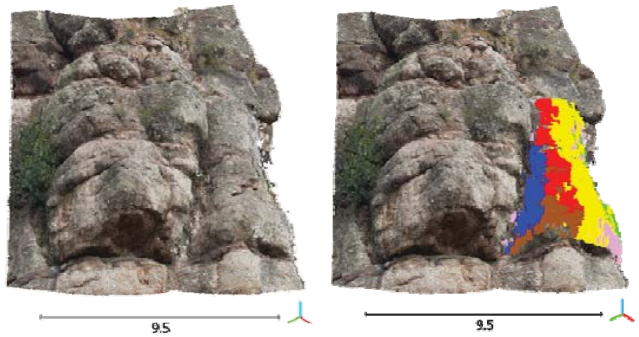

Number of surfaces in rockfall source

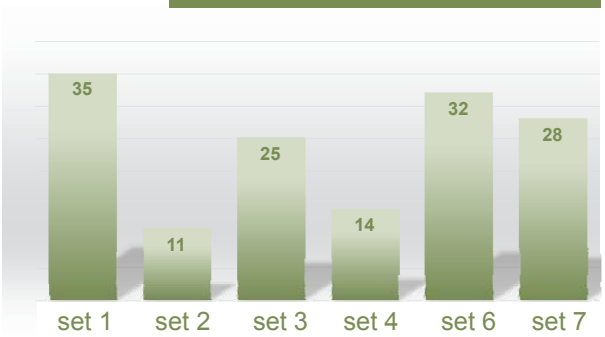

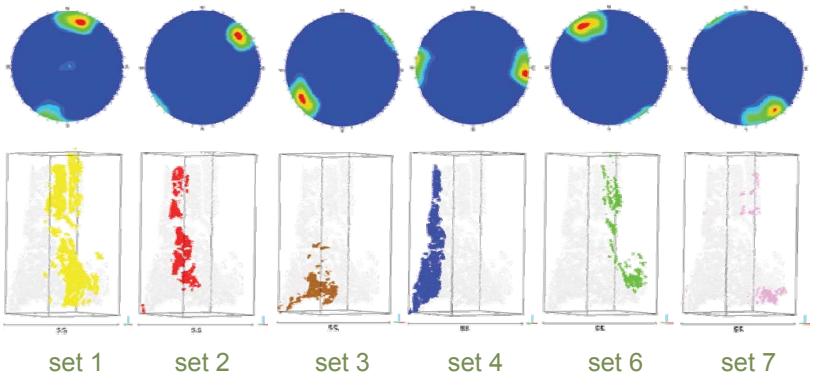

Joint Analysis (6 joint sets)

Set of joints	Dip/Dip Direction	Number of points
Set 1	75/196	552.785
Set 2	79/230	111.862
Set 3	81/274	597.755
Set 4	80/054	103.025
Set 6	78/147	248.430
Set 7	80/335	218.321

Conclusions

Joint sets	Dip/Dip Direction			
	Monestir Cliff	Degotalls Cliff	Collbató Cliff	Alsaker et al. (1996)
Set 1	71/182*	86/014	75/196*	Set E (W-E) / Set C (WNW-ESE)
Set 2	81/225*	85/038	79/230*	Set BNW (NW-SE)
Set 3	83/254*	85/065	80/054	
Set 4	73/103	78/096	81/274*	Set A (NNE-SSW)
Set 5	70/122	80/120		Set A (NNE-SSW)
Set 6	72/144	83/141	78/147	Set BNE (NE-SW)
Set 7			80/335*	Set BNE (NE-SW)

* Conjugate joint sets (± 180º)

Joint Analysis

- Set 1,2,3,4 and 6 joint sets affect the massif in a regional way. And they are detected in all locations.
- The limits of each dip direction range are subjective. And they are based on 3D observations of the points clouds.
- The joints surfaces are not a perfect and continuous faces and the orientation can be slightly changed along the massif.
- LiDAR data sets are a good way (quickly and contactless) to do structural analysis.

References

ALSAKER E, GABRIELSEN RH, ROCA E (1996) The significance of the joint patterns of Late-Eocene Mont-serrat fan-delta, Catalan Coastal Ranges (NE Spain). Tectonophysics 266, 465–91.

BLANCH X, GUINAU M, ROYÁN M J (2017) Caracterización geomorfológica y estructural de zonas de salida de bloques en una pared rocosa afectada por desprendimientos. IX Simposio Nacional sobre Taludes y Laderas Inestables. Santander.

GAL·LA REQUENA M (2010) Caracterització de les zones de sortida de despreniments de la paret de Degotalls (Montserrat). Trabajo Final de Carrera. http://hdl.handle.net/2099.1/12578

GARCÍA-SELLÉS D, FALIVENE O, ARBUES P, GRATACOS O, TAVANI S, MUNOZ JA (2011) Supervised identification and reconstruction of near-planar geological surfaces from terrestrial laser scanning. Computers & Geosciences, 37 1584-1594.

SABAT F (2011) Les diàclasis dels Degotalls de Montserrat. Universitat de Barcelona. (Unpublished report)

ROYÁN M J, GUINAU M, VILAPLANA J M, ABELLÁN A (2013) Análisis y seguimiento de las laderas del Monasterio de Montserrat mediante LiDAR Terrestre. VIII Simposio Nacional sobre Taludes y Laderas Inestables. Palma de Mallorca.

Rockfall risk management in the Montserrat massif

Field trip

Wednesday, 24 May 2017

4.03 Overview on the massif

Rockfall hazard and runout

Stop 3 (Degotalls)

M. Janeras & G. Domènech (ICGC)

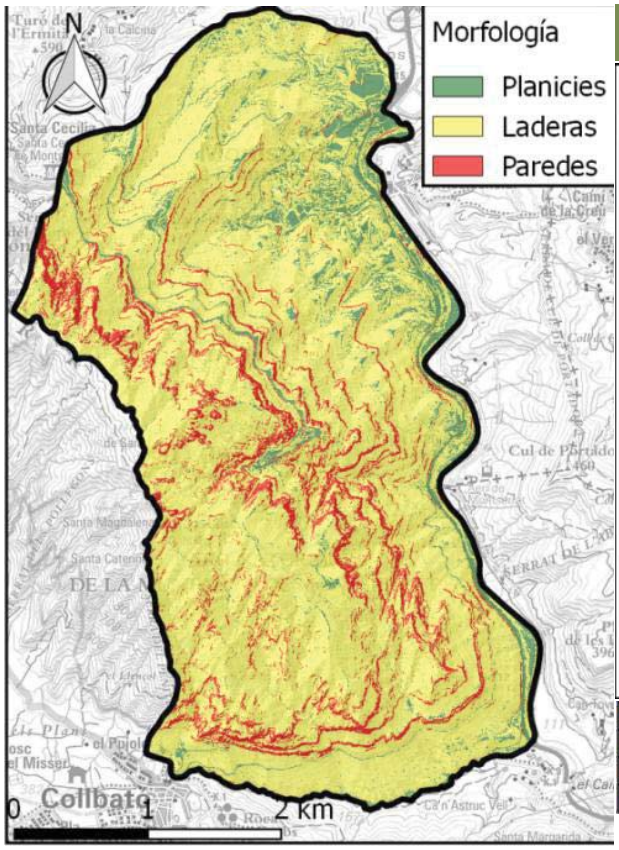

Morphometric analysis

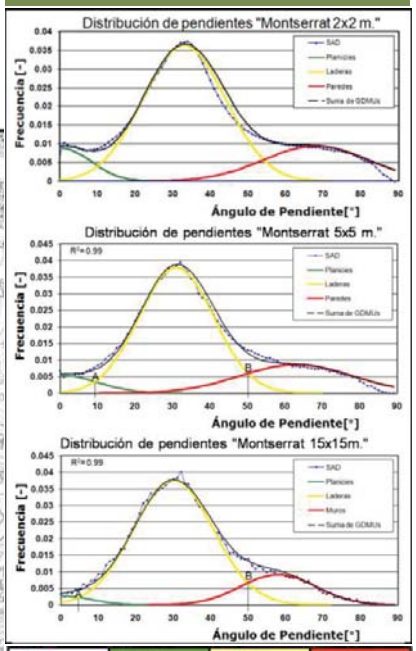

MET	Planicies	Laderas	Paredes
2x2	0° - 10°	10°-54°	54° – 90°
5x5	0° – 10°	10°-50°	50° – 90°
15x15	0° – 5°	5°- 50°	50° - 90°

Natural park: 3500 ha
Study area: 1438 ha (41%)
Rockfall source: 145ha (planimetry, 2D) = 10%
Rockface: 357 ha (pseudo-real, 2.5D)
Slope: mean rockface = 66º

Flow-R Approach

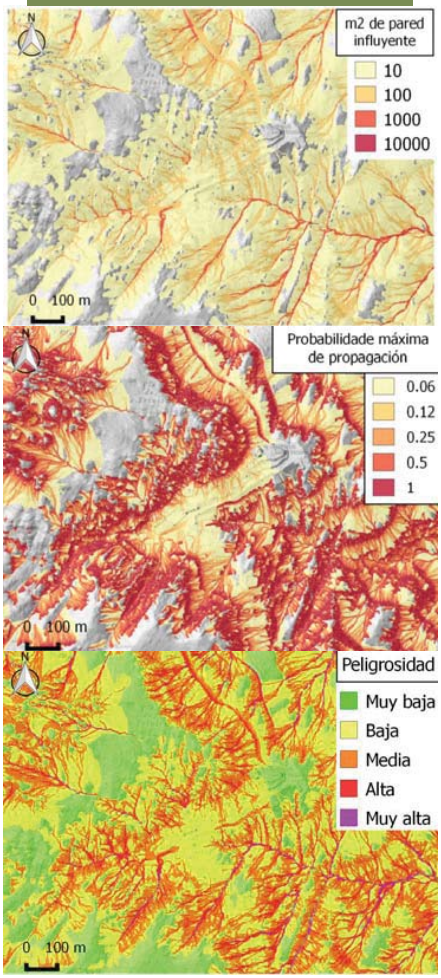

A. Carmona (2015) "Sectorización y zonificación de la peligrosidad por caída de rocas, aplicación en Montserrat". Master Thesis, Vilaplana & Janeras (Adv.) Universitat de Barcelona.

Rockfall inventory and runout susceptibility

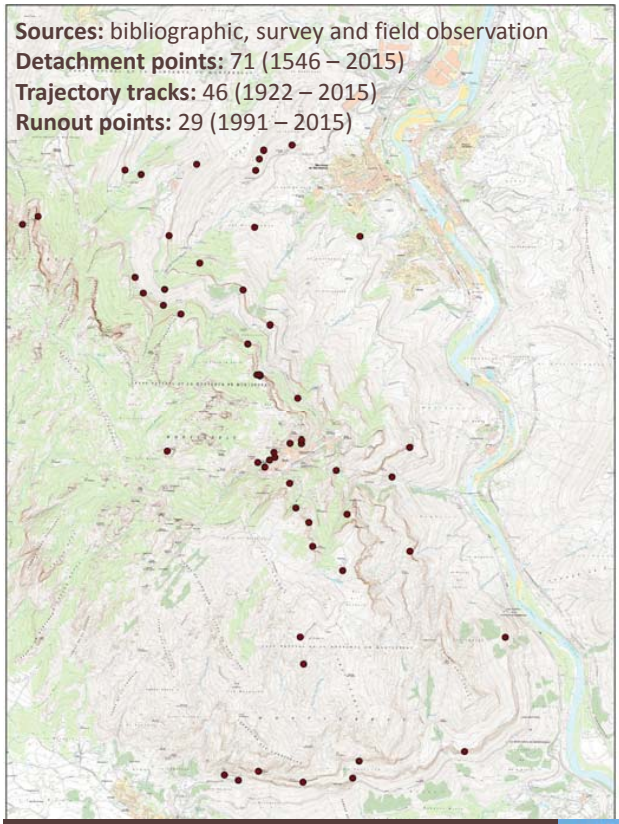

Sources: bibliographic, survey and field observation
Detachment points: 71 (1546 – 2015)
Trajectory tracks: 46 (1922 – 2015)
Runout points: 29 (1991 – 2015)

Degotalls 2007-08:
Volume 300 – 900m^3
Reach angle = 36-37º

Terrain type	reference value for the Reach angle
Open, planar slope	31º
Channelized path	36º
Highly deflected	45º or higher

Preliminary results

- Sanctuary & Monastery building area:

V >= 1 m^3 / **T** = 6 years
V >= 10 m^3 / **T** = 27 years

- The whole massif:

V >= 10 m^3 / **F** = 9 events/year

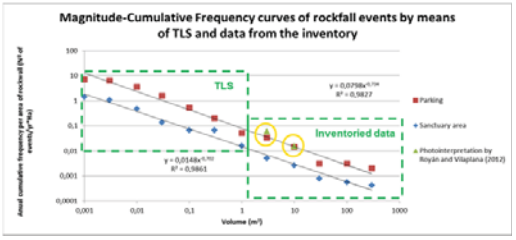

M. Janeras, G. Domènech, J. Pons, E. Prat, P. Buxó (2016) "Rockfall hazard assessment by means of the magnitude-frequency curves in the Montserrat Massif (central Catalonia, Spain): first insights". *EGU General Assembly 2016*, Vienna, *Geophysical Research Abstracts* Vol. 18, EGU2016-13341-2, 2016.

Field trip

Wednesday, 24 May 2017

4.04 Overview on the massif

Regional cartography: MPRG25k

Stop 4 (Sant Joan funicular)

P. Buxó, J. Pinyol & M. González (ICGC)

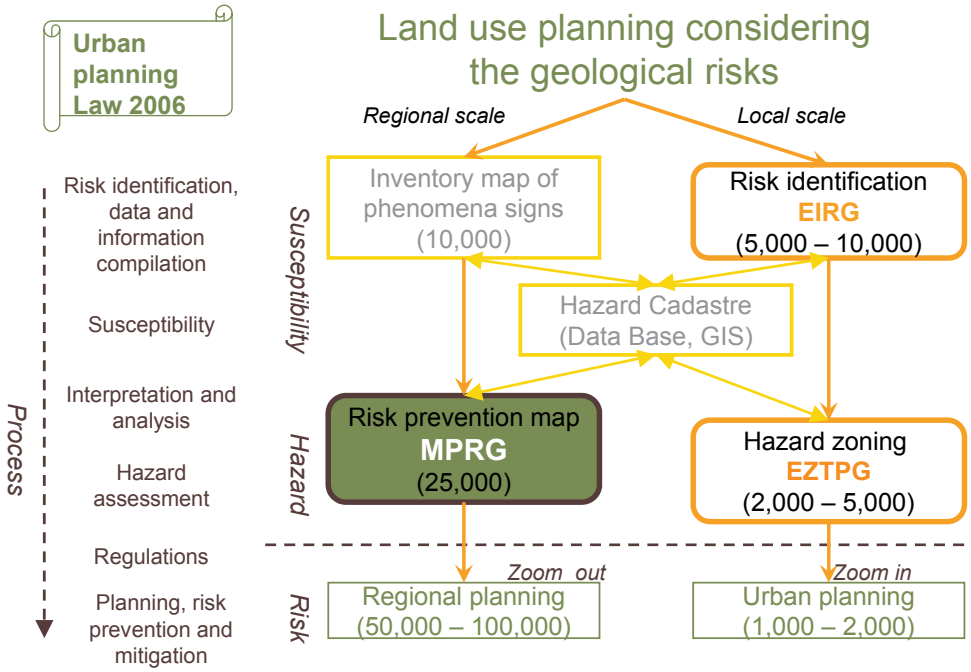

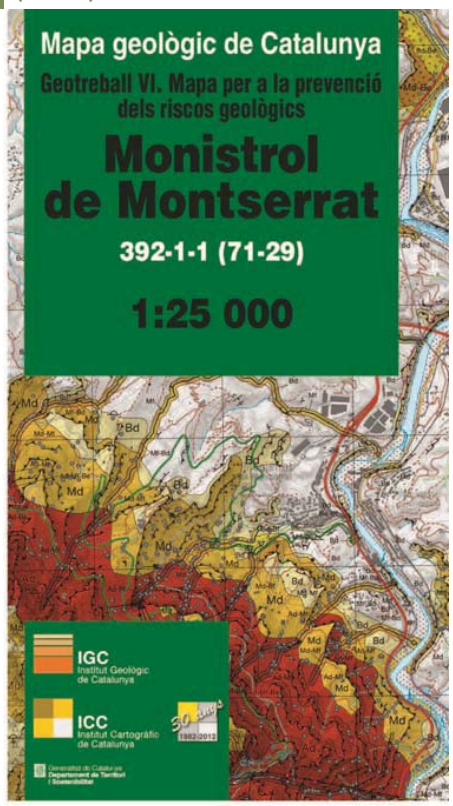

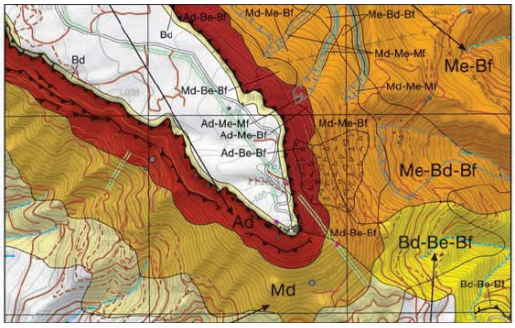

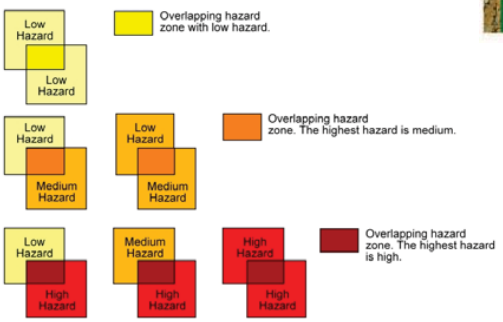

Multi-hazard map

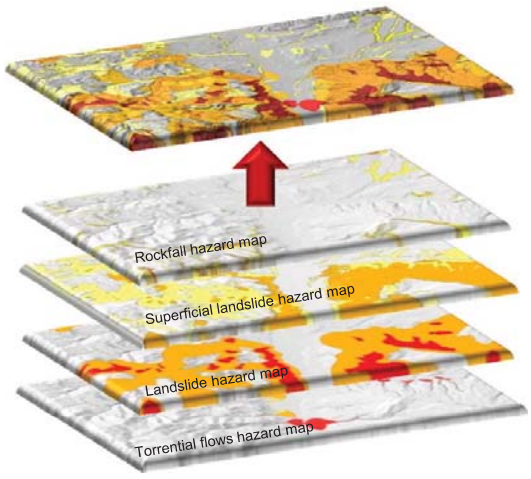

Example of hazard zoning for expected rockfall of 10-100 m^3

Magnitude	Medium		
Angle of reach	40º	33º	30º
Frequency to reach			
Frequency to inciciation: High	High	Medium	Low
Frequency to inciciation: Medium	Medium	Medium	Low
Frequency to inciciation: Low	Medium	Low	Low

Hazard boundaries based on the angle of reach for a 10-100 m high cliff, many instability evidences and potential rockfall volumes between 10-100 m3.

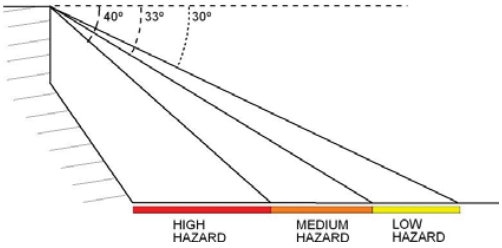

J. Pinyol, M. González, P. Oller (2016) "A regional methodology for rockfall hazard assessment in the hazard prevention map of Catalonia 1:25,000. A geomorphological approach". In: Aversa et al. (Eds.) *Landslides and Engineered Slopes. Experience, Theory and Practice*, Associazione Geotecnica Italiana, Rome, ISBN 978-1-138-02988-0, 1631-1636

Rockfall risk management in the Montserrat massif

Field trip

Wednesday, 24 May 2017

4.05 Rockfall gallery for the funicular

Hazard conditions

Stop 4 (Sant Joan funicular)
M. Janeras (ICGC)
D. Paret & A. Ferré (FGC)

Mass	>1 ton	100 – 500 kg	20 – 100 kg	5 – 20 kg	1 – 5 kg
Type	Massive slabs and plates, large blocks	Isolated blocks prone to disaggregate	Thin slabs or plates	Pebble aggregates	Pebbles and crusts

Constraints:

- Maximum velocity = 40 m/s (height jump of 80m)
- Railcar glass ceiling = 0.2 kJ
- Small opening of the mesh to retain also small boulders
- Landscape friendly design from external point of view
- As transparent as possible for the passengers

Dimensioning: 110 kJ
Under elastic behaviour (Service limit)

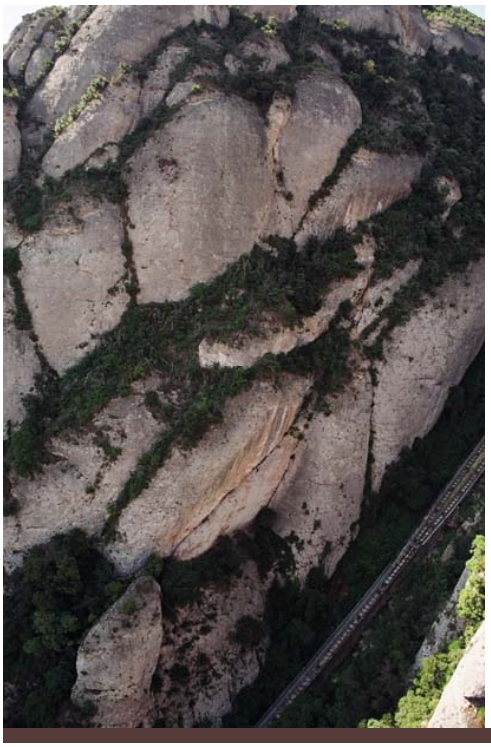

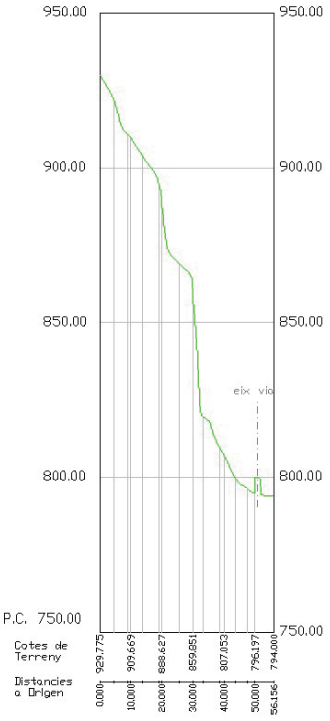

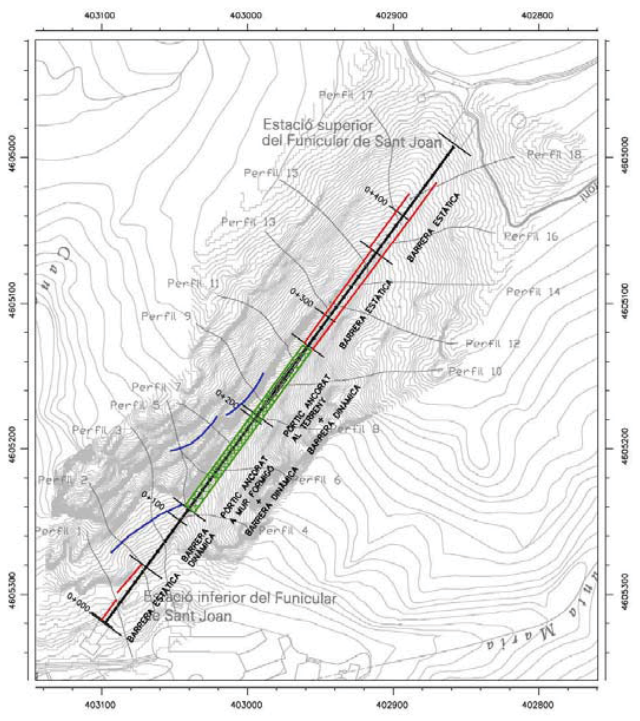

Rockfall risk management in the Montserrat massif

Field trip

Wednesday, 24 May 2017

4.06 Rockfall gallery for the funicular

Mesh test

Stop 4 (Sant Joan funicular)
M. Janeras (ICGC)
J.M. Velasco (AMATRIA)
D. Paret & A. Ferré (FGC)

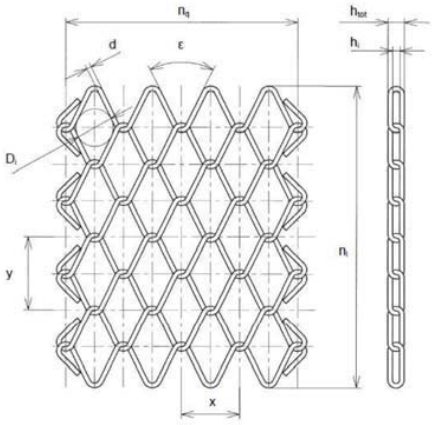

Test site: Walenstadt, Switzerland
Test date: 8-9/04/2010
Tester: Swiss Federal Research Institute WSL
Manufacturer: GEOBRUGG
Mesh: High-tensile steel wire mesh
Sample 1: ROMBO® G30/3mm wire
Sample 2: ROMBO® G30/4mm wire
Device: KTI-Frame (4 x 4 m)

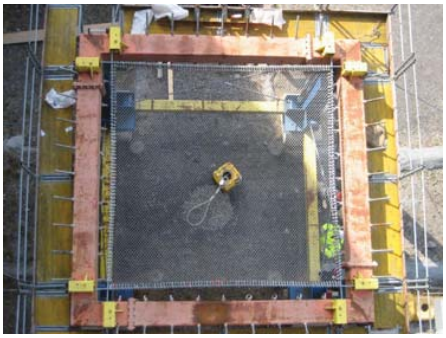

Level	E1	E2	E3
Energy (kJ)	20	45	100
Mass (kg)	160	160	320
Release height (m)	12.8	28.7	32
Velocity (m/s)	15.8	23.8	25

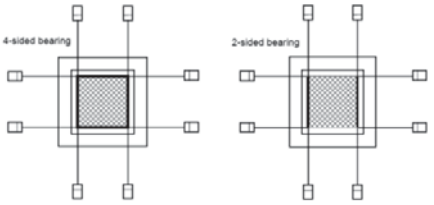

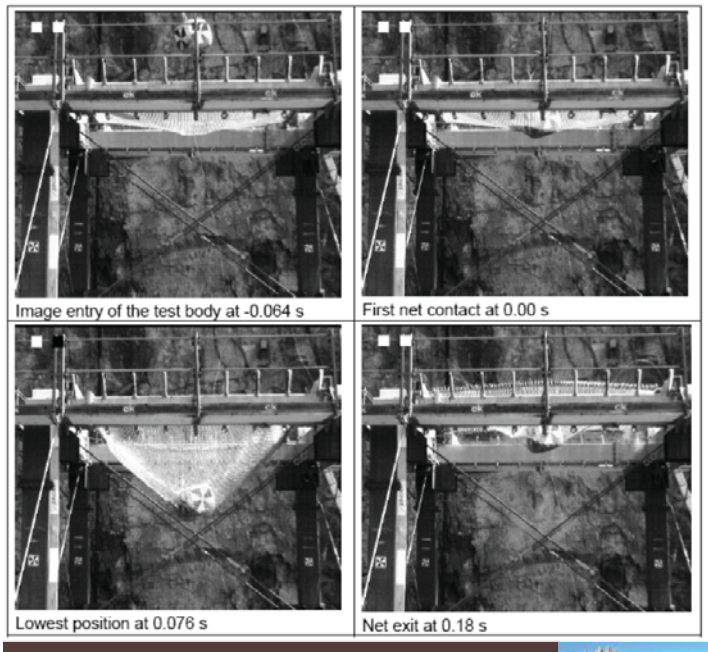

Dynamic Test: (Film 100408_d003)	Time t (s)	Height z (m)	Velocity (m/s)	Energy (kJ)
Data at image entry	-0.064	3.82	24.37	
Data at first net contact	0	2.24	25.00	100.01
Data at lowest position	0.076	1.10	0	
Brakdistance dynamic 1.14 m				1.79
Data at net exit	0.18	2.29	13.85	
Rebound height after net exit (m)		9.78		

Maximum pulse on the supporting wires:
- Longitudinal: 197kN @ 0.066s
- Transversal: 136kN @ 0.079s

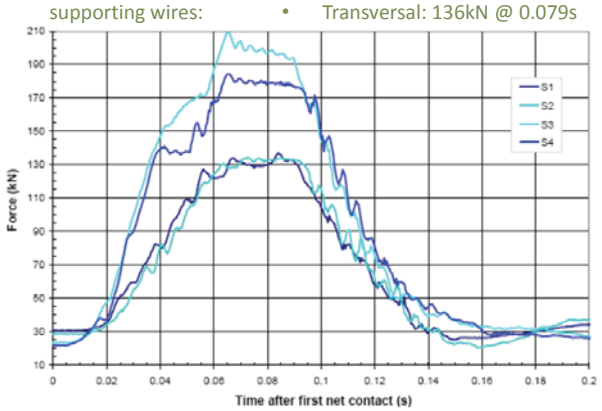

Rockfall risk management in the Montserrat massif

Field trip

Wednesday, 24 May 2017

4.06 Rockfall gallery for the funicular

Structure design

Stop 4 (Sant Joan funicular)

M. Janeras (ICGC)
J.M. Velasco (AMATRIA)
D. Paret & A. Ferré (FGC)

FGC Ferrocarrils de la Generalitat de Catalunya

amatria ingeniería

Model to reproduce the test

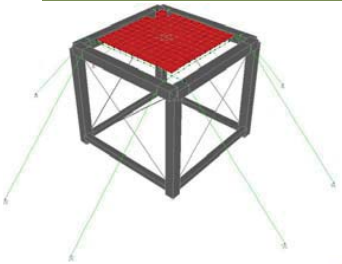

Shell like

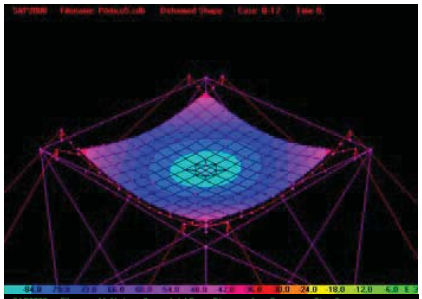

Mesh like

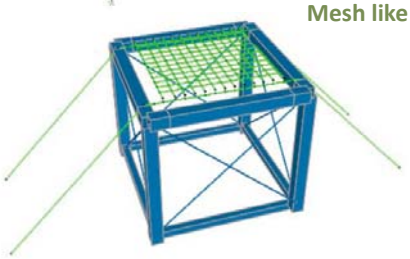

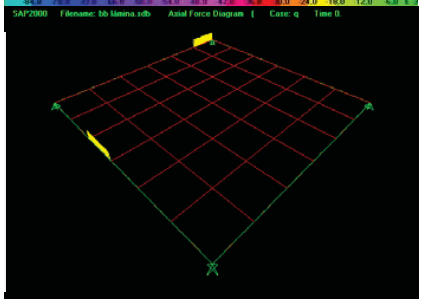

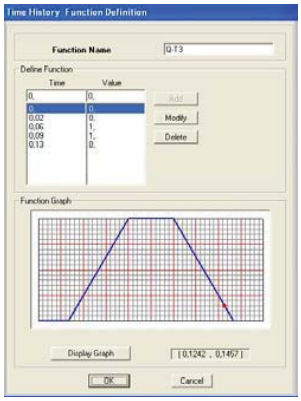

Single track

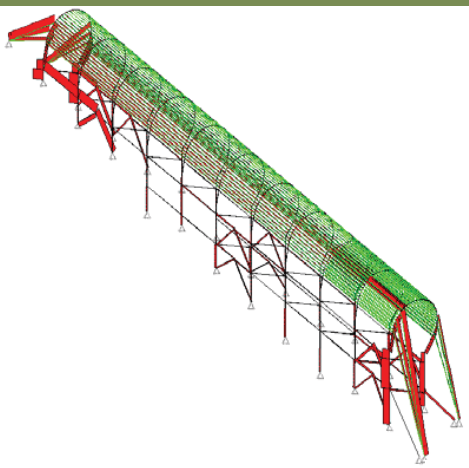

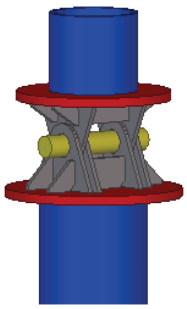

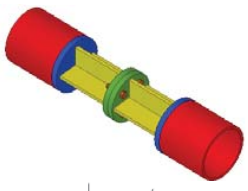

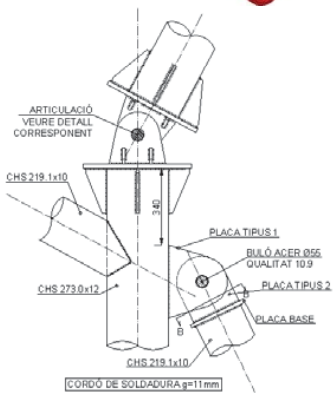

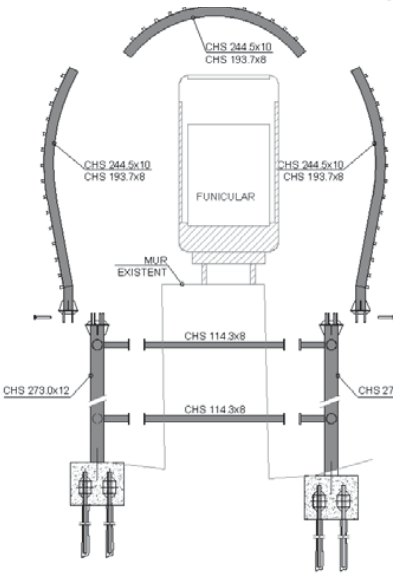

EXPLOSIÓ PÒRTIC VIA UNICA

Double track

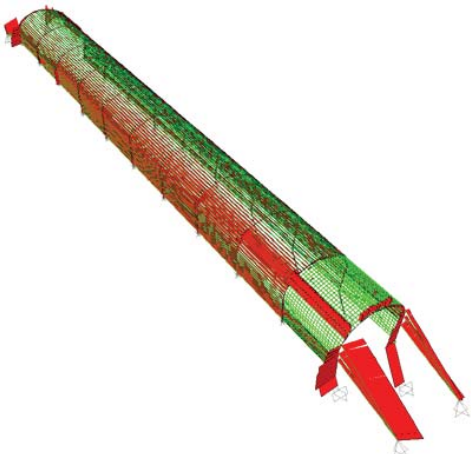

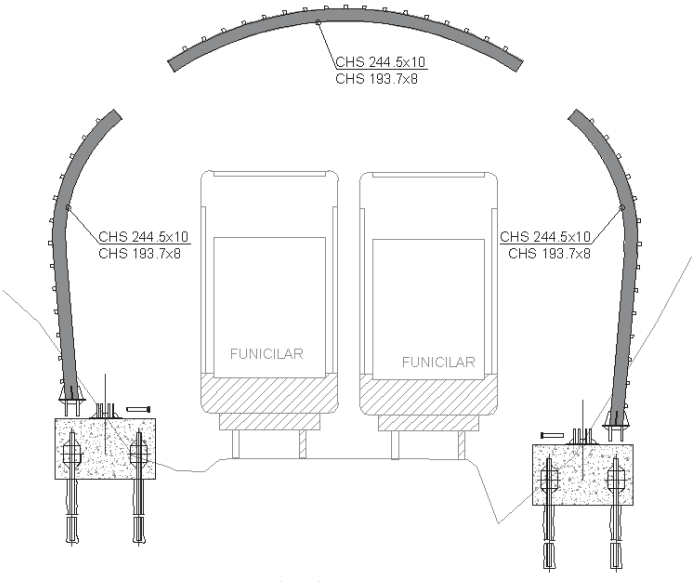

EXPLOSIÓ PÒRTIC VIA UNICA

ICGC
Institut
Cartogràfic i Geològic
de Catalunya

UNIVERSITAT POLITÈCNICA
DE CATALUNYA
BARCELONATECH

CIMNE

International Center
for Numerical Methods in Engineering